ISSN 1948-5204 (online)

World Journal of *Gastrointestinal Oncology*

World J Gastrointest Oncol 2022 December 15; 14(12): 2302-2421

Published by Baishideng Publishing Group Inc

World Journal of Gastrointestinal Oncology

Contents

Monthly Volume 14 Number 12 December 15, 2022

MINIREVIEWS

ORIGINAL ARTICLE

Basic Study

Retrospective Study

Observational Study

CASE REPORT

World Journal of Gastrointestinal Oncology

Monthly Volume 14 Number 12 December 15, 2022

Contents

ABOUT COVER

AIMS AND SCOPE

The primary aim of *World Journal of Gastrointestinal Oncology* (*WJGO*, *World J Gastrointest Oncol*) is to provide scholars and readers from various fields of gastrointestinal oncology with a platform to publish high-quality basic and clinical research articles and communicate their research findings online.

WJGO mainly publishes articles reporting research results and findings obtained in the field of gastrointestinal oncology and covering a wide range of topics including liver cell adenoma, gastric neoplasms, appendiceal neoplasms, biliary tract neoplasms, hepatocellular carcinoma, pancreatic carcinoma, cecal neoplasms, colonic neoplasms, colorectal neoplasms, duodenal neoplasms, esophageal neoplasms, gallbladder neoplasms, *etc*.

INDEXING/ABSTRACTING

The *WJGO* is now abstracted and indexed in PubMed, PubMed Central, Science Citation Index Expanded (SCIE, also known as SciSearch®), Journal Citation Reports/Science Edition, Scopus, Reference Citation Analysis, China National Knowledge Infrastructure, China Science and Technology Journal Database, and Superstar Journals Database. The 2022 edition of Journal Citation Reports® cites the 2021 impact factor (IF) for *WJGO* as 3.404; IF without journal self cites: 3.357; 5-year IF: 3.250; Journal Citation Indicator: 0.53; Ranking: 162 among 245 journals in oncology; Quartile category: Q3; Ranking: 59 among 93 journals in gastroenterology and hepatology; and Quartile category: Q3. The *WJGO*'s CiteScore for 2021 is 3.6 and Scopus CiteScore rank 2021: Gastroenterology is 72/149; Oncology is 203/360.

RESPONSIBLE EDITORS FOR THIS ISSUE

Production Editor: *Xiang-Di Zhang*; **Production Department Director:** *Xiang Li*; **Editorial Office Director:** *Jia-Ru Fan*.

NAME OF JOURNAL
World Journal of Gastrointestinal Oncology

ISSN
ISSN 1948-5204 (online)

LAUNCH DATE
February 15, 2009

FREQUENCY
Monthly

EDITORS-IN-CHIEF
Florin Burada, Monjur Ahmed

EDITORIAL BOARD MEMBERS
https://www.wjgnet.com/1948-5204/editorialboard.htm

PUBLICATION DATE
December 15, 2022

INSTRUCTIONS TO AUTHORS
https://www.wjgnet.com/bpg/gerinfo/204

GUIDELINES FOR ETHICS DOCUMENTS
https://www.wjgnet.com/bpg/GerInfo/287

GUIDELINES FOR NON-NATIVE SPEAKERS OF ENGLISH
https://www.wjgnet.com/bpg/gerinfo/240

PUBLICATION ETHICS
https://www.wjgnet.com/bpg/GerInfo/288

PUBLICATION MISCONDUCT
https://www.wjgnet.com/bpg/gerinfo/208

ARTICLE PROCESSING CHARGE
https://www.wjgnet.com/bpg/gerinfo/242

STEPS FOR SUBMITTING MANUSCRIPTS
https://www.wjgnet.com/bpg/GerInfo/239

ONLINE SUBMISSION
https://www.f6publishing.com

World Journal of Gastrointestinal Oncology

Submit a Manuscript: https://www.f6publishing.com

World J Gastrointest Oncol 2022 December 15; 14(12): 2302-2312

DOI: 10.4251/wjgo.v14.i12.2302

ISSN 1948-5204 (online)

MINIREVIEWS

Sarcopenia in pancreatic cancer: Effect on patient outcomes

Moon Hyung Choi, Seung Bae Yoon

Specialty type: Gastroenterology and hepatology

Provenance and peer review: Invited article; Externally peer reviewed.

Peer-review model: Single blind

Peer-review report's scientific quality classification

Grade A (Excellent): 0
Grade B (Very good): 0
Grade C (Good): C, C
Grade D (Fair): D
Grade E (Poor): 0

P-Reviewer: Marquardt JP, United States; Pan Y, China; Shariati MBH, Iran

Received: September 17, 2022
Peer-review started: September 17, 2022
First decision: October 19, 2022
Revised: October 29, 2022
Accepted: November 28, 2022
Article in press: November 28, 2022
Published online: December 15, 2022

Moon Hyung Choi, Department of Radiology, Eunpyeong St. Mary's Hospital, College of Medicine, The Catholic University of Korea, Seoul 03312, South Korea

Seung Bae Yoon, Division of Gastroenterology, Department of Internal Medicine, College of Medicine, The Catholic University of Korea, Seoul 03312, South Korea

Corresponding author: Seung Bae Yoon, MD, PhD, Associate Professor, Division of Gastroenterology, Department of Internal Medicine, College of Medicine, The Catholic University of Korea, 1021, Tongil Ro, Eunpyeong-gu, Seoul 03312, South Korea.
sbyoon@catholic.ac.kr

Abstract

Pancreatic cancer is a challenging disease with an increasing incidence and extremely poor prognosis. The clinical outcomes of pancreatic cancer depend on tumor biology, responses to treatments, and malnutrition or cachexia. Sarcopenia represents a severe catabolic condition defined by the age-related loss of muscle mass and strength and affects as much as 70% of malnourished pancreatic cancer patients. The lumbar skeletal muscle index, defined as the total abdominal muscle area at the L3 vertebral level adjusted by the square of the height, is widely used for assessing sarcopenia in patients with pancreatic cancer. Several studies have suggested that sarcopenia may be a risk factor for perioperative complications and decreased recurrence-free or overall survival in patients with pancreatic cancer undergoing surgery. Sarcopenia could also intensify chemotherapy-induced toxicities and worsen the quality of life and survival in the neoadjuvant or palliative chemotherapy setting. Sarcopenia, not only at the time of diagnosis but also during treatment, decreases survival in patients with pancreatic cancer. Theoretically, multimodal interventions may improve sarcopenia and clinical outcomes; however, no study has reported positive results. Further prospective studies are needed to confirm the prognostic role of sarcopenia and the effects of multimodal interventions in patients with pancreatic cancer.

Key Words: Sarcopenia; Pancreatic cancer; Skeletal muscle; Computed tomography; Outcomes; Survival

Core Tip: Despite advances in diagnosing and treating pancreatic cancer, the prognosis remains poor. More than half of patients with pancreatic cancer develop cachexia and sarcopenia, resulting in poor adherence to intensive treatments. Here, we introduced computed tomography-based body composition analysis, which has been used for analyzing sarcopenia in cancer patients, and covered controversial issues regarding the lack of consensus and diagnostic cutoff points. Recent studies analyzed the effect of sarcopenia on pancreatic cancer on surgery, neoadjuvant therapy, and palliative chemotherapy. Finally, we suggested recommendations for multimodal interventions for the management of sarcopenia and the design of future studies.

Citation: Choi MH, Yoon SB. Sarcopenia in pancreatic cancer: Effect on patient outcomes. *World J Gastrointest Oncol* 2022; 14(12): 2302-2312
URL: https://www.wjgnet.com/1948-5204/full/v14/i12/2302.htm
DOI: https://dx.doi.org/10.4251/wjgo.v14.i12.2302

INTRODUCTION

Pancreatic cancer is the fourth leading cause of cancer-related deaths in both men and women worldwide[1]. Although overall cancer mortality continues to decrease in both sexes, the mortality rate of pancreatic cancer is still increasing[2]. Further, despite advances in cancer treatment, the 5-year survival rate remains poor at approximately 8%. Less than 20% of patients are in a resectable state and can be treated with curative surgery, and approximately 80% of patients have locally advanced or metastatic disease at the time of diagnosis. As such, efforts have been recently made to improve pancreatic cancer treatment, including advanced surgical techniques, adjuvant chemotherapy, neoadjuvant therapy (NAT), and combination chemotherapy regimens [*e.g.*, folinic acid, fluorouracil, irinotecan hydrochloride, and oxaliplatin (FOLFIRINOX), and gemcitabine plus nab-paclitaxel][3,4].

The clinical outcomes of pancreatic cancer not only depend on tumor biology and treatment responses but are also strongly influenced by the nutrition and performance status of the patients. Before or during treatment, many patients experience early alteration of the metabolic state with rapid weight loss or treatment-related performance deterioration. Therefore, the assessment of nutritional status and performance status is crucial to determine the best treatment modality for extending survival with adequate quality of life.

The assessment of body composition typically refers to the measurement of fat and muscle mass. Sarcopenia is a term used to describe the age-related loss of muscle mass and strength. Beyond the quantification of the muscle mass, the importance of the muscle quality assessed for fat infiltration within the muscle is also emerging. A number of parameters have been analyzed for sarcopenic obesity, such as subcutaneous adipose tissue, visceral adipose tissue, and visceral fat-to-skeletal muscle ratio. Sarcopenia has been proven to be related to the prognosis of various diseases, especially in several types of cancer. A wide range of techniques such as body imaging modalities, including computed tomography (CT) and magnetic resonance imaging, bioimpedance analysis, or anthropometric measures, have been used to assess muscle mass; however, no gold standard diagnostic method for sarcopenia has been established yet[5]. Despite its high cost and radiation exposure, CT is the most accessible way to measure the fat and muscle area separately because of the regular follow-up CT examinations for cancer patients[6].

This study aimed to describe a method to assess body composition using CT images and the role of sarcopenia in the management and prognosis of pancreatic cancer.

CT-BASED BODY COMPOSITION ANALYSIS

Various methods have been introduced for CT-based body composition analysis. The total abdominal muscle area, including the entire abdominal wall and back muscle, is commonly measured on CT images. Muscle area can be measured on one axial slice, or muscle volume can be measured on several consecutive slices. Among the many different landmarks, the level of the transverse processes of the L3 vertebra is generally used. Measurement of the psoas muscle area is a simple method, and the psoas muscle area has been proven to be highly correlated with the total abdominal muscle area.

Thresholds of CT attenuation can affect the muscle area, as they determine the pixels that contain muscles and other tissues. If the threshold range is wider, more pixels are selected as the muscle area, leading to a larger muscle area. The use of intravenous contrast or slice thickness can affect body composition data[7]. The phase of CT acquisition (*e.g.*, arterial or portal) also affects the assessment of the skeletal muscle area because the contrast agent increases tissue attenuation. Therefore, the consistent use of certain thresholds and a particular phase of CT is important to obtain reliable results. In addition,

CT acquisition parameters should be reported together with body composition data using CT. As body habitus affects muscle mass, several methods are used to adjust the body habitus using the square of height and body weight. The most commonly used index is the skeletal muscle index, which is calculated as muscle area/height squared (cm^2/m^2). In pancreatic cancer, the lumbar skeletal muscle index (cm^2/m^2), defined as the total abdominal muscle area at the L3 vertebral level adjusted by the height square, is commonly used. Additionally, the mean density of the muscle reflecting the amount of intervening fat in the muscle may be related to muscle quality.

PANCREATIC CANCER AND SARCOPENIA

There is a lack of consensus regarding the definition of sarcopenia in patients with pancreatic cancer. Among the many definitions of sarcopenia, the cutoff values for sex-specific lumbar skeletal muscle index suggested by Prado *et al*[8] (52.4 cm^2/m^2 for males and 38.5 cm^2/m^2 for females) have been widely used in early Western studies[9-11]. These sex-specific cutoffs were obtained from the most significant *P* value by optimal stratification of mortality in obese cancer patients. In addition, Martin *et al*[12] reported a new sex- and body mass index-specific threshold value of sarcopenia applicable to both obese and non-obese cancer patients as follows: < 43 cm^2/m^2 for males with body mass index < 25 kg/m^2 or < 53 cm^2/m^2 for males with body mass index > 25 kg/m^2 and < 41 cm^2/m^2 for females. This definition of sarcopenia has also been widely used in studies on pancreatic cancer[13-17]. However, if the cutoff values based on Western studies are applied to Eastern cancer patients, the prevalence of sarcopenia is increased, with more than two-thirds of males classified as having sarcopenia, and a maldistribution between sexes occurs[18,19]. Therefore, many Eastern studies on pancreatic cancer have applied the following criteria based on a consensus report of the Asian Working Group for Sarcopenia[20]: 42 cm^2/m^2 for males and 38 cm^2/m^2 for females[21-23]. Because body composition can vary among ethnicities and tumor stages, a few studies have set their own cutoff values based on the lowest sex-specific tertile or quartile of the individual cohorts[18,24,25].

Pretreatment sarcopenia is present in 40%-73% of patients with pancreatic cancer. The incidence of sarcopenia and cancer cachexia is particularly higher in pancreatic cancer than in other malignancies [26], possibly owing to the high activation of host inflammatory response and its catabolic pathways in patients with pancreatic cancer. Pancreatic exocrine insufficiency also contributes to malnutrition and weight loss. Pancreatic enzymes are essential for the degradation and absorption of fat and liposoluble vitamins; thus, deficiency of pancreatic enzymes results in steatorrhea and severe maldigestion[27]. Finally, patients with pancreatic cancer can exhibit endocrine insufficiency, usually resulting in pancreatogenic diabetes.

SURGICAL TREATMENT

Surgical resection is the only curative treatment option for localized pancreatic cancer. However, pancreatic cancer surgery carries a high risk of perioperative morbidity and recurrence. Therefore, the role of sarcopenia in patients undergoing surgery is a major topic of interest in the field of pancreatic cancer. The main studies that analyzed the effect of sarcopenia on the surgical treatment of pancreatic cancer are summarized in Table 1[7,9,10,18,19,24,25,28-30]. In 2012, Peng *et al*[24] evaluated 557 patients with pancreatic cancer who underwent curative resection at Johns Hopkins University. Sarcopenia stratified by total psoas muscle area increased the 3-year mortality by 63%. A few years later, a study by Amini *et al*[7] showed that assessing the psoas muscle volume might be a better method than assessing the psoas muscle area to define sarcopenia. Most subsequent studies have evaluated the total abdominal muscle area instead of the psoas muscle area or volume.

The effect of sarcopenia in the surgical setting has been well-summarized in a recent meta-analysis [31]. Bundred *et al*[31] analyzed 43 studies assessing body composition in patients with pancreatic cancer before surgery, of which 30 studies assessed body composition using CT. Among these, 10 studies reported the impact of preoperative sarcopenia on postoperative outcomes. Sarcopenia was associated with perioperative mortality (odds ratio: 2.40; 95% confidence interval: 1.19-4.85) and overall survival (hazard ratio: 1.95; 95% confidence interval, 1.54-2.05) but not with overall complications (odds ratio: 0.96; 95% confidence interval, 0.78-1.19). This meta-analysis was limited by the heterogeneity in the methods and cutoff values for assessing sarcopenia in individual studies.

Patients with overweight or obesity and sarcopenia exhibit worse clinical outcomes than those with sarcopenia alone. In many studies, the combination of obesity and sarcopenia was associated with a higher incidence of perioperative complications and lower survival[9,10,28,30]. Sarcopenic obesity is a complex syndrome associated with aging and lifestyle changes. Reduced physical activity may result in accelerated muscle loss, decreased energy consumption, and adverse health effects such as hypertension, dyslipidemia, and insulin resistance. Sarcopenia and obesity should be comprehensively considered to stratify patients undergoing pancreatic cancer surgery into risk categories for predicting clinical outcomes.

Table 1 Studies analyzing the effect of sarcopenia on surgical outcomes of pancreatic cancer

Ref.	Country	No. of patients	Imaging modality	Level	Time	Definition and cutoff	Sarcopenia prevalence before surgery	Types of surgery	Perioperative complications	Survival	Additional meaningful findings or comments
Peng *et al*[24], 2012	United States	557	CT	L3	Before surgery	TPAI (mm^2/m^2), lowest quartile: < 564.2 (M), < 414.5 (F)	25%	PD, DP	(-)	(+) OS	Sarcopenia was an independent predictor of survival in multivariable analysis
Amini *et al*[7], 2015	United States	763	CT	L3	Before surgery	TPAI (mm^2/m^2), < 564.2 (M), 414.5 (F); TPVI (cm^3/m^2), < 17.2 (M), < 12.0 (F)	25% by TPAI, 20% by TPVI	PD, DP. TP	(+) Overall Cx. by TPVI	(+) OS by TPVI	TPVI was a better measure for defining sarcopenia rather than TPAI
Pecorelli *et al* [9], 2016	Italy	202	CT	L3	Before surgery	LSMI, < 52.4 cm^2/m^2 (M), < 38.5 cm^2/m^2 (F)[1]	65%	PD	(-)	NE	The combination of visceral obesity and sarcopenia was a predictor of perioperative Cx
Ninomiya *et al* [28], 2017	Japan	265	CT	L3	Before surgery	LSMI, < 43.75 cm^2/m^2 (M), < 38.5 cm^2/m^2 (F)	64%	PD, DP. TP	(-)	(-)	Sarcopenia was an independent prognostic factor only in patients with BMI ≥ 22 kg/m^2
Okumura *et al* [29], 2017	Japan	301	CT	L3	Before surgery	LSMI, clinically relevant cutoff: < 47.1 cm^2/m^2 (M), < 36.6 cm^2/m^2 (F)	40%	PD, DP. TP	(-)	(+) OS and RFS	Low muscle attenuation, as well as low muscle mass, was associated with worse OS and RFS
Choi *et al*[18], 2018	South Korea	180	CT	L3	Before and after 60 d of surgery	LSMI, the lowest tertile; < 45.3 cm^2/m^2 (M), < 39.3 cm^2/m^2 (F)	33%	PD, DP	(-)	(+) OS	Accelerated muscle loss after surgery negatively impacts OS
Sugimoto *et al* [19], 2018	United States	323	CT	L3	Before surgery	LSMI, < 55.4 cm^2/m^2 (M), < 38.9 cm^2/m^2 (F)	62%	PD, DP. TP	NE	(-)	Smaller sex-standardized LSMI as a continuous variable is associated with a shorter OS
Gruber *et al* [10], 2019	Austria	133	CT	L3	Before surgery	LSMI, < 52.4 cm^2/m^2 (M), < 38.5 cm^2/m^2 (F)[1]	59%	PD, DP	(-)	(+) OS	Obese patients (BMI ≥ 25) with sarcopenia have higher incidence of major post-operative Cx
Ryu *et al*[30], 2020	South Korea	548	CT	L3	Before surgery	LSMI, < 50.18 cm^2/m^2 (M), < 38.63 cm^2/m^2 (F)	46%	PD	(-)	(+) OS	Sarcopenic obesity is a predictive factor for post-operative pancreatic fistula after PD
Rom *et al*[25], 2022	Israel	111	CT	L3	Before surgery	LSMI, the lowest quartile: < 44; 35 cm^2/m^2 (M), < 34.82 cm^2/m^2 (F)	25%	PD, DP	(+) Overall Cx.	(+) OS, DSS, and RFS	High intramuscular adipose tissue content correlates with poor OS and DSS

[1]This cutoff value for sarcopenia was defined by Prado *et al*[8] (2008). BMI: Body mass index; CT: Computed tomography; Cx.: Complications; DP: Distal pancreatectomy; DSS: Disease-specific survival; F: Female; L3: Level of the lumbar 3 vertebral body; LSMI: Lumbar skeletal muscle index; M: Male; NE: Not evaluated; OS: Overall survival; PD: Pancreaticoduodenectomy; RFS: Recurrence-free survival; TPAI: Total psoas area index; TPVI: Total psoas volume index; TP: Total pancreatectomy.

The amount of skeletal muscle mass has been traditionally used as a criterion to determine sarcopenia. However, some studies reported that a decrease in muscle quality, represented by low skeletal muscle attenuation also negatively impacts prognosis after pancreatic cancer surgery[25,29]. Although the muscle mass remains normal, muscle strength and function may be reduced. In such cases, the deposition of intramuscular adipose tissue causes reduced muscle density, resulting in a decline in muscle quality. A previous study reported that skeletal muscle density decreased before the reduction in skeletal muscle mass in patients with cancer[32]. Thus, efforts should be made to evaluate and monitor muscle quantity and quality closely.

Choi *et al*[18] demonstrated that preoperative sarcopenia and post-operative accelerated muscle loss were associated with poor overall survival in pancreatic cancer patients undergoing surgery. Postoperative skeletal muscle changes were assessed based on the difference between the initial and follow-up CT scans at an approximately 60-d interval. Approximately 30% of their patients showed significant muscle loss of more than 10% over 60 d. Given that most patients undergoing pancreatic cancer surgery receive adjuvant chemotherapy, it may be necessary to maintain muscle mass through active nutritional support and rehabilitation exercise after surgery.

NAT

In recent years, NAT, including neoadjuvant chemotherapy and chemoradiation, has become the standard of care for borderline resectable or locally advanced pancreatic cancers. NAT may increase the rate of margin-negative resections and help clinicians screen patients with progressive disease during NAT who might not benefit from surgery[33]. In addition, NAT may be able to treat micrometastases at the time of diagnosis, which can reduce early lymph node or hepatic recurrence after surgery[34]. However, because not all patients receiving NAT are eligible for curative surgery and have increased survival, it is imperative to develop biomarkers that can predict responses to NAT. Recent studies that assessed the correlation of body composition with the response to and outcome of NAT in patients with pancreatic cancer are summarized in Table 2[13-15,35-37].

The prevalence of sarcopenia before NAT ranges from 40% to 63%. However, no studies have shown that sarcopenia at the time of diagnosis affects resectability after NAT. Meanwhile, in a recent study by Jin *et al*[37] in 2022, sarcopenia before NAT was associated with decreased overall survival and disease-free survival. Among 119 patients, 57 (47.9%) had sarcopenia before NAT. The median overall survival and disease-free survival for sarcopenia patients were 16.6 mo and 10.9 mo, respectively, which were significantly lower than those for non-sarcopenia patients (21.4 mo and 14.0 mo, respectively; all $P < 0.001$). However, because of the retrospective nature of this study, unavoidable biases were associated with variations in the NAT regimens and treatment durations.

Several studies have evaluated changes in body composition during NAT and their effect on clinical outcomes[13,14,35-37]. In these studies, most patients experienced further depletion of skeletal muscle during NAT and the degree of skeletal muscle loss correlated with resectability or survival. Sandini *et al*[13] reported that patients who underwent resection after NAT had skeletal muscle gain, whereas unresectable patients experienced muscle wasting during NAT. Therefore, skeletal muscle changes must be considered in the setting of NAT, and further efforts should focus on maintaining muscle mass during treatment.

PALLIATIVE CHEMOTHERAPY

Approximately 80% of pancreatic cancer patients are diagnosed at an advanced stage, including locally advanced or metastatic disease. Combination chemotherapy with FOLFIRINOX or gemcitabine plus nab-paclitaxel is associated with more prolonged overall survival than gemcitabine monotherapy, with acceptable adverse events[3,4]. Currently, these two combination regimens are considered the standard first-line treatments for advanced pancreatic cancer. Therefore, selecting appropriate patients who can tolerate aggressive palliative chemotherapy is crucial. In palliative chemotherapy settings, the occurrence of sarcopenia can be related to exacerbated chemotherapy toxicity, reduced adherence to treatment, or worsened survival.

Several recent studies evaluated the effect of sarcopenia on various clinical outcomes in patients with advanced pancreatic cancer receiving palliative chemotherapy (Table 3)[11,16,17,21-23,38-40]. Kim *et al*[17] investigated the clinical impact of sarcopenia in 330 patients with metastatic pancreatic cancer who were treated with first-line gemcitabine-based chemotherapy. All grade ≥ 3 toxicities developed at a significantly higher frequency in sarcopenia patients than in non-sarcopenia patients. This result might be explained by the link between body composition and the pharmacokinetics of chemotherapy drugs. In addition, a recent study by Emori *et al*[23] in 2022 showed that major adverse events, including hematologic toxicity, occurred more frequently in sarcopenia patients. Remarkably, the grade ≥ 3 neutropenia rate was significantly higher in sarcopenia patients than in non-sarcopenia patients (64% *vs* 40%, $P = 0.028$). Therefore, patients with sarcopenia should be considered for dose modification or

Table 2 Studies analyzing the effect of sarcopenia on neoadjuvant therapy outcomes of pancreatic cancer

Ref.	Country	No. of patients	Inclusion	Imaging modality	Level	Time	Definition and cutoff	Sarcopenia prevalence before NAT	Resectability	Survival	Additional meaningful findings or comments
Cooper *et al* [35], 2015	United States	89	RPC	CT	L3	Before and after NAT	LSMI, < 55.4 cm^2/m^2 (M), < 38.9 cm^2/m^2 (F)	55%	(-)	(-)	SKM loss during NAT was correlated with DFS
Cloyd *et al* [36], 2018	United States	127	RPC, BRPC, LAPC	CT	L3	Before and after NAT, 3 mo and 12 mo after surgery (PD)	LSMI, < 55.4 cm^2/m^2 (M), < 38.9 cm^2/m^2 (F)	63%	NE	(-)	SKM gain between the postoperative period and 1-yr follow-up was correlated with improved OS
Sandini *et al* [13], 2018	United States and Italy	193	BRPC, LAPC	CT	L3	Before and after NAT	LSMI, < 43 cm^2/m^2 (M) where BMI < 25 kg/m^2, < 53 cm^2/m^2 (M) where BMI > 25 kg/m^2, < 41 cm^2/m^2 (F)[1]	44%	(-)	NE	SKM gain during NAT is correlated with better resectability
Griffin *et al* [14], 2019	Ireland	78	BRPC	CT	L3	Before and after NAT	LSMI, < 43 cm^2/m^2 (M) where BMI < 25 kg/m^2, < 53 cm^2/m^2 (M) where BMI > 25 kg/m^2, < 41 cm^2/m^2 (F)[1]	50%	(-)	(-)	Low muscle attenuation before NAT and SKM loss during NAT was correlated with decreased OS
Takeda *et al* [15], 2021	Japan	62	RPC	CT	L3	Before NAT	LSMI, < 43 cm^2/m^2 (M) where BMI < 25 kg/m^2, < 53 cm^2/m^2 (M) where BMI > 25 kg/m^2, < 41 cm^2/m^2 (F)[1]	40%	(-)	NE	Sarcopenia before NAT did not correlate with antitumor response and toxicity of therapy
Jin *et al*[37], 2022	China	119	RPC	CT	L3	Before and after NAT	LSMI, < 41 cm^2/m^2 (M), < 38.5 cm^2/m^2 (F)	48%	NE	(+) OS, DFS	SKM and fat wasting during NAT was correlated with decreased OS and DFS

[1]This cutoff value for sarcopenia was defined by Martin *et al*[12] reported in 2013. BMI: Body mass index; BRPC: Borderline resectable pancreatic cancer; CT: Computed tomography; DFS: Disease-free survival; F: Female; L3: Level of the lumbar 3 vertebral body; LAPC: Locally advanced pancreatic cancer; LSMI: Lumbar skeletal muscle index; M: Male; NAT: Neoadjuvant therapy; NE: Not evaluated; OS: Overall survival; PD: Pancreaticoduodenectomy; RPC: Resectable pancreatic cancer; SKM: Skeletal muscle.

aggressive preventive interventions to reduce chemotherapy-related toxicity.

A study by Kurita *et al*[38] conducted on 82 pancreatic cancer patients treated with FOLFIRINOX showed that compared with non-sarcopenia patients, sarcopenia patients had a significantly lower median overall survival (11.3 mo *vs* 17.0 mo) and progression-free survival (3.0 mo *vs* 6.1 mo). In another study that evaluated 84 patients treated with gemcitabine plus nab-paclitaxel, the median overall and progression-free survival were also lower in sarcopenia patients than in non-sarcopenia patients (10.3 mo *vs* 18.1 mo and 5.0 mo *vs* 8.0 mo, respectively)[23]. Skeletal muscle mass can also be used as a critical prognostic factor in patients receiving second-line FOLFIFIRNOX chemotherapy for advanced pancreatic cancer[39]. In addition, body composition-based patient selection and dose determination may be clinically useful for patients receiving palliative chemotherapy to minimize toxicity and maximize therapeutic benefits.

Table 3 Studies analyzing the effect of sarcopenia on palliative chemotherapy outcomes of pancreatic cancer

Ref.	Country	No. of patients	Inclusion (%)	Imaging modality	Level	Time	Definition and cutoff	Sarcopenia prevalence before CTX	CTX regimen	CTX toxicity	PFS	OS	Additional meaningful findings or comments
Kays *et al* [11], 2018	United States	53	LAPC (49), MPC (51)	CT	L3	Before and during CTX (median 5.6 times)	LSMI, < 52.4 cm^2/m^2 (M), < 38.5 cm^2/m^2 (F)[1]	49%	1st line FOLFIRINOX	NE	NE	(-)	No muscle wasting during CTX improved OS
Basile *et al* [16], 2019	Italy	94	LAPC (50), MPC (50)	CT	L3	Before and after 12 wk of CTX	LSMI, < 43 cm^2/m^2 (M) where BMI < 25 kg/m^2, < 53 cm^2/m^2 (M) where BMI > 25 kg/m^2, < 41 cm^2/m^2 (F)[2]	73%	Various	NE	(-)	(-)	Loss of skeletal muscle mass (≥ 10%) was associated with worse OS and PFS
Kurita *et al* [38], 2019	Japan	82	LAPC (35), MPC (65)	CT	L3	Before CTX	LSMI, clinically relevant cut-off: < 45.3 cm^2/m^2 (M), < 37.1 cm^2/m^2 (F)	51%	1st line FOLFIRINOX	(-)	(+)	(+)	Sarcopenic obesity was associated with hematologic toxicity
Lee *et al* [39], 2019	South Korea	57	LAPC (5), MPC (95)	CT	L3	Before and after 8 wk of CTX	LSMI, median level: unknown	50%	2nd line FOLFIRINOX	NE	(+)	(+)	Baseline LSMI was an independent predictor of survival in multivariable analysis
Kim *et al* [17], 2021	South Korea	251	MPC (100)	CT	L3	Before and after 8 wk of CTX	LSMI, < 43 cm^2/m^2 (M) where BMI < 25 kg/m^2, < 53 cm^2/m^2 (M) where BMI > 25 kg/m^2, < 41 cm^2/m^2 (F)[2]	41%	1st line gemcitabine-based CTX	(+) Overall grade ≥ 3 toxicity	(-)	(-)	Sarcopenia was a prognostic factor for OS but not for PFS in multivariable analysis
Uemura *et al*[21], 2021	Japan	69	LAPC (29), MPC (71)	CT	L3	Before and after 8 wk of CTX	LSMI, < 42 cm^2/m^2 (M), < 38 cm^2/m^2 (F)[3]	48%	1st line FOLFIRINOX	(-)	(-)	(-)	Loss of skeletal muscle mass (≥ 7.9%) is associated with worse OS
Williet *et al* [40], 2021	France	79	MPC (100)	CT	L3	Before CTX	TPAI, clinically relevant cutoff: 5.73 cm^2/m^2 (M), 4.37 cm^2/m^2 (F)	38%	Various	(-)	(+)	(+)	Measuring TPAI was less time-consuming than measuring LSMI
Asama *et al* [22], 2022	Japan	124	LAPC (29), MPC (60), RePC (15)	CT	L3	Before CTX	LSMI, < 42 cm^2/m^2 (M), < 38 cm^2/m^2 (F)[3]	49%	1st line Gem-Nab	(-)	(-)	(-)	In elderly patients (> 70 yr), sarcopenia was associated with worse OS
Emori *et al* [23], 2022	Japan	176	LAPC (14), MPC (86)	CT	L3	Before CTX	LSMI, < 42 cm^2/m^2 (M), < 38 cm^2/m^2 (F)[3]	53%	1st line Gem-Nab	(+) Overall grade ≥ 3 toxicity	(+)	(+)	Propensity score matching analysis was performed

[1]This cutoff value for sarcopenia was defined by Prado *et al*[8] (2008).

[2]This cutoff value for sarcopenia was defined by Martin *et al*[12] (2013).

[3]This cutoff value for sarcopenia was defined by the Asian Working Group for Sarcopenia (Chen *et al*[20]) reported in 2014.

BMI: Body mass index; CT: Computed tomography; CTX: Chemotherapy; F: Female; FOLFIRINOX: Folinic acid, fluorouracil, irinotecan hydrochloride, and oxaliplatin; Gem-Nab: Gemcitabine plus nab-paclitaxel; L3: Level of the lumbar 3 vertebral body; LAPC: Locally advanced pancreatic cancer; LSMI: Lumbar skeletal muscle index; M: Male; MPC: Metastatic pancreatic cancer; NE: Not evaluated; OS: Overall survival; PFS: Progression-free survival; RePC:

Recurrent pancreatic cancer; TPAI: Total psoas area index.

Some studies have reported the negative impact of accelerated muscle loss during palliative chemotherapy on the clinical outcomes of advanced pancreatic cancer[16,21]. Basile *et al*[16] reported that early loss of skeletal muscle by more than 10% during the first 3 mo of chemotherapy was significantly associated with poor overall and progression-free survival. In a study by Uemura *et al*[21], patients with a greater decrease in skeletal muscle index (≥ 7.9%) 2 mo after the start of FOLFIRINOX therapy had a shorter survival (10.9 mo) than those who did not (21.0 mo, $P < 0.01$). The management of sarcopenia, not only at the time of diagnosis but also during palliative chemotherapy, is important in patients with advanced pancreatic cancer.

LIMITATIONS

There has been heterogeneity among studies regarding the threshold for sarcopenia based on low skeletal muscle index. The races of study participants, clinical stages, and treatment methods could affect skeletal muscle index. Therefore, caution is needed when synthesizing or comparing each study. Another limitation of the studies based on CT-assessed sarcopenia relates to the failure to include any functional measurement or patient-reported quality of life. Although the decrease and change of skeletal muscle mass is a major concern for supportive care in pancreatic cancer patients, physical functional assessments and quality of life measures have been highlighted as meaningful outcomes for cancer cachexia research.

FUTURE DIRECTIONS

Since sarcopenia adversely affects the outcomes of patients with pancreatic cancer in surgical or chemotherapy settings, interventions to improve sarcopenia may help increase survival rates. However, studies investigating the impact of nutritional or exercise interventions on survival are immature, and the results are still far from demonstrating their clinical efficacy. A phase II trial on inoperable pancreatic or lung cancer patients reported that multimodal intervention, including polyunsaturated fatty acid nutritional supplements, exercise, and anti-inflammatory medication is feasible and safe[41]. In the IMPACT study by Basile *et al*[16], more than half of the patients undergoing FOLFIRINOX chemotherapy were evaluated by a nutritionist and received dietary supplementation. Body weight loss during chemotherapy was the only factor associated with early dietary supplementation; however, nutritional support or intervention did not affect prognosis with respect to overall survival. A "Nutritional Oncology Board" has recently emerged as a good clinical practice tool of routine care for cancer patients[26]. Based on the adoption of this system, early nutritional assessment before or during oncological treatment can provide patient-tailored management for preventing or treating sarcopenia.

Although there has been increasing interest in the assessment of sarcopenia using CT-based methods, there are some areas to be improved in future studies[42]. It is recommended to use validated techniques and appropriate diagnostic criteria based on the study populations[43]. For sequential measurements, CT protocols should be controlled, including the timing of image acquisition and amount of contrast agent. It is also recommended to measure various physical performance measures (*e.g.*, gait speed or handgrip strength) as indicators of muscle quality along with skeletal muscle mass, which reflects muscle quantity. Through the application of artificial intelligence, CT-based body composition analysis, which is a time-consuming process, can be applied to routine clinical practice[44].

CONCLUSION

Sarcopenia has been recognized as a prognostic biomarker in patients with pancreatic cancer receiving surgical or chemotherapy treatments. The CT-based analysis is an objective and useful tool to assess sarcopenia and skeletal muscle changes during treatment. It may be helpful to consider sarcopenia when predicting patient outcomes and to minimize complications. However, whether early nutritional support or exercise improves sarcopenia and clinical outcomes remains unclear. Further prospective studies are necessary to confirm the prognostic role of sarcopenia and the effects of multimodal interventions in patients with pancreatic cancer.

FOOTNOTES

Author contributions: Choi MH and Yoon SB contributed equally to the conception, design, and literature search; Choi MH drafted the manuscript and prepared the tables; Yoon SB modified and revised the manuscript.

Supported by the National Research Foundation of Korea, No. NRF-2021 R1F1A1062255.

Conflict-of-interest statement: All the authors report having no relevant conflicts of interest for this article.

Country/Territory of origin: South Korea

ORCID number: Moon Hyung Choi 0000-0001-5962-4772; Seung Bae Yoon 0000-0002-6119-7236.

S-Editor: Gong ZM
L-Editor: Filipodia
P-Editor: Gong ZM

REFERENCES

1 **Siegel RL**, Miller KD, Fuchs HE, Jemal A. Cancer statistics, 2022. *CA Cancer J Clin* 2022; **72**: 7-33 [PMID: 35020204 DOI: 10.3322/caac.21708]
2 **Carioli G**, Malvezzi M, Bertuccio P, Boffetta P, Levi F, La Vecchia C, Negri E. European cancer mortality predictions for the year 2021 with focus on pancreatic and female lung cancer. *Ann Oncol* 2021; **32**: 478-487 [PMID: 33626377 DOI: 10.1016/j.annonc.2021.01.006]
3 **Conroy T**, Desseigne F, Ychou M, Bouché O, Guimbaud R, Bécouarn Y, Adenis A, Raoul JL, Gourgou-Bourgade S, de la Fouchardière C, Bennouna J, Bachet JB, Khemissa-Akouz F, Péré-Vergé D, Delbaldo C, Assenat E, Chauffert B, Michel P, Montoto-Grillot C, Ducreux M; Groupe Tumeurs Digestives of Unicancer; PRODIGE Intergroup. FOLFIRINOX versus gemcitabine for metastatic pancreatic cancer. *N Engl J Med* 2011; **364**: 1817-1825 [PMID: 21561347 DOI: 10.1056/NEJMoa1011923]
4 **Von Hoff DD**, Ervin T, Arena FP, Chiorean EG, Infante J, Moore M, Seay T, Tjulandin SA, Ma WW, Saleh MN, Harris M, Reni M, Dowden S, Laheru D, Bahary N, Ramanathan RK, Tabernero J, Hidalgo M, Goldstein D, Van Cutsem E, Wei X, Iglesias J, Renschler MF. Increased survival in pancreatic cancer with nab-paclitaxel plus gemcitabine. *N Engl J Med* 2013; **369**: 1691-1703 [PMID: 24131140 DOI: 10.1056/NEJMoa1304369]
5 **Cruz-Jentoft AJ**, Baeyens JP, Bauer JM, Boirie Y, Cederholm T, Landi F, Martin FC, Michel JP, Rolland Y, Schneider SM, Topinková E, Vandewoude M, Zamboni M; European Working Group on Sarcopenia in Older People. Sarcopenia: European consensus on definition and diagnosis: Report of the European Working Group on Sarcopenia in Older People. *Age Ageing* 2010; **39**: 412-423 [PMID: 20392703 DOI: 10.1093/ageing/afq034]
6 **Lee K**, Shin Y, Huh J, Sung YS, Lee IS, Yoon KH, Kim KW. Recent Issues on Body Composition Imaging for Sarcopenia

Evaluation. *Korean J Radiol* 2019; **20**: 205-217 [PMID: 30672160 DOI: 10.3348/kjr.2018.0479]
7 **Amini N**, Spolverato G, Gupta R, Margonis GA, Kim Y, Wagner D, Rezaee N, Weiss MJ, Wolfgang CL, Makary MM, Kamel IR, Pawlik TM. Impact Total Psoas Volume on Short- and Long-Term Outcomes in Patients Undergoing Curative Resection for Pancreatic Adenocarcinoma: a New Tool to Assess Sarcopenia. *J Gastrointest Surg* 2015; **19**: 1593-1602 [PMID: 25925237 DOI: 10.1007/s11605-015-2835-y]
8 **Prado CM**, Lieffers JR, McCargar LJ, Reiman T, Sawyer MB, Martin L, Baracos VE. Prevalence and clinical implications of sarcopenic obesity in patients with solid tumours of the respiratory and gastrointestinal tracts: a population-based study. *Lancet Oncol* 2008; **9**: 629-635 [PMID: 18539529 DOI: 10.1016/S1470-2045(08)70153-0]
9 **Pecorelli N**, Carrara G, De Cobelli F, Cristel G, Damascelli A, Balzano G, Beretta L, Braga M. Effect of sarcopenia and visceral obesity on mortality and pancreatic fistula following pancreatic cancer surgery. *Br J Surg* 2016; **103**: 434-442 [PMID: 26780231 DOI: 10.1002/bjs.10063]
10 **Gruber ES**, Jomrich G, Tamandl D, Gnant M, Schindl M, Sahora K. Sarcopenia and sarcopenic obesity are independent adverse prognostic factors in resectable pancreatic ductal adenocarcinoma. *PLoS One* 2019; **14**: e0215915 [PMID: 31059520 DOI: 10.1371/journal.pone.0215915]
11 **Kays JK**, Shahda S, Stanley M, Bell TM, O'Neill BH, Kohli MD, Couch ME, Koniaris LG, Zimmers TA. Three cachexia phenotypes and the impact of fat-only loss on survival in FOLFIRINOX therapy for pancreatic cancer. *J Cachexia Sarcopenia Muscle* 2018; **9**: 673-684 [PMID: 29978562 DOI: 10.1002/jcsm.12307]
12 **Martin L**, Birdsell L, Macdonald N, Reiman T, Clandinin MT, McCargar LJ, Murphy R, Ghosh S, Sawyer MB, Baracos VE. Cancer cachexia in the age of obesity: skeletal muscle depletion is a powerful prognostic factor, independent of body mass index. *J Clin Oncol* 2013; **31**: 1539-1547 [PMID: 23530101 DOI: 10.1200/JCO.2012.45.2722]
13 **Sandini M**, Patino M, Ferrone CR, Alvarez-Pérez CA, Honselmann KC, Paiella S, Catania M, Riva L, Tedesco G, Casolino R, Auriemma A, Salandini MC, Carrara G, Cristel G, Damascelli A, Ippolito D, D'Onofrio M, Lillemoe KD, Bassi C, Braga M, Gianotti L, Sahani D, Fernández-Del Castillo C. Association Between Changes in Body Composition and Neoadjuvant Treatment for Pancreatic Cancer. *JAMA Surg* 2018; **153**: 809-815 [PMID: 29801062 DOI: 10.1001/jamasurg.2018.0979]
14 **Griffin OM**, Duggan SN, Ryan R, McDermott R, Geoghegan J, Conlon KC. Characterising the impact of body composition change during neoadjuvant chemotherapy for pancreatic cancer. *Pancreatology* 2019; **19**: 850-857 [PMID: 31362865 DOI: 10.1016/j.pan.2019.07.039]
15 **Takeda T**, Sasaki T, Mie T, Furukawa T, Yamada Y, Kasuga A, Matsuyama M, Ozaka M, Sasahira N. The impact of body composition on short-term outcomes of neoadjuvant chemotherapy with gemcitabine plus S-1 in patients with resectable pancreatic cancer. *Jpn J Clin Oncol* 2021; **51**: 604-611 [PMID: 33479765 DOI: 10.1093/jjco/hyaa247]
16 **Basile D**, Parnofiello A, Vitale MG, Cortiula F, Gerratana L, Fanotto V, Lisanti C, Pelizzari G, Ongaro E, Bartoletti M, Garattini SK, Andreotti VJ, Bacco A, Iacono D, Bonotto M, Casagrande M, Ermacora P, Puglisi F, Pella N, Fasola G, Aprile G, Cardellino GG. The IMPACT study: early loss of skeletal muscle mass in advanced pancreatic cancer patients. *J Cachexia Sarcopenia Muscle* 2019; **10**: 368-377 [PMID: 30719874 DOI: 10.1002/jcsm.12368]
17 **Kim IH**, Choi MH, Lee IS, Hong TH, Lee MA. Clinical significance of skeletal muscle density and sarcopenia in patients with pancreatic cancer undergoing first-line chemotherapy: a retrospective observational study. *BMC Cancer* 2021; **21**: 77 [PMID: 33461517 DOI: 10.1186/s12885-020-07753-w]
18 **Choi MH**, Yoon SB, Lee K, Song M, Lee IS, Lee MA, Hong TH, Choi MG. Preoperative sarcopenia and post-operative accelerated muscle loss negatively impact survival after resection of pancreatic cancer. *J Cachexia Sarcopenia Muscle* 2018; **9**: 326-334 [PMID: 29399990 DOI: 10.1002/jcsm.12274]
19 **Sugimoto M**, Farnell MB, Nagorney DM, Kendrick ML, Truty MJ, Smoot RL, Chari ST, Moynagh MR, Petersen GM, Carter RE, Takahashi N. Decreased Skeletal Muscle Volume Is a Predictive Factor for Poorer Survival in Patients Undergoing Surgical Resection for Pancreatic Ductal Adenocarcinoma. *J Gastrointest Surg* 2018; **22**: 831-839 [PMID: 29392613 DOI: 10.1007/s11605-018-3695-z]
20 **Chen LK**, Liu LK, Woo J, Assantachai P, Auyeung TW, Bahyah KS, Chou MY, Chen LY, Hsu PS, Krairit O, Lee JS, Lee WJ, Lee Y, Liang CK, Limpawattana P, Lin CS, Peng LN, Satake S, Suzuki T, Won CW, Wu CH, Wu SN, Zhang T, Zeng P, Akishita M, Arai H. Sarcopenia in Asia: consensus report of the Asian Working Group for Sarcopenia. *J Am Med Dir Assoc* 2014; **15**: 95-101 [PMID: 24461239 DOI: 10.1016/j.jamda.2013.11.025]
21 **Uemura S**, Iwashita T, Ichikawa H, Iwasa Y, Mita N, Shiraki M, Shimizu M. The impact of sarcopenia and decrease in skeletal muscle mass in patients with advanced pancreatic cancer during FOLFIRINOX therapy. *Br J Nutr* 2021; **125**: 1140-1147 [PMID: 32883372 DOI: 10.1017/S0007114520003463]
22 **Asama H**, Ueno M, Kobayashi S, Fukushima T, Kawano K, Sano Y, Tanaka S, Nagashima S, Morimoto M, Ohira H, Maeda S. Sarcopenia: Prognostic Value for Unresectable Pancreatic Ductal Adenocarcinoma Patients Treated With Gemcitabine Plus Nab-Paclitaxel. *Pancreas* 2022; **51**: 148-152 [PMID: 35404889 DOI: 10.1097/MPA.0000000000001985]
23 **Emori T**, Itonaga M, Ashida R, Tamura T, Kawaji Y, Hatamaru K, Yamashita Y, Shimokawa T, Koike M, Sonomura T, Kawai M, Kitano M. Impact of sarcopenia on prediction of progression-free survival and overall survival of patients with pancreatic ductal adenocarcinoma receiving first-line gemcitabine and nab-paclitaxel chemotherapy. *Pancreatology* 2022; **22**: 277-285 [PMID: 35033425 DOI: 10.1016/j.pan.2021.12.013]
24 **Peng P**, Hyder O, Firoozmand A, Kneuertz P, Schulick RD, Huang D, Makary M, Hirose K, Edil B, Choti MA, Herman J, Cameron JL, Wolfgang CL, Pawlik TM. Impact of sarcopenia on outcomes following resection of pancreatic adenocarcinoma. *J Gastrointest Surg* 2012; **16**: 1478-1486 [PMID: 22692586 DOI: 10.1007/s11605-012-1923-5]
25 **Rom H**, Tamir S, Van Vugt JLA, Berger Y, Perl G, Morgenstern S, Tovar A, Brenner B, Benchimol D, Kashtan H, Sadot E. Sarcopenia as a Predictor of Survival in Patients with Pancreatic Adenocarcinoma After Pancreatectomy. *Ann Surg Oncol* 2022; **29**: 1553-1563 [PMID: 34716836 DOI: 10.1245/s10434-021-10995-y]
26 **Rovesti G**, Valoriani F, Rimini M, Bardasi C, Ballarin R, Di Benedetto F, Menozzi R, Dominici M, Spallanzani A. Clinical Implications of Malnutrition in the Management of Patients with Pancreatic Cancer: Introducing the Concept of the Nutritional Oncology Board. *Nutrients* 2021; **13** [PMID: 34684523 DOI: 10.3390/nu13103522]

27 **Vujasinovic M**, Valente R, Del Chiaro M, Permert J, Löhr JM. Pancreatic Exocrine Insufficiency in Pancreatic Cancer. *Nutrients* 2017; **9** [PMID: 28241470 DOI: 10.3390/nu9030183]

28 **Ninomiya G**, Fujii T, Yamada S, Yabusaki N, Suzuki K, Iwata N, Kanda M, Hayashi M, Tanaka C, Nakayama G, Sugimoto H, Koike M, Fujiwara M, Kodera Y. Clinical impact of sarcopenia on prognosis in pancreatic ductal adenocarcinoma: A retrospective cohort study. *Int J Surg* 2017; **39**: 45-51 [PMID: 28110029 DOI: 10.1016/j.ijsu.2017.01.075]

29 **Okumura S**, Kaido T, Hamaguchi Y, Kobayashi A, Shirai H, Yao S, Yagi S, Kamo N, Hatano E, Okajima H, Takaori K, Uemoto S. Visceral Adiposity and Sarcopenic Visceral Obesity are Associated with Poor Prognosis After Resection of Pancreatic Cancer. *Ann Surg Oncol* 2017; **24**: 3732-3740 [PMID: 28871520 DOI: 10.1245/s10434-017-6077-y]

30 **Ryu Y**, Shin SH, Kim JH, Jeong WK, Park DJ, Kim N, Heo JS, Choi DW, Han IW. The effects of sarcopenia and sarcopenic obesity after pancreaticoduodenectomy in patients with pancreatic head cancer. *HPB (Oxford)* 2020; **22**: 1782-1792 [PMID: 32354655 DOI: 10.1016/j.hpb.2020.04.004]

31 **Bundred J**, Kamarajah SK, Roberts KJ. Body composition assessment and sarcopenia in patients with pancreatic cancer: a systematic review and meta-analysis. *HPB (Oxford)* 2019; **21**: 1603-1612 [PMID: 31266698 DOI: 10.1016/j.hpb.2019.05.018]

32 **Hayashi N**, Ando Y, Gyawali B, Shimokata T, Maeda O, Fukaya M, Goto H, Nagino M, Kodera Y. Low skeletal muscle density is associated with poor survival in patients who receive chemotherapy for metastatic gastric cancer. *Oncol Rep* 2016; **35**: 1727-1731 [PMID: 26648321 DOI: 10.3892/or.2015.4475]

33 **Gugenheim J**, Crovetto A, Petrucciani N. Neoadjuvant therapy for pancreatic cancer. *Updates Surg* 2022; **74**: 35-42 [PMID: 34628591 DOI: 10.1007/s13304-021-01186-1]

34 **Sugimoto M**, Takahashi N, Farnell MB, Smyrk TC, Truty MJ, Nagorney DM, Smoot RL, Chari ST, Carter RE, Kendrick ML. Survival benefit of neoadjuvant therapy in patients with non-metastatic pancreatic ductal adenocarcinoma: A propensity matching and intention-to-treat analysis. *J Surg Oncol* 2019; **120**: 976-984 [PMID: 31452208 DOI: 10.1002/jso.25681]

35 **Cooper AB**, Slack R, Fogelman D, Holmes HM, Petzel M, Parker N, Balachandran A, Garg N, Ngo-Huang A, Varadhachary G, Evans DB, Lee JE, Aloia T, Conrad C, Vauthey JN, Fleming JB, Katz MH. Characterization of Anthropometric Changes that Occur During Neoadjuvant Therapy for Potentially Resectable Pancreatic Cancer. *Ann Surg Oncol* 2015; **22**: 2416-2423 [PMID: 25519927 DOI: 10.1245/s10434-014-4285-2]

36 **Cloyd JM**, Nogueras-González GM, Prakash LR, Petzel MQB, Parker NH, Ngo-Huang AT, Fogelman D, Denbo JW, Garg N, Kim MP, Lee JE, Tzeng CD, Fleming JB, Katz MHG. Anthropometric Changes in Patients with Pancreatic Cancer Undergoing Preoperative Therapy and Pancreatoduodenectomy. *J Gastrointest Surg* 2018; **22**: 703-712 [PMID: 29230694 DOI: 10.1007/s11605-017-3618-4]

37 **Jin K**, Tang Y, Wang A, Hu Z, Liu C, Zhou H, Yu X. Body Composition and Response and Outcome of Neoadjuvant Treatment for Pancreatic Cancer. *Nutr Cancer* 2022; **74**: 100-109 [PMID: 33629916 DOI: 10.1080/01635581.2020.1870704]

38 **Kurita Y**, Kobayashi N, Tokuhisa M, Goto A, Kubota K, Endo I, Nakajima A, Ichikawa Y. Sarcopenia is a reliable prognostic factor in patients with advanced pancreatic cancer receiving FOLFIRINOX chemotherapy. *Pancreatology* 2019; **19**: 127-135 [PMID: 30473464 DOI: 10.1016/j.pan.2018.11.001]

39 **Lee HS**, Kim SY, Chung MJ, Park JY, Bang S, Park SW, Song SY. Skeletal Muscle Mass Predicts Poor Prognosis in Patients with Advanced Pancreatic Cancer Undergoing Second-Line FOLFIRINOX Chemotherapy. *Nutr Cancer* 2019; **71**: 1100-1107 [PMID: 30955349 DOI: 10.1080/01635581.2019.1597906]

40 **Williet N**, Fovet M, Maoui K, Chevalier C, Maoui M, Le Roy B, Roblin X, Hag B, Phelip JM. A Low Total Psoas Muscle Area Index Is a Strong Prognostic Factor in Metastatic Pancreatic Cancer. *Pancreas* 2021; **50**: 579-586 [PMID: 33939672 DOI: 10.1097/MPA.0000000000001796]

41 **Solheim TS**, Laird BJA, Balstad TR, Stene GB, Bye A, Johns N, Pettersen CH, Fallon M, Fayers P, Fearon K, Kaasa S. A randomized phase II feasibility trial of a multimodal intervention for the management of cachexia in lung and pancreatic cancer. *J Cachexia Sarcopenia Muscle* 2017; **8**: 778-788 [PMID: 28614627 DOI: 10.1002/jcsm.12201]

42 **Griffin OM**, Bashir Y, O'Connor D, Peakin J, McMahon J, Duggan SN, Geoghegan J, Conlon KC. Measurement of body composition in pancreatic cancer: a systematic review, meta-analysis and recommendations for future study design. *Dig Surg* 2022; Online ahead of print [PMID: 35580571 DOI: 10.1159/000524575]

43 **Wu CH**, Chang MC, Lyadov VK, Liang PC, Chen CM, Shih TT, Chang YT. Comparing Western and Eastern criteria for sarcopenia and their association with survival in patients with pancreatic cancer. *Clin Nutr* 2019; **38**: 862-869 [PMID: 29503056 DOI: 10.1016/j.clnu.2018.02.016]

44 **Hsu TH**, Schawkat K, Berkowitz SJ, Wei JL, Makoyeva A, Legare K, DeCicco C, Paez SN, Wu JSH, Szolovits P, Kikinis R, Moser AJ, Goehler A. Artificial intelligence to assess body composition on routine abdominal CT scans and predict mortality in pancreatic cancer- A recipe for your local application. *Eur J Radiol* 2021; **142**: 109834 [PMID: 34252866 DOI: 10.1016/j.ejrad.2021.109834]

World Journal of Gastrointestinal Oncology

Submit a Manuscript: https://www.f6publishing.com

World J Gastrointest Oncol 2022 December 15; 14(12): 2313-2328

DOI: 10.4251/wjgo.v14.i12.2313

ISSN 1948-5204 (online)

ORIGINAL ARTICLE

Basic Study

N-myc downstream regulated gene 1 inhibition of tumor progression in Caco2 cells

Yi-Xiao He, Hong Shen, Yu-Zhu Ji, Hai-Rong Hua, Yu Zhu, Xiang-Fei Zeng, Fang Wang, Kai-Xin Wang

Specialty type: Oncology

Provenance and peer review: Unsolicited article; Externally peer reviewed.

Peer-review model: Single blind

Peer-review report's scientific quality classification

Grade A (Excellent): A
Grade B (Very good): 0
Grade C (Good): C
Grade D (Fair): 0
Grade E (Poor): 0

P-Reviewer: Ekine-Afolabi B, United Kingdom; Mohamed SY, Egypt

Received: July 14, 2022
Peer-review started: July 14, 2022
First decision: September 26, 2022
Revised: October 17, 2022
Accepted: November 22, 2022
Article in press: November 22, 2022
Published online: December 15, 2022

Yi-Xiao He, Yu-Zhu Ji, Department of Pathology, Mianyang Central Hospital, School of Medicine, University of Electronic Science and Technology of China, Mianyang 621000, Sichuan Province, China

Yi-Xiao He, Hai-Rong Hua, Fang Wang, Department of Pathology and Pathophysiology, Faculty of Basic Medical Sciences, Kunming Medical University, Kunming 650500, Yunnan Province, China

Hong Shen, Department of Pathology, Zhaotong First People's Hospital, Zhaotong 657000, Yunnan Province, China

Yu Zhu, School of Nursing, Henan Vocational College of Applied Technology, Kaifeng 450000, Henan Province, China

Xiang-Fei Zeng, Department of Clinical Pathology, West China Hospital, Sichuan University, Chengdu 610000, Sichuan Province, China

Kai-Xin Wang, Department of Pathology, Huazhong University of Science and Technology Union Shenzhen Hospital (Nanshan Hospital), Shenzhen 518052, Guangdong Province, China

Corresponding author: Kai-Xin Wang, MD, Associate Chief Physician, Department of Pathology, Huazhong University of Science and Technology Union Shenzhen Hospital (Nanshan Hospital), No. 89 Taoyuan Road, Nanshan District, Shenzhen 518052, Guangdong Province, China. 313683968@qq.com

Abstract

BACKGROUND

Invasion and migration are the irreversible stages of colorectal cancer (CRC). The key is to find a sensitive, reliable molecular marker that can predict the migration of CRC at an early stage. N-myc downstream regulated gene 1 (NDRG1) is a multifunctional gene that has been tentatively reported to have a strong relationship with tumor invasion and migration, however the current molecular role of NDRG1 in CRC remains unknown.

AIM

To explore the role of NDRG1 in the development of CRC.

METHODS

NDRG1 stably over-expressed Caco2 cell line was established by lentiviral

infection and NDRG1 knock-out Caco2 cell line was established by CRISPR/Cas9. Furthermore, the mRNA and protein levels of NDRG1 in Caco2 cells after NDRG1 over-expression and knockout were detected by real-time polymerase chain reaction and western blot. The cell proliferation rate was measured by the cell counting kit-8 method; cell cycle and apoptosis were detected by flow cytometry; invasion and migration ability were detected by the 24-transwell method.

RESULTS

NDRG1 over-expression inhibited Caco2 proliferation and the cell cycle could be arrested at the G1/S phase when NDRG1 was over-expressed, while the number of cells in the G2 phase was significantly increased when NDRG1 was knocked out. This suggests that NDRG1 inhibited the proliferation of Caco2 cells by arresting the cell cycle in the G1/S phase. Our data also demonstrated that NDRG1 promotes early cell apoptosis. Invasion and migration of cells were extensively inhibited when NDRG1 was over-expressed.

CONCLUSION

NDRG1 inhibits tumor progression in Caco2 cells which may represent a potential novel therapeutic strategy for the treatment of CRC.

Key Words: N-myc downstream regulated gene 1; Caco2; Colorectal cancer; Tumor progression; CRISPR/Cas9; Lentivirus infection

Core Tip: This study investigated the molecular functions of N-myc downstream regulated gene 1 (NDRG1) in the process of colorectal cancer (CRC) migration through stable over-expression or knockout of NDRG1 in the Caco2 CRC cell line. Our results showed that NDRG1 over-expression arrested the cell cycle at the G1/S phase, while its knock-out significantly increased the number of G2 phase cells. Altogether, our results highlight the fact that NDRG1 inhibits tumor progression in Caco2 cells which may provide a novel diagnostic or therapeutic tool in inhibiting the migration of CRC.

Citation: He YX, Shen H, Ji YZ, Hua HR, Zhu Y, Zeng XF, Wang F, Wang KX. N-myc downstream regulated gene 1 inhibition of tumor progression in Caco2 cells. *World J Gastrointest Oncol* 2022; 14(12): 2313-2328
URL: https://www.wjgnet.com/1948-5204/full/v14/i12/2313.htm
DOI: https://dx.doi.org/10.4251/wjgo.v14.i12.2313

INTRODUCTION

Malignant neoplasms are currently the leading cause of death in the world and the biggest obstacle to longer lives. Among new cancer cases in the world in 2018[1], colorectal cancer (CRC) accounted for 10.2% of new cancer cases and 9.2% of cancer deaths. CRC has become the third most common cancer and the incidence of CRC is increasing year by year.

Invasion and metastasis are two malignant features of CRC, involving the spreading of tumor cells from the primary tumor, penetrating into blood and lymphatic vessels and extravasation to the metastatic site. These are the main issues affecting the efficacy of treatment and the prognosis of CRC, and are the main cause of death in patients with CRC. Recent studies on the molecular biological mechanism of CRC indicate that the invasion and migration of CRC are associated with genes as well as microRNA[2]. It is the result of the combined action of multiple transfer-related genes and transfer-inhibitory genes. Many new biological indicators of prognosis and potential therapeutic targets related to CRC are being studied, however, early and sensitive biological indicators that can predict the migration of CRC at an early stage have not yet been discovered.

N-myc downstream regulated gene 1 (NDRG1) is a multifunctional gene. Recent studies have shown that NDRG1 is related to tumor invasion and migration[3], apoptosis[4], tumor cell proliferation[5], drug response and drug resistance of tumor cells[6]. Its expression in tumors is tissue-specific; it acts as a metastasis suppressor gene in prostate cancer[7] and ovarian cancer[8], but in lung cancer and esophageal squamous cell carcinoma, NDRG1 promotes tumor development[9]. The current role of NDRG1 in CRC is controversial. Many researchers have found that NDRG1 inhibits tumor invasion and migration in CRC[10-12], however, Wang *et al*[13] and Shah *et al*[14] found that NDRG1 promoted the development of CRC. Koshiji *et al*[15] found that the expression of NDRG1 differed with race and pathological stage of CRC patients.

To further investigate the role of NDRG1 in the development of CRC, we over-expressed and knocked out NDRG1 in the Caco2 CRC cell line, and then assessed cell proliferation, apoptosis, invasion and migration *in vitro*. We conducted these experiments to analyze the role of the NDRG1 gene in CRC, thus providing a theoretical basis for the early diagnosis and prognosis of CRC metastasis and a potential new molecular target for treatment of CRC.

MATERIALS AND METHODS

Cell culture

A Caco2 CRC cell line was purchased from the Kunming Cell Bank of the Kunming Institute of Zoology, Chinese Academy of Sciences. The Caco2 cell line was derived from a 72-year-old Caucasian male with colorectal adenocarcinoma. The 293T cells were provided by the Kunming Institute of Zoology, Chinese Academy of Sciences. The media required for culturing Caco2 and 293T cells was a Dulbecco's Minimum Essential Medium media (DMEM; Gibco, Thermo Fisher Scientific, Waltham, MA, United States) containing 10% fetal bovine serum (FBS; Gibco), 100 U/mL penicillin and 100 mg/mL streptomycin. All cell lines were incubated at 37 °C in a humidified atmosphere with 5% CO_2.

Establishment of cell lines

The lentiviral plasmid used for NDRG1 over-expression was GV358-NDRG1 (Genechem, Shanghai, China). The plasmid vector used for NDRG1 knockout was pL-CRISPR.EFS.GFP, which was kindly provided by the Kunming Institute of Zoology, Chinese Academy of Sciences. We designed three single-guide RNAs (sgRNAs) which were both located in exon 3 of the NDRG1 gene: sgRNA1, sgRNA2 and sgRNA3 (Table 1), inserting these three sgRNAs into the pL-CRISPR.EFS.GFP plasmid. All constructed plasmids were identified by sequencing. The empty GV358 and pL-CRISPR.EFS.GFP plasmids were used as a control. The plasmid (GV358-NDRG1, pL-CRISPR.EFS.GFP-sgRNA1, pL-CRISPR.EFS.GFP-sgRNA2, pL-CRISPR.EFS.GFP-sgRNA3, pL-control, GV358-control) and its corresponding packaging plasmid (Pspax2, PMD2.G) were co-transfected into 293T cells for virus packaging. Virus supernatants were then collected, concentrated and purified and finally, cells were infected with the virus. The cells successfully infected with the virus were sorted by flow cytometry. Then, the monoclonal NDRG1 knockout cells were sorted and isolated using flow cytometry. The monoclonal cells were expanded and cultured to extract DNA. The third exon of NDRG1 was amplified by polymerase chain reaction (PCR), the PCR product was sequenced and identified and the successfully identified cells were subjected to T-A cloning. The T-A cloning product was also sent for sequencing. All the primers used are shown in Table 1.

RNA extraction and quantitative PCR

The total cellular RNA was extracted (miRNeasy Kit; Qiagen, Hilden, Germany) and converted into cDNA (RevertAid First Strand cDNA Synthesis Kit; Thermo Fisher Scientific) according to the kit instructions. The ABI qPCR instrument was used for amplification of the reactants. The reaction procedure was: 95 °C for 10 min, 95 °C for 15 s, 60 °C for 1 min, 95 °C for 15 s for 40 cycles and 60 °C for 1 min. The results were normalized using GAPDH, and relative gene expression levels were calculated by the $\Delta\Delta$Ct method. Three replicate wells were repeated for each sample. All the primers used are shown in Table 2.

Western blotting

High-efficiency RIPA lysate was used to extract total cellular protein and protein concentrations were quantified using the BCA assay. An aliquot of 80 μg protein was separated by electrophoresis on a 10% SDS-polyacrylamide gel. Proteins were electrotransferred from the gel to a PVDF membrane, and then blocked with 5% non-fat milk solution for 2 h. Membranes were incubated with an anti-human NDRG1 monoclonal antibody (1:500, Cat. No. 9485S; CST, Danvers, MA, United States), β-tubulin (1:5000, Cat. No. 6046; Abcam, Cambridge, United Kingdom) was incubated for 1 h, and then incubated at 4 °C overnight. The next day, the corresponding secondary antibody (NDRG1 1:500, β-tubulin 1:10000, Cat. No. AS014; ABclonal, Woburn, MA, United States) was incubated for 1 h at room temperature. The membrane was washed and underwent detection using an enhanced enterochromaffin-like detection system.

Cell counting kit-8 assay

GV358-control, GV358-NDRG1, pL-control, and pL-NDRG1-knockout cells were seeded in 96-well plates at 2 × 10^3 cells per well for the cell counting kit-8 (CCK-8) cell proliferation assay (CCK-8 kit; Beyotime, Beijing, China), then cultured for 1, 2, 3, and 4 d, respectively. According to the manufacturer's instructions, the cells were incubated with the CCK-8 reagent at 37 °C for 1 h, with the absorbance of each sample scanned on a microplate reader equipped to read absorbance values at 450 nm.

Table 1 Primers used for the establishment of cell lines

Gene	Forward primer	Reverse primer
sgRNA1	5′-ATCCTCACCTACCATGACAT-3′	5′-ATGTCATGGTAGGTGAGGAT-3′
sgRNA2	5′-ACGCTGTGTGGGACTCCCAA-3′	5′-TTGGGAGTCCCACACAGCGT-3′
sgRNA3	5′-GTTCATGCCGATGTCATGG-3′	5′-ACCATGACATCGGCATGAAC-3′
NDRG1	5′-TTTGGTGCATTTAACAGCGCAGTCT-3′	5′-CAGGAAGTCCCAGGCAAAAAGAAAC-3′

NDRG1: N-myc downstream regulated gene 1; sgRNA: Single-guide RNA.

Table 2 Primers used for quantitative polymerase chain reaction

Gene	Forward primer	Reverse primer
GAPDH	5′-GCACCGTCAAGGCTGAGAA-3′	5′-TGGTGAAGACGCCAGTGGA-3′
NDRG1	5′-ATGTCTCGGGAGATGCAGGATGTAG-3′	5′-CTAGCAGGAGACCTCCATGGACTTG-3′

NDRG1: N-myc downstream regulated gene 1.

Assessment of cell cycle by flow cytometric analysis

For cell cycle synchronization, 5 × 10^5 cells were plated in 6-well plates. After the cells were completely adherent, the cells were cultured in the serum-free medium for 24 h and then cultured in a serum medium for 24 h. Cells were collected and fixed with pre-cooled 75% ethanol at 4 °C for 14-24 h. After fixation, propidium iodide and RNAase were added to the stained cells for 30 min in the dark, then detected by flow cytometry.

Assessment of apoptosis by flow cytometric analysis

Cells were trypsinized without EDTA then washed twice with cell staining buffer and resuspended with Annexin V Binding Buffer to adjust the cell concentration to (0.25-1.0) × 10^7/mL. 100 μL of the cell suspension was transferred into a new 1.5 mL centrifuge tube and 5 μL of APC Annexin V and 10 μL of propidium iodide solution were added, then incubated at room temperature for 15 min in the dark and tested by flow cytometry.

24-transwell for invasion and migration

Invasion experiments were done using the Chamber Matrigel Invasion 24-well DO (Cat. No. 354480; Biocoat Inc., Horsham, PA, United States), and migration experiments were done using a Transwell Chamber (Cat. No. 3422; Corning Inc., Corning, NY, United States). All experimental steps were carried out according to the given protocols. Cells were seeded at a concentration of 1 × 10^5 in the upper chamber. The lower chamber was filled with a DMEM medium containing 20% FBS. After 48 h, chambers were fixed in 4% paraformaldehyde, stained with 0.1% crystal violet, and the number of cells that passed through the Filter were observed. Cells stained with crystal violet were eluted using 33% acetic acid, and the absorbance of the eluate was measured by a microplate reader at 570 nm.

Statistical analysis

The data were statistically analyzed using GraphPad Prism 7.0 (La Jolla, CA, United States). Student's *t*-test was used for statistical analysis. Data are presented as a mean ± SD. $P < 0.05$ was considered statistically significant.

RESULTS

Flow cytometry sorting of cells

After viral infection of cells, positive cells (GFP-positive) were sorted by flow cytometry. The results showed that positive rates of GV358-control cells, GV358-NDRG1 cells, pL-control cells, and pL-NDRG1-knockout cells were 58.3%, 54.1%, 0.506%, and 0.461%, respectively (Figures 1A-D). The cells in the selected NDRG1 over-expression group (GV358-control cells, GV358-NDRG1 cells) were expanded and cultured. For knockout cells (pL-NDRG1-knockout cells), we used flow cytometry to sort for monoclonal cells with an efficiency of 4.73% (Figure 2).

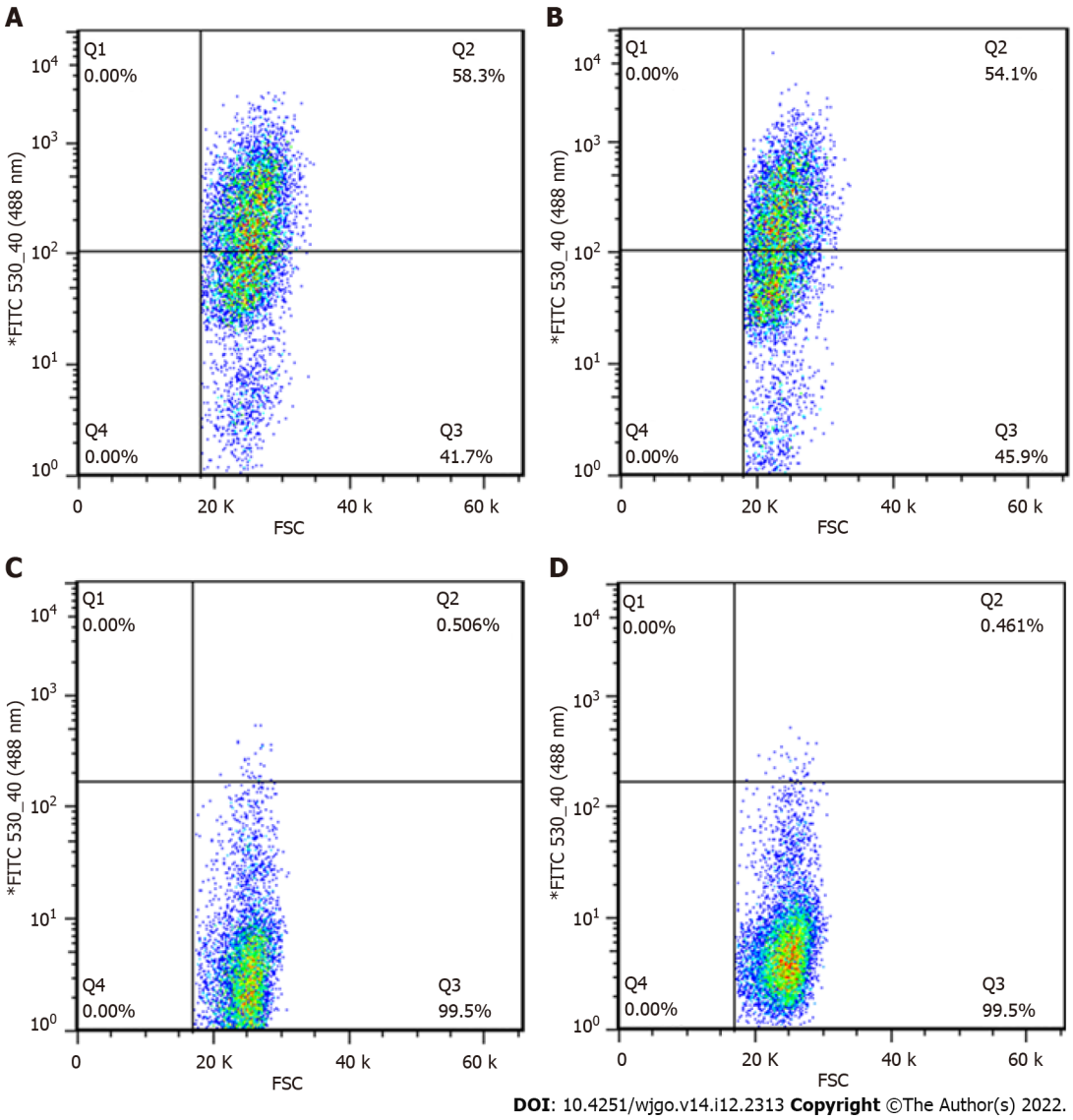

DOI: 10.4251/wjgo.v14.i12.2313 **Copyright** ©The Author(s) 2022.

Figure 1 Sorting efficiency of cells. A: Sorting efficiency of GV358-control cells (58.3%); B: Sorting efficiency of GV358-N-myc downstream regulated gene 1 (NDRG1) cells (54.1%); C: Sorting efficiency of pL-control cells (0.506%); D: Sorting efficiency of pL-NDRG1-knockout cells (0.461%).

Identification of gene knockout cell sequences

After monoclonal cells were expanded and cultured, cell DNA was extracted, the third exon of NDRG1 was amplified and products were sent for sequencing. Sequencing results showed that a DNA strand nick was generated on the third exon of NDRG1, then an A base was inserted. An analysis of the NDRG1 sequence in which the A base was inserted was performed using SnapGene software, and it was found that a TGA stop codon was formed after the inserted A base, thereby terminating the translation of NDRG1. The amplified exon of NDRG1 was identified by T-A cloning and sent for sequencing again. The sequencing results were consistent with previous results (Figure 3).

Verification of NDRG1 stable over-expression and knockout of the Caco2 cell line

After sorting GFP-positive cells by flow cytometry and sequencing identification, we detected the changes in NDRG1 mRNA and protein expression levels by quantitative PCR (qPCR) and western blotting. The relative expression level of NDRG1 mRNA of GV358-NDRG1 cells increased about three-fold compared with the control group ($P = 0.0006$). In the pL-NDRG1-knockout cells, NDRG1 mRNA levels were clearly diminished relative to the controls ($P < 0.0001$) (Figure 4A). Western blotting revealed that the protein levels in the over-expressed cells approximately doubled ($P < 0.0001$). After NDRG1 gene knockout, the level reduced significantly ($P < 0.0001$) (Figures 4B-D). All cells were expanded (Figure 5).

NDRG1 arrested the cell cycle in the G1/S phase, which inhibited the proliferation of Caco2 cells

In different tumor cells, NDRG1 can either promote or inhibit the proliferation of tumor cells. To

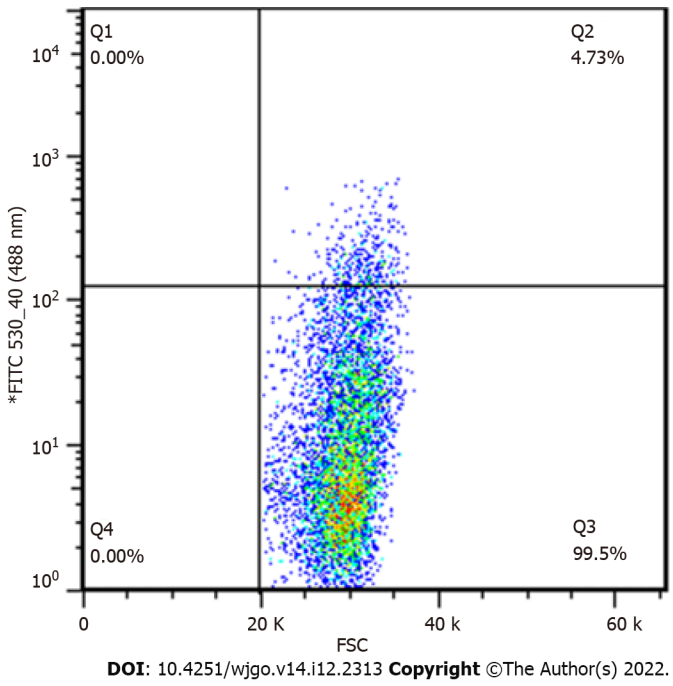

DOI: 10.4251/wjgo.v14.i12.2313 **Copyright** ©The Author(s) 2022.

Figure 2 Sorting efficiency of monoclonal cells. Sorting efficiency of pL-N-myc downstream regulated gene 1-knockout cells for monoclonal cells (4.73%).

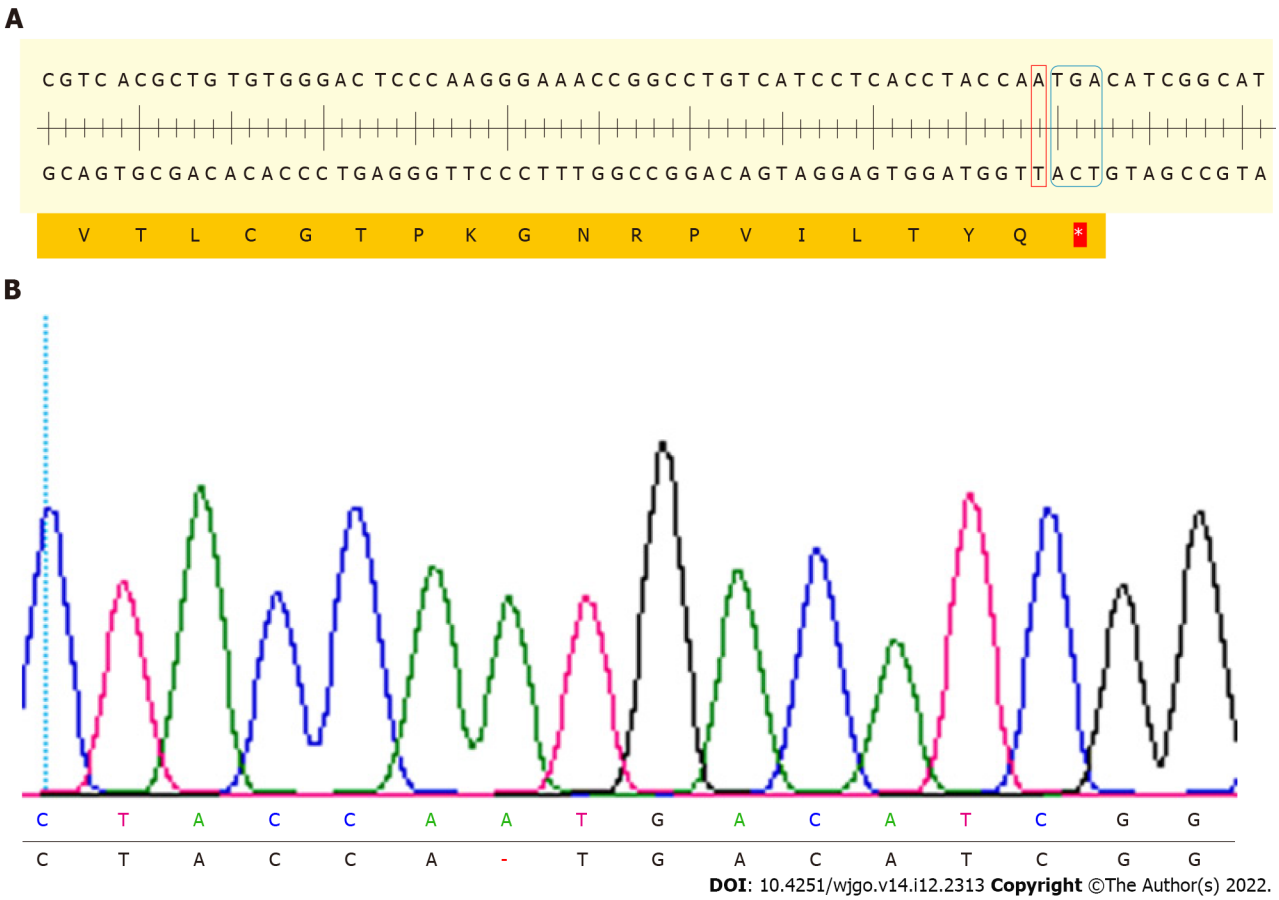

DOI: 10.4251/wjgo.v14.i12.2313 **Copyright** ©The Author(s) 2022.

Figure 3 Sequencing results of N-myc downstream regulated gene 1 exon3 T-A clone of N-myc downstream regulated gene 1 knockout cell. A: DNA strand nick was generated on the third exon of N-myc downstream regulated gene 1 (NDRG1), then an A base was inserted. An analysis of the NDRG1 sequence was performed using SnapGene software; B: Sequencing results of NDRG1 exon 3 of NDRG1 knockout cells.

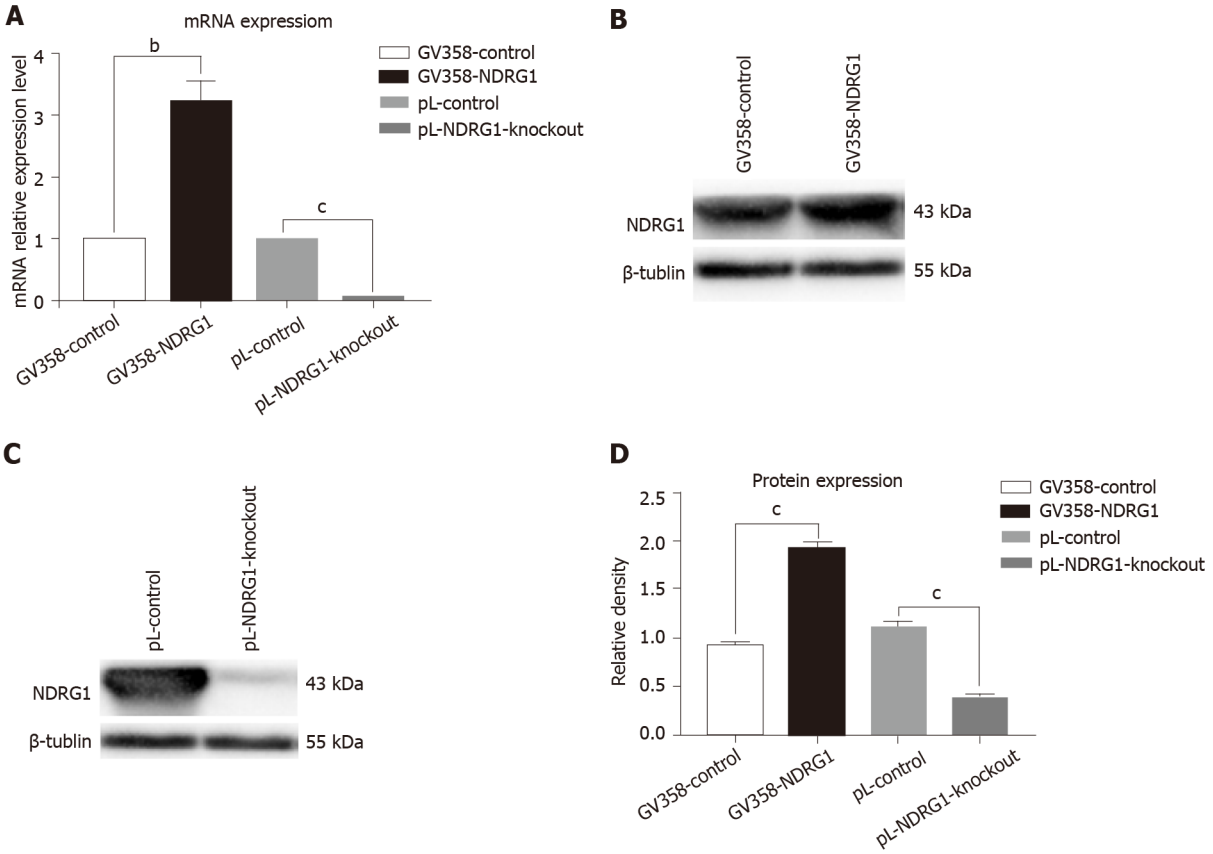

DOI: 10.4251/wjgo.v14.i12.2313 **Copyright** ©The Author(s) 2022.

Figure 4 The results of quantitative polymerase chain reaction and western blotting after N-myc downstream regulated gene 1 over-expression and knockout. A: The mRNA levels of N-myc downstream regulated gene 1 (NDRG1) were detected using real-time polymerase chain reaction. The relative levels of NDRG1 mRNA were calculated using the $\Delta\Delta$Ct method, and normalized to GAPDH expression; B-D: Representative western blot bands and statistical results of NDRG1 protein expression normalized to β-tubulin. $^{a}P < 0.05$, $^{b}P < 0.01$, $^{c}P < 0.001$ *vs* control cells. Experiments were repeated three times.

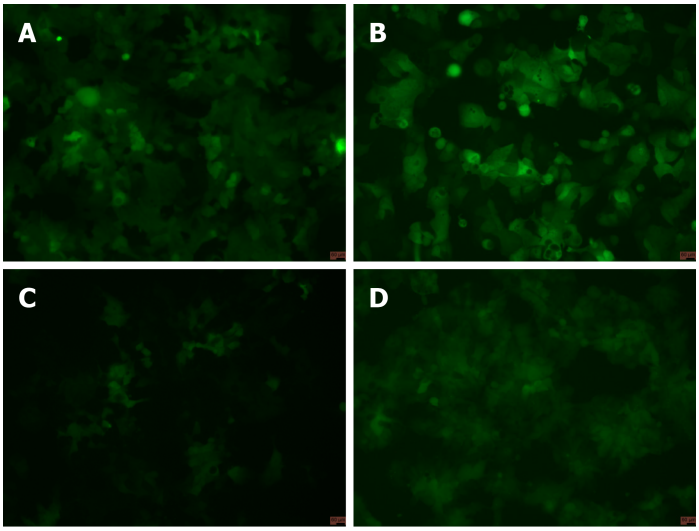

DOI: 10.4251/wjgo.v14.i12.2313 **Copyright** ©The Author(s) 2022.

Figure 5 Cells under a fluorescence microscope. A: GV358-Control cells (Scale bar: 60 μm); B: GV358-N-myc downstream regulated gene 1 (NDRG1) cells (Scale bar: 60 μm); C: pL-control cells (Scale bar: 60 μm); D: pL-NDRG1-knockout cells (Scale bar: 60 μm).

confirm the role of NDRG1 in Caco2 cells, we detected cell proliferation using the CCK-8 assay and flow cytometry. As shown in Figure 6, the relative proliferative activity of GV358-NDRG1 cells was decreased at 48 h, 72 h and 96 h compared with the GV358-control cells ($P < 0.001$) (Figures 6A and 6B), while pL-NDRG1-knockout cells were higher than pL-control cells at 24 h, 48 h, 72 h and 96 h ($P < 0.01$)

(Figures 6C and 6D), which indicates that over-expression of NDRG1 could inhibit the proliferation of Caco2 cells. Flow cytometry may illuminate the underlying mechanism. The proportion of G1 phase cells was significantly increased ($P < 0.0001$) (Figures 6E-G) after over-expression of NDRG1, while G2 phase cells were increased after NDRG1 knockout ($P < 0.0001$) (Figures 6H-J). The above results show that NDRG1 inhibits the proliferation of Caco2 cells by arresting the cell cycle in the G1/S phase.

NDRG1 inhibited migration and invasion of Caco2 cells

NDRG1 was also involved in tumor invasion and metastasis. Metastatic ability is also called exercise ability. Invasion and metastasis are two complementary processes. Invasive ability can be regarded as the basis of tumor cell metastasis. Thus, we also detected changes in the invasion and migration ability of cells using a 24- well transwell chamber. The number of cells passing through the chamber decreased after over-expression of NDRG1 ($P = 0.0001$) but increased after NDRG1 knockout ($P = 0.0001$). These results indicate that NDRG1 inhibited migration and invasion of Caco2 cells (Figure 7).

NDRG1 promoted early apoptosis of Caco2 cells

In order to further investigate the effect of NDRG1 on Caco2 cells, we used flow cytometry to detect cell apoptosis. The early apoptosis of the cells was increased after the over-expression of NDRG1 ($P = 0.0002$) (Figures 8A-C), and the rate of pL-NDRG1-knockout cells was decreased compared with pL-control cells ($P = 0.0013$) (Figures 8D-F), indicating that NDRG1 promoted early apoptosis of Caco2 cells.

DISCUSSION

According to the 2018 Global Cancer Statistics Report[1], CRC is the third most common cancer after lung cancer and breast cancer, and represents a serious threat to life and health worldwide. In addition, the incidence and mortality of CRC is on the rise, with the mortality rate reaching 95% for people over 45-years-old. CRC is a common malignant tumor which seriously threatens the life and health of patients. Unfortunately, the cause of this malignant disease is still unclear. Recent studies have shown that an excessive intake of red meat and processed meat increases the risk of CRC[16-18]. A large alcohol intake is also a risk factor[17-18] and a high-fat diet may also be related to CRC[19].

Invasion and metastasis are two malignant features of CRC. Tumor invasion and metastasis are multi-step, multi-stage, complex and orderly processes of interaction between tumor and host. They are the synergistic results of a variety of factors that promote the transfer mechanism of tumor cells in response to changes in the host environment. In addition, in recent years the molecular biology mechanisms of tumor invasion and metastasis research has shown that these processes are related to metastasis promoter gene activation and metastasis suppressor gene inactivation, as mutations of a variety of oncogenes and tumor suppressor genes can induce or enhance the metastatic potential of cancer cells. Therefore, tumor invasion and metastasis are the result of the combined action of multiple genes that promote and inhibit metastasis[20]. Clinically, the vast majority of CRC patients die, not from the primary tumor, but from multiple organ damage caused by tumor invasion and metastasis. Thus, the search for CRC metastasis suppressor genes is particularly important in current research. Further research on metastasis-associated genes in CRC cells will guide the early diagnosis of CRC, predicting early metastasis of cancer which is important for reducing the mortality of patients with CRC.

NDRG 1 is a member of the NDRG family. Human NDRG genes include NDRG1, NDRG2, NDRG3 and NDRG4, which are located on different chromosomes. The NDRG family belongs to an α/β hydrolase superfamily, but there is no hydrolase catalytic site. NDRG1 is located on human chromosome 8q24.3, is about 60 kb in length, and contains 16 exons and 15 introns. The full length of the mRNA is about 3 kb, and is composed of 394 amino acids and is highly conserved. The protein encoded by the gene is 43 kDa, and exists mainly in the cytoplasm, and to a lesser extent in the nucleus. NDRG1 is a multifunctional protein involved in cell growth[21], apoptosis[4], cell cycle regulation[22], tumor cell proliferation[5,23] and tumor invasion and metastasis[3]. It can be induced by a variety of drugs such as induced differentiation agents[24,25], and not only regulates homeostatic and genomic stability[26], but is also involved in the regulation of epidermal growth factor[27]. In addition, NDRG1 is related to the regulation of multiple signaling pathways, including the noncanonical nuclear factor-kappaB pathway [12,25], the PI3K/AKT/mTOR pathway[28,29], the RAS/RAF/MEK/ERK pathway[28,29], the transforming growth factor-beta pathway[30], and the Wnt/β-catenin pathways[3,9], suggesting it plays an important role in the development of tumors.

Recent studies have shown that NDRG1 may promote or inhibit the development of cancers, but its exact function in the process remains undefined. Some scholars believe that NDRG1 promotes the progression of liver cancer[31-33], lung cancer[34-36], bladder cancer[37], and gastric cancer[38,39]. However, other researchers have found that NDRG1 inhibits the development of prostate cancer[7,40], nasopharyngeal carcinoma[41], oropharyngeal squamous cell carcinoma[42], and ovarian cancer[8]. The role of NDRG1 in CRC is not conclusively understood.

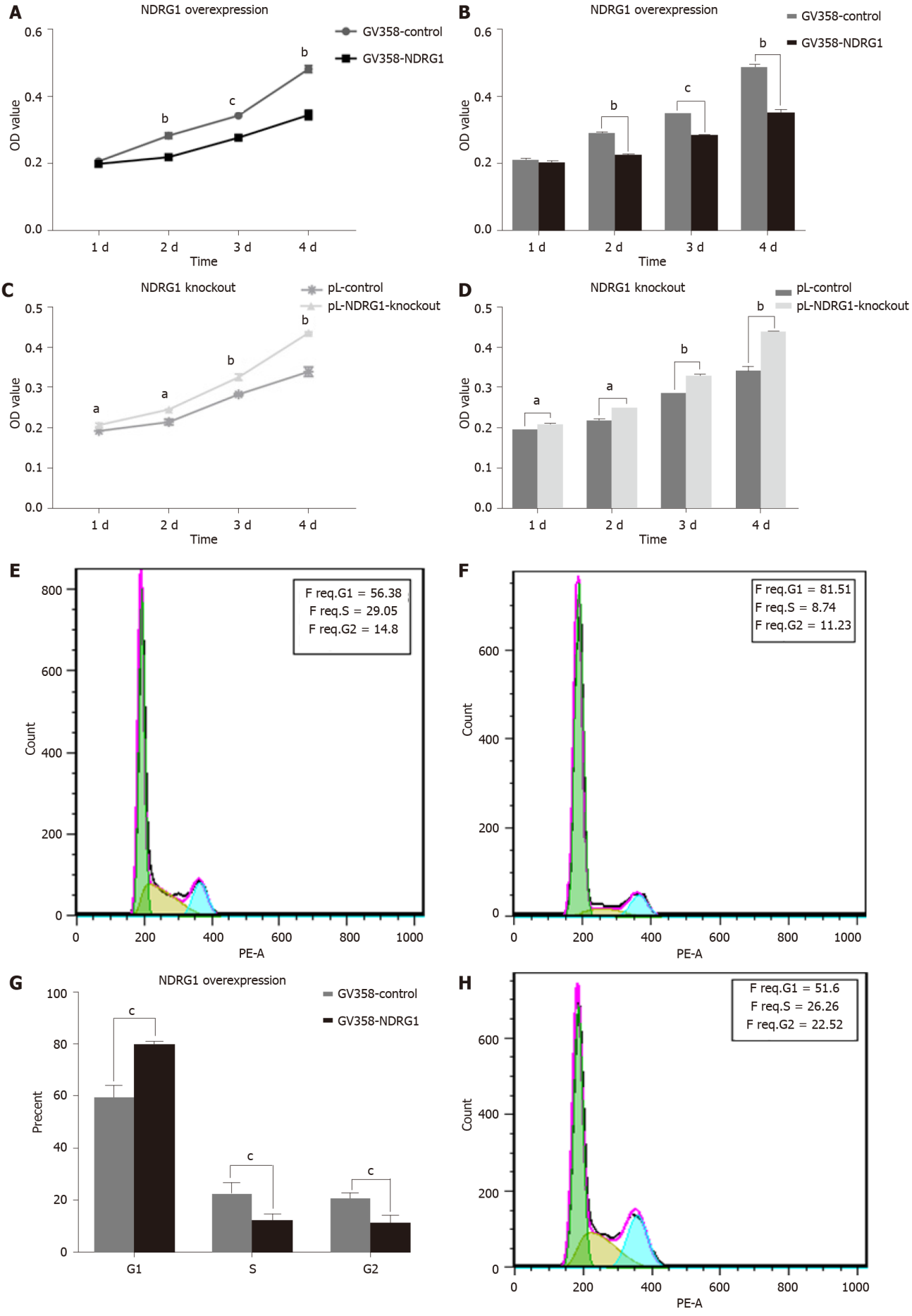
A
NDRG1 overexpression
GV358-control
GV358-NDRG1
OD value
Time
1 d
2 d
3 d
4 d
B
NDRG1 overexpression
GV358-control
GV358-NDRG1
OD value
Time
C
NDRG1 knockout
pL-control
pL-NDRG1-knockout
OD value
Time
D
NDRG1 knockout
pL-control
pL-NDRG1-knockout
OD value
Time
E
F req.G1 = 56.38
F req.S = 29.05
F req.G2 = 14.8
Count
PE-A
F
F req.G1 = 81.51
F req.S = 8.74
F req.G2 = 11.23
Count
PE-A
G
NDRG1 overexpression
GV358-control
GV358-NDRG1
Precent
G1
S
G2
H
F req.G1 = 51.6
F req.S = 26.26
F req.G2 = 22.52
Count
PE-A

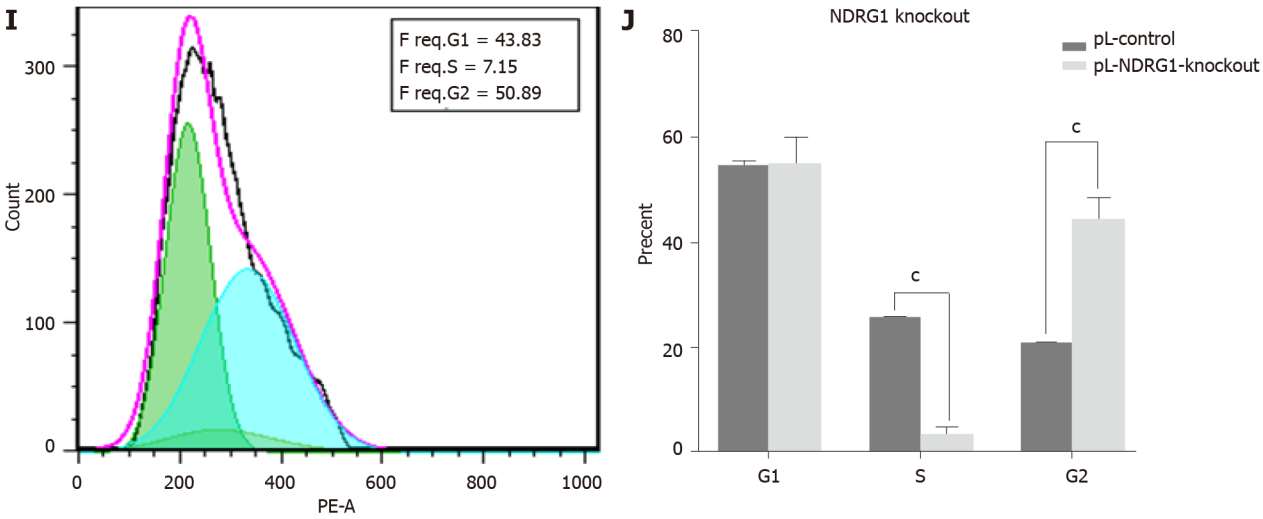

DOI: 10.4251/wjgo.v14.i12.2313 **Copyright** ©The Author(s) 2022.

Figure 6 N-myc downstream regulated gene 1 inhibits the proliferation of Caco2 cells. Cell viability was measured using the cell counting kit-8 assay. The cell cycle was measured using flow cytometry. A: Proliferation curves of Caco2 cells at 24 h, 48 h, 72 h and 96 h after N-myc downstream regulated gene 1 (NDRG1) over-expression; B: Statistical histogram of proliferation activity of Caco2 cells at 24 h, 48 h, 72 h and 96 h after NDRG1 over-expression; C: Proliferation curves of Caco2 cells at 24 h, 48 h, 72 h and 96 h after NDRG1 knockout; D: Statistical histogram of proliferation activity of Caco2 cells at 24 h, 48 h, 72 h and 96 h after NDRG1 knockout; E: Cell cycle diagram of GV358-control group; F: Cell cycle diagram of GV358-NDRG1-over-expression group; G: Statistical histogram of proportions of G1, S, and G2 cells after NDRG1 over-expression; H: Cell cycle diagram of pL-control group; I: Cell cycle diagram of pL-NDRG1-knockout group; J: Statistical histogram of proportions of G1, S, and G2 cells after NDRG1 knockout. $^{a}P < 0.05$, $^{b}P < 0.01$, $^{c}P < 0.001$ *vs* control. Experiments were repeated three times.

Vaes *et al*[43] found that NDRG1 mRNA levels were significantly reduced in CRC tissues compared to normal colon tissue. Wang *et al*[10] showed that silencing NDRG1 expression in CRC cells increased cell growth, invasion and migration. Mi *et al*[11] also found that NDRG1 inhibited epithelial-mesenchymal transition, invasion and migration of CRC cells by promoting ubiquitination of caveolin-1 (Cav1). These studies indicate that NDRG1 is a positive regulator of CRC. Interestingly, Koshiji *et al*[15] found that the expression of NDRG1 was different in CRC patients of different races and at different pathological stages, which resulted in different clinical outcomes. Some research also supports the premise that NDRG1 is a transfer-promoting gene[13,44]. It has also been observed that NDRG1 locates at the centrosome of CRC cells and participates in the cell cycle as a microtubule-associated protein and mitotic site. In p53 deficient tumor cell lines, NDRG1 inhibits polyploid development and increases the number of cells by inducing cell cycle arrest. Therefore, NDRG1 can protect cells from uncontrolled proliferation, suggesting that NDRG1 possesses different effects in different cancer cells, and may be related to specific cell types and pleiotropic functions of genes.

To further investigate the role of NDRG1 in the development of CRC, lentivirus infection was used to establish stable NDRG1 over-expression in the Caco2 CRC cell line, and CRISPR/Cas9 was used to establish stable NDRG1 knock down in the Caco2 cells. Relative mRNA expression and protein expression of the cloned cells were detected by flow cytometry, qPCR and western blot. The results showed that NDRG1 mRNA levels increased by 3.218 times on average after over-expression, and western blot results showed that protein expression increased by about 2 times on average after NDRG1 over-expression. The relative mRNA expression level after NDRG1 was knockout and was only about 0.07, and the protein expression of NDRG1 after knockout was about 0.3. Following verification of over-expression and knock down, changes in cell proliferative ability, cell cycle, apoptosis, invasion and migratory ability were measured.

The results showed that the rate of cell proliferation was slowed down after NDRG1 over-expression, while the rate of cell proliferation was increased after NDRG1 gene knockout, both of which were statistically significant ($P < 0.01$). Cell cycle assay results showed that after NDRG1 over-expression, the proportion of cells in G1 phase increased significantly ($P < 0.0001$), while the proportion of cells in S and G2 phase decreased. After NDRG1 was knocked out, the proportion of cells in S phase decreased significantly, however, there was an increased number of cells in G2 phase indicating that the proportion of cells in the proliferation phase increased, and cell growth remained active. Combining the results of the two experiments, we concluded that NDRG1 over-expression arrested the cell cycle in G1/S phase and sequentially inhibited the cell growth rate of Caco2 cells. In contrast, NDRG1 knockout could enhance the mitosis of Caco2 cells, thus promoting cell growth. Then, flow cytometry was used to analyze the effect of NDRG1 on apoptosis of Caco2 cells. After NDRG1 over-expression, both the rates of early apoptosis and total apoptosis of cells increased ($P < 0.05$), indicating that NDRG1 over-expression promoted the apoptosis of Caco2 cells. In contrast, after NDRG1 was knocked out, both the rates of early apoptosis and total apoptosis of Caco2 cells decreased ($P < 0.05$), indicating that NDRG1

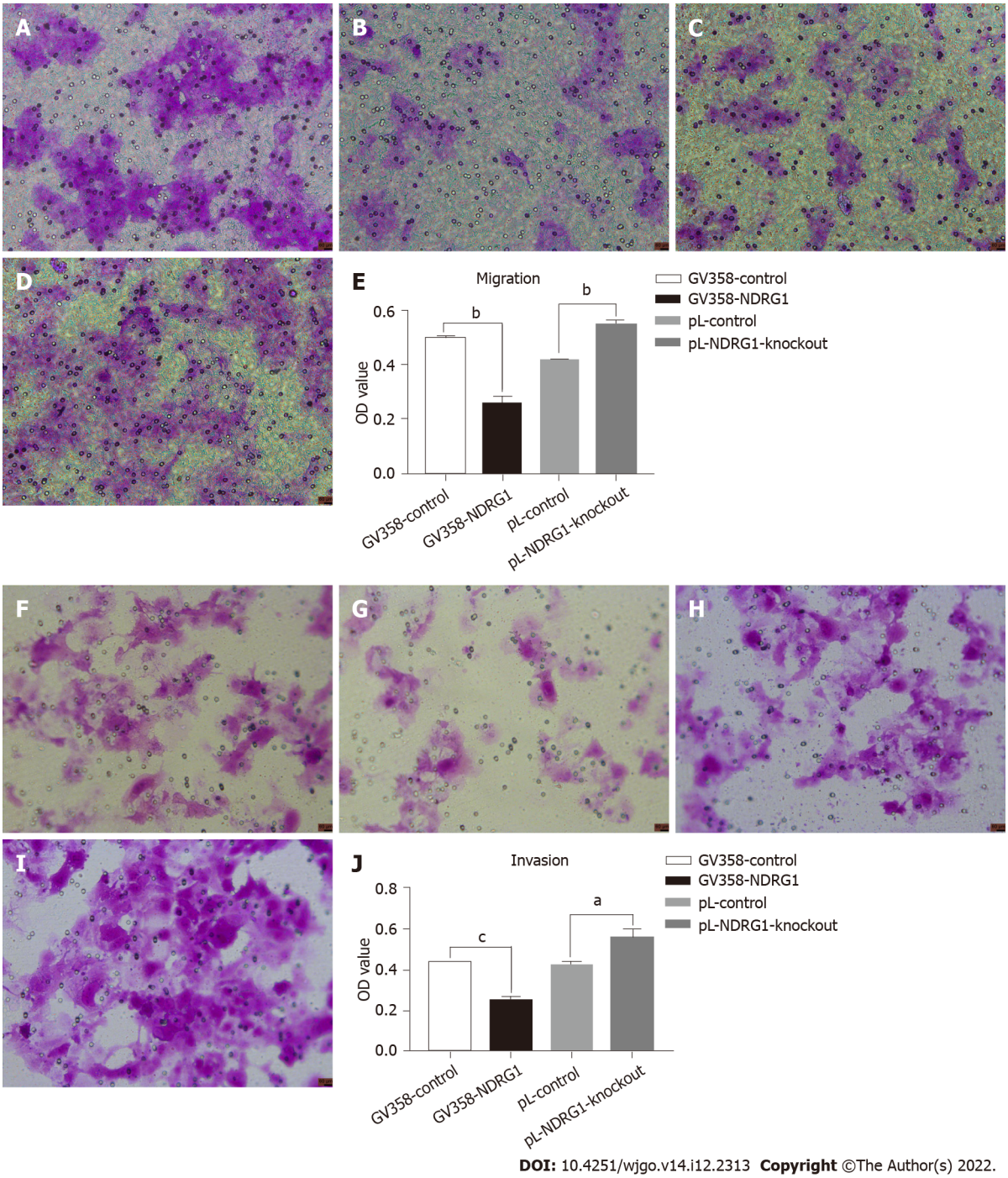

DOI: 10.4251/wjgo.v14.i12.2313

Figure 7 N-myc downstream regulated gene 1 inhibited migration and invasion of Caco2 cells. 24-well transwell chambers were used to detect migration and invasion. Cells were stained with crystal violet, eluted with 33% acetic acid, and the absorbance of the eluate was measured at 570 nm. The number of cells passing through the chamber at 48 h of the migration experiment (A-E). The number of cells passing through the chamber at 48 h of the invasion experiment (F-J). A: Number of cells passing through the chamber at 48 h of migration assay in GV358-control group (Scale bar: 60 μm); B: Number of cells passing through the chamber at 48 h of migration assay in GV358-N-myc downstream regulated gene 1 (NDRG1)-over-expression group (Scale bar: 60 μm); C: Number of cells passing through the chamber at 48 h of migration assay in pL-control group (Scale bar: 60 μm); D: Number of cells passing through the chamber at 48 h of migration assay in pL-NDRG1-knockout group (Scale bar: 60 μm); E: Statistical histograms of OD values eluted by crystal violet after NDRG1 over-expression and knockdown at 48h of migration assay; F: Number of cells passing through the chamber at 48 h of invasion assay in GV358-control group (Scale bar: 60 μm); G: Number of cells passing through the chamber at 48 h of invasion assay in GV358-NDRG1-over-expression group (Scale bar: 60 μm); H: Number of cells passing through the chamber at 48 h of invasion assay in pL-control group (Scale bar: 60 μm); I: Number of cells passing through the chamber at 48 h of invasion assay in pL-NDRG1-knockout group (Scale bar: 60 μm); J: Statistical histograms of OD values eluted by crystal violet after NDRG1 over-expression and knockdown at 48h of invasion assay. $^{a}P < 0.05$, $^{b}P < 0.01$, $^{c}P < 0.001$ *vs* control. Experiments were repeated three times.

knockout can inhibit the apoptosis of Caco2 cells. Invasion and migration are two complementary processes, and migratory ability (also known as motor ability) can be regarded as the basis for invasion of tumor cells. In this experiment, we used a 24-well transwell chamber to detect the invasion and migration of cells at 48 h. The results showed that NDRG1 over-expression inhibited cell invasion and

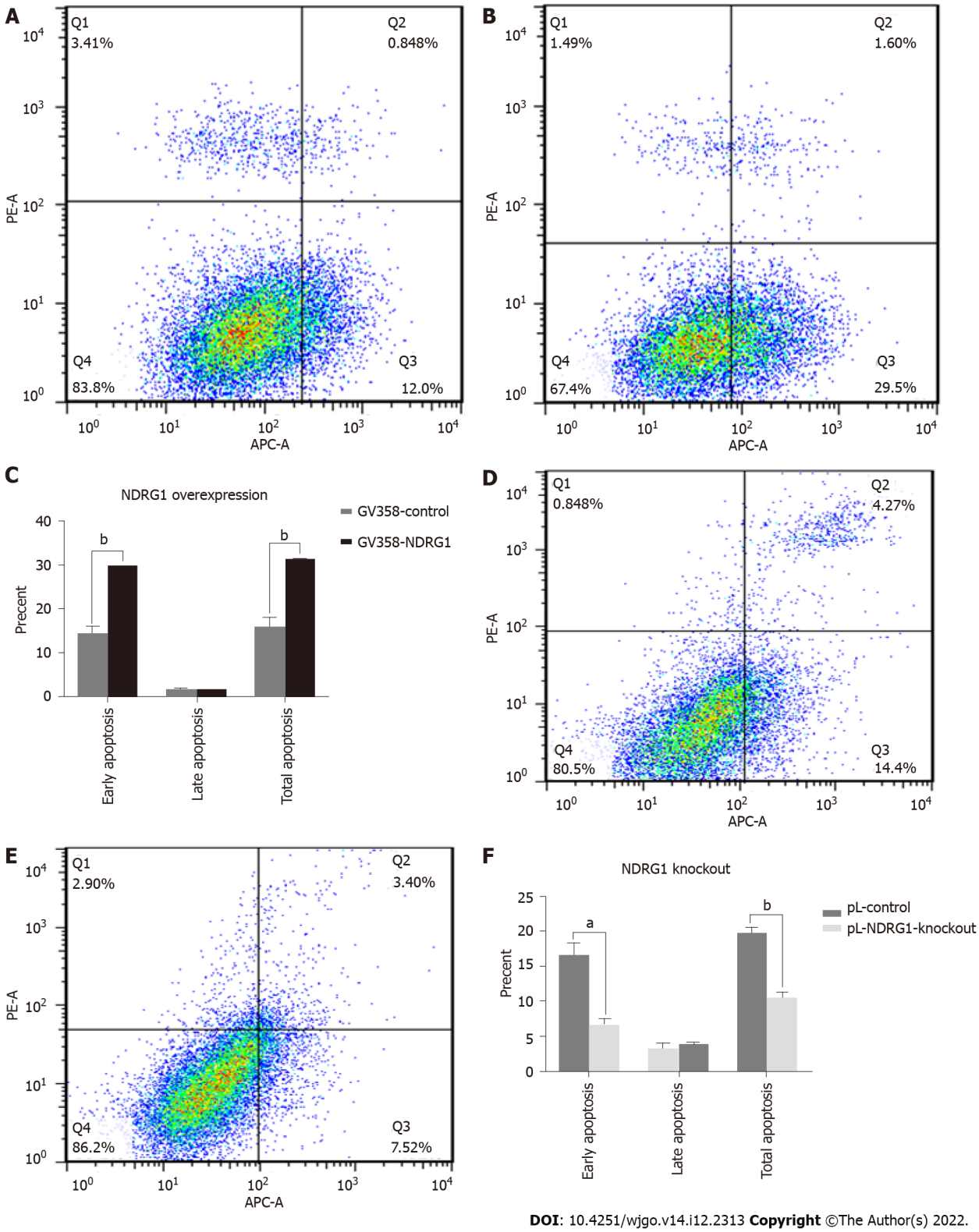

DOI: 10.4251/wjgo.v14.i12.2313

Figure 8 N-myc downstream regulated gene 1 promoted early apoptosis of Caco2 cells. Annexin V-APC/propidium iodide (PI) staining by flow cytometry was performed to detect the apoptosis of cells. Early apoptosis (Annexin V-APC+/PI-), late apoptosis (Annexin V-APC+/PI+), and necrosis (Annexin V-APC-/PI+). A: Apoptosis rate of Caco2 cells in GV358-control group; B: Apoptosis rate of Caco2 cells in GV358-N-myc downstream regulated gene 1 (NDRG1)-over-expression group; C: Statistical histogram of apoptosis rate of Caco2 cells after NDRG1 over-expression; D: Apoptosis rate of Caco2 cells in pL-control group; E: Apoptosis rate of Caco2 cells in pL-NDRG1-knockout group; F: Statistical histogram of apoptosis rate of Caco2 cells after NDRG1 knockout. $^{a}P < 0.05$, $^{b}P < 0.01$, $^{c}P < 0.001$ *vs* control. Experiments were repeated three times.

migration, while cell invasion and migration were promoted after knockout. In conclusion, NDRG1 can inhibit the proliferation of Caco2 cells by arresting the cell cycle in G1/S phase, promoting early apoptosis of cells, and inhibiting the invasive and migratory ability of cells. Thus, NDRG1 is a tumor

metastasis suppressor gene in Caco2 cells.

NDRG1 has been shown to be a key player in the spread of cancer and the proliferation of cancer cells. However, the effects of NDRG1 on tumor invasion and metastasis, along with the mechanisms behind it are poorly understood. Aikemu *et al*[45] provided *in silico* evidence that NDRG1 plays a crucial role in actin reorganization in CRC. They found that NDRG1 loss disrupts the binding between RhoGDI α and CDC42, triggers the activation of CDC42 and the downstream PAK1/Cofilin cascade, thereby promoting the formation of filopodia and invasion of CRC. The knockdown of NDRG1 led to enhanced mobility of CRC cells *in vivo* and correlates with active CDC42 expression. In addition, Aikemu *et al*[45] found an elevated level of active CDC42 in patients with advanced T stage cancer that was negatively correlated with NDRG1 expression. In sum, these results uncover a mechanism utilized by NDRG1 to regulate CDC42 activity in coordinating cytoskeleton reorganization, which is crucial in cancer invasion. Claudin-2 (CLDN2), a well-defined component of cellular tight junction, has also been suggested to be associated with CRC progression. Wei *et al*[46] demonstrated that CLDN2 is up-regulated in CRC samples and associated with poor survival. Additionally, CLDN2 depletion significantly promoted NDRG1 transcription, leading to termination of CRC growth and metastasis *in vitro* and *in vivo*. NDRG1 is a key regulator that interacts with many classic tumor signaling pathways, including some molecules downstream of the epidermal growth factor receptor (EGFR). Yang *et al*[47] demonstrated that NDRG1 inhibited the expression of EGFR, blocked EGFR phosphorylation, and reduced the distribution of EGFR distribution in the cell membrane, cytoplasm and nucleus. NDRG1 suppression of EGFR subsequently suppressed pathways downstream of EGFR, including the RAS/RAF/ERK and PI3k/AKT/mTOR pathways. NDRG1 was also able to attenuate endocytosis and degradation of EGFR induced by Cav1. NDRG1 could be a promising biomarker to predict optimum responses to cyclophosphamide (commonly known as CTX) and a key target to enhance CTX activity in the treatment of metastatic CRC.

To further clarify the mechanism by which NDRG1 inhibits tumorigenesis, we are proceeding to observe the relevant signal pathway and the abilities of NDRG1 in nude mice. This preliminary basic research is useful in providing new potential targets for molecular therapy in CRC.

CONCLUSION

In conclusion, we conducted analyses on the effect of NDRG1 on the Caco2 cell line. Through the analyses of the NDRG1 on the biological behaviors of Caco2 cell line, we found that NDRG1 would reduce the proliferation, apoptosis, migration and invasion abilities of Caco2 cell line. NDRG1 may have potential application value as a molecular biological index to predict the early invasion and metastasis of CRC.

ARTICLE HIGHLIGHTS

Research background

In American colorectal cancer patients, the expression of N-myc downstream regulated gene 1 (NDRG1) in primary colorectal cancer was always less than that in adjacent normal tissues. Our study on clinical samples showed the opposite. Therefore, the effect of NDRG1 in cancer may be related to the ethnic backgrounds of colorectal cancer. The future research direction is to find out whether the role of NDRG1 in the development of colorectal tumors is related to ethnic differences through *in vivo* and *in vitro* experiments.

Research motivation

This study identifies the *in vitro* role of NDRG1 in Caucasian large intestine tumors as inhibition of tumor cell invasion and migration.

Research objectives

This study only showed the *in vitro* effect of NDRG1 in Caucasian large intestine tumors, and the question remains to be solved about the effect of NDRG1 in large intestine tumors of other races.

Research methods

RNA extraction and quantitative polymerase chain reaction, western blotting, cell counting kit-8 assay, assessment of cell cycle by flow cytometric analysis, assessment of apoptosis by flow cytometric analysis, 24-transwell for invasion and migration were used in the experiments. GraphPad Prism 7.0. student's *t*-test was used for statistical analysis.

Research results

The primary objective was to investigate the role of NDRG1 in the development and progression of colorectal tumors. The objective has been to investigate the *in vitro* role of NDRG1 in the development of Caucasian human bowel tumors. The significance of achieving these goals for future research in this area is to provide clinicians with a theoretical basis for selecting therapies for colorectal cancer.

Research conclusions

The research topic is NDRG1 and the key problem to be solved is the role of NDRG1 in the occurrence and development of colorectal tumors. The results can provide a certain basis for the selection of treatment options for colorectal tumors.

Research perspectives

In 2004, our research group published an article in the *World Journal of Gastroenterology* on our research data with a large clinical sample (150 cases): "Correlation of N-myc downstream-regulated gene 1 over-expression with progressive growth of colorectal neoplasm.", which carried significance on the association of NDRG1 with colorectal cancer progression.

ACKNOWLEDGEMENTS

We thank the Department of Comparative Genomics Group of the Institute of Zoology, the Chinese Academy of Sciences for providing experimental sites and technical support in this study.

FOOTNOTES

Author contributions: He YX, Shen H and Ji YZ have contributed equally to the work; He YX, Shen H and Ji YZ performed the experiments, analyzed the data and wrote the manuscript; Hua HR and Zhu Y contributed analysis tools, acquired and analyzed data; Zeng XF helped perform the analysis with constructive discussions; Wang F and Wang KX conceived and designed the experiments as well as an acquired research grant; and all authors read and approved the final version of the article.

Supported by the National Natural Science Foundation of China, No. 81260361; and Incubation Project of Mianyang Central Hospital, No. 2020FH05.

Conflict-of-interest statement: He YX, Shen H, Ji YZ, Zhu Y, Zeng XF and Wang KX were previously postgraduate students at Kunming Medical University. Wang Fang was a teacher at Kunming Medical University. All the authors report no relevant conflicts of interest for this article.

Data sharing statement: No additional data are available.

Country/Territory of origin: China

ORCID number: Yu-Zhu Ji 0000-0003-2563-8118; Fang Wang 0000-0002-3562-8434; Kai-Xin Wang 0000-0002-9938-8011.

S-Editor: Wang JJ
L-Editor: Filipodia
P-Editor: Wang JJ

REFERENCES

1 **Bray F**, Ferlay J, Soerjomataram I, Siegel RL, Torre LA, Jemal A. Global cancer statistics 2018: GLOBOCAN estimates of incidence and mortality worldwide for 36 cancers in 185 countries. *CA Cancer J Clin* 2018; **68**: 394-424 [PMID: 30207593 DOI: 10.3322/caac.21492]
2 **Ye H**, Pang L, Wu Q, Zhu Y, Guo C, Deng Y, Zheng X. A critical role of mir-199a in the cell biological behaviors of colorectal cancer. *Diagn Pathol* 2015; **10**: 65 [PMID: 26065676 DOI: 10.1186/s13000-015-0260-x]
3 **Jin R**, Liu W, Menezes S, Yue F, Zheng M, Kovacevic Z, Richardson DR. The metastasis suppressor NDRG1 modulates

the phosphorylation and nuclear translocation of β-catenin through mechanisms involving FRAT1 and PAK4. *J Cell Sci* 2014; **127**: 3116-3130 [PMID: 24829151 DOI: 10.1242/jcs.147835]

4 **Chen B**, Zaveri PG, Longtine MS, Nelson DM. N-myc downstream-regulated gene 1 (NDRG1) mediates pomegranate juice protection from apoptosis in hypoxic BeWo cells but not in primary human trophoblasts. *Placenta* 2015; **36**: 847-853 [PMID: 26028238 DOI: 10.1016/j.placenta.2015.05.009]

5 **Chang X**, Xu X, Ma J, Xue X, Li Z, Deng P, Zhang S, Zhi Y, Chen J, Dai D. NDRG1 expression is related to the progression and prognosis of gastric cancer patients through modulating proliferation, invasion and cell cycle of gastric cancer cells. *Mol Biol Rep* 2014; **41**: 6215-6223 [PMID: 24985974 DOI: 10.1007/s11033-014-3501-2]

6 **Verma N**, Müller AK, Kothari C, Panayotopoulou E, Kedan A, Selitrennik M, Mills GB, Nguyen LK, Shin S, Karn T, Holtrich U, Lev S. Targeting of PYK2 Synergizes with EGFR Antagonists in Basal-like TNBC and Circumvents HER3-Associated Resistance *via* the NEDD4-NDRG1 Axis. *Cancer Res* 2017; **77**: 86-99 [PMID: 27793840 DOI: 10.1158/0008-5472.CAN-16-1797]

7 **Lee JE**, Kim JH. Valproic acid inhibits the invasion of PC3 prostate cancer cells by upregulating the metastasis suppressor protein NDRG1. *Genet Mol Biol* 2015; **38**: 527-533 [PMID: 26692161 DOI: 10.1590/S1415-475738420150028]

8 **Wang B**, Li J, Ye Z, Li Z, Wu X. N-myc downstream regulated gene 1 acts as a tumor suppressor in ovarian cancer. *Oncol Rep* 2014; **31**: 2279-2285 [PMID: 24626771 DOI: 10.3892/or.2014.3072]

9 **Ai R**, Sun Y, Guo Z, Wei W, Zhou L, Liu F, Hendricks DT, Xu Y, Zhao X. NDRG1 overexpression promotes the progression of esophageal squamous cell carcinoma through modulating Wnt signaling pathway. *Cancer Biol Ther* 2016; **17**: 943-954 [PMID: 27414086 DOI: 10.1080/15384047.2016.1210734]

10 **Wangpu X**, Yang X, Zhao J, Lu J, Guan S, Kovacevic Z, Liu W, Mi L, Jin R, Sun J, Yue F, Ma J, Lu A, Richardson DR, Wang L, Zheng M. The metastasis suppressor, NDRG1, inhibits "stemness" of colorectal cancer *via* down-regulation of nuclear β-catenin and CD44. *Oncotarget* 2015; **6**: 33893-33911 [PMID: 26418878 DOI: 10.18632/oncotarget.5294]

11 **Mi L**, Zhu F, Yang X, Lu J, Zheng Y, Zhao Q, Wen X, Lu A, Wang M, Zheng M, Ji J, Sun J. The metastatic suppressor NDRG1 inhibits EMT, migration and invasion through interaction and promotion of caveolin-1 ubiquitylation in human colorectal cancer cells. *Oncogene* 2017; **36**: 4323-4335 [PMID: 28346422 DOI: 10.1038/onc.2017.74]

12 **Ma J**, Gao Q, Zeng S, Shen H. Knockdown of NDRG1 promote epithelial-mesenchymal transition of colorectal cancer *via* NF-κB signaling. *J Surg Oncol* 2016; **114**: 520-527 [PMID: 27338835 DOI: 10.1002/jso.24348]

13 **Wang Z**, Wang F, Wang WQ, Gao Q, Wei WL, Yang Y, Wang GY. Correlation of N-myc downstream-regulated gene 1 overexpression with progressive growth of colorectal neoplasm. *World J Gastroenterol* 2004; **10**: 550-554 [PMID: 14966915 DOI: 10.3748/wjg.v10.i4.550]

14 **Shah MA**, Kemeny N, Hummer A, Drobnjak M, Motwani M, Cordon-Cardo C, Gonen M, Schwartz GK. Drg1 expression in 131 colorectal liver metastases: correlation with clinical variables and patient outcomes. *Clin Cancer Res* 2005; **11**: 3296-3302 [PMID: 15867226 DOI: 10.1158/1078-0432.CCR-04-2417]

15 **Koshiji M**, Kumamoto K, Morimura K, Utsumi Y, Aizawa M, Hoshino M, Ohki S, Takenoshita S, Costa M, Commes T, Piquemal D, Harris CC, Tchou-Wong KM. Correlation of N-myc downstream-regulated gene 1 expression with clinical outcomes of colorectal cancer patients of different race/ethnicity. *World J Gastroenterol* 2007; **13**: 2803-2810 [PMID: 17569115 DOI: 10.3748/wjg.v13.i20.2803]

16 **Magalhães B**, Peleteiro B, Lunet N. Dietary patterns and colorectal cancer: systematic review and meta-analysis. *Eur J Cancer Prev* 2012; **21**: 15-23 [PMID: 21946864 DOI: 10.1097/CEJ.0b013e3283472241]

17 **Garcia-Larsen V**, Morton V, Norat T, Moreira A, Potts JF, Reeves T, Bakolis I. Dietary patterns derived from principal component analysis (PCA) and risk of colorectal cancer: a systematic review and meta-analysis. *Eur J Clin Nutr* 2019; **73**: 366-386 [PMID: 30050075 DOI: 10.1038/s41430-018-0234-7]

18 **Godos J**, Bella F, Torrisi A, Sciacca S, Galvano F, Grosso G. Dietary patterns and risk of colorectal adenoma: a systematic review and meta-analysis of observational studies. *J Hum Nutr Diet* 2016; **29**: 757-767 [PMID: 27412573 DOI: 10.1111/jhn.12395]

19 **Fu T**, Coulter S, Yoshihara E, Oh TG, Fang S, Cayabyab F, Zhu Q, Zhang T, Leblanc M, Liu S, He M, Waizenegger W, Gasser E, Schnabl B, Atkins AR, Yu RT, Knight R, Liddle C, Downes M, Evans RM. FXR Regulates Intestinal Cancer Stem Cell Proliferation. *Cell* 2019; **176**: 1098-1112.e18 [PMID: 30794774 DOI: 10.1016/j.cell.2019.01.036]

20 **Chui MH**. Insights into cancer metastasis from a clinicopathologic perspective: Epithelial-Mesenchymal Transition is not a necessary step. *Int J Cancer* 2013; **132**: 1487-1495 [PMID: 22833228 DOI: 10.1002/ijc.27745]

21 **Larkin J**, Chen B, Shi XH, Mishima T, Kokame K, Barak Y, Sadovsky Y. NDRG1 deficiency attenuates fetal growth and the intrauterine response to hypoxic injury. *Endocrinology* 2014; **155**: 1099-1106 [PMID: 24424031 DOI: 10.1210/en.2013-1425]

22 **Matsugaki T**, Zenmyo M, Hiraoka K, Fukushima N, Shoda T, Komiya S, Ono M, Kuwano M, Nagata K. N-myc downstream-regulated gene 1/Cap43 expression promotes cell differentiation of human osteosarcoma cells. *Oncol Rep* 2010; **24**: 721-725 [PMID: 20664979 DOI: 10.3892/or_00000913]

23 **Lu WJ**, Chua MS, So SK. Suppressing N-Myc downstream regulated gene 1 reactivates senescence signaling and inhibits tumor growth in hepatocellular carcinoma. *Carcinogenesis* 2014; **35**: 915-922 [PMID: 24302615 DOI: 10.1093/carcin/bgt401]

24 **Kalinowski DS**, Stefani C, Toyokuni S, Ganz T, Anderson GJ, Subramaniam NV, Trinder D, Olynyk JK, Chua A, Jansson PJ, Sahni S, Lane DJ, Merlot AM, Kovacevic Z, Huang ML, Lee CS, Richardson DR. Redox cycling metals: Pedaling their roles in metabolism and their use in the development of novel therapeutics. *Biochim Biophys Acta* 2016; **1863**: 727-748 [PMID: 26844773 DOI: 10.1016/j.bbamcr.2016.01.026]

25 **Xi R**, Pun IH, Menezes SV, Fouani L, Kalinowski DS, Huang ML, Zhang X, Richardson DR, Kovacevic Z. Novel Thiosemicarbazones Inhibit Lysine-Rich Carcinoembryonic Antigen-Related Cell Adhesion Molecule 1 (CEACAM1) Coisolated (LYRIC) and the LYRIC-Induced Epithelial-Mesenchymal Transition *via* Upregulation of N-Myc Downstream-Regulated Gene 1 (NDRG1). *Mol Pharmacol* 2017; **91**: 499-517 [PMID: 28275050 DOI: 10.1124/mol.116.107870]

26 **Croessmann S**, Wong HY, Zabransky DJ, Chu D, Mendonca J, Sharma A, Mohseni M, Rosen DM, Scharpf RB, Cidado J, Cochran RL, Parsons HA, Dalton WB, Erlanger B, Button B, Cravero K, Kyker-Snowman K, Beaver JA, Kachhap S,

Hurley PJ, Lauring J, Park BH. NDRG1 links p53 with proliferation-mediated centrosome homeostasis and genome stability. *Proc Natl Acad Sci U S A* 2015; **112**: 11583-11588 [PMID: 26324937 DOI: 10.1073/pnas.1503683112]

27 **Menezes SV**, Kovacevic Z, Richardson DR. The metastasis suppressor NDRG1 down-regulates the epidermal growth factor receptor *via* a lysosomal mechanism by up-regulating mitogen-inducible gene 6. *J Biol Chem* 2019; **294**: 4045-4064 [PMID: 30679310 DOI: 10.1074/jbc.RA118.006279]

28 **Kovacevic Z**, Chikhani S, Lui GY, Sivagurunathan S, Richardson DR. The iron-regulated metastasis suppressor NDRG1 targets NEDD4L, PTEN, and SMAD4 and inhibits the PI3K and Ras signaling pathways. *Antioxid Redox Signal* 2013; **18**: 874-887 [PMID: 22462691 DOI: 10.1089/ars.2011.4273]

29 **McCubrey JA**, Steelman LS, Abrams SL, Bertrand FE, Ludwig DE, Bäsecke J, Libra M, Stivala F, Milella M, Tafuri A, Lunghi P, Bonati A, Martelli AM. Targeting survival cascades induced by activation of Ras/Raf/MEK/ERK, PI3K/PTEN/Akt/mTOR and Jak/STAT pathways for effective leukemia therapy. *Leukemia* 2008; **22**: 708-722 [PMID: 18337766 DOI: 10.1038/leu.2008.27]

30 **Hu ZY**, Xie WB, Yang F, Xiao LW, Wang XY, Chen SY, Li ZG. NDRG1 attenuates epithelial-mesenchymal transition of nasopharyngeal cancer cells *via* blocking Smad2 signaling. *Biochim Biophys Acta* 2015; **1852**: 1876-1886 [PMID: 26071641 DOI: 10.1016/j.bbadis.2015.06.009]

31 **Luo Q**, Wang CQ, Yang LY, Gao XM, Sun HT, Zhang Y, Zhang KL, Zhu Y, Zheng Y, Sheng YY, Lu L, Jia HL, Yu WQ, Liu J, Dong QZ, Qin LX. FOXQ1/NDRG1 axis exacerbates hepatocellular carcinoma initiation *via* enhancing crosstalk between fibroblasts and tumor cells. *Cancer Lett* 2018; **417**: 21-34 [PMID: 29248714 DOI: 10.1016/j.canlet.2017.12.021]

32 **Zhao K**, Zhao Y, Zhu JY, Dong H, Cong WM, Yu Y, Wang H, Zhu ZZ, Xu Q. A Panel of Genes Identified as Targets for 8q24.13-24.3 Gain Contributing to Unfavorable Overall Survival in Patients with Hepatocellular Carcinoma. *Curr Med Sci* 2018; **38**: 590-596 [PMID: 30128866 DOI: 10.1007/s11596-018-1918-x]

33 **Liu Y**, Wang D, Li Y, Yan S, Dang H, Yue H, Ling J, Chen F, Zhao Y, Gou L, Tang P, Huang A, Tang H. Long noncoding RNA CCAT2 promotes hepatocellular carcinoma proliferation and metastasis through up-regulation of NDRG1. *Exp Cell Res* 2019; **379**: 19-29 [PMID: 30922920 DOI: 10.1016/j.yexcr.2019.03.029]

34 **Zhang JZ**, Liu ZL, Zhang YX, Lin HJ, Zhang ZJ. Lipoxin A4 Ameliorates Lipopolysaccharide-Induced A549 Cell Injury through Upregulation of N-myc Downstream-Regulated Gene-1. *Chin Med J (Engl)* 2018; **131**: 1342-1348 [PMID: 29786049 DOI: 10.4103/0366-6999.232788]

35 **Dai T**, Dai Y, Murata Y, Husni RE, Nakano N, Sakashita S, Noguchi M. The prognostic significance of N-myc downregulated gene 1 in lung adenocarcinoma. *Pathol Int* 2018; **68**: 224-231 [PMID: 29431240 DOI: 10.1111/pin.12644]

36 **Chiang CT**, Demetriou AN, Ung N, Choudhury N, Ghaffarian K, Ruderman DL, Mumenthaler SM. mTORC2 contributes to the metabolic reprogramming in EGFR tyrosine-kinase inhibitor resistant cells in non-small cell lung cancer. *Cancer Lett* 2018; **434**: 152-159 [PMID: 30036610 DOI: 10.1016/j.canlet.2018.07.025]

37 **Li A**, Zhu X, Wang C, Yang S, Qiao Y, Qiao R, Zhang J. Upregulation of NDRG1 predicts poor outcome and facilitates disease progression by influencing the EMT process in bladder cancer. *Sci Rep* 2019; **9**: 5166 [PMID: 30914736 DOI: 10.1038/s41598-019-41660-w]

38 **Kawahara A**, Akiba J, Hattori S, Yamaguchi T, Abe H, Taira T, Ureshino H, Murakami Y, Watari K, Koufuji K, Shirouzu K, Kuwano M, Ono M, Kage M. Nuclear expression of N-myc downstream regulated gene 1/Ca(2+)-associated protein 43 is closely correlated with tumor angiogenesis and poor survival in patients with gastric cancer. *Exp Ther Med* 2011; **2**: 471-479 [PMID: 22977527 DOI: 10.3892/etm.2011.222]

39 **Ureshino H**, Murakami Y, Watari K, Izumi H, Kawahara A, Kage M, Arao T, Nishio K, Yanagihara K, Kinoshita H, Kuwano M, Ono M. N-myc downstream regulated gene 1 (NDRG1) promotes metastasis of human scirrhous gastric cancer cells through epithelial mesenchymal transition. *PLoS One* 2012; **7**: e41312 [PMID: 22844455 DOI: 10.1371/journal.pone.0041312]

40 **Sharma A**, Mendonca J, Ying J, Kim HS, Verdone JE, Zarif JC, Carducci M, Hammers H, Pienta KJ, Kachhap S. The prostate metastasis suppressor gene NDRG1 differentially regulates cell motility and invasion. *Mol Oncol* 2017; **11**: 655-669 [PMID: 28371345 DOI: 10.1002/1878-0261.12059]

41 **Chiang KC**, Yang SW, Chang KP, Feng TH, Chang KS, Tsui KH, Shin YS, Chen CC, Chao M, Juang HH. Caffeic Acid Phenethyl Ester Induces *N*-myc Downstream Regulated Gene 1 to Inhibit Cell Proliferation and Invasion of Human Nasopharyngeal Cancer Cells. *Int J Mol Sci* 2018; **19** [PMID: 29738439 DOI: 10.3390/ijms19051397]

42 **Lee JC**, Chiang KC, Feng TH, Chen YJ, Chuang ST, Tsui KH, Chung LC, Juang HH. The Iron Chelator, Dp44mT, Effectively Inhibits Human Oral Squamous Cell Carcinoma Cell Growth in Vitro and in Vivo. *Int J Mol Sci* 2016; **17** [PMID: 27589737 DOI: 10.3390/ijms17091435]

43 **Vaes N**, Schonkeren SL, Brosens E, Koch A, McCann CJ, Thapar N, Hofstra RMW, van Engeland M, Melotte V. A combined literature and in silico analysis enlightens the role of the NDRG family in the gut. *Biochim Biophys Acta Gen Subj* 2018; **1862**: 2140-2151 [PMID: 30033230 DOI: 10.1016/j.bbagen.2018.07.004]

44 **Song Y**, Lv L, Du J, Yue L, Cao L. Correlation of N-myc downstream-regulated gene 1 subcellular localization and lymph node metastases of colorectal neoplasms. *Biochem Biophys Res Commun* 2013; **439**: 241-246 [PMID: 23973486 DOI: 10.1016/j.bbrc.2013.08.049]

45 **Aikemu B**, Shao Y, Yang G, Ma J, Zhang S, Yang X, Hong H, Yesseyeva G, Huang L, Jia H, Wang C, Zang L, Sun J, Zheng M. NDRG1 regulates Filopodia-induced Colorectal Cancer invasiveness *via* modulating CDC42 activity. *Int J Biol Sci* 2021; **17**: 1716-1730 [PMID: 33994856 DOI: 10.7150/ijbs.56694]

46 **Wei M**, Zhang Y, Yang X, Ma P, Li Y, Wu Y, Chen X, Deng X, Yang T, Mao X, Qiu L, Meng W, Zhang B, Wang Z, Han J. Claudin-2 promotes colorectal cancer growth and metastasis by suppressing NDRG1 transcription. *Clin Transl Med* 2021; **11**: e667 [PMID: 34965023 DOI: 10.1002/ctm2.667]

47 **Yang G**, Huang L, Jia H, Aikemu B, Zhang S, Shao Y, Hong H, Yesseyeva G, Wang C, Li S, Sun J, Zheng M, Ma J. NDRG1 enhances the sensitivity of cetuximab by modulating EGFR trafficking in colorectal cancer. *Oncogene* 2021; **40**: 5993-6006 [PMID: 34385595 DOI: 10.1038/s41388-021-01962-8]

World Journal of Gastrointestinal Oncology

Submit a Manuscript: https://www.f6publishing.com

World J Gastrointest Oncol 2022 December 15; 14(12): 2329-2339

DOI: 10.4251/wjgo.v14.i12.2329

ISSN 1948-5204 (online)

ORIGINAL ARTICLE

Basic Study

Expression of nucleus accumbens-1 in colon cancer negatively modulates antitumor immunity

Zhao-Hua Shen, Wei-Wei Luo, Xing-Cong Ren, Xiao-Yan Wang, Jin-Ming Yang

Specialty type: Medicine, general and internal

Provenance and peer review: Unsolicited article; Externally peer reviewed.

Peer-review model: Single blind

Peer-review report's scientific quality classification

Grade A (Excellent): 0
Grade B (Very good): 0
Grade C (Good): C, C
Grade D (Fair): 0
Grade E (Poor): 0

P-Reviewer: Bondre MF, Oman; Kirkik D, Turkey

Received: July 10, 2022
Peer-review started: July 10, 2022
First decision: September 26, 2022
Revised: October 16, 2022
Accepted: November 21, 2022
Article in press: November 21, 2022
Published online: December 15, 2022

Zhao-Hua Shen, Wei-Wei Luo, Xiao-Yan Wang, Department of Gastroenterology, Third Xiangya Hospital, Central South University, Changsha 410013, Hunan Province, China

Xing-Cong Ren, Jin-Ming Yang, Department of Cancer Biology and Toxicology, University of Kentucky College of Medicine, Lexington, MA 40506, United States

Corresponding author: Jin-Ming Yang, Doctor, Academic Editor, Department of Cancer Biology and Toxicology, University of Kentucky College of Medicine, 101 Main Building Lexington, MA 40506, United States. yangjinming285@sina.com

Abstract

BACKGROUND

Nucleus accumbens-1 (NAC-1) is highly expressed in a variety of tumors, including colon cancer, and is closely associated with tumor recurrence, metastasis, and invasion.

AIM

To determine whether and how NAC-1 affects antitumor immunity in colon cancer.

METHODS

NAC-1-siRNA was transfected into RKO colon cancer cells to knock down NAC expression; tumor cells with or without knockdown of NAC-1 were treated with $CD8^+$T cells to test their cytocidal effect. The level of the immune checkpoint programmed death receptor-1 ligand (PD-L1) in colon cancer cells with or without knockdown of NAC-1 was analyzed using Quantitative real-time polymerase chain reaction and Western blotting. A double luciferase reporter assay was used to examine the effects of NAC-1 on the transcription of PD-L1. Mice bearing MC-38-OVA colon cancer cells expressing NAC-shRNA or control-shRNA were treated with OT-I mouse $CD8^+$T cells to determine the tumor response to immunotherapy. Immune cells in the tumor tissues were analyzed using flow cytometry. NAC-1, PD-L1 and $CD8^+$T cells in colon cancer specimens from patients were examined using immunohistochemistry staining.

RESULTS

Knockdown of NAC-1 expression in colon cancer cells significantly enhanced the cytocidal effect of $CD8^+$T cells in cell culture experiments. The sensitizing effect of NAC-1 knockdown on the antitumor action of cytotoxic $CD8^+$T cells was recapit-

ulated in a colon cancer xenograft animal model. Furthermore, knockdown of NAC-1 in colon cancer cells decreased the expression of PD-L1 at both the mRNA and protein levels, and this effect could be rescued by transfection of an RNAi-resistant NAC-1 expression plasmid. In a reporter gene assay, transient expression of NAC-1 in colon cancer cells increased the promoter activity of PD-L1, indicating that NAC-1 regulates PD-L1 expression at the transcriptional level. In addition, depletion of tumoral NAC-1 increased the number of $CD8^+$ T cells but decreased the number of suppressive myeloid-derived suppressor cells and regulatory T cells.

CONCLUSION
Tumor expression of NAC-1 is a negative determinant of immunotherapy.

Key Words: Nucleus accumbens-1; Colon cancer; Tumor immunity; Programmed death receptor-1/programmed death receptor-1 ligand; CD8+T cells

Core Tip: We determined whether and how nucleus accumbens-1 (NAC-1) affects antitumor immunity in colon cancer. Knockdown of NAC-1 expression in colon cancer cells significantly enhanced the cytocidal effect of $CD8^+$ T cells. Knockdown of NAC-1 in colon cancer cells decreased the expression of programmed death receptor-1 ligand. Depletion of tumoral NAC-1 increased the amount of $CD8^+$ T cells but decreased the amount of suppressive myeloid-derived suppressor cells and regulatory T cells. It comes to a conclusion that tumoral expression of NAC-1 is a negative determinant of immunotherapy.

Citation: Shen ZH, Luo WW, Ren XC, Wang XY, Yang JM. Expression of nucleus accumbens-1 in colon cancer negatively modulates antitumor immunity. *World J Gastrointest Oncol* 2022; 14(12): 2329-2339
URL: https://www.wjgnet.com/1948-5204/full/v14/i12/2329.htm
DOI: https://dx.doi.org/10.4251/wjgo.v14.i12.2329

INTRODUCTION

Upregulation of nucleus accumbens-1 (NAC-1), a member of the Bric-a-brac/poxvirus and zinc finger (BTB/POZ) family, has been reported in a variety of cancers, including colorectal cancer, pancreatic cancer, and breast cancer[1]. The expression of NAC-1 is associated with cancer invasion, recurrence, proliferation and metastasis[2,3] and is related to patient survival, disease severity and prognosis[4,5]. We previously showed that NAC-1 could affect the expression of high mobility group box-1 protein (HMGB1) to promote autophagy and cisplatin resistance in ovarian cancer and NAC-1 dysfunction can promote cell senescence and block tumor cell proliferation and canceration[6,7]. In recent years, immunotherapy has achieved impressive progress in the treatment of various cancers; however, its clinical outcome remains unsatisfactory due to a variety of factors, including coinhibltory signals that can inhibit anticancer immunity. Immune checkpoint proteins such as programmed death receptor-1 (PD-1) have an important role in dampening the antitumor immune response. In this study, we found that tumoral expression of NAC-1 can negatively modulate the antitumor immune response, which is likely associated with its promotive effect on PD-1 ligand (PD-L1) transcription, suppressive myeloid-derived suppressor cells (MDSCs) and regulatory T cells (Tregs) in the tumor microenvironment. Our study suggests that targeting tumoral NAC-1 may be explored as a potential therapeutic strategy to enhance cancer immunotherapy.

MATERIALS AND METHODS

Mice, cells and clinical specimens

The human colon cancer cell line RKO was purchased from ATCC, and the mouse colon cancer cell line MC-38 transfected with ovalbumin (OVA) into MC-38 cells was a gift from the Department of Immunology, University of Pennsylvania School of Medicine. The cell line was cultured using DMEM (HyClone, United States). Construction of the NAC-1 knockout MC-38-OVA stable transfection cell line: SuperFect® Transfection Reagent (QIAGEN) was used to transfer NAC-1 shRNA and control plasmids into MC-38-OVA mouse colon cancer cells to culture for 72 h. Puromycin (PM) (0, 1.0, 2.5, 5.0, 7.5, and 10.0 μg/mL) (GEMINI, United States) was added for treatment for 7-10 d, and the culture containing puromycin was replaced every two days. The concentration of puromycin at which all cells died at 3 d

was selected as the optimal screening concentration.

Human $CD8^+$ T cells were purchased from the Immunology Laboratory of the University of Pennsylvania. The cells were placed in a 24-well plate precoated with CD3 antibody (2 μg/mL) (Biolegend), CD8 (5 μg/mL) (Biolegend) and IL-2 (100 U/mL) (Biolegend) and activated for approximately 3 d for use. Eight-week-old OT-I mice were euthanized, and then the spleens were removed, cleavage red blood cells were lysed, and CD8 immunomagnetic beads (EasySepTM) were used to isolate $CD8^+$ T cells from OT-I mice. The activation method is the same as above.

All procedures involving animals were reviewed and approved by the IRB of Third Xiangya Hospital, Central South University (No. 2020-S298). Wild-type C57BL/6 mice and OT-I mice were purchased from The Jackson Laboratory and the Experimental Animal Center of Xiangya Medical College, Central South University and were raised in a specific pathogen-free (SPF) laboratory. The study followed the guidelines for the Care and Use of Laboratory Animals published by the National Institutes of Health (NIH).

Clinical specimens were collected from 20 patients with colon cancer admitted to the Third Xiangya Hospital of Central South University in Changsha, Hunan Province, from 2018.01-2018.12. Thirteen out of 20 patients were older than 60 years. Seven patients were younger than 60 years. Out of 20 patients, 11 were female, and 9 were male. The TNM stage of the patients was stage I-II for 15 patients and III-IV for 5 patients. Ten patients had a tumor of a size of less than 5 cm, while the other 10 patients had a tumor larger than 5 cm. The tumor tissues were removed, fixed, dehydrated, paraffin embedded, and sectioned for later use. All clinical specimens were collected with informed consent from the patients.

siRNA and plasmid transfection

siRNA transfection: Colon cells were made into a single cell suspension and seeded in a six-well plate at 5×10^5 cells/well. After adherence, a mixture of transfection reagent and NAC-1-siRNA was prepared. The whole experimental process was carried out strictly in accordance with the liposome 3000 (Lipofectamine 3000, Lipo3000) transfection reagent instructions, and the experiment was repeated at least 3 times. See Table 1 for the siRNA sequence required for the experiment.

Transient expression plasmid transfection: The plasmid was thoroughly mixed with SuperFect® Transfection Reagent (Roche), allowed to stand for 15 min, and replaced with fresh culture medium.

CytoTox 96® nonradioactive cytotoxicity assay

Different concentration ratios (1:1, 2:1, 5:1, 10:1) of $CD8^+$ T cells were cocultured with RKO and RKO NAC-1-siRNA human colon cancer cells for 12 h, and the supernatant was collected for the detection of cytotoxicity, which was carried out according to the instructions of the kit (Promega).

Quantitative real-time polymerase chain reaction

After collecting the cells, TRIzol reagent was used to extract the total RNA of the cells, which was then reverse transcribed to synthesize cDNA, which was used as a template for real-time polymerase chain reaction (PCR). The PCR sequence required for the experiment is shown in Table 2.

Western blot

After collecting the cells, RIPA lysis buffer was used to extract the total protein, and the protein concentration was determined. The total protein sample was loaded, SDS-PAGE electrophoresis was performed, and the membrane was transferred and blocked with 5% skimmed milk powder. Then, PD-L1 antibody (Proteintech) was added and incubated overnight at 4 °C. After washing, anti-rabbit or anti-mouse secondary antibody was added and incubated for 1 h. After washing and exposure, ImageJ software was used to analyze the gray value of the band, and the relative expression of the target protein was expressed as the ratio of the gray value of the band to the gray value of the internal reference band.

Dual-luciferase reporter assay

The classic PD-L1 transcriptional regulators, including STAT1/3, STAT2/5 and IRF-1, are mainly located within -400 bp of the PD-L1 promoter region[8]. Based on this, we constructed a luciferase plasmid containing the PD-L1 classic transcription factor binding segment (from -456 bp to -1 bp) and PD-L1 full promoter region to investigate whether NAC-1 can enhance the promoter region transcription of the PD-L1 segment. We transfected colon cancer cells into Renilla plasmid, luciferase plasmid, and pcDNA3.1-NACC1 transient expression plasmid or the corresponding empty load. After 48 h of culture, the cells were lysed, and the fluorescence value was measured by the dual luciferase method. The fluorescence value of Renilla was used as a reference. Then, the transcriptional activity of the corresponding segment of the PD-L1 promoter was obtained.

Experimental design and animal groups

The experiment was divided into 6 groups: The control group, NAC-1-KD group, control + CTLs group, NAC-1-KD + CTLs group, control + CTLs + MEKi group, and NAC-1-KD + CTLs + MEKi group. Each group had 6 mice (3 males and 3 females) that were 8 wk old.

Table 1 siRNA sequences used in gene knockdown

Gene name		Primer sequence (5'→3')
Negative control	Sense	UUCUCCGAACGUGUCACGUTT
	Anti-sence	ACGUGACACGUUCGGAGAATT
siNAC-1	Sense	GGACAUGAUGAGCAUGGAATT
	Anti-sence	UUCCAUGCUCAUCAUGUCCTT
siCD274	Sense	GAGGAAGACCUGAAGGUUCAGCAUA
	Anti-sence	UAUGCUGAACCUUCAGGUCUUCCUC

NAC-1: Nucleus accumbens-1.

Table 2 Human primers used in quantitative real-time-polymerase chain reaction

Gene name		Primer sequence (5'→3')
NAC-1	Forward	TTCTTTGACCGGAACACGCT
	Reverse	TGGCATTCATCTCGCTCTCC
PD-L1	Forward	CCCTAATTTGAGGGTCAGTTCCT
	Reverse	CTCAGTCATGCAGAAAACAAATTGA
GAPDH	Forward	GACAGTCAGCCGCATCTTCT
	Reverse	TTAAAAGCAGCCCTGGTGAC

NAC-1: Nucleus accumbens-1; PD-L1: Programmed death receptor-1 ligand.

Construction of a homogenous subcutaneous tumor model: A total of 100 μL of 1 × 10^6 colon cancer cells was slowly injected into the right flanks of mice. The size of the mouse subcutaneous tumor was observed and measured [calculation method of tumor volume: tumor volume= (length × $width^2$) × 0.52].

Treatment group: When the tumor volume reached 200 mm^3, $CD8^+$ T cells were injected in the tail vein at a quantity of 4 × 10^6 per mouse, or cobimetinib at 7.5 mg/kg was injected intraperitoneally 3 times a week. When the tumor volume reached 1800 mm^3, the mice were sacrificed.

Flow cytometry

After the mice were euthanized, the tumor tissue was removed to prepare a cell suspension and stained with PE-conjugated anti-CD3, APC-conjugated anti-CD45, and BV650-conjugated anti-CD8 antibodies (BioLegend, United States). CD3- and CD45-positive cells were detected by an LSRII flow cytometer (BD), and then $CD8^+$ positive cells were chosen. The cells were stained with APC-Gr-1 and FITC-conjugated anti-CD11b antibodies, and the proportion of MDSCs was detected by flow cytometry. Then, the samples were treated with predigested solution (1 × HBSS + 5 mmol/L EDTA + 1 mmol/L DTT) and with digestive solution (1 ×, containing type IV collagenase (1 mg/mL, Sigma), hyaluronidase (1%, Sigma), DNase I (0.25%, Sigma) to digest the tissues. Percoll was further purified and then stained with FITC-conjugated anti-CD4 and APC-conjugated anti-CD25 antibodies (Biolegend, United States). After breaking the nucleus and staining with PE-Foxp3 antibody (Biolegend, United States), flow cytometry was used to detect the proportion of $CD4^+$ $CD25^+$ $Foxp3^+$ triple-positive cells.

Immunohistochemistry

Tumor tissue and adjacent tissue samples from colon cancer patients were immersed in 4% formaldehyde and fixed for more than 48 h. The tissue was dehydrated in a dehydrator, embedded in paraffin, and the paraffin was sectioned to obtain a section with a thickness of 4 μm. The slices were boiled in sodium citrate repair solution (pH 6.0, Google Bio, Wuhan, Hubei Province, China) for 17 min and cooled at room temperature. Then, the sections were incubated with NAC-1, CD274, and CD8 antibodies at 4 °C overnight and incubated with the corresponding secondary antibody (Google Bio, Wuhan, China) for 15 min. Then, a DAB kit (Mixin Biotechnology Development Company, Fuzhou, Fujian Province, China) was used to develop color.

Statistical analysis

GraphPad Prism 6 was used to statistically analyze the data. A significant difference between the two groups was determined by Student's-test, and the statistical data of 3 groups or more was determined by one-way ANOVA. NS, $P > 0.05$, $^{a}P < 0.05$, $^{b}P < 0.01$, and $^{c}P < 0.001$. The correlation analysis of NAC-1, PD-L1 and CD8 expression adopted the Pearson correlation coefficient test. Among them, the correlation coefficient $r = 0.0$-0.2 is a very weak correlation or no correlation, $r = 0.2$-0.4 is a weak correlation, $r = 0.4$-0.6 is a medium degree correlation, $r = 0.6$-0.8 is a strong correlation, and $r = 0.8$-1.0 is a very strong degree correlation. Pearson's significance test $P < 0.05$ indicates that the correlation between the two variables is statistically significant.

RESULTS

Knockdown of NAC-1 sensitizes colon cancer cells to the cytocidal effect of CD8$^+$ T cells In vitro and in vivo

To determine whether the expression of NAC-1 in colon cancer cells affects their response to cytotoxic CD8$^+$ T cells, we cocultured CD8$^+$ T cells with RKO colon cancer cells with or without NAC-1 knockdown, and at the end of treatment, the killing effect of CD8$^+$ T cells was analyzed using the CytoTox 96® assay. Figure 1A shows that knockdown of NAC-1 in cancer cells significantly enhanced the toxicity of CD8$^+$ T cells compared with the control.

To recapitulate the effect of tumoral NAC-1 on the cytotoxicity of CD8$^+$ T cells *in vivo*, we inoculated C57BL/6 homologous mice subcutaneously with MC-38-OVA colon cancer cells transfected with NAC-1-shRNA or control shRNA. CD8$^+$ T cells isolated from the spleen of OT-I mice that can recognize OVA were then injected into the mouse subcutaneously. Figure 1B shows that the growth of tumors with depletion of NAC-1 was slower than that of NAC-1-expressing tumors in the absence or presence of CTLs; cotreatment with CTLs and cobimetinib, a small molecule inhibitor of MEK1, further inhibited tumor growth in mice.

Effect of NAC-1 on the expression of PD-L1

To explore how NAC-1 affects the tumor response to CTLs, we next determined the effect of NAC-1 on the expression of PD-L1, an immune checkpoint protein that inhibits the killing effect of CTLs. We found that knockdown of NAC-1 reduced the expression of PD-L1 at both the transcriptional and translational levels, as evidenced by the decreased mRNA and protein levels of PD-L1 (Figure 2A and B). To validate the effect of NAC-1 on PD-L1, we assessed whether the RNAi-resistant NAC-1 expression plasmid could rescue the effect of siRNA on PD-L1 expression. Figure 2C and D shows that transfection of RNAi-resistant cells blocked the silencing effect of NAC-1 siRNA. These results demonstrate that NAC-1 has a positive role in regulating the expression of PD-L1. To explore the mechanism by which NAC-1 regulates the expression of PD-L1, we constructed a luciferase plasmid containing the full PD-L1 promoter region and the transcription factor binding segment. We showed that transient expression of the NAC-1 plasmid in colon cancer cells increased the promoter activity of PD-L1 (Figure 2E and F), suggesting that NAC-1 promotes PD-L1 expression at the transcriptional level.

Effect of NAC-1 on the tumor immune microenvironment

Tumoral expression of NAC-1 also affects immune cells in the tumor microenvironment (TME) of colon cancer. Using flow cytometry, we analyzed the proportions of CD8$^+$T cells, MDSCs, a group of heterogeneous cells derived from bone marrow that have the ability to suppress CD8$^+$ T-cell function, and Tregs, a subpopulation of T cells that can exert a negative immunomodulatory effect by directly contacting target cells or secreting TGF-β/IL-10 in tumor tissues. Our results showed that in the tumors subjected to depletion of NAC-1, CD8$^+$ T cells were significantly increased (Figure 3A and B), whereas MDSCs were significantly decreased, as evidenced by reductions in Gr-1$^+$ CD11b$^+$ cells (Figure 3C and D), when treated with CTLs and MEK inhibitor. Tregs were also reduced in NAC-depleted tumor tissues, as determined by significant decreases in CD4$^+$CD25$^+$ Foxp3$^+$ cells (Figure 3E and F). These results suggest that the expression of NAC-1 in colon cancer may suppress antitumor immunity *via* its effects on immune cells in the TME.

NAC-1, PD-L1, and CD8 expression in patients

To investigate the clinical implications of tumor NAC-1 in immunotherapy, we analyzed the correlations between NAC-1, PD-L1 and CD8 T cells using paraffin embedding and serial sectioning of tumor tissues and adjacent tissues from 20 colon cancer patients. Immunohistochemical staining was performed, and Image-Pro Plus software was used to quantitatively analyze the integrated optical density (IOD) of NAC-1- and PD-L1-positive areas. The IOD of the positive area was divided by the IOD of the entire area to obtain the positive protein expression rate. Taking the average of the positive expression rates of NAC-1 and PD-L1 proteins, a 0.00-0.25 positive rate is expressed as +, a 0.25-0.50 positive rate is expressed as + + , and a positive rate above 0.50 is expressed as + + +[9]. The results

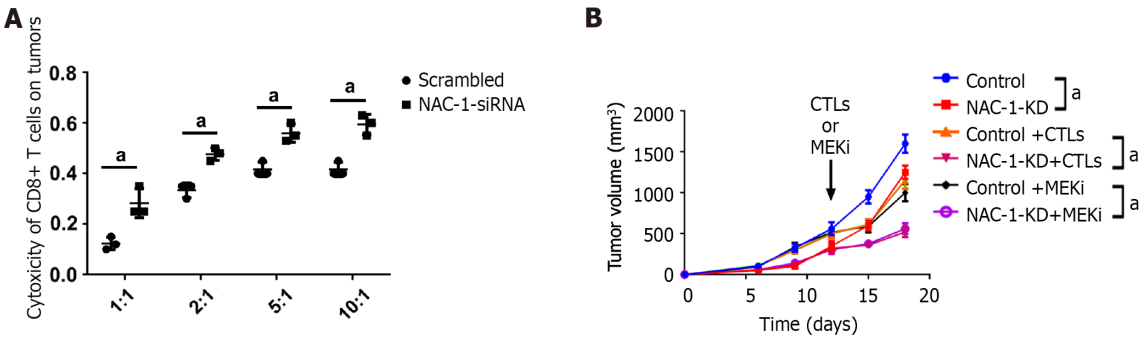

DOI: 10.4251/wjgo.v14.i12.2329 **Copyright** ©The Author(s) 2022.

Figure 1 *In vitro* and *in vivo* cytotoxicity experiments of nucleus accumbens-1 on colon cancer cells. A: The effect of nucleus accumbens-1 (NAC-1) on the toxicity of CD8⁺ T cells on the colon cancer cell line RKO; B: The effects of NAC-1, CD8⁺ T cells and MEK inhibitors on tumor killing *in vivo* ($^aP < 0.05$). NAC-1: Nucleus accumbens-1.

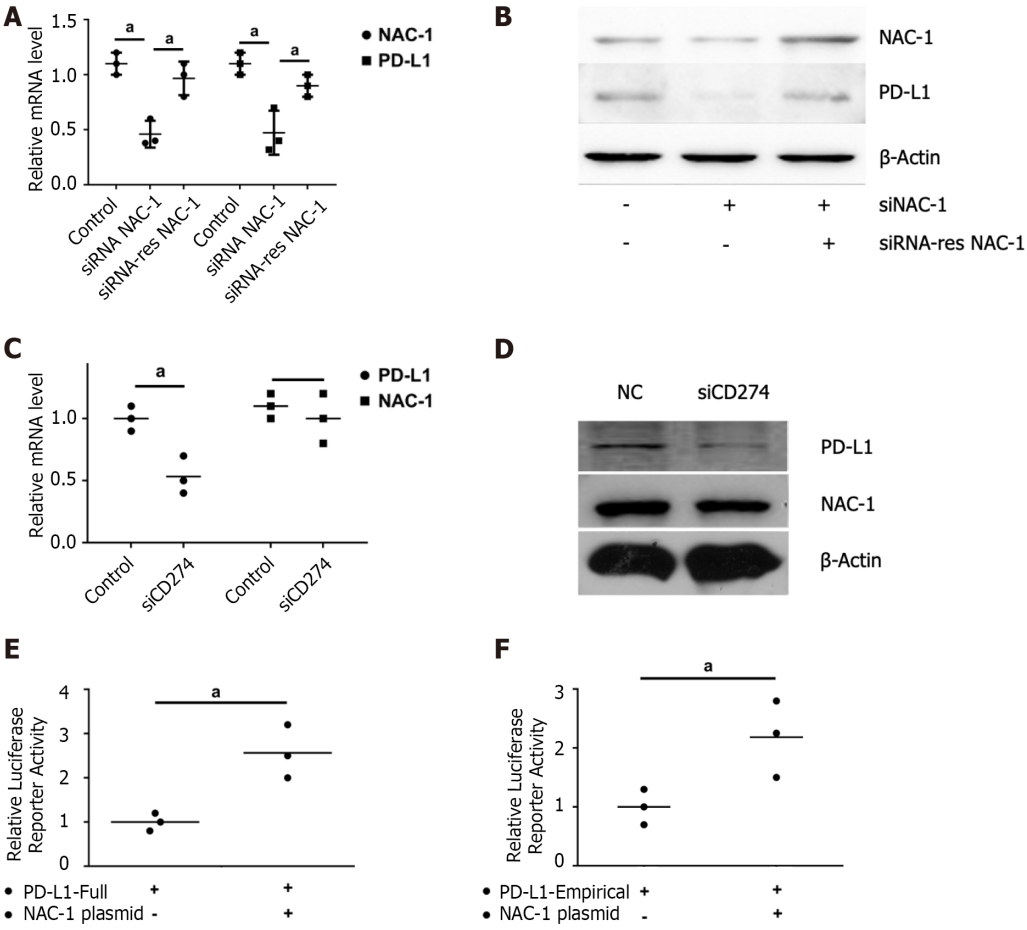

DOI: 10.4251/wjgo.v14.i12.2329 **Copyright** ©The Author(s) 2022.

Figure 2 Effect of nucleus accumbens-1 on the expression of programmed death receptor-1 ligand. A: Effect of nucleus accumbens-1 (NAC-1) on the mRNA expression of programmed death receptor-1 ligand (PD-L1); B: Effect of NAC-1 on the protein expression of PD-L1; C: The effect of PD-L1 on the transcription level of NAC-1; D: The effect of PD-L1 on the translation level of NAC-1; E: The effect of NAC-1 on the full promoter region of PD-L1; F: The effect of NAC-1 on the PD-L1 classic transcription factor binding segment (1:1, 2:1, 5:1, 10:1 are the ratios of CD8⁺ T cells to RKO; $^aP < 0.05$). NAC-1: Nucleus accumbens-1; PD-L1: Programmed death receptor-1 ligand.

showed that compared with adjacent tissues, the expression of NAC-1 and PD-L1 in colon cancer tissues was increased, and the expression of CD8 was decreased ($P < 0.05$) (Figure 4). These results suggest that the expression of NAC-1 in colon cancer may be further studied as a potential predictive biomarker for immunotherapy.

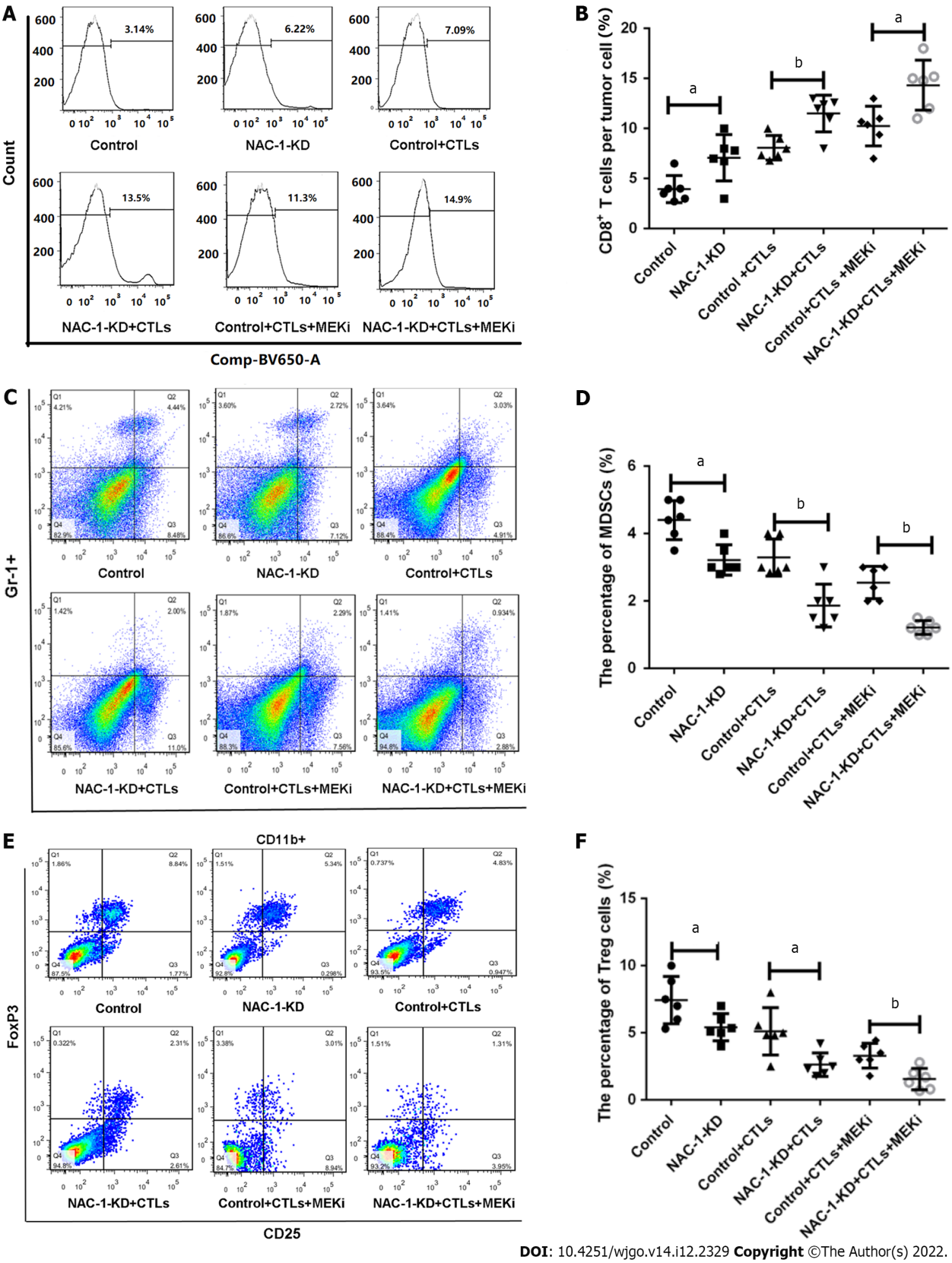

DOI: 10.4251/wjgo.v14.i12.2329

Figure 3 The effect of nucleus accumbens-1 on CD8⁺ T cells, myeloid-derived suppressor cells and regulatory T cells in the mouse colon cancer tumor microenvironment. A: Flow cytometric detection of the effects of nucleus accumbens-1 (NAC-1), CD8⁺ T cells and MEK inhibitors on the expression of CD8⁺ T cells; B: Statistical analysis of CD8⁺ T-cell expression levels in each group; C: Flow cytometric detection of the effect of NAC-1 on the expression of myeloid-derived suppressor cells (MDSCs); D: Statistical analysis of the expression of MDSCs in each group; E: Flow cytometric detection of the effect of NAC-1 on the expression of regulatory T cell (Treg) cells; F: Statistical analysis of Treg expression in each group ($^aP < 0.05$, $^bP < 0.01$). NAC-1: Nucleus accumbens-1.

DISCUSSION

In this study, we showed that knockdown of NAC-1 in colon cancer cells can enhance the cytocidal activity of $CD8^+$ T cells and reduce the expression of PD-L1. The combination of $DR8^+$ T cells with a MEK inhibitor further increases the antitumor immune response. In a colon cancer animal model, we showed that colon cancer deficient in NAC-1 was more sensitive to CTLs. This might be associated with the decreases in PD-L1 and suppressive immune cells in the TME. We further demonstrated that NAC-1 modulates PD-L1 expression at the transcriptional level.

Nucleus accumbens-associated protein 1 (NACC1) is a potential cancer-related gene that can regulate the expression of the cell transcription factor NAC-1. The expression of NAC-1 is elevated in colon cancer and other malignant tumors. NAC-1 is a transcription factor, a member of the BTB/POZ family, and is closely related to tumor occurrence, development, proliferation, and apoptosis[10]. NAC-1 modulates autoimmunity by suppressing regulatory T cell–mediated tolerance[11].

Tumor immunity is a current research hotspot. Tumor immunotherapy that targets immune checkpoints has attracted increasing attention. Immune checkpoints are molecules that play a protective function in the body's immune system. The activation of T lymphocytes requires activation signals regulated by costimulatory molecules. At the same time, there are coinhibitory molecules on the surface of T cells. After they bind to the corresponding ligands, they can inhibit the activation and function of T cells. These coinhibitory molecules are called immune checkpoints[12]. Various tumor cells use this feature to escape the body's immune monitoring, thereby promoting the proliferation of tumor cells. Immune checkpoints include CTLA-4, PD-1/PD-L1, LMTK3, Fibrinogen-like protein 1 (FGL1)[13,14].

Previous research found that NAC-1 can affect the tumor microenvironment, but there is no research regarding colon cancer. We used colon cancer cell and $CD8^+$ T-cell coculture experiments. The results suggest that NAC-1 knockdown can enhance the toxicity of $CD8^+$ T cells to colon cancer cells and further indicate that NAC-1 may affect the body's tumor immunity. How does NAC-1 affect the body's tumor immunity? The immune checkpoint is a very important molecule in tumor immunity. An increasing number of immune checkpoint inhibitors are being used in clinical research, including PD-1 antibodies and PD-L1 antibodies, in the treatment of colon cancer. Targeting PD-L1 is related to a significant clinical response in many cancer patients[15]. Therefore, does NAC-1 affect immune checkpoints, especially PD-L1, which has great clinical application value? The results of the study found that NAC-1 can positively regulate the expression of PD-L1 and may increase its expression by promoting the transcription of the classic transcription factor binding segment of PD-L1.

We found at the cellular level that NAC-1 can inhibit the toxicity of CTLs to colon cancer by upregulating the immune checkpoint PD-L1. Is there a similar function in the mouse animal model? We constructed a subcutaneous tumor model with NAC-1 knockdown and found that NAC-1 can promote tumor growth and that $CD8^+$ T cells can exert a toxic effect to kill tumor cells. NAC-1 may downregulate the number of $CD8^+$ T cells and positively regulate the number of MDSCs and Treg cells, thereby suppressing tumor immunity. MDSCs are defined by their T cell immunosuppressive functions[15]. In addition, NAC-1 can inhibit the killing effect of $CD8^+$ T cells and MEKi on colon cancer.

At the tissue level, we explored the relationship between NAC-1, PD-L1, and CD8 through immunohistochemical detection of tumor tissues in colon cancer patients. Compared with adjacent tissues, the expression of NAC-1 and PD-L1 in colon cancer tissues increased, and the expression of CD8 decreased. The expression of NAC-1 and PD-L1 showed a positive correlation, and the expression of NAC-1 and CD8 showed a negative correlation. This further supports the conclusion that "NAC-1 promotes the expression of PD-L1 and reduces the toxicity of $CD8^+$ T cells and chemotherapeutic drugs to colon cancer".

CONCLUSION

In this project, we studied the impact of NAC-1 on the tumor microenvironment of colon cancer, explored its mechanism, explored its relationship with immune checkpoints, and further revealed its mechanisms of colon cancer regulation. This study provides a theoretical basis for the occurrence and development of colon cancer and tumor immunotherapy.

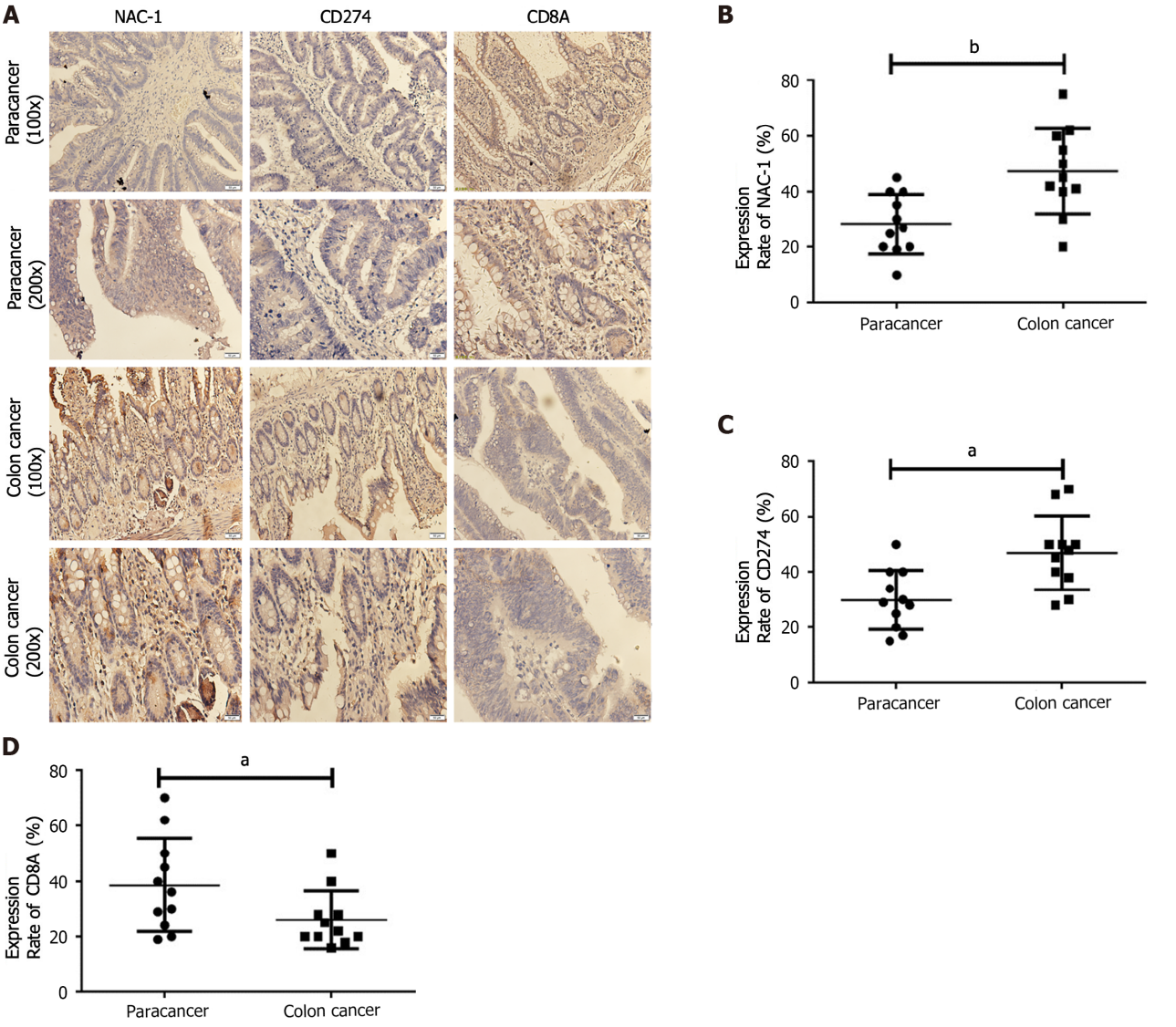

DOI: 10.4251/wjgo.v14.i12.2329

Figure 4 Exploring the relationship between nucleus accumbens-1, programmed death receptor-1 ligand and CD8 at the clinical level. A: Nucleus accumbens-1 (NAC-1), programmed death receptor-1 ligand (PD-L1), and CD8 staining results of typical tissue samples from several patients, scale bar = 50 μm; B: NAC-1 expression in tumor tissues and adjacent tissues; C: PD-L1 expression in tumor tissues and adjacent tissues; D: The expression of CD8 in tumor tissues and adjacent tissues. NAC-1: Nucleus accumbens-1.

ARTICLE HIGHLIGHTS

Research background

Nucleus accumbens-1 (NAC-1) is highly expressed in a variety of tumors, and is closely associated with tumor recurrence, metastasis, and invasion.

Research motivation

We determined whether and how NAC-1 affects antitumor immunity in colon cancer.

Research objectives

To determine whether and how NAC-1 affects tumor microenvironment in colon cancer.

Research methods

NAC-1-siRNA, cytocidal test, quantitative real-time polymerase chain reaction, and Western blotting, a double luciferase reporter assay were used.

Research results

Knockdown of NAC-1 expression in colon cancer cells significantly enhanced the cytocidal effect of

CD8$^+$ T cells in cell culture experiments. The sensitizing effect of NAC-1 knockdown on the antitumor action of cytotoxic CD8$^+$ T cells was recapitulated in a colon cancer xenograft animal model. Furthermore, knockdown of NAC-1 in colon cancer cells decreased the expression of PD-L1 at both the mRNA and protein levels, and this effect could be rescued by transfection of an RNAi-resistant NAC-1 expression plasmid. In a reporter gene assay, transient expression of NAC-1 in colon cancer cells increased the promoter activity of PD-L1, indicating that NAC-1 regulates PD-L1 expression at the transcriptional level. In addition, depletion of tumoral NAC-1 increased the number of CD8$^+$ T cells but decreased the number of suppressive myeloid-derived suppressor cells and regulatory T cells.

Research conclusions

Tumor expression of NAC-1 is a negative determinant of immunotherapy.

Research perspectives

Our study suggests that targeting tumoral NAC-1 may be explored as a potential therapeutic strategy to enhance cancer immunotherapy.

FOOTNOTES

Author contributions: Yang JM and Wang XY supervised the project and revised the manuscript; Shen ZH performed the *in vitro* and *in vivo* experiments, generated the figures, and revised the manuscript; Luo WW completed the analysis of the results; Ren XC contributed to the study design.

Supported by the Changsha Municipal Natural Science Foundation, No. kq2014258.

Institutional review board statement: The study was reviewed and approved by the IRB of Third Xiangya Hospital, Central South University (Approval No. 2020-S195).

Institutional animal care and use committee statement: All procedures involving animals were reviewed and approved by the IRB of Third Xiangya Hospital, Central South University (No. 2020-S298).

Informed consent statement: All study participants, or their legal guardian, provided informed written consent prior to study enrollment.

Conflict-of-interest statement: The authors declare that there are no conflicts of interest.

Data sharing statement: Data can be acquired from the corresponding author.

ARRIVE guidelines statement: The authors have read the ARRIVE Guidelines, and the manuscript was prepared and revised according to the ARRIVE Guidelines.

Country/Territory of origin: China

ORCID number: Zhao-Hua Shen 0000-0003-3518-8202; Wei-Wei Luo 0000-0003-3476-7376; Xiao-Yan Wang 0000-0003-0467-445; Jin-Ming Yang 0000-0002-7307-1649.

S-Editor: Chen YL
L-Editor: A
P-Editor: Zhang XD

REFERENCES

1 **Nakayama K**, Nakayama N, Davidson B, Sheu JJ, Jinawath N, Santillan A, Salani R, Bristow RE, Morin PJ, Kurman RJ, Wang TL, Shih IeM. A BTB/POZ protein, NAC-1, is related to tumor recurrence and is essential for tumor growth and survival. *Proc Natl Acad Sci U S A* 2006; **103**: 18739-18744 [PMID: 17130457 DOI: 10.1073/pnas.0604083103]
2 **Koob GF**. Drug addiction: the yin and yang of hedonic homeostasis. *Neuron* 1996; **16**: 893-896 [PMID: 8630244 DOI: 10.1016/s0896-6273(00)80109-9]
3 **Nakayama K**, Nakayama N, Miyazaki K. Development of a novel ovarian cancer molecular target therapy against cancer-related transcriptional factor, NAC1. *J Obstet Gynaecol Res* 2013; **39**: 18-25 [PMID: 22845777 DOI:

10.1111/j.1447-0756.2012.01946.x]

4 **Ishikawa M**, Nakayama K, Yeasmin S, Katagiri A, Iida K, Nakayama N, Miyazaki K. NAC1, a potential stem cell pluripotency factor expression in normal endometrium, endometrial hyperplasia and endometrial carcinoma. *Int J Oncol* 2010; **36**: 1097-1103 [PMID: 20372782 DOI: 10.3892/ijo_00000591]

5 **Yeasmin S**, Nakayama K, Ishibashi M, Katagiri A, Iida K, Purwana IN, Nakayama N, Miyazaki K. Expression of the bric-a-brac tramtrack broad complex protein NAC-1 in cervical carcinomas seems to correlate with poorer prognosis. *Clin Cancer Res* 2008; **14**: 1686-1691 [PMID: 18347169 DOI: 10.1158/1078-0432.CCR-07-4085]

6 **Zhang Y**, Cheng Y, Ren X, Zhang L, Yap KL, Wu H, Patel R, Liu D, Qin ZH, Shih IM, Yang JM. NAC1 modulates sensitivity of ovarian cancer cells to cisplatin by altering the HMGB1-mediated autophagic response. *Oncogene* 2012; **31**: 1055-1064 [PMID: 21743489 DOI: 10.1038/onc.2011.290]

7 **Zhang Y**, Cheng Y, Ren X, Hori T, Huber-Keener KJ, Zhang L, Yap KL, Liu D, Shantz L, Qin ZH, Zhang S, Wang J, Wang HG, Shih IeM, Yang JM. Dysfunction of nucleus accumbens-1 activates cellular senescence and inhibits tumor cell proliferation and oncogenesis. *Cancer Res* 2012; **72**: 4262-4275 [PMID: 22665267 DOI: 10.1158/0008-5472.CAN-12-0139]

8 **Lee SJ**, Jang BC, Lee SW, Yang YI, Suh SI, Park YM, Oh S, Shin JG, Yao S, Chen L, Choi IH. Interferon reguLatory factor-1 is prerequisite to the constitutive expression and IFN-gamma induced upregulation of B7-H1 (CD274). *FEBS Lett* 2006; **580**: 755-762 [PMID: 16413538 DOI: 10.1016/j.febslet.2005.12.093]

9 **Al-Batran SE**, Rafiyan MR, Atmaca A, Neumann A, Karbach J, Bender A, Weidmann E, Altmannsberger HM, Knuth A, Jäger E. Intratumoral T-cell infiltrates and MHC class I expression in patients with stage IV melanoma. *Cancer Res* 2005; **65**: 3937-3941 [PMID: 15867394 DOI: 10.1158/0008-5472.CAN-04-4621]

10 **Nakayama K**, Rahman MT, Rahman M, Yeasmin S, Ishikawa M, Katagiri A, Iida K, Nakayama N, Miyazaki K. Biological role and prognostic significance of NAC1 in ovarian cancer. *Gynecol Oncol* 2010; **119**: 469-478 [PMID: 20869761 DOI: 10.1016/j.ygyno.2010.08.031]

11 **Yang JM**, Ren Y, Kumar A, Xiong X, Das JK, Peng HY, Wang L, Ren X, Zhang Y, Ji C, Cheng Y, Zhang L, Alaniz RC, de Figueiredo P, Fang D, Zhou H, Liu X, Wang J, Song J. NAC1 modulates autoimmunity by suppressing regulatory T cell-mediated tolerance. *Sci Adv* 2022; **8**: eabo0183 [PMID: 35767626 DOI: 10.1126/sciadv.abo0183]

12 **Drake CG**, Lipson EJ, Brahmer JR. Breathing new Life into immunotherapy: review of melanoma, lung and kidney cancer. *Nat Rev Clin Oncol* 2014; **11**: 24-37 [PMID: 24247168 DOI: 10.1038/nrclinonc.2013.208]

13 **Qian W**, Zhao M, Wang R, Li H. Fibrinogen-like protein 1 (FGL1): the next immune checkpoint target. *J Hematol Oncol* 2021; **14**: 147 [PMID: 34526102 DOI: 10.1186/s13045-021-01161-8]

14 **Sacher AG**, Gandhi L. Biomarkers for the Clinical Use of PD-1/PD-L1 Inhibitors in Non-Small-Cell Lung Cancer: A Review. *JAMA Oncol* 2016; **2**: 1217-1222 [PMID: 27310809 DOI: 10.1001/jamaoncol.2016.0639]

15 **Liu J**, Chen Z, Li Y, Zhao W, Wu J, Zhang Z. PD-1/PD-L1 Checkpoint Inhibitors in Tumor Immunotherapy. *Front Pharmacol* 2021; **12**: 731798 [PMID: 34539412 DOI: 10.3389/fphar.2021.731798]

World Journal of Gastrointestinal Oncology

Submit a Manuscript: https://www.f6publishing.com

World J Gastrointest Oncol 2022 December 15; 14(12): 2340-2352

DOI: 10.4251/wjgo.v14.i12.2340

ISSN 1948-5204 (online)

ORIGINAL ARTICLE

Basic Study

Inhibition of bromodomain-containing protein 4 enhances the migration of esophageal squamous cell carcinoma cells by inducing cell autophagy

Wen-Qian Yang, Rui Liang, Man-Qi Gao, Yu-Zhen Liu, Bo Qi, Bao-Sheng Zhao

Specialty type: Gastroenterology and hepatology

Provenance and peer review: Unsolicited article; Externally peer reviewed.

Peer-review model: Single blind

Peer-review report's scientific quality classification

Grade A (Excellent): 0
Grade B (Very good): B, B
Grade C (Good): C
Grade D (Fair): 0
Grade E (Poor): 0

P-Reviewer: Anandan H, India; Gassler N, Germany

Received: August 11, 2022
Peer-review started: August 11, 2022
First decision: October 5, 2022
Revised: October 17, 2022
Accepted: November 16, 2022
Article in press: November 16, 2022
Published online: December 15, 2022

Wen-Qian Yang, Rui Liang, Man-Qi Gao, Yu-Zhen Liu, Bo Qi, Bao-Sheng Zhao, Department of Thoracic Surgery, The First Affiliated Hospital of Xinxiang Medical University, Weihui 453100, Henan Province, China

Wen-Qian Yang, Rui Liang, Man-Qi Gao, Yu-Zhen Liu, Bao-Sheng Zhao, Esophageal Cancer Institute, Xinxiang Medical University, Weihui 453100, Henan Province, China

Wen-Qian Yang, Rui Liang, Yu-Zhen Liu, Life Science Research Center, The First Affiliated Hospital of Xinxiang Medical University, Weihui 453100, Henan Province, China

Corresponding author: Bao-Sheng Zhao, BMed, Chief Physician, Professor, Department of Thoracic Surgery, The First Affiliated Hospital of Xinxiang Medical University, No. 88 Jiankang Road, Weihui 453100, Henan Province, China. drbszhao@xxmu.edu.cn

Abstract

BACKGROUND

Esophageal squamous cell carcinoma (ESCC), the predominant type of esophageal cancer, has a 5-year survival rate less than 20%. Although the cause of poor prognosis is the high incidence and mortality of ESCC, the high rate of metastasis after esophageal cancer surgery is the main cause of death after the surgery. Bromodomain-containing protein 4 (BRD4), an epigenetic reader of chromatin-acetylated histones in tumorigenesis and development, plays an essential role in regulating oncogene expression. BRD4 inhibition and BRD4 inhibition-based treatment can potentially suppress ESCC growth. However, the effects and mechanisms of action of BRD4 on ESCC cell migration remain unclear.

AIM

To explore the effect of BRD4 on cell migration of ESCC *in vitro* and its possible molecular mechanism.

METHODS

Human ESCC cell lines KYSE-450 and KYSE-150 were used. The 3-(4,5-dimethyl-2-thiazolyl)-2,5-diphenyl-2-H-tetrazolium bromide assay was performed to examine cell proliferation, and the transwell migration assay was conducted to test ESCC cell migration. JQ1, a BRD4 inhibitor, was applied to cells, and BRD4 siRNA was transfected into ESCC cells to knockdown endogenous BRD4. GFP-

RFP-LC3 adenovirus was infected into ESCC cells to evaluate the effect of JQ1 on autophagy. Western blotting was performed to determine the protein levels of BRD4, E-cadherin, vimentin, AMP-activated protein kinase (AMPK), and p-AMPK.

RESULTS

BRD4 was either downregulated by small interfering RNA or pretreated with JQ1 in ESCC cells, leading to increased tumor migration in ESCC cells in a dose- and time-dependent manner. Inhibition of BRD4 not only significantly suppressed cell proliferation but also strongly increased cell migration by inducing epithelial-mesenchymal transition (EMT). The protein expression of vimentin was increased and E-cadherin decreased in a dose-dependent manner, subsequently promoting autophagy in KYSE-450 and KYSE-150 cells. Pretreatment with JQ1, a BRD4 inhibitor, inhibited BRD4-induced LC3-II activation and upregulated AMPK phosphorylation in a dose-dependent manner. Additionally, an increased number of autophagosomes and autolysosomes were observed in JQ1-treated ESCC cells. The autophagy inhibitor 3-methyladenine (3-MA) reversed the effects of BRD4 knockdown on ESCC cell migration and blocked JQ1-induced cell migration. 3-MA also downregulated the expression of vimentin and upregulation E-cadherin.

CONCLUSION

BRD4 inhibition enhances cell migration by inducing EMT and autophagy in ESCC cells *via* the AMPK-modified pathway. Thus, the facilitating role on ESCC cell migration should be considered for BRD4 inhibitor clinical application to ESCC patients.

Key Words: JQ1; Bromodomain-containing protein 4; Cell migration; Cell autophagy; Epithelial-mesenchymal transition; Esophageal squamous cell carcinoma

Core Tip: It has been demonstrated that bromodomain-containing protein 4 (BRD4) as a transcriptional regulator promotes tumor development. Thus, targeting of BRD4 has recently emerged as a promising anti-cancer therapeutic strategy. We present here that BRD4 inhibition suppresses esophageal squamous cell carcinoma (ESCC) cell proliferation, but promotes ESCC cell migration by induction of autophagy, which further facilities epithelial-mesenchymal transition process. Our study implies that the migration-promoting effect should be carefully considered when clinical targeting BRD4 as anti-cancer approach and combination with autophagy inhibitor might be a new therapeutic strategy to avoid the deleterious role of BRD4-targeted strategies.

Citation: Yang WQ, Liang R, Gao MQ, Liu YZ, Qi B, Zhao BS. Inhibition of bromodomain-containing protein 4 enhances the migration of esophageal squamous cell carcinoma cells by inducing cell autophagy. *World J Gastrointest Oncol* 2022; 14(12): 2340-2352
URL: https://www.wjgnet.com/1948-5204/full/v14/i12/2340.htm
DOI: https://dx.doi.org/10.4251/wjgo.v14.i12.2340

INTRODUCTION

Esophageal squamous cell carcinoma (ESCC), one of the most common and aggressive digestive system cancers, is the main histological type of esophageal carcinoma in East Asian countries such as China[1]. Despite significant advancements in ESCC treatment, the prognosis remains dismal owing to its invasive growth and high frequencies of lymph node metastases[2]. Therefore, understanding the molecular mechanisms of metastasis in ESCC will facilitate the discovery of new therapeutic strategies to promote novel drug development with the goal of improving patient survival.

Bromodomain-containing protein 4 (BRD4) is an epigenetic regulator of the bromodomain and extra-terminal domain (BET) protein family. The structural features of BRD4 are its two bromodomains and one extra-terminal domain[3]. Bromodomain contains a hydrophobic pocket that recognizes acetylated lysine residues and thus acts as the "reader" of lysine acetylation. Therefore, the bromodomain is responsible for transducing the signal carried by acetylated lysine residues. The extra-terminal domain is the focal point for recruiting multiple and varied chromatin or transcriptional regulators[4]. Based on these properties, BRD4 is a pivotal transcriptional and epigenetic regulator. BRD4 has also been demonstrated to play a critical role in cancer development; high expression of BRD4 has been found in several types of cancers, such as colorectal cancer, breast cancer, and lung cancer[5-7]. Several small-

molecule inhibitors of BRD4 have been studied, such as JQ1, which has therapeutic uses in combating hematological and solid malignancies[8-10]. In esophageal cancer, inhibition of BRD4 blocked cell proliferation by binding to the promoter region of the chromosome condensation 2 (RCC2) regulator to downregulate RCC2 expression[11]. The finding that enhancer or promoter-associated BRD4 stimulates the expression of oncogenic drivers suggests that BRD4 is a promising target for anti-cancer drug development, but BRD4's role as a tumor suppressor in tumorigenesis is apparent in lung and breast cancer patient samples[12,13]. Crawford *et al*[12] also reported that ectopic expression of BRD4 reduced the migration and invasion of the metastatic mouse mammary tumor cell line Mvt-1 without affecting the growth rate, indicating the counteracting oncogenic function of BRD4. Thus, BRD4 probably has diverse functions that are cancer type-dependent. Although the oncogenic function of BRD4 has been well elucidated, given the importance of BRD4-targeted therapy, whether inhibition of BRD4 promotes tumor cell migration has not been clarified.

BRD4 functions as a histone chaperone by interacting with acetylated histones or non-histone proteins and participating in gene expression[14]. In our previous study, we found that trichostatin A (TSA), a histone deacetylase (HDAC) inhibitor, promoted the migration of ESCC cells, and JQ1 attenuated the cell migratory effects induced by TSA and that JQ1 alone promoted ESCC cell migration [15], indicating that BRD4 is involved in hyperacetylation-initiated ESCC cell migration but has an inhibitory effect on ESCC cell migration in the absence of hyperacetylation. Thus, the ability to promote tumor cell migration after inhibition of BRD4 signaling without hyperacetylation represents a crucial research direction regarding the prospect of BRD4 inhibition as an anti-cancer therapeutic approach.

Autophagy is a membrane trafficking process that directs the degradation of cytoplasmic material in lysosomes. Autophagy has been demonstrated to create a tumor-suppressing environment by inhibiting early tumorigenesis through the prevention of chronic tissue damage and regeneration[16]. However, autophagy deteriorates the migration and invasion of tumor cells *in vitro* while aggravating metastasis *in vivo*[17]; thus, autophagy elicits a double-sided biological role in tumorigenesis and development. Reports have demonstrated that inhibition of BRD4 induces AMP-activated protein kinase (AMPK)-mTOR-ULK1 modulated autophagy-associated cell death by blocking the BRD4-AMPK interaction in breast cancer cells[18]. Moreover, Jang *et al*[19] found that JQ1 induced cell autophagy in leukemia stem cells by activating the AMPK/ULK pathway. These reports suggest that inhibition of BRD4 may trigger autophagy *via* the activation of AMPK signaling.

In this study, we explored the effects of JQ1 on ESCC cell migration and its potential mechanisms of action. We found that JQ1 suppressed ESCC cell proliferation but promoted ESCC cell migration by inducing epithelial-mesenchymal transition (EMT). Knockdown of BRD4 in ESCC cells further confirmed the role of JQ1 in ESCC cell migration. Mechanistically, JQ1 induced autophagy, which is achieved *via* AMPK activation, which might mediate the promoting role of JQ1 in ESCC cell migration. These data provide new insights into the diverse functions of BRD4 in ESCC cell proliferation and migration, as well as caveats for BRD4-targeted clinical strategies.

MATERIALS AND METHODS

Reagents and antibodies

Bromodomain inhibitor (+) - JQ1 was purchased from APEXBIO (Houston, TX, United States), dissolved in dimethyl sulfoxide (DMSO), and diluted to the desired concentration before use. 3-(4,5-dimethylthiazol-2-yl)-2,5-diphenyl-terazolium bromide (MTT) was purchased from Beyotime Biotechnology (Shanghai, China). 3-methyladenine (3-MA) was purchased from Selleck (Shanghai, China), dissolved in PBS, and diluted to the desired concentration. Anti-E-cadherin (3195), AMPK (5831), p-AMPK (2535), and LC3-II (12741) antibodies were purchased from Cell Signaling Technology (Danvers, MA, United States). Anti-vimentin (WL00742) and anti-GAPDH (WL01114) were purchased from Wanleibio (Shenyang, China).

Cell culture and transfection

Two human ESCC cell lines, KYSE-450 (Cobioer Biosciences, Nanjing, China) and KYSE-150 (Cell Bank of the Typical Culture Preservation Committee of the Chinese Academy of Sciences, Shanghai, China), were used. Both cell lines were grown in PRMI-1640 medium (Corning, New York, United States) and supplemented with 10% fetal bovine serum (FBS; Biological Industries, Israel), 100 μg/mL penicillin, and 100 μg/mL streptomycin (Solarbio, Shanghai, China). The cells were cultured at 37 °C in a humidified atmosphere with 50 mL/L CO_2. BRD4 small interfering RNA (siBRD4) and control siRNA were purchased from Santa Cruz Biotechnology (sc-43639, Carlsbad, CA, United States). Cells cultured in a 6-well plate at 60% density were transfected with siRNA at a final concentration of 100 nmol/L using Lipofectamine 2000 (Invitrogen, Carlsbad, CA, United States), according to the manufacturer's protocol. After 24 h, the cells were collected for transwell and western blot assays.

Cell proliferation assay

The effect of JQ1 on cellular growth was determined using an MTT assay. Cells (4×10^3 cells/well) were seeded in 96-well plates, incubated for 24 h, and treated with different doses of JQ1 or vehicle. After incubation for 24, 48, and 72 h, cell proliferation was analyzed using an MTT assay. Ten microliters of MTT dye (5 mg/mL) was added to each well and incubated for 4 h. DMSO (100 μL/well) was added to dissolve formazan crystals. Absorbance at 490 nm was measured using a Multisken Spectrum microplate reader (Thermo Fisher Scientific, Carlsbad, CA, United States). Each experiment was repeated thrice.

Cell morphological observation

KYSE-450 and KYSE-150 cells were seeded in six-well plates (KYSE-150 and KYSE-150 2.0×10^5 cells/well). After overnight culture, cells were treated with or without JQ1 for 48 h. Five different fields were selected to observe cell phenotypic changes using a phase-contrast microscope (Nikon).

Cell migration assay

The cell migration assay was performed using a 6.5 mm transwell chamber with 8 μm micropores (Corning Costar, Manassas, Virginia, United States). Cells at 1×10^5 cells/200 μL per well in serum-free medium were seeded into the transwell chamber with or without application of the drug as follows: JQ1 (APExBIO) or 3-MA (Selleck), both of which were cultured in 24-well plates with 600 μL RPMI-1640 medium supplemented with 10% FBS. After allowing the cells to migrate for 24 h, non-migrated cells on the upper side of the chamber were cleaned with a cotton swab. Migrated cells on the bottom surface of the chamber were fixed with 4% formaldehyde and stained with 0.1% crystal violet. The migrated cells in five different fields of each membrane were captured using a phase-contrast microscope (Nikon), and the migrated cells were counted.

Western blot assay

Total protein was extracted from KYSE-150 and KYSE-450 cells using RIPA buffer. A BCA assay (DingGuo, Beijing, China) was used to measure the protein concentration. Next, 30 μg protein from each sample was separated using 10% SDS-PAGE and transferred to a PVDF membrane (Millipore, Billerica, MA, United States). The membrane was blocked using 5% nonfat dry milk for 1 h at room temperature and incubated with primary antibodies overnight at 4 °C (all in a 1:1000 dilution). Next, the membrane was washed thrice by TBST and incubated with HRP-conjugated secondary antibodies (Boster, Wuhan, China) for 1 h. After washing, the PVDF membrane was processed with a BeyoECL chemiluminescence kit (Beyotime Biotechnology, Shanghai, China) and detected using the Amersham™ Imager 600 System (GE Healthcare Bio-Sciences, Pittsburgh, PA, United States).

Detection of autophagosomes and autolysosomes

GFP-RFP-LC3 virus is widely used to detect autophagic flux. The cells were transfected with the GFP-RFP-LC3 expression virus (Hanbio, Wuhan, China) using Lipofectamine 2000, according to the manufacturer's instructions. After 48 h of transfection, cells were treated with JQ1 for an additional 24 h. GFP-RFP-LC3 fluorescence was observed using a Nikon Eclipse E800 microscope and photographed with a Nikon digital camera DS-U3 (Nikon, Tokyo, Japan). Afterward, autophagosomes (yellow dots) and autolysosomes (red dots) in each cell were counted.

Statistical analysis

The experimental results are expressed as the mean ± SD. The significance of differences between the two groups was tested by Student's *t* test. A value of $P < 0.05$ was considered statistically significant.

RESULTS

JQ1 inhibits cell proliferation but promotes cell migration via regulation of EMT in ESCC cells

To study the role of BRD4 in ESCC, we first examined its effect on ESCC cell proliferation. A BRD4 inhibitor, JQ1 was applied to KYSE-450 and KYSE-150 cells. The cell viability was measured at various time points. The results showed that JQ1 significantly inhibited KYSE-450 cell proliferation after treatment with all doses (0.5, 1, 5, 10, and 20 μmol/L) at all tested time points (24, 48, and 72 h) (Figure 1A). JQ1 had significant suppressive effects on KYSE-150 cell proliferation at 48 and 72 h after treatment with JQ1 at 1, 5, 10, and 20 μmol/L. When compared with the reaction of KYSE-150 cells to the proliferation-inhibition effects of JQ1, KYSE-450 cells were observed to be more sensitive to JQ1 in a dose-dependent manner. These results indicate an inhibitory effect of JQ1 on the proliferation of esophageal cancer cells. Compared with the control, we also noticed that JQ1-treated KYSE-150 and KYSE-450 cells had stretched and had an elongated spindle-like phenotype, which is a separable feature of the mesenchymal cells (Figure 1B).

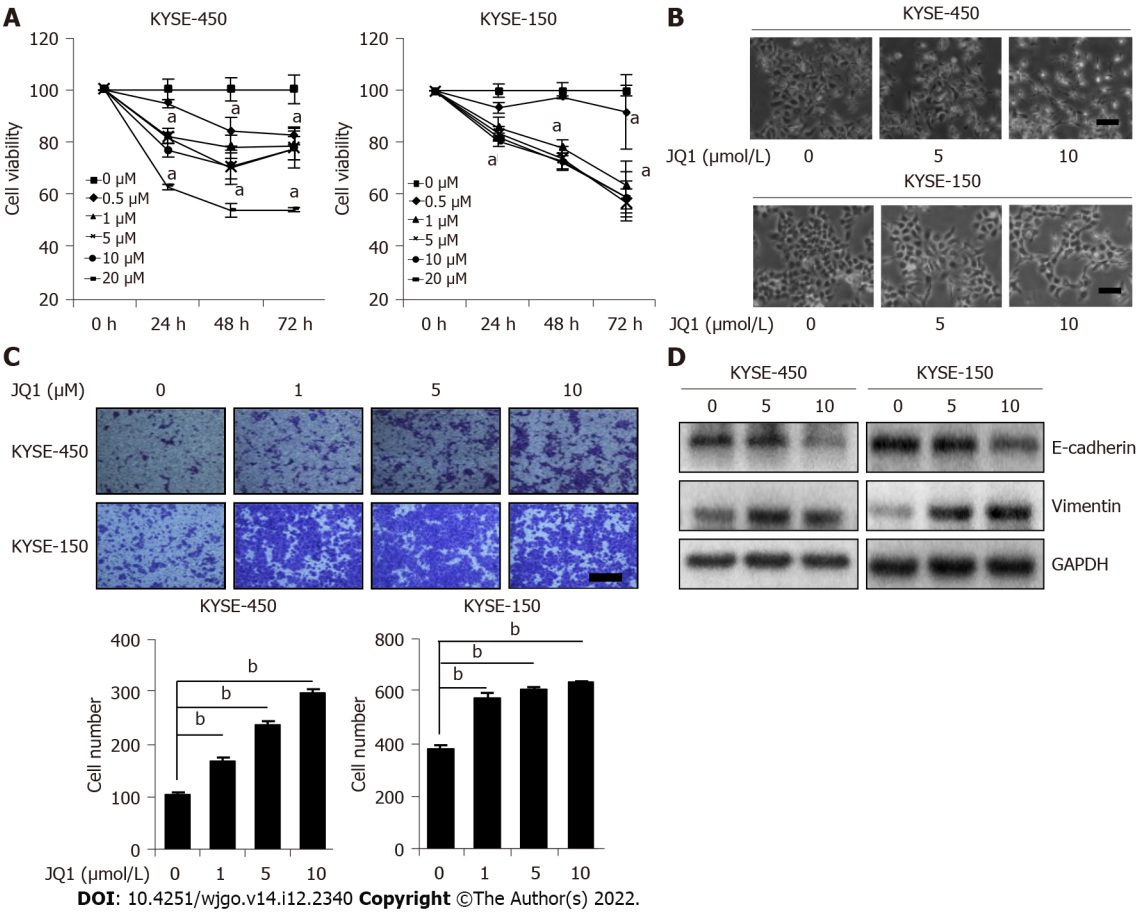

DOI: 10.4251/wjgo.v14.i12.2340 **Copyright** ©The Author(s) 2022.

Figure 1 Effects of JQ1, an inhibitor of bromodomain-containing protein 4, on esophageal squamous cell carcinoma cell proliferation and migration. A: 3-(4,5-dimethylthiazol-2-yl)-2,5-diphenyl-terazolium bromide assay was conducted to detect cell viability of KYSE-450 cells and KYSE-150 cells after treatment with JQ1 at various fixed dosages at different time points; B: Phase contrast images of esophageal squamous cell carcinoma cells treated with JQ1 were captured by a Nikon digital microscope. C: Transwell assay was performed to examine cell migration in KYSE-450 cells and KYSE-150 cells after treatment with JQ1 at various fixed dosages; D: Western blot was carried out to measure the expression levels of E-cadherin and vimentin in KYSE-450 cells and KYSE-150 cells after treatment with JQ1 at various fixed dosages. GAPDH was used as the protein loading control. $^{a}P < 0.05$, $^{b}P < 0.01$. Scale bars in (B) and (C) are 100 μm.

We further explored the effect of JQ1 on ESCC cell migration by treating the cells with JQ1 before performing a transwell migration assay. The results revealed that JQ1 at 1, 5, and 10 μmol/L enhanced cell migration more than the control treatment and that this dose-dependent promotion was more apparent in KYSE-450 cells than in KYSE-150 cells (Figure 1C). EMT is an important initiation step during epithelial-derived cancer cell migration, a process that leads to cancer invasion and metastasis [20]. Therefore, we evaluated whether JQ1 promotes cell migration through EMT induction. KYSE-450 and KYSE-150 cells were treated with 5 μmol/L of JQ1 and 10 μmol/L JQ1, respectively. Western blotting was used to examine the EMT marker E-cadherin, which is a marker for epithelia, and vimentin, a mesenchymal marker. We observed that E-cadherin protein levels decreased and vimentin protein levels increased in JQ1-treated cells (Figure 1D). These data suggest that JQ1 facilitates ESCC cell migration by promoting EMT.

Knockdown of BRD4 promotes ESCC cell migration

To confirm the role of inhibition BRD4 in ESCC cell migration, siBRD4 was transfected with ESCC cells to knock down endogenous BRD4. Cell migration was examined in siBRD4-transfected KYSE-450 and KYSE-150 cells. As shown in Figure 2A, compared with that in the negative control cells (siNC), a significant increase in the number of migrated cells was observed in siBRD4-transfested KYSE-450 cells and KYSE-150 cells. Western blotting confirmed the knockdown of BRD4 after transfection with siBRD4 in KYSE-450 and KYSE-150 cells. Western blotting also revealed that BRD4 knockdown decreased the level of E-cadherin but increased the level of vimentin in both cell lines (Figure 2B), which is consistent with the results of JQ1 treatment of KYSE-450 and KYSE-150 cells. These findings indicate that inhibition of BRD4 facilitates ESCC cell migration, which is possibly mediated by EMT induction.

JQ1 induces cell autophagy and activates AMPK signaling in ESCC cells

Increasing evidence has revealed that autophagy can promote the metastasis of cancer cells[21,22]. In a

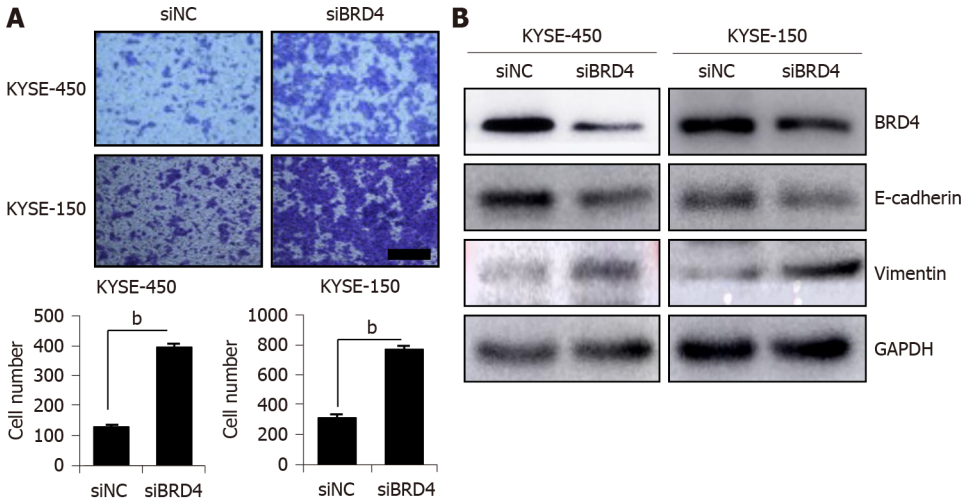

DOI: 10.4251/wjgo.v14.i12.2340 **Copyright** ©The Author(s) 2022.

Figure 2 Knockdown of bromodomain-containing protein 4 promotes esophageal squamous cell carcinoma cell migration. A: Transwell assay was performed to detect cell migration in KYSE-450 and KYSE-150 after transfection with siBRD4; B: Western blot was conducted to measure the levels of E-cadherin and vimentin after transfection with siBRD4. GAPDH was used as the protein loading control. $^{a}P < 0.05$, $^{b}P < 0.01$. Scale bar in (A) is 100 μm.

study on acute myeloid leukemia, JQ1 induced cell autophagy with little effect on cell apoptosis[19]; therefore, we speculated that autophagy might participate in JQ1-induced ESCC cell migration. To explore the role of JQ1 in autophagy, the GFP-RFP-LC3 double fluorescent autophagy indicator system was used to mark and track changes in LC3 and autophagy flow. KYSE-450 and KYSE-150 cells were infected with GFP-RFP-LC3 virus, as shown in Figure 3A. The number of red dots (indicating autolysosomes) and yellow dots (indicating autophagosomes) were significantly increased after treatment with 5 μmol/L of JQ1. Western blots in Figure 3B showed that the level of LC3-II, an autophagy marker, was significantly increased after treatment with JQ1 at doses of 5 and 10 μmol/L (Figure 3B). AMPK is known to regulate many cellular processes, including autophagy; therefore, we examined AMPK phosphorylation. The addition of JQ1 caused an increase in the level of phosphorylated AMPK (Figure 3B) in KYSE-450 and KYSE-150 cells. These results collectively suggest that JQ1 induces autophagy, which may be triggered by AMPK activation in ESCC cells.

Inhibition of autophagy blocks JQ1-caused cell migration and EMT in ESCC cells

To examine whether JQ1-induced cell migration was due to autophagy activation, we used 3-MA, a classic autophagy inhibitor, to arrest autophagy at an early stage. 3-MA works by inhibiting the class III phosphoinositide 3-kinase (PI3K) complex, thus exhibiting an inhibitory role in the formation and development of autophagosomes. As shown in Figure 4, compared with that in cells treated with only JQ1, a significant decrease in the number of migrated cells was observed in cells treated with both JQ1 and 3-MA. This finding indicates that JQ1 facilitates ESCC migration *via* the induction of autophagy. Next, we explored whether the JQ1-promoted EMT process is related to the induction of autophagy. As shown in Figure 4B, 3-MA treatment noticeably blocked the JQ1-induced upregulation of LC3-II, indicating that 3-MA prevents JQ1-induced autophagy. Moreover, it was revealed that combination treatment with 3-MA and JQ1 increased the level of E-cadherin while lowering the level of vimentin when compared with that of JQ1 alone treatment, which showed activation of the EMT process. These findings suggest that JQ1-induced ESCC migration may be related to the autophagy-activated EMT process in ESCC cells.

DISCUSSION

Upregulation or translocation of the BET family frequently occurs in different tumor types, including hematological malignancies and solid tumors[23]. Targeting BET family members is a promising therapeutic strategy in anti-cancer medicine development. For instance, BRD4, a member of the BET family, has been reported as a novel therapeutic candidate target for incurable subtypes of human squamous carcinoma, such as respiratory mucosa cancer[24]. JQ1, a BET bromodomain inhibitor, exhibits anti-cancer activity by competitively displacing BRD4 to bind nuclear chromatin[25], repressing the transcription of BRD4-controlled downstream genes, such as c-Myc[26]. JQ1 has been demonstrated to suppress multi-organ cancer cell proliferation, and multi-organ cancer cell migration and invasion[27-29]. However, Nagarajan *et al*[30] reported that BRD4 was required for epithelium-specific gene

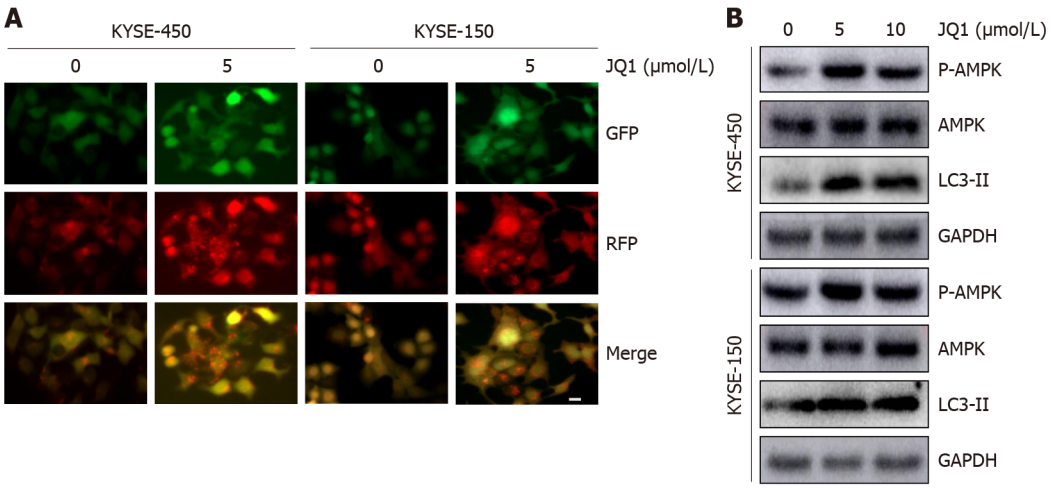

DOI: 10.4251/wjgo.v14.i12.2340 **Copyright** ©The Author(s) 2022.

Figure 3 JQ1 induces cell autophagy and activates AMP-activated protein kinase. A: Cells infected by the GFP-RFP-LC3 virus were treated with dimethyl sulfoxide or JQ1 dissolved in dimethyl sulfoxide (5 μmol/L) for 24 h, then fluorescence microscopy images were photographed. Bar = 20 μm; B: Cells were either untreated or treated with JQ1 at doses of 0, 5, or 10 μmol/L for 24 h. Western blots were performed to examine the levels of LC3-II, AMP-activated protein kinase (AMPK) and p-AMPK in KYSE-450 cells and KYSE-150 cells. GAPDH was used as the protein loading control.

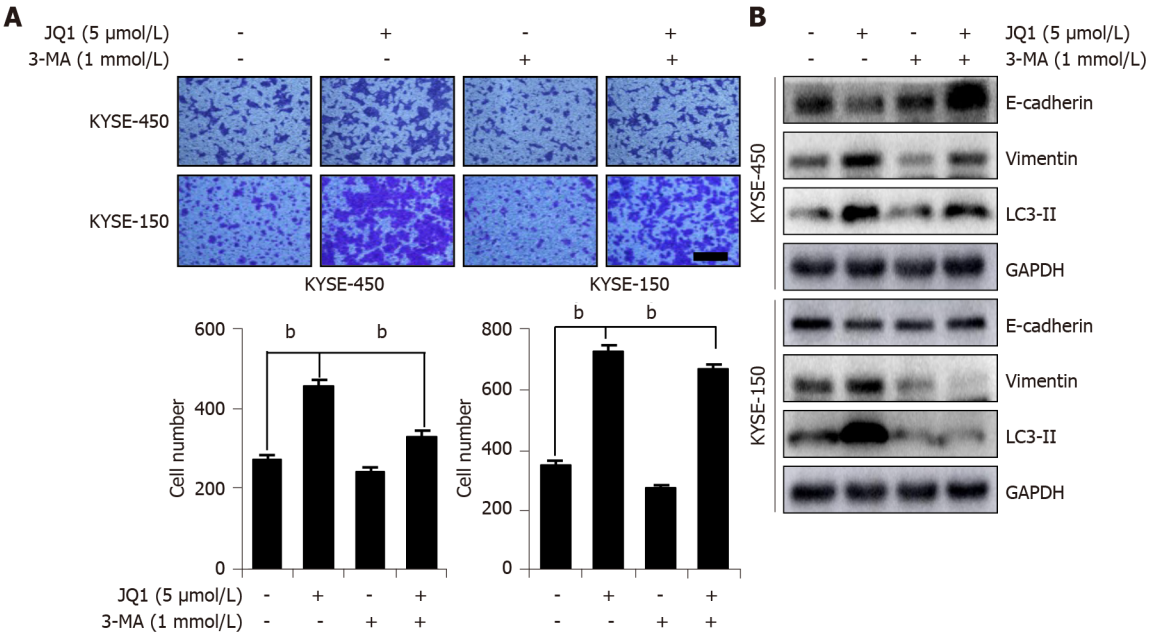

DOI: 10.4251/wjgo.v14.i12.2340 **Copyright** ©The Author(s) 2022.

Figure 4 Inhibition of autophagy blocks JQ1-caused cell migration and epithelial-mesenchymal transition. A: Transwell assay was performed to detect cell migration of KYSE-450 and KYSE-150 after treatment with JQ1 (5 μmol/L) along or combination with 3-methyladenine (3-MA) (1 mmol/L); B: Western blots were performed to measure the levels of LC3-II, E-cadherin, and vimentin in KYSE-450 cells and KYSE-150 cells after treatment of JQ1 along or combination with 3-MA. GAPDH was used as the protein loading control. $^{b}P < 0.01$. Scale bar in (A) is 100 μm.

expression and cellular phenotype expression in mammary epithelial cells, and knockdown of BRD4 or application of JQ1 promoted epithelial transformation and migration of mammary cells. Thus, concerns associated with the induction of unwanted cell characteristics should be cautiously considered in the clinical use of BET domain inhibitors. In this study, our data revealed that JQ1 suppressed the growth of ESCC cells (Figure 1A), which is consistent with reports on JQ1's anti-tumor effect involving anti-ESCC cell proliferation. Our data also revealed that JQ1 and BRD4 knockdown promoted ESCC cell migration. Thus, improving the understanding of the mechanism underlying the promoting role of JQ1 on cell migration is urgently necessary to design strategies to improve its efficiency and overcome its role in promoting cell migration.

BRD4 is not only recruited to histones by acetylated lysine but also interacts directly with transcription factors that determine cell-specific functions and fates[31-33]. The two tandem bromodomain domains of BRD4 recognize acetylated lysine residues in nucleosomal histones and recruit transcriptional proteins to chromatin. The literature has suggested that the first bromodomain of BRD4 may specifically bind to acetylated histones, and the second bromodomain may bind to acetylated lysine residues in cell-specific transcription factors[31,34]. We previously reported that JQ1 or knockdown of BRD4 noticeably counteracted the promoting effect of TSA (an HDAC inhibitor that causes histone acetylation) on ESCC cell migration and that this counteractive mechanism might be involved in the recruitment of BRD4 to TSA-induced acetylated histones[15]. Shi *et al*[31] reported that by overexpressing twist and BRD4 in HEK293 cells, TSA increases the interaction between twist and BRD4 *via* twist acetylation promotion. By binding to acetylated twist, BRD4 is recruited to twist target gene promoters/enhancers to direct gene transcription (*i.e.*, directing the transcription of WNT5A in basal-like breast cancer cells), ultimately resulting in BRD4-regulated cell migration and invasion processes. In summary, the function of BRD4 is regulated by post-translational modifications and interactor switches that reshape the genomic landscape, leading to the reorganization of transcriptional programs at specific genetic loci[35]. This reorganization results in differing downstream gene diversification and effects on the migratory behavior of tumor cells. Based on these results, our hypothesis was that the function of BRD4 is dependent on the level of acetylated histones or transcription factors/cofactors. In our study, either JQ1 or knockdown of BRD4 significantly promoted the migration of ESCC cells (Figures 1B and 2A), effectively showing that ESCC cell migration was opposite to that of other cells. This finding indicates a protective role of BRD4 in ESCC cell migration. Our data suggest that inhibition of BRD4 not only represses ESCC cell proliferation but also activates cancer progressing genes that affect cell migration to disrupt the therapeutic anti-cancer effects of BRD4 inhibition in ESCC. Combination treatment strategies that selectively overcome JQ1-induced cell migration could potentially provide maximum anti-cancer therapeutic benefits.

We explored the possible mechanism by which JQ1 promotes ESCC cell migration and provided new insights that support the clinical application of JQ1. A study reported that ubenimex, a classical anti-cancer drug, inhibited glioma cell autophagy to enhance JQ1 sensitivity, which induces cell death by upregulation of hexamethylene bisacetamide-inducible protein 1. The most notable finding in that study was that cell migration and autophagy did not respond to JQ1-only treatment, in contrast with the increased inhibition of cell migration and increased autophagy in cells treated with ubenimex-adjuvant JQ1[36].

Autophagy participates in various intracellular processes; therefore, disordered autophagy is involved in the progression of many diseases and some processes, such as cancer, lysosomal storage diseases, neurodegenerative diseases, aging, development and immune function[37-39]. In addition, the regulation of autophagy is unique and selective. In some growth situations, BRD4 acts as a transcriptional suppressor by working with the methyltransferase EHMT2 to negatively regulate autophagy. Moreover, inhibition of BRD4 resulted in increased autophagy. When nutrient deprivation occurs, AMPK signaling cascades, rather than BRD4, and binds to chromatin, which promotes autophagy gene activation and cell survival[40,41]. Thus, BRD4 can negatively regulate cellular autophagy, and the unique role of BRD4 in the selective regulation of autophagy may facilitate future therapeutic strategies for treating various diseases. In addition, activation of AMPK, a major metabolic energy sensor, triggers activation of downstream autophagy[42,43]. In this study, we found that AMPK may mediate JQ1-induced autophagy in ESCC cells and detect increased phosphorylation of AMPK. Compared with those in the control, the levels of LC3-II and autophagosome/autolysosome increased in JQ1-treated cells because of the activation of AMPK signaling (Figure 3A and B). Utilizing the autophagy inhibitor 3-MA reduced the effect of JQ1-induced upregulation of LC3-II. Further research is necessary to explore the molecular mechanisms of autophagy in relation to JQ1-induced cell migration in esophageal squamous cell carcinoma.

Autophagy has been shown to play an important role in cancer metastasis[44]. In HepG2 cells, fluid shear stress induces cell migration and invasion by activating autophagy[45]. The induction of autophagy leads to loss of the metastatic phenotype by promoting autophagy-mediated degradation of Snail and Twist in breast cancer cells[46]. The literature has also reported that sirtuin-1 induced EMT by promoting autophagy degradation of E-cadherin in melanoma cells[47]. In addition, in a study on hepatocellular carcinoma, plant homeodomain finger protein 8, an EMT activator, promoted metastasis *via* FIP200-dependent autophagic degradation of E-cadherin[48]. In this study, we demonstrated that JQ1-induced autophagy might promote EMT. Inhibition of autophagy blocks JQ1-induced cell migration and EMT. The transwell assay showed that 3-MA treatment suppressed JQ1-induced cell migration in KYSE-450 and KYSE-150 cell lines (Figure 4A). EMT drives migratory properties that cause adherent cells to adopt a mesenchymal phenotype and enhance cell fate plasticity[49]. E-cadherin is an epithelial marker, and β-catenin and vimentin are mesenchymal markers involved in EMT. In this study, we showed that inhibition of BRD4, either by siBRD4 transfection or by JQ1 treatment, not only facilitated ESCC cell migration by promoting the EMT process (Figure 1C, 2A and B) but also induced the upregulation of E-cadherin and downregulation of vimentin. Compared with those in JQ1-only treated cells, the protein level of E-cadherin was increased and vimentin was reduced in ESCC cells treated with JQ1 combined with 3-MA (Figure 4B). This study showed that cell autophagy is involved in

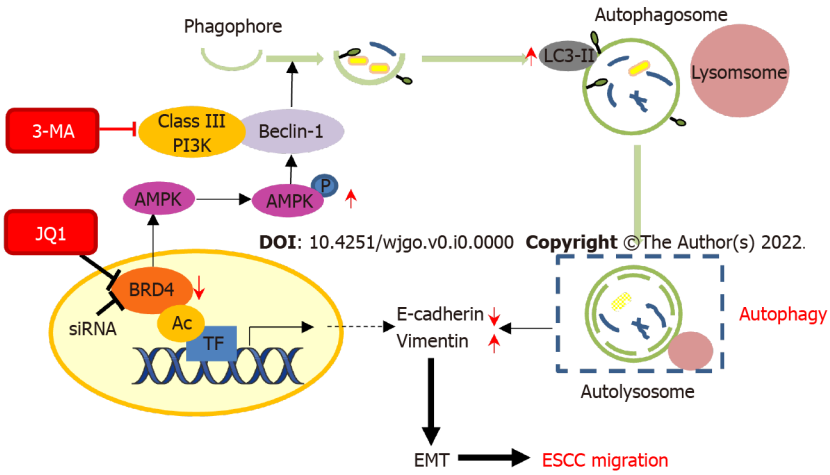

DOI: 10.4251/wjgo.v14.i12.2340 Copyright ©The Author(s) 2022.

Figure 5 Schematic model of the effect of JQ1 or inhibition of bromodomain-containing protein 4 on cell migration in esophageal squamous cell carcinoma cells. JQ1 treatment or siRNA inhibition of bromodomain-containing protein 4 can lead to increased phosphorylation of AMP-activated protein kinase, resulting in upregulation of LC3-II protein level in order to activate autophagy. In addition, the activation of autophagy promotes the epithelial-mesenchymal transition process of esophageal squamous cell carcinoma cells, thus promoting the JQ1-induced migration of esophageal cancer cells. Finally, this pro-migration effect can be inhibited by the autophagy inhibitor 3-methyladenine. AMPK: AMP-activated protein kinase; TF: Transcription factor; BRD4: Bromodomain-containing protein 4; EMT: Epithelial-mesenchymal transition; ESCC: Esophageal squamous cell carcinoma; AC: Acetylation.

BRD4 regulated cell migration in ESCC. Therefore, the downregulation of BRD4 or JQ1 treatment augments cell migration by promoting autophagy in ESCC cells. Our data indicate that inhibition of autophagy is a potential therapeutic strategy for JQ1-treated ESCC (Figure 5).

After reviewing the literature, we determined that this study is the first to show that JQ1 or inhibition of BRD4 augments the migration of ESCC cells by inducing autophagy, which promotes the EMT process. To determine whether BRD4 effects are specific for ESCC cells, we observed the effect of JQ1 on human glioma cell line U251 cell migration, and found that JQ1 obviously repressed U251 cell migration (data not shown). On the basis of our observations, we speculate that the promoting effect on cell migration induced by BRD4 inhibition is not ESCC cell specific. In the future work, we will explore whether this role occurs on other types of cancer cell. Collectively, our work implies that the migration-promoting effect should be carefully considered when applying JQ1 or targeting BRD4 as an anti-cancer approach. JQ1, in combination with an autophagy inhibitor, might be a new therapeutic strategy to overcome the effects of JQ1 on cancer cell migration.

CONCLUSION

Our research shows that the downregulation of BRD4 by JQ1 treatment or knockdown of BRD4 promotes the upregulation of AMPK phosphorylation, which might induce autophagy by activating Beclin-1 (a mammalian homolog of yeast Atg6) and class III PI3K complex signaling. Once these signaling pathways are activated, LC3-II level increases, which generates autophagosomes and autolysosomes. Autophagy leads to EMT molecular changes that promote events related to the migration behavior of ESCC cells.

ARTICLE HIGHLIGHTS

Research background

Bromodomain-containing protein 4 (BRD4) as a transcriptional regulator promotes tumor development. Thus, targeting of BRD4 has recently emerged as a promising anti-cancer therapeutic strategy. Although it has been reported that BRD4 inhibition repressed esophageal squamous cell carcinoma (ESCC) cell proliferation, the role of BRD4 inhibition in ESCC cell migration remains unclear.

Research motivation

To explore the role of targeting BRD4 on ESCC cell migration for developing BRD4 inhibitor combination therapies when clinical application of BRD4 inhibitor as anti-cancer therapy.

Research objectives
To explore the effect of BRD4 inhibition on ESCC cell migration and the potential mechanism.

Research methods
Human ESCC cell lines KYSE-450 and KYSE-150 were cultured. 3-(4,5-dimethylthiazol-2-yl)-2,5-diphenyl-terazolium bromide assay was performed to examine cell proliferation and transwell assay was conducted to cell migration. JQ1 was used to inhibit BRD4 function and siBRD4 was transfected into ESCC cells to knockdown endogenous BRD4. GFP-RFP-LC3 adenovirus was infected into ESCC cells to evaluate the effect of JQ1 on autophagy. Western blot was performed to determine the protein levels of BRD4, E-cadherin, vimentin, AMP-activated protein kinase (AMPK), and p-AMPK.

Research results
JQ1 inhibited ESCC cell proliferation, but JQ1 or knockdown of BRD4 promoted ESCC cell migration as well as epithelial-mesenchymal transition (EMT). Application of JQ1 increased autophagosomes and autolysosomes in ESCC cells and enhanced level of LC3-II and AMPK phosphorylation in a dose-dependent manner. The autophagy inhibitor 3-MA blocked JQ1-induced cell migration and EMT.

Research conclusions
Inhibition of BRD4 promotes ESCC cell migration and EMT mediated by activation of autophagy.

Research perspectives
The migration-promoting effect should be carefully considered when applying JQ1 or targeting BRD4 as an anti-cancer approach. JQ1, in combination with an autophagy inhibitor, might be a new therapeutic strategy to overcome the effects of JQ1 on cancer cell migration.

ACKNOWLEDGEMENTS

We thank Chen-Fang Qi who works at Cedars-Sinai Medical Center, 8700 Beverly Blvd, Los Angeles, CA 90048, United States, for providing language editorial assistance.

FOOTNOTES

Author contributions: Liu YZ and Zhao BS designed and coordinated the study; Yang WQ, Liang R, Gao MQ and Qi B performed the experiments, acquired and analyzed data; Yang WQ, Liu YZ and Zhao BS interpreted the data; Yang WQ, Liu YZ and Zhao BS wrote the manuscript; all authors approved the final version of the article.

Supported by the Key Project of Science and Technology of Xinxiang, No. GG2020027; and the Health Commission of Henan Province of China, No. SBGJ202102188.

Conflict-of-interest statement: The authors declare that no conflict of interest exists in this study.

Data sharing statement: No additional data are available.

Country/Territory of origin: China

ORCID number: Wen-Qian Yang 0000-0001-7940-0637; Yu-Zhen Liu 0000-0001-8329-1795; Bo Qi 0000-0002-1477-8513; Bao-Sheng Zhao 0000-0002-7854-111X.

S-Editor: Zhang H
L-Editor: A
P-Editor: Zhang H

REFERENCES

1 **Lin Y**, Totsuka Y, He Y, Kikuchi S, Qiao Y, Ueda J, Wei W, Inoue M, Tanaka H. Epidemiology of esophageal cancer in Japan and China. *J Epidemiol* 2013; **23**: 233-242 [PMID: 23629646 DOI: 10.2188/jea.je20120162]

2 **Huang JX**, Chen WC, Lin M, Zhang YL, Li FY, Song ZX, Xiao W, Chen P, Qian RY, Salminen E, Yu H. Clinicopathological significance of cyclooxygenase-2 and cell cycle-regulatory proteins expression in patients with esophageal squamous cell carcinoma. *Dis Esophagus* 2012; **25**: 121-129 [PMID: 21762277 DOI: 10.1111/j.1442-2050.2011.01219.x]

3 **Zhang W**, Prakash C, Sum C, Gong Y, Li Y, Kwok JJ, Thiessen N, Pettersson S, Jones SJ, Knapp S, Yang H, Chin KC. Bromodomain-containing protein 4 (BRD4) regulates RNA polymerase II serine 2 phosphorylation in human CD4+ T cells. *J Biol Chem* 2012; **287**: 43137-43155 [PMID: 23086925 DOI: 10.1074/jbc.M112.413047]

4 **Belkina AC**, Denis GV. BET domain co-regulators in obesity, inflammation and cancer. *Nat Rev Cancer* 2012; **12**: 465-477 [PMID: 22722403 DOI: 10.1038/nrc3256]

5 **Hu Y**, Zhou J, Ye F, Xiong H, Peng L, Zheng Z, Xu F, Cui M, Wei C, Wang X, Wang Z, Zhu H, Lee P, Zhou M, Jiang B, Zhang DY. BRD4 inhibitor inhibits colorectal cancer growth and metastasis. *Int J Mol Sci* 2015; **16**: 1928-1948 [PMID: 25603177 DOI: 10.3390/ijms16011928]

6 **Marcotte R**, Sayad A, Brown KR, Sanchez-Garcia F, Reimand J, Haider M, Virtanen C, Bradner JE, Bader GD, Mills GB, Pe'er D, Moffat J, Neel BG. Functional Genomic Landscape of Human Breast Cancer Drivers, Vulnerabilities, and Resistance. *Cell* 2016; **164**: 293-309 [PMID: 26771497 DOI: 10.1016/j.cell.2015.11.062]

7 **Liao YF**, Wu YB, Long X, Zhu SQ, Jin C, Xu JJ, Ding JY. High level of BRD4 promotes non-small cell lung cancer progression. *Oncotarget* 2016; **7**: 9491-9500 [PMID: 26840017 DOI: 10.18632/oncotarget.7068]

8 **Herrmann H**, Blatt K, Shi J, Gleixner KV, Cerny-Reiterer S, Müllauer L, Vakoc CR, Sperr WR, Horny HP, Bradner JE, Zuber J, Valent P. Small-molecule inhibition of BRD4 as a new potent approach to eliminate leukemic stem- and progenitor cells in acute myeloid leukemia AML. *Oncotarget* 2012; **3**: 1588-1599 [PMID: 23249862 DOI: 10.18632/oncotarget.733]

9 **Shimamura T**, Chen Z, Soucheray M, Carretero J, Kikuchi E, Tchaicha JH, Gao Y, Cheng KA, Cohoon TJ, Qi J, Akbay E, Kimmelman AC, Kung AL, Bradner JE, Wong KK. Efficacy of BET bromodomain inhibition in Kras-mutant non-small cell lung cancer. *Clin Cancer Res* 2013; **19**: 6183-6192 [PMID: 24045185 DOI: 10.1158/1078-0432.CCR-12-3904]

10 **Asangani IA**, Dommeti VL, Wang X, Malik R, Cieslik M, Yang R, Escara-Wilke J, Wilder-Romans K, Dhanireddy S, Engelke C, Iyer MK, Jing X, Wu YM, Cao X, Qin ZS, Wang S, Feng FY, Chinnaiyan AM. Therapeutic targeting of BET bromodomain proteins in castration-resistant prostate cancer. *Nature* 2014; **510**: 278-282 [PMID: 24759320 DOI: 10.1038/nature13229]

11 **Wu Q**, Liu F, Ge M, Laster KV, Wei L, Du R, Jiang M, Zhang J, Zhi Y, Jin G, Zhao S, Kim DJ, Dong Z, Liu K. BRD4 drives esophageal squamous cell carcinoma growth by promoting RCC2 expression. *Oncogene* 2022; **41**: 347-360 [PMID: 34750516 DOI: 10.1038/s41388-021-02099-4]

12 **Crawford NP**, Alsarraj J, Lukes L, Walker RC, Officewala JS, Yang HH, Lee MP, Ozato K, Hunter KW. Bromodomain 4 activation predicts breast cancer survival. *Proc Natl Acad Sci U S A* 2008; **105**: 6380-6385 [PMID: 18427120 DOI: 10.1073/pnas.0710331105]

13 **Fernandez P**, Scaffidi P, Markert E, Lee JH, Rane S, Misteli T. Transformation resistance in a premature aging disorder identifies a tumor-protective function of BRD4. *Cell Rep* 2014; **9**: 248-260 [PMID: 25284786 DOI: 10.1016/j.celrep.2014.08.069]

14 **Kanno T**, Kanno Y, LeRoy G, Campos E, Sun HW, Brooks SR, Vahedi G, Heightman TD, Garcia BA, Reinberg D, Siebenlist U, O'Shea JJ, Ozato K. BRD4 assists elongation of both coding and enhancer RNAs by interacting with acetylated histones. *Nat Struct Mol Biol* 2014; **21**: 1047-1057 [PMID: 25383670 DOI: 10.1038/nsmb.2912]

15 **Liu D**, Liu Y, Qi B, Gu C, Huo S, Zhao B. Trichostatin A promotes esophageal squamous cell carcinoma cell migration and EMT through BRD4/ERK1/2-dependent pathway. *Cancer Med* 2021; **10**: 5235-5245 [PMID: 34160902 DOI: 10.1002/cam4.4059]

16 **White E**. The role for autophagy in cancer. *J Clin Invest* 2015; **125**: 42-46 [PMID: 25654549 DOI: 10.1172/JCI73941]

17 **Sharifi MN**, Mowers EE, Drake LE, Collier C, Chen H, Zamora M, Mui S, Macleod KF. Autophagy Promotes Focal Adhesion Disassembly and Cell Motility of Metastatic Tumor Cells through the Direct Interaction of Paxillin with LC3. *Cell Rep* 2016; **15**: 1660-1672 [PMID: 27184837 DOI: 10.1016/j.celrep.2016.04.065]

18 **Ouyang L**, Zhang L, Liu J, Fu L, Yao D, Zhao Y, Zhang S, Wang G, He G, Liu B. Discovery of a Small-Molecule Bromodomain-Containing Protein 4 (BRD4) Inhibitor That Induces AMP-Activated Protein Kinase-Modulated Autophagy-Associated Cell Death in Breast Cancer. *J Med Chem* 2017; **60**: 9990-10012 [PMID: 29172540 DOI: 10.1021/acs.jmedchem.7b00275]

19 **Jang JE**, Eom JI, Jeung HK, Cheong JW, Lee JY, Kim JS, Min YH. AMPK-ULK1-Mediated Autophagy Confers Resistance to BET Inhibitor JQ1 in Acute Myeloid Leukemia Stem Cells. *Clin Cancer Res* 2017; **23**: 2781-2794 [PMID: 27864418 DOI: 10.1158/1078-0432.CCR-16-1903]

20 **Behrens J**, Mareel MM, Van Roy FM, Birchmeier W. Dissecting tumor cell invasion: epithelial cells acquire invasive properties after the loss of uvomorulin-mediated cell-cell adhesion. *J Cell Biol* 1989; **108**: 2435-2447 [PMID: 2661563 DOI: 10.1083/jcb.108.6.2435]

21 **Liu H**, Ma Y, He HW, Zhao WL, Shao RG. SPHK1 (sphingosine kinase 1) induces epithelial-mesenchymal transition by promoting the autophagy-linked lysosomal degradation of CDH1/E-cadherin in hepatoma cells. *Autophagy* 2017; **13**: 900-913 [PMID: 28521610 DOI: 10.1080/15548627.2017.1291479]

22 **Li J**, Yang B, Zhou Q, Wu Y, Shang D, Guo Y, Song Z, Zheng Q, Xiong J. Autophagy promotes hepatocellular carcinoma cell invasion through activation of epithelial-mesenchymal transition. *Carcinogenesis* 2013; **34**: 1343-1351 [PMID: 23430956 DOI: 10.1093/carcin/bgt063]

23 **Spriano F**, Stathis A, Bertoni F. Targeting BET bromodomain proteins in cancer: The example of lymphomas. *Pharmacol Ther* 2020; **215**: 107631 [PMID: 32693114 DOI: 10.1016/j.pharmthera.2020.107631]

24 **French CA**, Miyoshi I, Aster JC, Kubonishi I, Kroll TG, Dal Cin P, Vargas SO, Perez-Atayde AR, Fletcher JA. BRD4

bromodomain gene rearrangement in aggressive carcinoma with translocation t(15;19). *Am J Pathol* 2001; **159**: 1987-1992 [PMID: 11733348 DOI: 10.1016/S0002-9440(10)63049-0]

25 **Filippakopoulos P**, Qi J, Picaud S, Shen Y, Smith WB, Fedorov O, Morse EM, Keates T, Hickman TT, Felletar I, Philpott M, Munro S, McKeown MR, Wang Y, Christie AL, West N, Cameron MJ, Schwartz B, Heightman TD, La Thangue N, French CA, Wiest O, Kung AL, Knapp S, Bradner JE. Selective inhibition of BET bromodomains. *Nature* 2010; **468**: 1067-1073 [PMID: 20871596 DOI: 10.1038/nature09504]

26 **Delmore JE**, Issa GC, Lemieux ME, Rahl PB, Shi J, Jacobs HM, Kastritis E, Gilpatrick T, Paranal RM, Qi J, Chesi M, Schinzel AC, McKeown MR, Heffernan TP, Vakoc CR, Bergsagel PL, Ghobrial IM, Richardson PG, Young RA, Hahn WC, Anderson KC, Kung AL, Bradner JE, Mitsiades CS. BET bromodomain inhibition as a therapeutic strategy to target c-Myc. *Cell* 2011; **146**: 904-917 [PMID: 21889194 DOI: 10.1016/j.cell.2011.08.017]

27 **Zhou S**, Zhang S, Wang L, Huang S, Yuan Y, Yang J, Wang H, Li X, Wang P, Zhou L, Xu Y, Gao H, Zhang Y, Lv Y, Zou X. BET protein inhibitor JQ1 downregulates chromatin accessibility and suppresses metastasis of gastric cancer *via* inactivating RUNX2/NID1 signaling. *Oncogenesis* 2020; **9**: 33 [PMID: 32157097 DOI: 10.1038/s41389-020-0218-z]

28 **Wen N**, Guo B, Zheng H, Xu L, Liang H, Wang Q, Wang D, Chen X, Zhang S, Li Y, Zhang L. Bromodomain inhibitor jq1 induces cell cycle arrest and apoptosis of glioma stem cells through the VEGF/PI3K/AKT signaling pathway. *Int J Oncol* 2019; **55**: 879-895 [PMID: 31485609 DOI: 10.3892/ijo.2019.4863]

29 **Wang L**, Wu X, Huang P, Lv Z, Qi Y, Wei X, Yang P, Zhang F. JQ1, a small molecule inhibitor of BRD4, suppresses cell growth and invasion in oral squamous cell carcinoma. *Oncol Rep* 2016; **36**: 1989-1996 [PMID: 27573714 DOI: 10.3892/or.2016.5037]

30 **Nagarajan S**, Bedi U, Budida A, Hamdan FH, Mishra VK, Najafova Z, Xie W, Alawi M, Indenbirken D, Knapp S, Chiang CM, Grundhoff A, Kari V, Scheel CH, Wegwitz F, Johnsen SA. BRD4 promotes p63 and GRHL3 expression downstream of FOXO in mammary epithelial cells. *Nucleic Acids Res* 2017; **45**: 3130-3145 [PMID: 27980063 DOI: 10.1093/nar/gkw1276]

31 **Shi J**, Wang Y, Zeng L, Wu Y, Deng J, Zhang Q, Lin Y, Li J, Kang T, Tao M, Rusinova E, Zhang G, Wang C, Zhu H, Yao J, Zeng YX, Evers BM, Zhou MM, Zhou BP. Disrupting the interaction of BRD4 with diacetylated Twist suppresses tumorigenesis in basal-like breast cancer. *Cancer Cell* 2014; **25**: 210-225 [PMID: 24525235 DOI: 10.1016/j.ccr.2014.01.028]

32 **Wu SY**, Lee AY, Lai HT, Zhang H, Chiang CM. Phospho switch triggers Brd4 chromatin binding and activator recruitment for gene-specific targeting. *Mol Cell* 2013; **49**: 843-857 [PMID: 23317504 DOI: 10.1016/j.molcel.2012.12.006]

33 **Roe JS**, Mercan F, Rivera K, Pappin DJ, Vakoc CR. BET Bromodomain Inhibition Suppresses the Function of Hematopoietic Transcription Factors in Acute Myeloid Leukemia. *Mol Cell* 2015; **58**: 1028-1039 [PMID: 25982114 DOI: 10.1016/j.molcel.2015.04.011]

34 **Shi J**, Vakoc CR. The mechanisms behind the therapeutic activity of BET bromodomain inhibition. *Mol Cell* 2014; **54**: 728-736 [PMID: 24905006 DOI: 10.1016/j.molcel.2014.05.016]

35 **Chiang CM**. Brd4 engagement from chromatin targeting to transcriptional regulation: selective contact with acetylated histone H3 and H4. *F1000 Biol Rep* 2009; **1**: 98 [PMID: 20495683 DOI: 10.3410/B1-98]

36 **Han L**, Zhao Q, Liang X, Wang X, Zhang Z, Ma Z, Zhao M, Wang A, Liu S. Ubenimex enhances Brd4 inhibition by suppressing HEXIM1 autophagic degradation and suppressing the Akt pathway in glioma cells. *Oncotarget* 2017; **8**: 45643-45655 [PMID: 28484091 DOI: 10.18632/oncotarget.17314]

37 **Mizushima N**, Levine B, Cuervo AM, Klionsky DJ. Autophagy fights disease through cellular self-digestion. *Nature* 2008; **451**: 1069-1075 [PMID: 18305538 DOI: 10.1038/nature06639]

38 **Martinez-Vicente M**, Cuervo AM. Autophagy and neurodegeneration: when the cleaning crew goes on strike. *Lancet Neurol* 2007; **6**: 352-361 [PMID: 17362839 DOI: 10.1016/S1474-4422(07)70076-5]

39 **Kimmelman AC**. The dynamic nature of autophagy in cancer. *Genes Dev* 2011; **25**: 1999-2010 [PMID: 21979913 DOI: 10.1101/gad.17558811]

40 **Wen X**, Klionsky DJ. BRD4 is a newly characterized transcriptional regulator that represses autophagy and lysosomal function. *Autophagy* 2017; **13**: 1801-1803 [PMID: 28837371 DOI: 10.1080/15548627.2017.1364334]

41 **Sakamaki JI**, Wilkinson S, Hahn M, Tasdemir N, O'Prey J, Clark W, Hedley A, Nixon C, Long JS, New M, Van Acker T, Tooze SA, Lowe SW, Dikic I, Ryan KM. Bromodomain Protein BRD4 Is a Transcriptional Repressor of Autophagy and Lysosomal Function. *Mol Cell* 2017; **66**: 517-532.e9 [PMID: 28525743 DOI: 10.1016/j.molcel.2017.04.027]

42 **Pineda-Ramírez N**, Alquisiras-Burgos I, Ortiz-Plata A, Ruiz-Tachiquín ME, Espinoza-Rojo M, Aguilera P. Resveratrol Activates Neuronal Autophagy Through AMPK in the Ischemic Brain. *Mol Neurobiol* 2020; **57**: 1055-1069 [PMID: 31667715 DOI: 10.1007/s12035-019-01803-6]

43 **Wu Q**, Li J, Li Z, Sun S, Zhu S, Wang L, Wu J, Yuan J, Zhang Y, Wang C. Exosomes from the tumour-adipocyte interplay stimulate beige/brown differentiation and reprogram metabolism in stromal adipocytes to promote tumour progression. *J Exp Clin Cancer Res* 2019; **38**: 223 [PMID: 31138258 DOI: 10.1186/s13046-019-1210-3]

44 **Choi AM**, Ryter SW, Levine B. Autophagy in human health and disease. *N Engl J Med* 2013; **368**: 651-662 [PMID: 23406030 DOI: 10.1056/NEJMra1205406]

45 **Yan Z**, Su G, Gao W, He J, Shen Y, Zeng Y, Liu X. Fluid shear stress induces cell migration and invasion *via* activating autophagy in HepG2 cells. *Cell Adh Migr* 2019; **13**: 152-163 [PMID: 30663937 DOI: 10.1080/19336918.2019.1568141]

46 **Lv Q**, Wang W, Xue J, Hua F, Mu R, Lin H, Yan J, Lv X, Chen X, Hu ZW. DEDD interacts with PI3KC3 to activate autophagy and attenuate epithelial-mesenchymal transition in human breast cancer. *Cancer Res* 2012; **72**: 3238-3250 [PMID: 22719072 DOI: 10.1158/0008-5472.CAN-11-3832]

47 **Sun T**, Jiao L, Wang Y, Yu Y, Ming L. SIRT1 induces epithelial-mesenchymal transition by promoting autophagic degradation of E-cadherin in melanoma cells. *Cell Death Dis* 2018; **9**: 136 [PMID: 29374154 DOI: 10.1038/s41419-017-0167-4]

48 **Zhou W**, Gong L, Wu Q, Xing C, Wei B, Chen T, Zhou Y, Yin S, Jiang B, Xie H, Zhou L, Zheng S. PHF8 upregulation contributes to autophagic degradation of E-cadherin, epithelial-mesenchymal transition and metastasis in hepatocellular carcinoma. *J Exp Clin Cancer Res* 2018; **37**: 215 [PMID: 30180906 DOI: 10.1186/s13046-018-0890-4]

49 **Aiello NM**, Kang Y. Context-dependent EMT programs in cancer metastasis. *J Exp Med* 2019; **216**: 1016-1026 [PMID: 30975895 DOI: 10.1084/jem.20181827]

World Journal of Gastrointestinal Oncology

Submit a Manuscript: https://www.f6publishing.com

World J Gastrointest Oncol 2022 December 15; 14(12): 2353-2366

DOI: 10.4251/wjgo.v14.i12.2353

ISSN 1948-5204 (online)

ORIGINAL ARTICLE

Basic Study

Anti-silencing function 1B knockdown suppresses the malignant phenotype of colorectal cancer by inactivating the phosphatidylinositol 3-kinase/AKT pathway

Gen-Hua Yu, Xu-Feng Gong, Ying-Ying Peng, Jun Qian

Specialty type: Oncology

Provenance and peer review: Unsolicited article; Externally peer reviewed.

Peer-review model: Single blind

Peer-review report's scientific quality classification

Grade A (Excellent): A
Grade B (Very good): 0
Grade C (Good): C, C
Grade D (Fair): D
Grade E (Poor): 0

P-Reviewer: Ekine-Afolabi B, United Kingdom; Martinou E, United Kingdom; Tanabe S, Japan

Received: June 29, 2022
Peer-review started: June 29, 2022
First decision: August 6, 2022
Revised: August 31, 2022
Accepted: November 4, 2022
Article in press: November 4, 2022
Published online: December 15, 2022

Gen-Hua Yu, Xu-Feng Gong, Ying-Ying Peng, Department of Radiation Oncology, Zhebei Mingzhou Hospital, Huzhou 313000, Zhejiang Province, China

Jun Qian, Department of Colorectal Surgery, The Cancer Hospital of the University of Chinese Academy of Sciences (Zhejiang Cancer Hospital), Hangzhou 310022, Zhejiang Province, China

Corresponding author: Jun Qian, MD, PhD, Professor, Surgeon, Department of Colorectal Surgery, The Cancer Hospital of the University of Chinese Academy of Sciences (Zhejiang Cancer Hospital), No. 1 Banshan East Road, Gongshu District, Hangzhou 310022, Zhejiang Province, China. qianj1973@aliyun.com

Abstract

BACKGROUND

Mounting studies have highlighted the pivotal influence of anti-silencing function 1B (ASF1B) on the malignancy of cancers.

AIM

To explore the influence and mechanism of ASF1B in colorectal cancer (CRC).

METHODS

Quantitative real-time polymerase chain reaction (qRT-PCR) was used to detect mRNA expression of ASF1B. Immunohistochemical staining was performed to detect protein expression of ASF1B and Ki67 in tumor tissues. Western blot analysis was used to determine levels of ASF1B and proliferation/epithelial mesenchymal transition (EMT)/stemness-related proteins. In addition, the proliferation of CRC cells was assessed using Cell Counting Kit-8 and 5-Ethynyl-2′-Deoxyuridine assays. The migration and invasion of CRC cells were evaluated using transwell assays. Stemness of CRC cells was tested using the sphere formation assay. To construct a xenograft tumor model, HCT116 cells were introduced into mouse flanks *via* subcutaneous injection.

RESULTS

ASF1B expression was markedly increased in CRC tissues and cells, and it was inversely correlated with overall survival of CRC patients and was positively associated with the tumor node metastasis (TNM) stage of CRC patients. Silencing of ASF1B suppressed proliferation, migration, invasion, stemness and EMT of

CRC cells as well as tumorigenesis of xenograft mice. Furthermore, protein levels of P-phosphatidylinositol 3-kinase (p-PI3K) and p-AKT were decreased after silencing of ASF1B in CRC cells. The inhibitory effects of ASF1B knockdown on cell proliferation, stemness and EMT were partly abolished by PI3K activator in CRC cells.

CONCLUSION

Silencing of ASF1B inactivated the PI3K/AKT pathway to suppress CRC malignancy *in vitro*.

Key Words: Colorectal cancer; Anti-silencing function 1B; Phosphatidylinositol 3-kinase/AKT; Stemness; Epithelial mesenchymal transition

Core Tip: Anti-silencing function 1B (ASF1B) expression was increased in colorectal cancer (CRC) tissues and cells, and was negatively associated with prognosis of CRC patients. Functionally, ASF1B knockdown repressed the malignant behaviors of CRC cells *in vitro* and tumorigenesis *in vivo*, therefore having potential for CRC treatment. Moreover, our findings showed that ASF1B down-regulation suppressed the malignant behaviors of CRC cells by inactivating the PI3K/AKT pathway.

Citation: Yu GH, Gong XF, Peng YY, Qian J. Anti-silencing function 1B knockdown suppresses the malignant phenotype of colorectal cancer by inactivating the phosphatidylinositol 3-kinase/AKT pathway. *World J Gastrointest Oncol* 2022; 14(12): 2353-2366

URL: https://www.wjgnet.com/1948-5204/full/v14/i12/2353.htm

DOI: https://dx.doi.org/10.4251/wjgo.v14.i12.2353

INTRODUCTION

Colorectal cancer (CRC) is a malignant gastrointestinal tumor, accounting for 8% of cancer-related deaths in 2018[1,2]. According to statistics, it leads to over 1 million deaths every year[3,4]. Despite great progress in CRC treatment including surgery, chemotherapy and combined therapy, CRC prognosis is still poor[5,6]. Therefore, deeper exploration of CRC pathogenesis and treatment targets is of importance to improve CRC therapy.

For the past few years, molecular targeting treatment has emerged as a research hotspot in CRC therapy[7,8]. Anti-silencing function 1 (ASF1), a conserved histone H3-H4 chaperone protein, is involved in the regulation of many processes such as transcription, DNA damage repair and DNA replication[9,10]. Of note, it includes two paralogous forms: ASF1A histone chaperone and ASF1B[11]. ASF1A is primarily implicated in regulation of DNA repair and cellular senescence, while ASF1B acts as a crucial regulator of cellular proliferation and cell cycle progression[10,12]. As a subtype of ASF1, up-regulated expression of ASF1B is reported to be associated with the poor prognosis of lung adenocarcinoma and breast cancer patients[13,14]. More importantly, ASF1B down-regulation is demonstrated to have anti-tumor ability in many cancers. For example, ASF1B knockdown suppresses cell proliferation, and promotes cell cycle arrest and apoptosis in cervical cancer[15]. ASF1B knockdown impairs proliferation, migration and invasion of lung cancer cells[16]. Silencing of ASF1B represses growth of hepatocellular carcinoma (HCC) cells, and induces cell cycle arrest[17]. Overall, ASF1B is gaining attention as an important player in the development of diverse cancers. However, the function and mechanistic understanding of ASF1B have rarely been reported in CRC.

The phosphatidylinositol 3-kinase (PI3K)/AKT pathway is widely found in tumors, and plays an important role in the growth and proliferation of tumor cells[18]. Notably, the PI3K/AKT pathway has been demonstrated to be involved in regulation of CRC progression and development[19,20]. For example, pleckstrin homology like domain family A member 2 down-regulation inactivates the PI3K/AKT pathway to inhibit proliferation, invasion and migration of CRC cells[19]. Pyrroline-5-carboxylate reductase 2 down-regulation suppresses the PI3K/AKT pathway to prevent proliferation, migration and invasion of CRC cells[20]. Inosine 5′-monophosphate dehydrogenase type II knockdown attenuates proliferation, invasion and migration abilities of CRC cells by inactivating the PI3K/AKT pathway[21]. In particular, ASF1B was revealed to affect the malignant behaviors of prostate cancer cells and pancreatic cancer cells by regulating the PI3K/AKT pathway[22,23]. Thus, we assumed that ASF1B may regulate the PI3K/AKT pathway to affect malignant progression of CRC. In this study, the expression pattern of ASF1B as well as the role of ASF1B was determined in CRC *in vitro* and *in vivo*. Furthermore, the molecular mechanism of ASF1B-mediated carcinogenesis was explored in CRC cells.

MATERIALS AND METHODS

Tissue samples

A total of 68 pairs of CRC tissues and adjacent normal tissues (3.0 cm away from the tumor margin) were obtained from CRC patients between June 2019 and January 2021, which were transported in liquid nitrogen to the laboratory and then stored at -80 °C until use. Pathological diagnosis of CRC patients (age range, 23-61 years; 35 males and 33 females) was conducted by three pathologists based on the eighth edition of the Union for International Cancer Control and the American Joint Committee on Cancer tumor node metastasis (TNM) classification[24,25]. The inclusion criteria were as follows: (1) Complete general information (including gender, age, ethnicity, past history and family history); and (2) Patients who underwent bidirectional endoscopy (colonoscopy performed immediately after gastroscopy). The exclusion criteria were as follows: (1) History of gastric cancer, peptic ulcer and other cancers; (2) Received antibiotics, proton pump inhibitors or glucocorticoids in the past month; (3) Patients who underwent chemotherapy, radiation therapy and other treatments for tumors; (4) Previous history of gastrointestinal surgery; (5) Presence of inflammatory bowel disease, Gardner's syndrome (a disease that affects the incidence of CRC) or familial adenoma; and (6) A history of systemic diseases. The current study obtained permission from the Ethics Committee of Zhebei Mingzhou Hospital (ZBMZYYLL211028), and all subjects signed informed consents. In addition, CRC patients were divided into ASF1B high or low-expression groups based on the median value of ASF1B expression.

Follow-up

The survival of patients was followed for 90 mo through the records of reexamination or the telephone.

Online website

The online website GEPIA (http://gepia.cancer-pku.cn/detail.php) was used to compare the expression of ASF1B between tumor tissues and normal tissues in CRC.

Cell culture

A human normal colorectal mucosal cell line (FHC) and CRC cell lines (HT29, HCT116, LOVO, SW480 and SW620) were bought from the American Type Culture Collection (ATCC, Manassas, VA, United States). All cells were cultured in Roswell Park Memorial Institute (RPMI) 1640 medium (Invitrogen, Carlsbad, CA, United States) containing 10% fetal bovine serum (FBS) (Gibco, Gaithersburg, MD, United States) and 1% penicillin/streptomycin (Gibco), which were incubated at 37 °C under 5% CO_2. To eliminate mycoplasma contamination, all cells were routinely examined using MycAway (Yeasen, Shanghai, China).

Cell transfection

Short hairpin RNAs against ASF1B (sh-ASF1B#1, sh-ASF1B#2 and sh-ASF1B#3) and sh-negative control (sh-NC) were bought from RiboBio (Guangzhou, China). Then HCT116 and SW620 cells were seeded in six-well plates to adjust the cell density to 5×10^5/mL. When the cell confluence reached 70%-80%, the above plasmids (final concentrations, 50 nM) were transiently transfected into cells through Lipofectamine 3000 (Invitrogen) for 48 h. To further explore the role of the PI3K/AKT pathway in CRC cells, transfected HCT116 cells were treated with PI3K activator (740 Y-P, 50 μg/mL, MedChemexpress, Shanghai, China) for 90 min[26].

Quantitative real-time polymerase chain reaction

Total RNAs in CRC tissues were isolated using TRIzol reagent (Invitrogen), and then used for synthesis of complementary DNAs (cDNAs) according to the instructions of a PrimeScript RT reagent kit (Takara, Dalian, China). Next, cDNAs and the SYBR Green polymerase chain reaction (PCR) kit (Takara) were used to perform quantitative real-time PCR (qRT-PCR) on a LightCycler 480 Real-Time PCR system (Roche, Shanghai, China). Reaction procedures for PCR were displayed as follows: 5 min at 94 °C, 38 cycles of 25 s at 94 °C, 1 min at 60 °C and 2 min at 72 °C. Primers bought from Sangon (Shanghai, China) were as follows: ASF1B-F, GATCAGCTTCGAGTGCAGTG; ASF1B-R, TGGTAGGTGCAGGTGATGAG; GAPDH-F, CCATCTTCCAGGAGCGAGAT; GAPDH-R, TGCTGATGATCTTGAGGCTG. Relative mRNA expression of ASF1B, which was normalized to GAPDH, was calculated using the $2^{-\Delta\Delta ct}$ method.

Cell Counting Kit-8 assay

Proliferation of HCT116 and SW620 cells was assessed through a Cell Counting Kit-8 (CCK-8) kit (Beyotime, Shanghai, China). Briefly, transfected cells (5×10^3 cells/well) were plated into 96-well plates, followed by incubation for 0 h, 24 h, 48 h, 72 h and 96 h. After that, CCK-8 solution (10 μL) was added to each well and the cells were incubated at 37 °C for 2 h. Finally, the optical density at 450 nm was measured using a microplate reader (MG LABTECH, Durham, NC, United States).

5-Ethynyl-2'-Deoxyuridine assay

Proliferation of HCT116 and SW620 cells was assessed using the 5-Ethynyl-2'-Deoxyuridine (EDU) proliferation assay (RiboBio). In detail, HCT116 and SW620 cells (1×10^5 cells/well) were plated to 96-well plates. Then these cells were exposed to 50 μM EDU at 37 °C for 2 h, and fixed with 4% formaldehyde for 30 min and permeabilized with 0.1% Triton X-100 for 20 min. The EDU solution was then added to the culture, followed by staining of nuclei *via* Hoechst. EDU-positive cells were observed using a fluorescent microscope.

Transwell assay

The invasion of HCT116 and SW620 cells was assessed using the transwell chamber (8.0 μm pore size; Millipore, Billerica, MA, United States) coated with Matrigel. In brief, cells (100000 cells/well) re-suspended in FBS-free medium were placed onto the upper compartment. Subsequently, the upper compartment was filled with 600 μL culture medium with 10% FBS. The chambers were then incubated for 24 h, and cells in the lower surface were fixed with 4% paraformaldehyde and dyed with 0.1% crystal violet. Invasive cells were counted under an optical microscope. In contrast, cell migration was assessed in the upper chamber without Matrigel, and the procedures were the same as the invasion evaluation.

Sphere formation assay

Stemness of HCT116 and SW620 cells was evaluated by the sphere formation assay. Briefly, cells (250 cells/well) were placed into 24-well plates with ultra-low attachment, which were cultured in RPMI 1640 medium containing 10 ng/mL fibroblast growth factor, 10 μg/mL insulin, 10 ng/mL epidermal growth factor and 2% B-27. After 10 d of incubation, representative fields were photographed using a Nikon microscope.

Western blot analysis

Protein extraction of CRC tissues and cells was performed using RIPA lysis buffer (Beyotime). The lysates were then centrifuged (12000 r/min) for 10 min at 4 °C, and 5 × loading buffer was added to the supernatant to denature at 100 °C for 5 min. Determination of protein concentration was performed using a BCA Protein Assay Kit (Beyotime). Subsequently, the sodium dodecyl sulfate-polyacrylamide gel with 5% stacking gel and 10% separation gel was prepared, and these protein samples (10 μL) were separated by electrophoresis in 1 × buffer [500 mL ddH_2O, 9.4 g glycine, 1.51 g Tris-base and 0.5 g sodium dodecyl sulfate (SDS)] at 80 V for 30 min and at 120 V for 1 h. Next, the proteins were subjected to 10% SDS polyacrylamide gel electrophoresis, after which the proteins were transferred to polyvinylidene difluoride membranes (Millipore, Darmstadt, Germany). After being blocked with 5% skim milk, primary antibodies (Abcam, Cambridge, CA, United States) including anti-ASF1B (1:1000, ab276071), anti-E-cadherin (1:10000, ab40772), anti-N-cadherin (1:1000, ab245117), anti-SOX2 (1:1000, ab92494), anti-OCT4 (1:10000, ab200834), anti-p-PI3K (1:500, ab278545), anti-PI3K (1:1000, ab32089), anti-p-AKT (1:500, ab38449), anti-AKT (1:500, ab8805) and anti-β-actin (1:200, ab115777) were added to immerse the membranes at 4 °C overnight. Then the secondary antibody (1:2000, ab6721) was added. Finally, the ECL chemiluminescent system was used to examine protein blots and Image J software (NIH, United States) was used to analyze the intensity of protein blots.

Immunohistochemistry staining

Mouse tumor tissues fixed with 4% paraformaldehyde were embedded using paraffin and cut into sections (4 μm), and then dried at 62 °C for 1 h. Next, these sections were deparaffinized using xylene for 20 min, and soaked in 100%, 95%, 90%, 80% and 70% ethyl alcohol for 5 min. Antigen repair was then performed at 120 °C in citrate buffer (pH 6.0), and the tissue sections were cooled at room temperature. After being washed with phosphate buffered saline (PBS), incubated in H_2O_2 and washed with PBS again, sections were blocked using bovine serum albumin (5%) for 1 h. Subsequently, primary antibodies including anti-ASF1B (1:200, ab235358, Abcam) and anti-Ki67 (1:200, ab16667, Abcam) were added and incubated overnight. The secondary antibody (1:500, ab6112, Abcam) was added, followed by addition of 3,3'-diaminobenzidine substrate solution. Finally, hematoxylin was used to stain the samples, and staining areas were observed by microscopy.

Xenograft assay

Animal experiments received permission from the Institutional Animal Care and Use Committee of Beijing Viewsolid Biotechnology Co., Ltd (VS212601454), which complied with the National Institutes of Health Guide for the Care and Use of Laboratory Animals as well as ARRIVE guidelines. Female BALB/C nude mice (5-wk old), were purchased from the Chinese Academy of Sciences (Shanghai, China), and were kept at 25 °C under a 12 h light/dark cycle and 50% humidity.

To establish a xenograft mouse model, 5×10^6 HCT116 cells transfected with sh-NC or sh-ASF1B#1 were introduced into the right flank of mice *via* subcutaneous injection[27]. The mice were randomly divided into two groups (n = 5/group): The sh-NC group and the sh-ASF1B#1 group. The tumor size was gauged every week after injection. Tumor volume was calculated using the formula V = (shortest

diameter)^2 × (longest diameter) × 0.5. On the 35th d after the injection, the mice were anesthetized by an intraperitoneal injection of sodium pentobarbital (50 mg/kg) and then euthanized by cervical dislocation. Finally, the tumors were collected for further analysis.

Statistical analysis

Data from three separate experiments are presented as mean ± SD. GraphPad Prism 7.0 (GraphPad Software Inc., La Jolla, CA, United States) was used to perform statistical analysis. Student's *t*-test was performed to analyze differences between two groups. Survival curves were plotted using the Kaplan-Meier method and differences between survival curves were assessed using the log-rank test. Clinicopathological characteristics between patients who demonstrated high ASF1B expression *vs* those with low expression were compared using the χ^2 test. Differences of $P < 0.05$ were considered statistically significant.

RESULTS

High expression of ASF1B is observed in CRC tissues and is associated with adverse clinicopathological CRC characteristics

We firstly analyzed ASF1B expression in the TCGA database, and observed up-regulation of ASF1B expression in tissues of colon adenocarcinoma and rectum adenocarcinoma in contrast to corresponding noncancerous tissues (Figure 1A, $P < 0.05$). We validated mRNA expression of ASF1B using qRT-PCR. As expected, the mRNA expression of ASF1B was increased in CRC tissues relative to that in normal tissues (Figure 1B, $P < 0.01$). Moreover, the protein expression of ASF1B was detected by immunohistochemistry staining and western blot, and higher ASF1B expression was found in tumor tissues than in normal tissues (Figures 1C and 1D, $P < 0.05$). We further investigated the clinical significance of ASF1B in CRC and found that ASF1B expression was significantly associated with TNM stage, lymph node metastasis and distant metastasis (Table 1). The expression of ASF1B was markedly higher in CRC patients at TNM stage III/IV than in CRC patients at TNM stage I/II (Figure 1E, $P < 0.01$). ASF1B up-regulation resulted in poor survival of CRC patients (Figure 1F, $P < 0.01$).

Silencing of ASF1B impairs proliferation of CRC cells

The protein expression of ASF1B was detected by western blot in a normal colorectal mucosal cell line (FHC) and CRC cell lines. Examination by western blot showed that ASF1B expression was increased in HT29, HCT116, LOVO, SW480 and SW620 cells compared to FHC cells ($P < 0.001$) and especially in SW620 and HCT116 cells. Therefore, the impact of ASF1B on CRC cell proliferation was investigated through loss-of-function assays in the HCT116 and SW620 cell lines.

Next, the impact of ASF1B on proliferation of CRC cells was probed through loss-of-function assays. Firstly, ASF1B was silenced by transfection of sh-ASF1B#1 and sh-ASF1B#2 in HCT116 and SW620 cells (Figure 2B, $P < 0.01$), and sh-ASF1B#1 and sh-ASF1B#2 were utilized for subsequent function experiments. The influence of ASF1B on proliferation of CRC cells was then determined by CCK-8 and EDU assays. It was found that the proliferation ability of HCT116 and SW620 cells was attenuated by ASF1B knockdown (Figures 2C and 2D, $P < 0.05$). In addition, we found that protein levels of proliferation markers (Ki67 and PCNA) were decreased after ASF1B knockdown in HCT116 and SW620 cells (Figure 2E, $P < 0.01$).

ASF1B down-regulation represses migration, invasion, stemness and epithelial mesenchymal transition of CRC cells

When we explored the influence of ASF1B on cell migration and invasion, and suppression of migration and invasion caused by ASF1B knockdown was found in HCT116 cells and SW620 cells (Figures 3A and 3B, $P < 0.001$). In addition, we detected the influence of ASF1B on cell stemness and EMT. It was demonstrated that ASF1B down-regulation led to an evident decrease in sphere formation of HCT116 and SW620 cells (Figure 3C), indicating that ASF1B down-regulation suppressed cell stemness. We also examined the levels of EMT-related proteins (E-cadherin and N-cadherin) and stemness marker proteins (SOX2 and OCT) using western blot. As expected, we observed an increased level of E-cadherin and a decreased level of N-cadherin as well as decreased levels of SOX2 and OCT after ASF1B down-regulation in HCT116 and SW620 cells (Figure 3D, $P < 0.05$).

PI3K activator reverses the inhibitory impact of ASF1B down-regulation on proliferation, stemness and EMT of CRC cells

In order to examine the underlying mechanism involved in the regulatory impact of ASF1B on CRC malignancy, subsequent experiments were conducted. It was demonstrated that p-PI3K and p-AKT levels were reduced in response to ASF1B knockdown in HCT116 and SW620 cells (Figure 4A, $P < 0.01$). In addition, reduction of p-PI3K and p-AKT levels caused by ASF1B knockdown was reversed by

Table 1 Association between clinical parameters of colorectal cancer patients and anti-silencing function 1B expression

Variable	Total	ASF1B expression (*n* = 68)		*P* value
		Low (*n* = 34)	High (*n* = 34)	
Age				0.622
< 45 yr	28 (3.69 ± 0.74)	15 (3.11 ± 0.33)	13 (4.41 ± 0.37)	
45 yr	40 (3.73 ± 0.62)	19 (3.20 ± 0.39)	21 (4.21 ± 0.37)	
Gender				0.4667
Female	33 (3.68 ± 0.68)	18 (3.16 ± 0.35)	15 (4.30 ± 0.41)	
Male	35 (3.74 ± 0.66)	16 (3.17 ± 0.39)	19 (4.24 ± 0.37)	
Tumor size				0.4921
< 2 cm	24 (3.77 ± 0.71)	11 (3.14 ± 0.42)	13 (4.31 ± 0.36)	
≥ 2 cm	44 (3.68 ± 0.65)	24 (3.20 ± 0.35)	20 (4.26 ± 0.40)	
TNM stage				0.0035[b]
I/II	41 (3.54 ± 0.64)	27 (3.16 ± 0.38)	14 (4.26 ± 0.35)	
III/IV	27 (3.99 ± 0.62)	8 (3.25 ± 0.35)	19 (4.30 ± 0.40)	
Lymph node metastasis				0.0158[a]
Negative	36 (3.32 ± 0.68)	29 (2.97 ± 0.35)	7 (4.21 ± 0.42)	
Positive	32 (3.95 ± 0.55)	17 (3.40 ± 0.24)	15 (4.30 ± 0.37)	
Distant metastasis				0.0040[b]
Negative	30 (3.39 ± 0.64)	20 (3.02 ± 0.33)	10 (4.12 ± 0.43)	
Positive	38 (3.98 ± 0.57)	12 (3.31 ± 0.28)	26 (4.28 ± 0.38)	

[a]$P < 0.05$.
[b]$P < 0.01$.
TNM: Tumor node metastasis; ASF1B: Anti-silencing function 1B.

addition of PI3K activator (740 Y-P) in HCT116 cells (Figure 4B, $P < 0.05$). More importantly, the inhibitory effect of ASF1B knockdown on proliferation was partly abolished by the addition of PI3K activator in HCT116 cells (Figure 4C). The inhibitory effects of ASF1B knockdown on protein levels of N-cadherin, SOX2 and OCT as well as the promoting effect of ASF1B knockdown on the level of E-cadherin were partly reversed by addition of PI3K activator in HCT116 cells (Figure 4D, $P < 0.05$). These results implied that ASF1B down-regulation had an impact on CRC malignancy by regulating the PI3K/AKT pathway.

Silencing of ASF1B represses CRC tumorigenesis in mice

After detecting the function of ASF1B in CRC *in vitro*, we next verified its function *in vivo*. As illustrated in Figures 5A-C, silencing of ASF1B inhibited tumor growth, and reduced tumor volume and weight in xenograft mice ($P < 0.05$). Likewise, protein levels of Ki67 and ASF1B were reduced after ASF1B knockdown in tumor tissues of mice (Figure 5D).

DISCUSSION

Over the past years, the mortality rate of CRC patients is increasing and limited prognosis poses a severe threat to CRC patients[28-30]. Thus, developing new effective therapies for CRC patients is imperative. Emerging evidence has uncovered that ASF1B is highly expressed and shows potential clinical value for the prognosis of cancer patients[13,17]. For instance, ASF1B shows high expression in HCC tissues, and ASF1B up-regulation is correlated with poor survival of HCC patients[17]. ASF1B expression is increased in tissues of lung adenocarcinoma, and ASF1B up-regulation is correlated with worse overall survival in lung adenocarcinoma patients[13]. Here, we also found up-regulation of ASF1B expression in CRC tissues and cells, and our outcome was consistent with prior reports[14,31]. We also discovered that ASF1B expression was significantly associated with TNM stage, lymph node metastasis and distant metastasis. In addition, ASF1B expression was inversely relevant to survival data

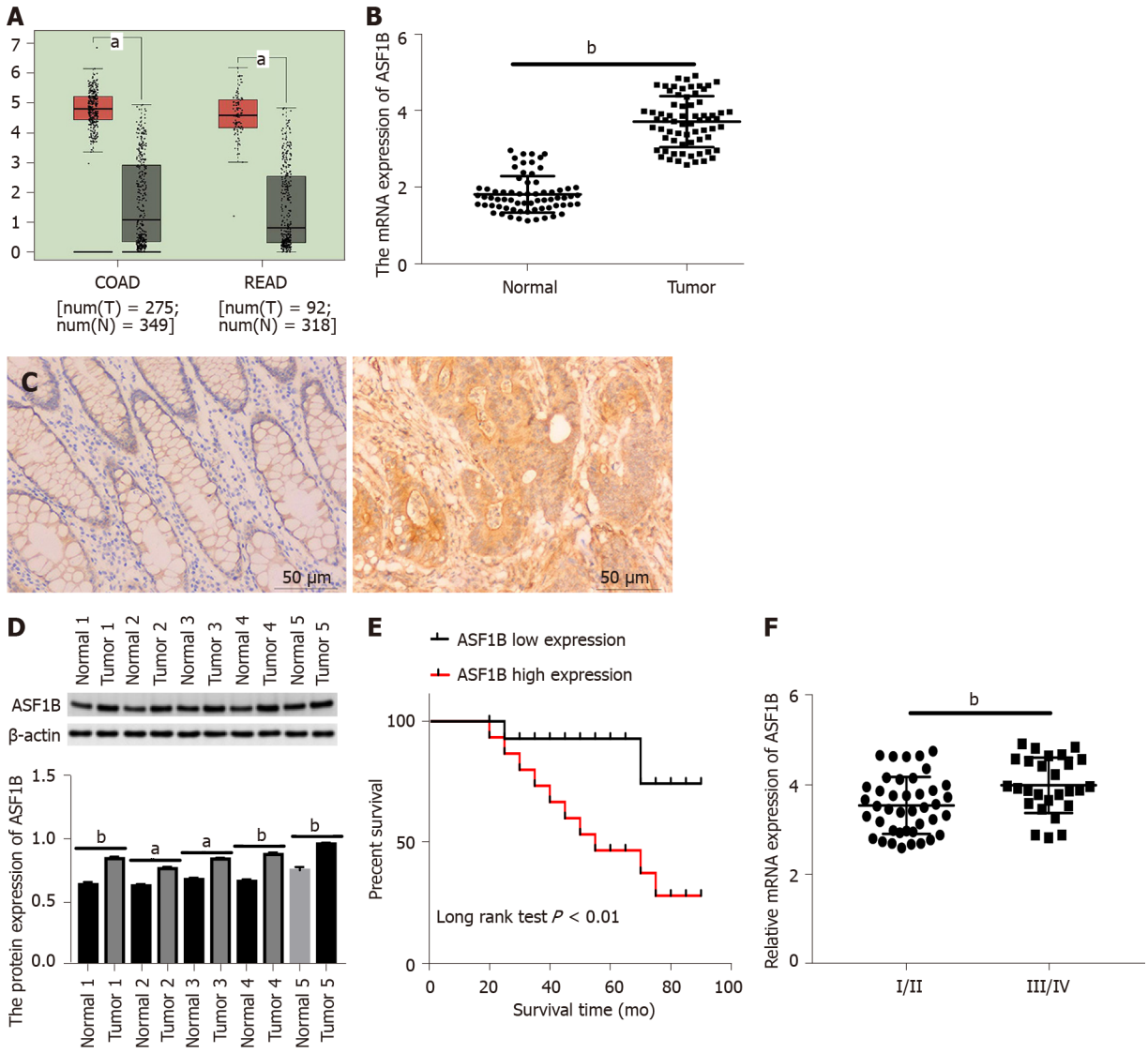

DOI: 10.4251/wjgo.v14.i12.2353

Figure 1 High expression of anti-silencing function 1B is observed in colorectal cancer tissues. A: The expression of anti-silencing function 1B (ASF1B) in tumor tissues and adjacent normal tissues was predicted based on The Cancer Genome Atlas database; B: Relative mRNA expression of ASF1B was detected by quantitative real-time polymerase chain reaction (qRT-PCR) in adjacent normal tissues and tumor tissues of colorectal cancer (CRC) patients; C: The protein expression of ASF1B in normal tissues and tumor tissues was detected by immunohistochemical staining; D: The protein expression of ASF1B in normal tissues and tumor tissues was detected by western blot; E: Relative expression of ASF1B at tumor node metastasis (TNM) stage I/II and TNM stage III/IV was determined by qRT-PCR in tumors; F: Kaplan-Meier analysis of the correlation between ASF1B expression and overall survival of CRC patients. $^{a}P < 0.05$, $^{b}P < 0.01$. Each experiment was repeated three times. ASF1B: Anti-silencing function 1B.

of CRC patients, and was markedly higher in CRC patients with advanced TNM stages than in patients with earlier stages. These results suggested that ASF1B may be a useful marker for prognosis and diagnosis assessment in CRC patients.

In previous studies, ASF1B was reported to be a key regulator in cancer progression[15,16]. For instance, ASF1B knockdown prevents cervical cancer cells from proliferating, migrating and invading, and suppresses tumor growth in mice[15]. ASF1B knockdown inhibits migration, invasion and EMT of lung cancer cells, and retards tumor growth in xenograft mice as well as the expression of Ki67[16]. Similarly, our outcomes *in vitro* displayed that ASF1B down-regulation distinctly attenuated proliferation, migration and invasion abilities of HCT116 and SW620 cells, and inhibited EMT and stemness of HCT116 and SW620 cells. As an important cancer hallmark in metastases and the "cadherin switch", EMT was demonstrated to initiate CRC metastasis from the primary tumor to distant sites, especially to liver and lymph nodes[32,33]. It was reported that loss of E-cadherin can cause metastatic dissemination and activation of EMT transcription factors in cancer cells[34]. Many invasive and metastatic cancers are associated with high expression of E-cadherin, notably in prostate cancer[35], ovarian cancer[36], and glioblastoma[37], suggesting that E-cadherin facilitates metastasis in several tumors instead of inhibiting tumor progression. In addition, N-cadherin is reported to act as an indicator of ongoing EMT and N-cadherin down-regulation can cause metastatic dissemination[38]. In our study, we found that the

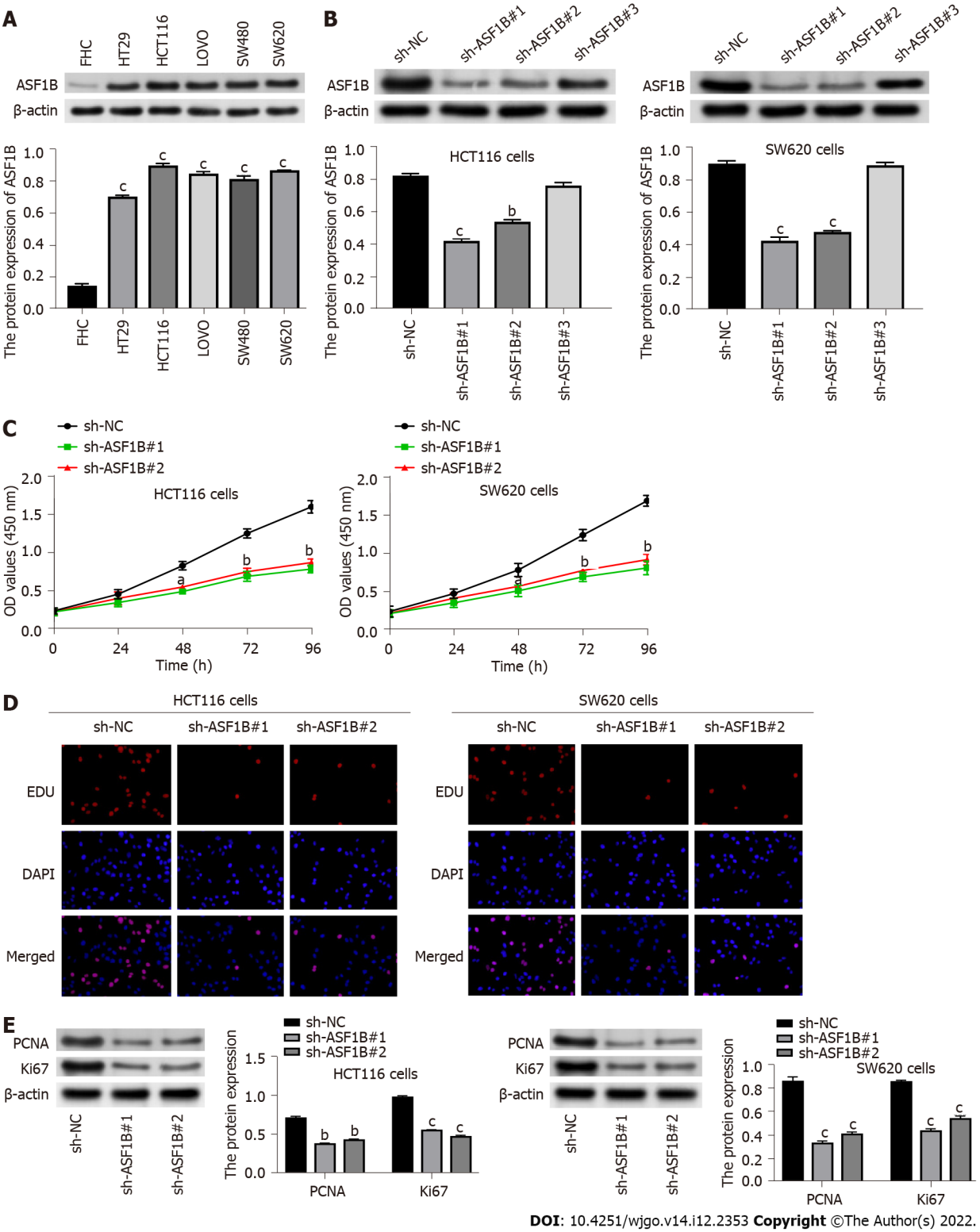

Figure 2 Silencing of anti-silencing function 1B impairs proliferation of colorectal cancer cells. A: The protein expression of anti-silencing function 1B (ASF1B) was detected by western blot in FHC, HT29, HCT116, LOVO, SW480 and SW620 cells; B: The protein expression of ASF1B was detected by western blot in HCT116 and SW620 cells after transfection of sh-ASF1B#1, sh-ASF1B#2 or sh-ASF1B#3; C and D: The proliferation of HCT116 and SW620 cells was evaluated by Cell Counting Kit-8 and 5-Ethynyl-2'-Deoxyuridine assays after transfection of sh-ASF1B#1 or sh-ASF1B#2; E: Protein levels of PCNA and Ki67 were examined by western blot in HCT116 and SW620 cells after transfection of sh-ASF1B#1 or sh-ASF1B#2. $^{a}P < 0.05$, $^{b}P < 0.01$, $^{c}P < 0.001$. Each experiment was repeated three times. ASF1B: Anti-silencing function 1B; NC: Negative control.

silencing of ASF1B results in a reverse cadherin switch phenomenon, indicating a potentially important role of ASF1B silencing in reducing the metastatic potential of CRC cells *in vitro*. In addition, our *in vivo* results indicated that ASF1B down-regulation suppressed tumor growth in xenograft mice as well as Ki67 expression. These findings provided evidence of the anti-tumor role of ASF1B knockdown in CRC,

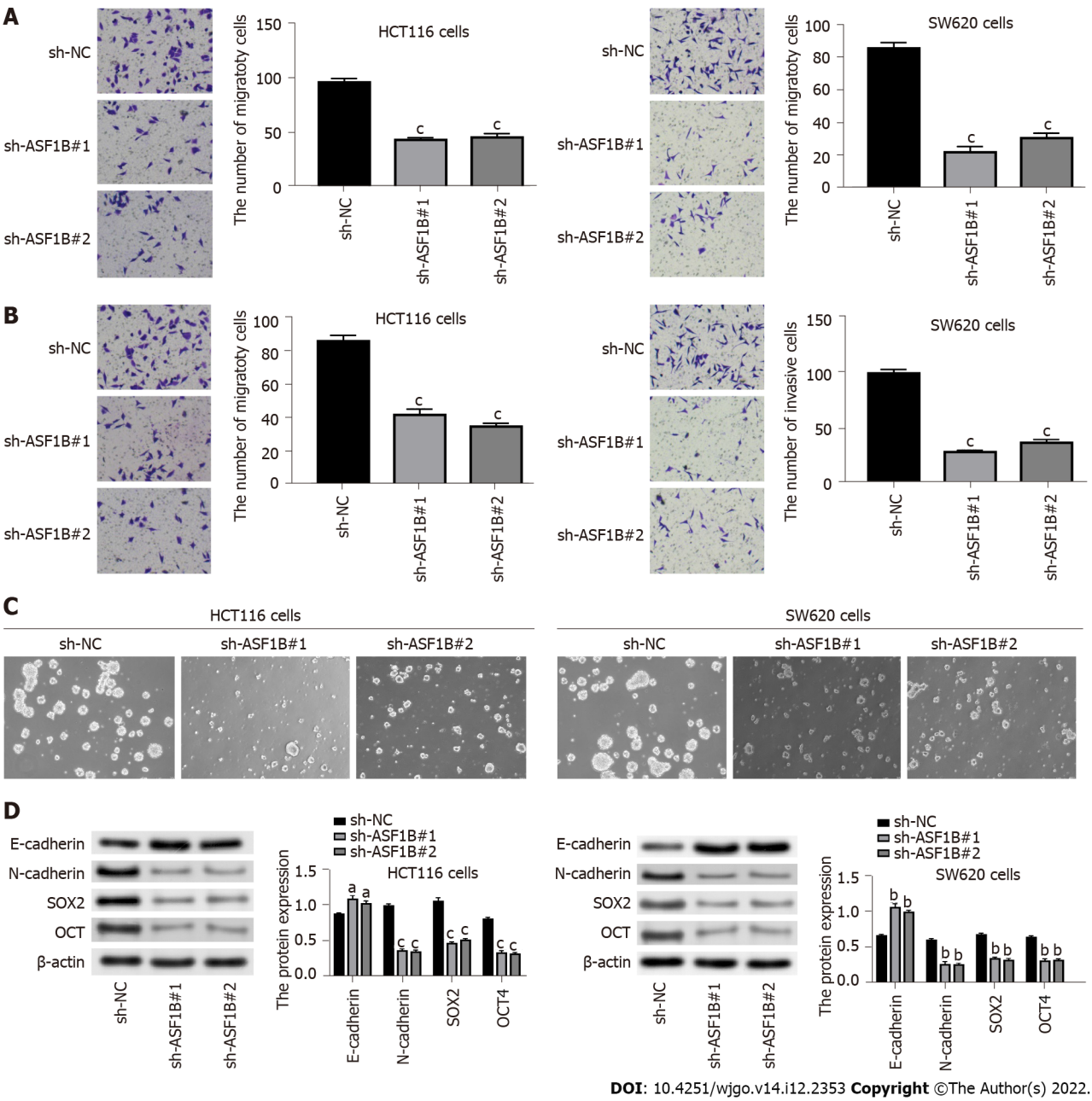

DOI: 10.4251/wjgo.v14.i12.2353 **Copyright** ©The Author(s) 2022.

Figure 3 Anti-silencing function 1B down-regulation represses migration, invasion, stemness and epithelial mesenchymal transition of colorectal cancer cells. A and B: Migration and invasion of HCT116 and SW620 cells were detected by transwell assay after transfection of sh-anti-silencing function 1B (ASF1B)#1 or sh-ASF1B#2; C: The stemness of HCT116 and SW620 cells was measured using the sphere formation assay after transfection of sh-ASF1B#1 or sh-ASF1B#2; D: Protein levels of E-cadherin, N-cadherin, SOX2 and OCT4 were detected by western blot in HCT116 and SW620 cells after transfection of sh-ASF1B#1 or sh-ASF1B#2. $^{a}P < 0.05$, $^{b}P < 0.01$, $^{c}P < 0.001$. Each experiment was repeated three times. ASF1B: Anti-silencing function 1B; NC: Negative control.

and shed light on exploring promising therapeutic agents for CRC treatment.

Considering the important function of ASF1B in CRC, we attempted to examine how ASF1B affected CRC progression and development. It is noteworthy that ASF1B has been proved to affect progression and development of cancers by regulating the PI3K/AKT pathway[22,23]. For instance, suppression of the PI3K/AKT pathway is pertinent to the influence of ASF1B knockdown on prostate cancer[22]. Silencing of ASF1B impairs cell proliferation by inactivating the PI3K/AKT pathway in pancreatic cancer[23]. In this study, we also investigated whether the PI3K/AKT pathway participated in ASF1B knockdown-mediated tumor inhibition in CRC cells. It was found that protein levels of p-PI3K and p-AKT were decreased due to ASF1B knockdown in HCT116 and SW620 cells. Concurrently, suppressive influences of ASF1B knockdown on proliferation, stemness and EMT of HCT116 cells were reversed by PI3K activator. Combining the above findings, we concluded that ASF1B knockdown repressed the malignant behaviors of CRC cells by inactivation of the PI3K/AKT pathway.

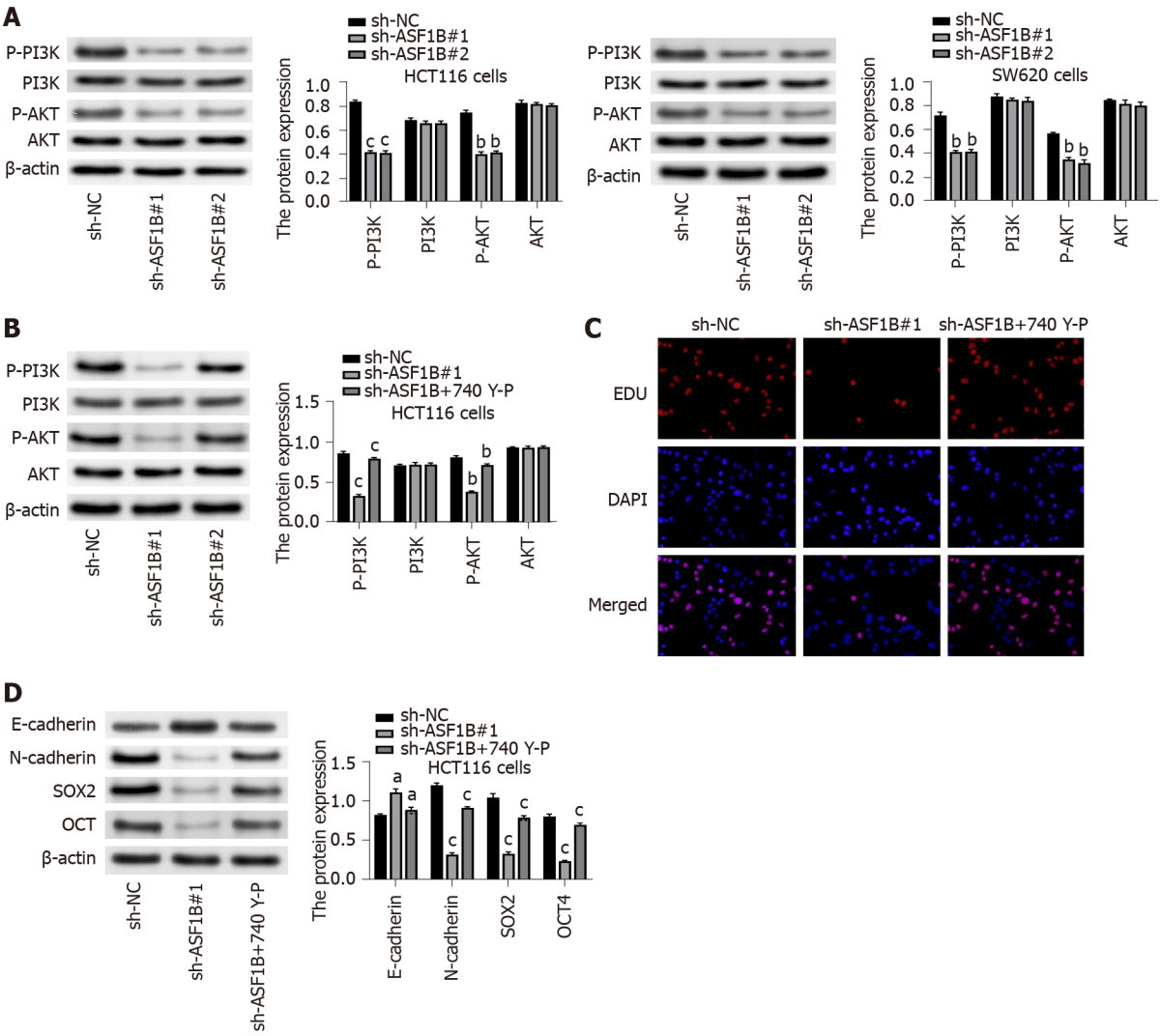

DOI: 10.4251/wjgo.v14.i12.2353 **Copyright** ©The Author(s) 2022.

Figure 4 Phosphatidylinositol 3-kinase activator reverses the inhibitory impact of anti-silencing function 1B down-regulation on proliferation, stemness and epithelial mesenchymal transition of colorectal cancer cells. A: Protein levels of p-phosphatidylinositol 3-kinase (PI3K), PI3K, p-AKT and AKT were detected by western blot in HCT116 and SW620 cells after transfection of sh-anti-silencing function 1B (ASF1B)#1 or sh-ASF1B#2; B: Protein levels of p-PI3K, PI3K, p-AKT and AKT were detected by western blot in HCT116 cells. Short hairpin RNA against ASF1B (sh-ASF1B#1) *vs* sh-negative control (NC), sh-ASF1B+740 Y-P *vs* sh-ASF1B#1; C: The proliferation of HCT116 cells was evaluated by the 5-Ethynyl-2'-Deoxyuridine assay; D: Protein levels of E-cadherin, N-cadherin, SOX2 and OCT4 were detected by western blot in HCT116 cells. sh-ASF1B#1 *vs* sh-NC, sh-ASF1B + 740 Y-P *vs* sh-ASF1B#1. $^{a}P < 0.05$, $^{b}P < 0.01$, $^{c}P < 0.001$. Each experiment was repeated three times. ASF1B: Anti-silencing function 1B; NC: Negative control.

However, there were three limitations in our study. Firstly, we only explored the role of ASF1B knockdown in CRC, and the overexpression experiment of ASF1B should be performed to further validate the influence of ASF1B on CRC. Secondly, only *in vitro* studies have been performed and therefore *in vivo* studies are recommended to strengthen the study's hypothesis. Thirdly, we failed to perform a-priori sample calculation, and we determined the sample size through a literature search. Overall, the novelty of this study included two aspects. Firstly, we demonstrated the role of ASF1B in CRC *in vitro* and *in vivo* for the first time. Secondly, we uncovered a new mechanism by which ASF1B impacted CRC cells.

CONCLUSION

In summary, ASF1B expression was increased in CRC tissues and cells, and was negatively associated with the prognosis of CRC patients. Functionally, ASF1B knockdown repressed the malignant behaviors of CRC cells *in vitro* and tumorigenesis *in vivo*, therefore having potential for CRC treatment. Moreover, our findings revealed that ASF1B down-regulation repressed impaired behaviors of CRC cells by inactivating the PI3K/AKT pathway. Our study provides new insights into the functional importance of ASF1B in CRC, and indicates that ASF1B may be a promising prognostic marker and a target for the

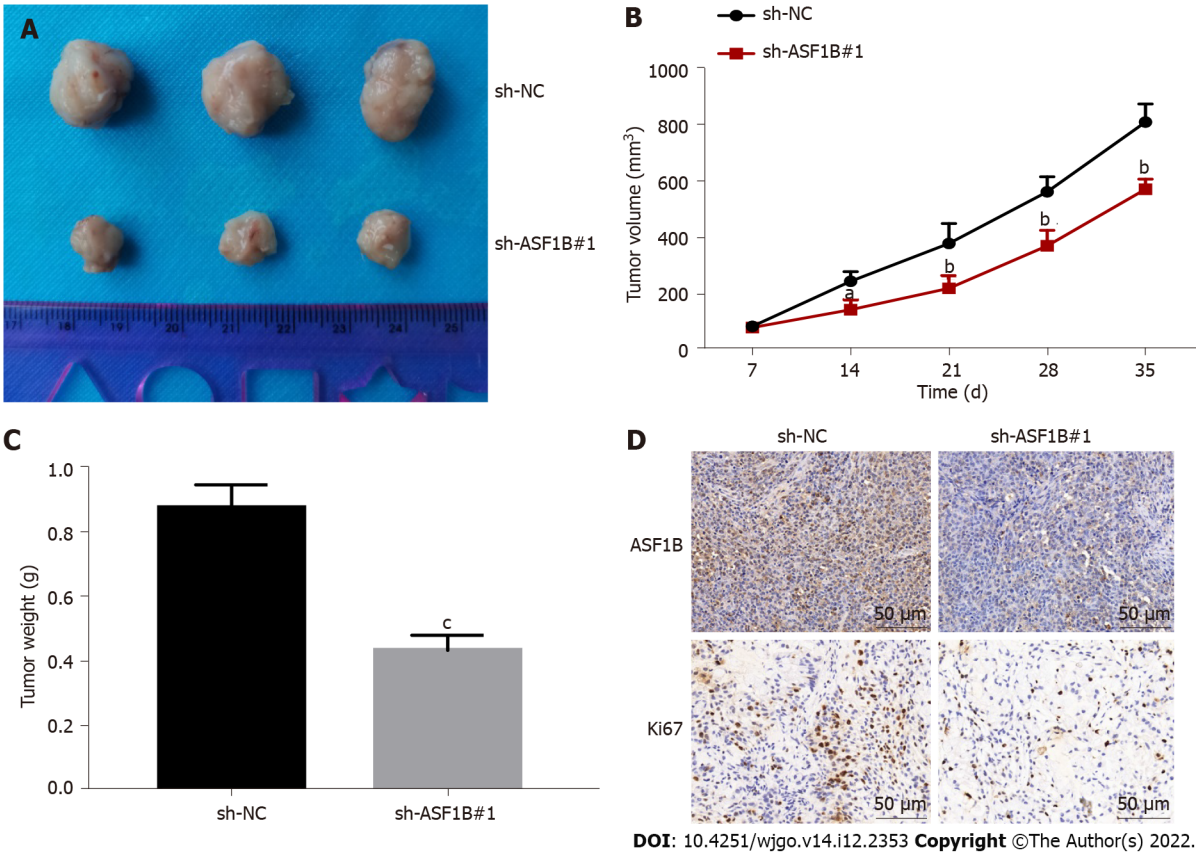

DOI: 10.4251/wjgo.v14.i12.2353

Figure 5 Silencing of anti-silencing function 1B represses colorectal cancer tumorigenesis in mice. A: Representative images of tumors in xenograft mice; B: The tumor volume in xenograft mice was monitored every 7 d and then the tumor growth curves of mice were constructed; C: Average tumor weight of xenograft mice was gauged; D: Protein levels of Ki67 and anti-silencing function 1B in tumor tissues of xenograft mice were determined by immunohistochemical staining. $^{a}P < 0.05$, $^{b}P < 0.01$, $^{c}P < 0.001$. $n = 5$. ASF1B: Anti-silencing function 1B; NC: Negative control.

management of CRC.

ASF1B may be a potential diagnostic and prognostic biomarker for improving CRC patients' outcome. More importantly, ASF1B may be a novel target for the treatment of CRC, showing promising prospects in clinical practice. In our future studies, we plan to perform *in vivo* studies to validate the role of ASF1B in CRC. Moreover, we expect more investigations into the other mechanisms of ASF1B in cancers.

ARTICLE HIGHLIGHTS

Research background

Colorectal cancer (CRC) is identified as a malignant gastrointestinal tumor, with high prevalence and mortality. Abundant studies have proved the important role of anti-silencing function 1B (ASF1B) in cancers, but little is known about ASF1B in CRC.

Research motivation

In order to identify the prognosis biomarker and treatment target for CRC.

Research objectives

To evaluate the role and mechanism of ASF1B in CRC.

Research methods

The mRNA expression of ASF1B was detected by quantitative real-time polymerase chain reaction. The clinical value of ASF1B for diagnosis and prognosis of CRC was assessed. The function of ASF1B was evaluated using *in vitro* assays and *in vivo* tumor formation experiments. The molecular mechanism of ASF1B on the phosphatidylinositol 3-kinase (PI3K)/AKT pathway was explored *via* the addition of PI3K activator.

Research results

The expression level of ASF1B was markedly increased in CRC tissues and cells, which was inversely associated with survival time of CRC patients and positively associated with tumor node metastasis stage of CRC patients. Biological functional analyses indicated that ASF1B knockdown may suppress the malignancy of CRC cells by regulating the PI3K/AKT pathway.

Research conclusions

ASF1B is highly expressed in CRC tissues and cells, showing potential as a diagnostic and prognostic biomarker for CRC. Silencing of ASF1B inactivated the PI3K/AKT pathway to inhibit CRC malignancy *in vitro*.

Research perspectives

Other mechanisms of ASF1B in CRC may be investigated in the future, and its application in anti-tumor therapy will be extended.

FOOTNOTES

Author contributions: Yu GH, Gong XF and Qian J were involved in the conceptualization; Peng YY and Qian J contributed to the formal analysis and investigation; Yu GH and Gong XF wrote the original draft.

Supported by Huzhou Science and Technology Bureau Foundation, No. 2018GY09.

Institutional review board statement: The current study received permission from the Ethics Committee of Zhebei Mingzhou Hospital (ZBMZYYLL211028).

Institutional animal care and use committee statement: Animal experiments obtained permission from the Institutional Animal Care and Use Committee of Beijing Viewsolid Biotechnology Co., Ltd (VS212601454), which complied with the National Institutes of Health Guide for the Care and Use of Laboratory Animals as well as ARRIVE guidelines.

Informed consent statement: All subjects signed informed consents.

Conflict-of-interest statement: All the authors report no relevant conflicts of interest for this article.

Data sharing statement: All the data used to support the findings of this study are included within the article.

ARRIVE guidelines statement: The authors have read the ARRIVE guidelines, and the manuscript was prepared and revised according to the ARRIVE guidelines.

Country/Territory of origin: China

ORCID number: Jun Qian 0000-0001-8569-3560.

S-Editor: Wang JJ
L-Editor: Webster JR
P-Editor: Wang JJ

REFERENCES

1 **Siegel RL**, Miller KD, Jemal A. Cancer statistics, 2019. *CA Cancer J Clin* 2019; **69**: 7-34 [PMID: 30620402 DOI: 10.3322/caac.21551]
2 **Bray F**, Ferlay J, Soerjomataram I, Siegel RL, Torre LA, Jemal A. Global cancer statistics 2018: GLOBOCAN estimates of incidence and mortality worldwide for 36 cancers in 185 countries. *CA Cancer J Clin* 2018; **68**: 394-424 [PMID: 30207593 DOI: 10.3322/caac.21492]
3 **Siegel RL**, Miller KD, Fedewa SA, Ahnen DJ, Meester RGS, Barzi A, Jemal A. Colorectal cancer statistics, 2017. *CA Cancer J Clin* 2017; **67**: 177-193 [PMID: 28248415 DOI: 10.3322/caac.21395]
4 **Arnold M**, Sierra MS, Laversanne M, Soerjomataram I, Jemal A, Bray F. Global patterns and trends in colorectal cancer

incidence and mortality. *Gut* 2017; **66**: 683-691 [PMID: 26818619 DOI: 10.1136/gutjnl-2015-310912]
5 **Mármol I**, Sánchez-de-Diego C, Pradilla Dieste A, Cerrada E, Rodriguez Yoldi MJ. Colorectal Carcinoma: A General Overview and Future Perspectives in Colorectal Cancer. *Int J Mol Sci* 2017; **18** [PMID: 28106826 DOI: 10.3390/ijms18010197]
6 **Siegel RL**, Miller KD, Goding Sauer A, Fedewa SA, Butterly LF, Anderson JC, Cercek A, Smith RA, Jemal A. Colorectal cancer statistics, 2020. *CA Cancer J Clin* 2020; **70**: 145-164 [PMID: 32133645 DOI: 10.3322/caac.21601]
7 **Pang SW**, Awi NJ, Armon S, Lim WW, Low JS, Peh KB, Peh SC, Teow SY. Current Update of Laboratory Molecular Diagnostics Advancement in Management of Colorectal Cancer (CRC). *Diagnostics (Basel)* 2019; **10** [PMID: 31877940 DOI: 10.3390/diagnostics10010009]
8 **Müller MF**, Ibrahim AE, Arends MJ. Molecular pathological classification of colorectal cancer. *Virchows Arch* 2016; **469**: 125-134 [PMID: 27325016 DOI: 10.1007/s00428-016-1956-3]
9 **Peng H**, Nogueira ML, Vogel JL, Kristie TM. Transcriptional coactivator HCF-1 couples the histone chaperone Asf1b to HSV-1 DNA replication components. *Proc Natl Acad Sci U S A* 2010; **107**: 2461-2466 [PMID: 20133788 DOI: 10.1073/pnas.0911128107]
10 **Messiaen S**, Guiard J, Aigueperse C, Fliniaux I, Tourpin S, Barroca V, Allemand I, Fouchet P, Livera G, Vernet M. Loss of the histone chaperone ASF1B reduces female reproductive capacity in mice. *Reproduction* 2016; **151**: 477-489 [PMID: 26850882 DOI: 10.1530/REP-15-0327]
11 **Soniat M**, Cağatay T, Chook YM. Recognition Elements in the Histone H3 and H4 Tails for Seven Different Importins. *J Biol Chem* 2016; **291**: 21171-21183 [PMID: 27528606 DOI: 10.1074/jbc.M116.730218]
12 **Paul PK**, Rabaglia ME, Wang CY, Stapleton DS, Leng N, Kendziorski C, Lewis PW, Keller MP, Attie AD. Histone chaperone ASF1B promotes human β-cell proliferation *via* recruitment of histone H3.3. *Cell Cycle* 2016; **15**: 3191-3202 [PMID: 27753532 DOI: 10.1080/15384101.2016.1241914]
13 **Feng Z**, Zhang J, Zheng Y, Wang Q, Min X, Tian T. Elevated expression of *ASF1B* correlates with poor prognosis in human lung adenocarcinoma. *Per Med* 2021; **18**: 115-127 [PMID: 33576264 DOI: 10.2217/pme-2020-0112]
14 **Corpet A**, De Koning L, Toedling J, Savignoni A, Berger F, Lemaître C, O'Sullivan RJ, Karlseder J, Barillot E, Asselain B, Sastre-Garau X, Almouzni G. Asf1b, the necessary Asf1 isoform for proliferation, is predictive of outcome in breast cancer. *EMBO J* 2011; **30**: 480-493 [PMID: 21179005 DOI: 10.1038/emboj.2010.335]
15 **Liu X**, Song J, Zhang Y, Wang H, Sun H, Feng X, Hou M, Chen G, Tang Q, Ji M. ASF1B promotes cervical cancer progression through stabilization of CDK9. *Cell Death Dis* 2020; **11**: 705 [PMID: 32848135 DOI: 10.1038/s41419-020-02872-5]
16 **Wang W**, Xiao L, Pan D, Hu L. ASF1B enhances migration and invasion of lung cancers cell *via* regulating the P53-mediated epithelial-mesenchymal transformation (EMT) signaling pathway. *Neoplasma* 2022; **69**: 361-369 [PMID: 35103478 DOI: 10.4149/neo_2021_210818N1181]
17 **Ouyang X**, Lv L, Zhao Y, Zhang F, Hu Q, Li Z, Zhu D, Li L. ASF1B Serves as a Potential Therapeutic Target by Influencing Cell Cycle and Proliferation in Hepatocellular Carcinoma. *Front Oncol* 2021; **11**: 801506 [PMID: 35087760 DOI: 10.3389/fonc.2021.801506]
18 **Davis WJ**, Lehmann PZ, Li W. Nuclear PI3K signaling in cell growth and tumorigenesis. *Front Cell Dev Biol* 2015; **3**: 24 [PMID: 25918701 DOI: 10.3389/fcell.2015.00024]
19 **Ma Z**, Lou S, Jiang Z. PHLDA2 regulates EMT and autophagy in colorectal cancer *via* the PI3K/AKT signaling pathway. *Aging (Albany NY)* 2020; **12**: 7985-8000 [PMID: 32385195 DOI: 10.18632/aging.103117]
20 **Yin F**, Huang X, Xuan Y. Pyrroline-5-Carboxylate Reductase-2 Promotes Colorectal Cancer Progression *via* Activating PI3K/AKT/mTOR Pathway. *Dis Markers* 2021; **2021**: 9950663 [PMID: 34512817 DOI: 10.1155/2021/9950663]
21 **Duan S**, Huang W, Liu X, Chen N, Xu Q, Hu Y, Song W, Zhou J. IMPDH2 promotes colorectal cancer progression through activation of the PI3K/AKT/mTOR and PI3K/AKT/FOXO1 signaling pathways. *J Exp Clin Cancer Res* 2018; **37**: 304 [PMID: 30518405 DOI: 10.1186/s13046-018-0980-3]
22 **Han G**, Zhang X, Liu P, Yu Q, Li Z, Wei X. Knockdown of anti-silencing function 1B histone chaperone induces cell apoptosis *via* repressing PI3K/Akt pathway in prostate cancer. *Int J Oncol* 2018; **53**: 2056-2066 [PMID: 30132513 DOI: 10.3892/ijo.2018.4526]
23 **Wang K**, Hao Z, Fu X, Li W, Jiao A, Hua X. Involvement of elevated ASF1B in the poor prognosis and tumorigenesis in pancreatic cancer. *Mol Cell Biochem* 2022; **477**: 1947-1957 [PMID: 35362843 DOI: 10.1007/s11010-022-04404-5]
24 **Bertero L**, Massa F, Metovic J, Zanetti R, Castellano I, Ricardi U, Papotti M, Cassoni P. Eighth Edition of the UICC Classification of Malignant Tumours: an overview of the changes in the pathological TNM classification criteria-What has changed and why? *Virchows Arch* 2018; **472**: 519-531 [PMID: 29209757 DOI: 10.1007/s00428-017-2276-y]
25 **Amin MB**, Greene FL, Edge SB, Compton CC, Gershenwald JE, Brookland RK, Meyer L, Gress DM, Byrd DR, Winchester DP. The Eighth Edition AJCC Cancer Staging Manual: Continuing to build a bridge from a population-based to a more "personalized" approach to cancer staging. *CA Cancer J Clin* 2017; **67**: 93-99 [PMID: 28094848 DOI: 10.3322/caac.21388]
26 **Sun C**, Zhang Z, He P, Zhou Y, Xie X. Involvement of PI3K/Akt pathway in the inhibition of hepatocarcinoma cell invasion and metastasis induced by SASH1 through downregulating Shh-Gli1 signaling. *Int J Biochem Cell Biol* 2017; **89**: 95-100 [PMID: 28600143 DOI: 10.1016/j.biocel.2017.06.006]
27 **Zheng Z**, Li X, You H, Zheng X, Ruan X. LncRNA SOCS2-AS1 inhibits progression and metastasis of colorectal cancer through stabilizing SOCS2 and sponging miR-1264. *Aging (Albany NY)* 2020; **12**: 10517-10526 [PMID: 32437330 DOI: 10.18632/aging.103276]
28 **Torre LA**, Bray F, Siegel RL, Ferlay J, Lortet-Tieulent J, Jemal A. Global cancer statistics, 2012. *CA Cancer J Clin* 2015; **65**: 87-108 [PMID: 25651787 DOI: 10.3322/caac.21262]
29 **Sadanandam A**, Lyssiotis CA, Homicsko K, Collisson EA, Gibb WJ, Wullschleger S, Ostos LC, Lannon WA, Grotzinger C, Del Rio M, Lhermitte B, Olshen AB, Wiedenmann B, Cantley LC, Gray JW, Hanahan D. A colorectal cancer classification system that associates cellular phenotype and responses to therapy. *Nat Med* 2013; **19**: 619-625 [PMID: 23584089 DOI: 10.1038/nm.3175]

30 **Nishihara R**, Wu K, Lochhead P, Morikawa T, Liao X, Qian ZR, Inamura K, Kim SA, Kuchiba A, Yamauchi M, Imamura Y, Willett WC, Rosner BA, Fuchs CS, Giovannucci E, Ogino S, Chan AT. Long-term colorectal-cancer incidence and mortality after lower endoscopy. *N Engl J Med* 2013; **369**: 1095-1105 [PMID: 24047059 DOI: 10.1056/NEJMoa1301969]

31 **Rosty C**, Sheffer M, Tsafrir D, Stransky N, Tsafrir I, Peter M, de Crémoux P, de La Rochefordière A, Salmon R, Dorval T, Thiery JP, Couturier J, Radvanyi F, Domany E, Sastre-Garau X. Identification of a proliferation gene cluster associated with HPV E6/E7 expression level and viral DNA load in invasive cervical carcinoma. *Oncogene* 2005; **24**: 7094-7104 [PMID: 16007141 DOI: 10.1038/sj.onc.1208854]

32 **Vu T**, Datta PK. Regulation of EMT in Colorectal Cancer: A Culprit in Metastasis. *Cancers (Basel)* 2017; **9** [PMID: 29258163 DOI: 10.3390/cancers9120171]

33 **Yang C**, Dou R, Wei C, Liu K, Shi D, Zhang C, Liu Q, Wang S, Xiong B. Tumor-derived exosomal microRNA-106b-5p activates EMT-cancer cell and M2-subtype TAM interaction to facilitate CRC metastasis. *Mol Ther* 2021; **29**: 2088-2107 [PMID: 33571679 DOI: 10.1016/j.ymthe.2021.02.006]

34 **Onder TT**, Gupta PB, Mani SA, Yang J, Lander ES, Weinberg RA. Loss of E-cadherin promotes metastasis *via* multiple downstream transcriptional pathways. *Cancer Res* 2008; **68**: 3645-3654 [PMID: 18483246 DOI: 10.1158/0008-5472.CAN-07-2938]

35 **Putzke AP**, Ventura AP, Bailey AM, Akture C, Opoku-Ansah J, Celiktaş M, Hwang MS, Darling DS, Coleman IM, Nelson PS, Nguyen HM, Corey E, Tewari M, Morrissey C, Vessella RL, Knudsen BS. Metastatic progression of prostate cancer and e-cadherin regulation by zeb1 and SRC family kinases. *Am J Pathol* 2011; **179**: 400-410 [PMID: 21703419 DOI: 10.1016/j.ajpath.2011.03.028]

36 **Reddy P**, Liu L, Ren C, Lindgren P, Boman K, Shen Y, Lundin E, Ottander U, Rytinki M, Liu K. Formation of E-cadherin-mediated cell-cell adhesion activates AKT and mitogen activated protein kinase *via* phosphatidylinositol 3 kinase and ligand-independent activation of epidermal growth factor receptor in ovarian cancer cells. *Mol Endocrinol* 2005; **19**: 2564-2578 [PMID: 15928314 DOI: 10.1210/me.2004-0342]

37 **Lewis-Tuffin LJ**, Rodriguez F, Giannini C, Scheithauer B, Necela BM, Sarkaria JN, Anastasiadis PZ. Misregulated E-cadherin expression associated with an aggressive brain tumor phenotype. *PLoS One* 2010; **5**: e13665 [PMID: 21060868 DOI: 10.1371/journal.pone.0013665]

38 **Lammens T**, Swerts K, Derycke L, De Craemer A, De Brouwer S, De Preter K, Van Roy N, Vandesompele J, Speleman F, Philippé J, Benoit Y, Beiske K, Bracke M, Laureys G. N-cadherin in neuroblastoma disease: expression and clinical significance. *PLoS One* 2012; **7**: e31206 [PMID: 22355346 DOI: 10.1371/journal.pone.0031206]

World Journal of Gastrointestinal Oncology

Submit a Manuscript: https://www.f6publishing.com

World J Gastrointest Oncol 2022 December 15; 14(12): 2367-2379

DOI: 10.4251/wjgo.v14.i12.2367

ISSN 1948-5204 (online)

ORIGINAL ARTICLE

Retrospective Study

Evaluation of short-term effects of drug-loaded microspheres and traditional transcatheter arterial chemoembolization in the treatment of advanced liver cancer

Ting Ye, Shi-Han Shao, Kan Ji, Shu-Lin Yao

Specialty type: Radiology, nuclear medicine and medical imaging

Provenance and peer review: Unsolicited article; Externally peer reviewed.

Peer-review model: Single blind

Peer-review report's scientific quality classification

Grade A (Excellent): 0
Grade B (Very good): B, B, B
Grade C (Good): 0
Grade D (Fair): 0
Grade E (Poor): 0

P-Reviewer: Andersen JB, Denmark; Pandya S, United States; Shroff RT, United States

Received: August 1, 2022
Peer-review started: August 1, 2022
First decision: August 21, 2022
Revised: August 29, 2022
Accepted: November 16, 2022
Article in press: November 16, 2022
Published online: December 15, 2022

Ting Ye, Shu-Lin Yao, Department of Nuclear Medicine, First Medical Center, PLA General Hospital, Beijing 100039, China

Shi-Han Shao, Department of Hepatobiliary Surgery, The Sixth Medical Center, PLA General Hospital, Beijing 100048, China

Kan Ji, Department of Interventional Radiology, First Medical Center, PLA General Hospital, Beijing 100071, China

Corresponding author: Shu-Lin Yao, MD, Associate Chief Technician, Statistical Worker, Department of Nuclear Medicine, First Medical Center, PLA General Hospital, No. 28 Fuxing Road, Haidian District, Beijing 100039, China. yaoshulinvip@126.com

Abstract

BACKGROUND

Liver cancer is a malignant tumor with high morbidity and mortality. Transcatheter arterial chemoembolization (TACE) is the main method for surgically unresectable liver cancer. In recent years, drug-loaded microspheres have been gradually applied in TACE technology. There are some controversies about the therapeutic effects of drug-loaded microspheres TACE (D-TACE) and traditional TACE.

AIM

To explore the short-term efficacy of D-TACE and traditional TACE in the treatment of advanced liver cancer.

METHODS

The clinical data of 73 patients with advanced liver cancer admitted to the First and Sixth Medical Centers of Chinese PLA General Hospital from January 2017 to October 2019 were retrospectively analyzed. Among them, 15 patients were treated with D-TACE, and 58 patients were treated with traditional TACE. Clinical baseline characteristics, perioperative laboratory indices, postoperative adverse reactions and postoperative complications were compared between the two groups.

RESULTS

There was no statistical difference between the two groups for the postoperative response: The highest postoperative body temperature of the drug-loaded microsphere group was 38.0 ± 0.9℃ and the postoperative highest body temperature of the traditional TACE group was 38.3 ± 0.7℃ (t = -1.414, P = 0.162). For the 24 h postoperative nausea and vomiting after surgery in terms of scoring and postoperative pain scores, the traditional TACE group was higher than the drug-loaded microsphere group (χ^2 = 14.33, P = 0.014; χ^2 = 32.967, P = 0.000) and the two groups had significant statistical differences. The disease control rate at 3 mo after treatment in the drug-loaded microsphere group was 60% and the disease control rate at 3 mo after treatment in the traditional TACE group was 75.9% (χ^2 = 4.091, P = 0.252). There was no statistical difference between the two groups of data. During the follow-up period, the number of interventional treatments received was once in the drug-loaded microsphere group and the traditional TACE group received an average of 1.48 treatments (χ^2 = 10.444 P = 0.005). There was a statistical difference between the two groups.

CONCLUSION

Compared with traditional TACE, D-TACE may have some advantages in the treatment of advanced hepatocellular carcinoma with a large tumor load in the short term, but the long-term clinical efficacy needs additional follow-up studies. In addition, compared with the traditional group, the patients in the drug-loaded microsphere group had better subjective tolerance and could reduce the number of interventional treatments. Therefore, D-TACE is worthy of clinical promotion.

Key Words: Primary liver cancer; Hepatocellular carcinoma; Drug-loaded microsphere transcatheter arterial chemoembolization; Traditional transcatheter arterial chemoembolization; Treatment; Short-term efficacy

Core Tip: Hepatocellular carcinoma with a very high mortality rate is insidious and about 80 per cent of patients have no chance of surgery when diagnosed. Transcatheter arterial chemoembolization (TACE) is recommended as a first-line treatment. Traditional TACE uses iodized oil and gelatin sponge as the main embolization materials, and the chemotherapeutic drugs are mixed with iodized oil and injected into the tumor feeding artery to achieve the dual role of embolization and chemotherapy. Some scholars believe that liver cancer cells are not sensitive to chemotherapy drugs, so the role of chemotherapy drugs in TACE treatment is controversial. In recent years, drug-loaded microspheres have been gradually applied in TACE technology, which can significantly improve the killing effect of drugs on tumor tissues, and significantly reduce the systemic drug concentration, thereby reducing the side effects of chemotherapy drugs. In this study, the effects of using the same size of embolization particles and drug-eluting beads during TACE were compared. To investigate the effect and systemic response of chemotherapy drugs in TACE under the new local drug delivery mode.

Citation: Ye T, Shao SH, Ji K, Yao SL. Evaluation of short-term effects of drug-loaded microspheres and traditional transcatheter arterial chemoembolization in the treatment of advanced liver cancer. *World J Gastrointest Oncol* 2022; 14(12): 2367-2379

URL: https://www.wjgnet.com/1948-5204/full/v14/i12/2367.htm

DOI: https://dx.doi.org/10.4251/wjgo.v14.i12.2367

INTRODUCTION

The prevalence of liver cancer ranks fourth among malignant tumors and its fatality rate ranks second among all tumors[1]. Surgical resection, liver transplantation and ablation are the main treatment methods for early liver cancer. However, due to the insidious onset of liver cancer, approximately 80% of patients have no chance of surgery when they are diagnosed[2]. For such patients, transcatheter arterial chemoembolization (TACE) is recommended as the first-line treatment[3-6]. Traditional TACE (conventional TACE, cTACE) uses iodized oil and gelatin sponges as the main embolization materials and injects chemotherapeutic drugs and iodized oil into the tumor feeding artery to achieve a dual effect of embolization and chemotherapy. Previously, some researchers thought that liver cancer cells were not sensitive to chemotherapeutic drugs, so the role of chemotherapeutic drugs in cTACE treatment was controversial[7].

In recent years, drug-eluting beads (DEBs) have been gradually applied in TACE technology. A DEB is a nonabsorbable embolic microsphere loaded with chemotherapeutic drugs that immediately causes embolization after reaching the tumor tissue. At the same time, local high concentrations due to the continuous release of chemotherapeutic drugs significantly improves the killing effect of drugs on tumor tissue and significantly reduces the systemic drug concentration, thereby reducing the side effects of chemotherapeutic drugs[7,8]. In addition, D-TACE is easier to standardize than cTACE[9].

There are some previous clinical studies comparing D-TACE and cTACE. Some studies have shown that D-TACE can have better therapeutic effects[10-14], but other studies found no significant difference in the therapeutic effect between the two groups[15-19]. For these studies, we found that there were some differences in the selection and use of the cTACE embolization agent. When comparing the embolization effect between the two groups, the curative effect difference caused by embolization agents and technical reasons cannot be excluded. Based on the above reasons, this study compared the effect of using the same size of embolization particles and DEB during TACE. We investigated the effect and systemic response of chemotherapy drugs in TACE under the new local drug delivery mode.

MATERIALS AND METHODS

Patient's information

We retrospectively analyzed the clinical data of 73 patients with advanced liver cancer treated with D-TACE and traditional TACE at the First Medical Center and the Sixth Medical Center of the PLA General Hospital from January 2017 to October 2019. All patients signed informed consent before surgery, were informed of the risk of surgery, and voluntarily chose D-TACE or traditional TACE treatment. Patients' inclusion criteria: (1) Comply with the diagnostic criteria of primary liver cancer in the diagnostic and therapeutic norms of primary liver cancer (2019 edition), and the primary lesion cannot be removed by surgery; (2) Child–Pugh A or B liver function classification; (3) The Eastern Cooperative Oncology Group (ECOG) score was 0–2; (4) The patient's expected survival time was more than 3 mo; (5) The Barcelona stage of liver cancer was B and C; (6) In patients with massive hepatocellular carcinoma (HCC), the tumors accounted for less than 70% of the liver mass; and (7) The portal vein trunk was not completely blocked. Exclusion criteria: (1) A combination of active hepatitis [hepatitis B e antigen (HBeAg) positive + male, alanine transaminase (ALT) ≥ 30 IU/L/female ALT ≥ 19 IU/L or HBeAg negative + hepatitis B virus (HBV) DNA ≥ 1×10^5 cps/mL + male ALT ≥ 30 IU/L/female ALT ≥ 19 IU/L] or a severe infection that cannot be treated simultaneously; (2) Tumors have extensive distant metastasis; (3) Severe heart and kidney dysfunction; (4) Peripheral white blood cells < 3.0×10^9 L and platelets < 50×10^9/L, which cannot be corrected by oral drugs, injection of injections, transfusion of white blood cells or platelets; (5) With other malignant tumors; (6) Other treatments (ablation, radiotherapy, targeted therapy, *etc.*) during the follow-up period after TACE; and (7) Missing or incomplete information during the follow-up period.

Methods

Preoperative laboratory examination included routine blood, urine, stool, liver and kidney function, coagulation, alpha-fetoprotein, and eight preoperative items (HBV five, hepatitis C, syphilis, human immunodeficiency viruses antibody). Imaging examination included abdominal dynamic enhanced magnetic resonance imaging (MRI) or computed tomography (CT), which was completed within one month before TACE. In addition, head and lung CT and electrocardiogram examinations were performed to screen for extrahepatic metastasis and to examine the cardiac function.

Treatment methods included D-TACE and traditional TACE. All patients underwent the modified Seldinger technique, percutaneous femoral artery puncture, superior mesenteric artery, abdominal artery or common hepatic artery angiography. Before embolization, combined with abdominal enhanced MRI or CT, the corresponding arteries (including subphrenic artery, left gastric artery, intercostal artery, adrenal artery, lumbar artery, *etc.*) were explored according to the location of lesions that may have collateral circulation, and a cone beam CT (CBCT) examination was performed if necessary. After defining the responsible vessels, the microcatheter superselective technique was used to superselect the target vessels. TACE group: Pirarubicin (50 mg), oxaliplatin/cisplatin (100/50 mg), and fluorouracil (750 mg) were used as chemotherapy drugs. Embolization materials were 100-300 μm CalliSpheres drug-loaded microspheres, chemotherapy drug loading, and 1-1.2 times of a nonionic contrast agent, left to stand for 5 min before use. Traditional TACE group: Conventional TACE group: chemotherapy drugs with pirarubicin/epirubicin 50 mg, oxaliplatin/cisplatin 100/50 mg, fluorouracil (750 mg perfusion), embolization materials with iodized oil, polyethylene embolization particles 100-300 μm (polyvinyl alcohol, PVA), and a gelatin sponge. During embolization, the chemotherapeutic drugs (pirarubicin and platinum) were mixed evenly with the iodized oil to prepare an emulsion before use. When the lesion could not be over selected, the embolization agent was iodized oil or iodized oil plus chemotherapy (because the ischemic effect caused by iodized oil is transient). The endpoint of embolization is to slow down the blood flow in the target artery, and the use of the contrast agent shows that the blood vessels are "dead branches", which can be considered to have achieved the endpoint of

embolization. After the operation, the catheter and sheath were removed, the puncture site was compressed for 10 min and then pressurized for 6-10 h. The color of the punctured lower limbs and the pulsation of the dorsal pedis artery were observed.

The common complications after postoperative treatment include fever, nausea, vomiting, liver pain, abnormal liver function, bone marrow suppression, infection, *etc.* After the operation, symptomatic treatments, such as gastric protection and acid suppression, antiemetics, liver protection, pain relief, and anti-infection, are routinely given[20,21]. Routine blood examination, liver and kidney function and other indicators were reviewed before discharge and discharge was only arranged after the indicators were close to normal, and the patients were asked to attend one month after discharge.

Follow-up and efficacy evaluation

The clinical follow-up data were obtained by admission review, telephone or letter follow-up. The follow-up data were independently evaluated by two experienced physicians above the specialist level, and consensus was reached after consultation when there was disagreement. The imaging data were mainly abdominal enhanced CT or MRI at 1 and 3 mo after the operation. The modified solid tumor efficacy evaluation criteria were used to evaluate the efficacy: All target lesions without enhancement in the arterial phase were considered complete remission (CR); the total diameter of the target lesion in the arterial phase was reduced by ≥ 30% for partial remission (PR); the disease was stable (SD) when the total diameter of the lesion was reduced by less than 30% or increased by less than 20%; when the total diameter of the target lesion in the arterial phase increased by ≥ 20% or new lesions developed was defined as disease progression. The objective response of the tumor was equal to the sum of CR and PR. Disease control equals the sum of CR, PR and SD.

Statistical analysis

EmpowerStats software was used for data analysis. Measurement data with an approximate normal distribution are expressed as mean ± SD, and a *t*-test was used for comparisons between groups. Measurement data with a nonnormal distribution are expressed as the mean (SD), median and P25, P75 values. Rank sum tests were used for comparisons between groups. Count data are expressed as the number of cases and percentage. χ^2 tests were used for comparisons between groups. $P < 0.05$ indicated that the difference was statistically significant. Age, tumor size and body temperature were the measurement data that conformed to or approximately conformed to the normal distribution. Sex, liver cirrhosis, portal vein tumor thrombus, ECOG physical status score, Child–Pugh score, number of tumors, Barcelona stage, HBV infection, postoperative 24 h postoperative nausea and vomiting (PONV) score, postoperative pain score, number of treatments, and 1 and 3 mo of follow-up were recorded.

The objective response rate was count data. The changes in aspartate aminotransferase, alanine aminotransferase, total bilirubin, serum albumin, white blood cells, red blood cells, platelets, and alpha-fetoprotein before and after surgery were nonnormally distributed measurement data.

RESULTS

General information of patients

The general information of patients is shown in Table 1. There were no statistical differences between the drug-loaded microsphere group and the conventional TACE group in terms of age, gender, presence of cirrhosis, presence of portal vein cancer thrombosis, ECOG physical status score, Child-Pugh score, preoperative methemoglobin, tumor number and Barcelona stage. There were statistical differences between the two groups in terms of preoperative tumor size (longest diameter) and whether they were infected with HBV, with the preoperative tumor size of 102.7 ± 44.4 mm in the drug-loaded microsphere group being larger than that of 75.0 ± 34.1 mm in the conventional TACE group; in terms of HBV infection, there were 6 cases in the drug-loaded microsphere group (40.0% of the whole group) and 48 cases in the conventional TACE group (82.8% of the whole group). The HBV infection rate was higher in the conventional TACE group.

Laboratory indexes of patients before and after surgery

The laboratory test indexes of patients before surgery and on the 3rd day after surgery are shown in Table 2. There were no statistical differences in the values of glutamic oxalyl transaminase, glutamic alanine transaminase, total bilirubin, serum albumin, leukocytes, red blood cells, and platelets before and after surgery in the drug-laden microsphere group and the conventional TACE group.

Postoperative reactions of patients

The common postoperative reactions of the patients are shown in Table 3. In terms of postoperative fever (maximum body temperature) in the drug-loaded microsphere group and the conventional TACE group, the drug-loaded microsphere group was 38.0 ± 0.9 °C, the conventional TACE group was 38.3 ± 0.7 °C, while the mean body temperature in the conventional TACE group was slightly higher but not

Table 1 General situation of the patients, *n* (%)

Influencing factors	D-TACE (15 cases)	C-TACE (58 cases)	t/χ^2 value	*P* value
Age (yr)	57.3 ± 11.5	59.9 ± 10.7	-0.836[1]	0.406
The longest tumor size before surgery (mm)	102.7 ± 44.4	75.0 ± 34.1	2.626[1]	0.011
Gender			1.907	0.167
Female	1 (6.7)	13 (22.4)		
Male	14 (93.3)	45 (77.6)		
Whether infected with HBV			11.317	0.0008
No	9 (60.0)	10 (17.2)		
Yes	6 (40.0)	48 (82.8)		
Whether there is liver cirrhosis			3.137	0.069
No	9 (60.0)	18 (31.0)		
Yes	6 (40.0)	40 (69.0)		
Is there a portal vein tumor thrombus			0.602	0.438
No	13 (86.7)	45 (77.6)		
Yes	2 (13.3)	13 (22.4)		
ECOG stamina score			3.769	0.152
0 points	2 (13.3)	13 (22.4)		
1points	9 (60.0)	40 (69.0)		
2points	4 (26.7)	5 (8.6)		
Child-Pugh classification			1.668	0.196
A	6 (40.0)	34 (58.6)		
B	9 (60.0)	24 (41.4)		
Number of tumors			1.237	0.744
1	3 (20.0)	7 (12.1)		
2	1 (6.7)	2 (3.4)		
3	0 (0.0)	1 (1.7)		
Multiple (> 3)	11 (73.3)	48 (82.8)		
Barcelona staging			0.434	0.510
B	9 (60)	40 (69)		
C	6 (40)	18 (31)		

[1]Result of *t* test.

ECOG: The Eastern Cooperative Oncology Group; D-TACE: Drug-loaded microspheres transcatheter arterial chemoembolization; C-TACE: Traditional/conventional transcatheter arterial chemoembolization.

statistically different between the two groups. In the postoperative 24 h PONV score and postoperative pain score, the traditional TACE group was higher than the drug-loaded microsphere group, and the data of the two groups were statistically different.

Patients were followed up 1 and 3 mo after surgery

The tumor control status of the patients at 1 and 3 mo after surgery is shown in Table 4. The objective tumor response rate (CR + PR) was 66.6% and the disease control rate (CR + PR + SD) was 86.6% in the drug-loaded microsphere group, while the objective tumor response rate (CR + PR) was 70.7% and the disease control rate (CR + PR + SD) was 82.8% in the conventional TACE group at 1 mo after treatment. There was no statistical difference between the data of the two groups. The objective tumor response rate (CR + PR) and disease control rate (CR + PR + SD) were 60% at 3 mo after treatment in the drug-loaded microsphere group, while the objective tumor response rate (CR + PR) and disease control rate (CR + PR + SD) were 67.2% and 75.9% at 3 mo after treatment in the conventional TACE group, and

Table 2 Laboratory indicators of patients before and after operation [median (P25, P75)]

Laboratory indicators	D-TACE (15 cases)	C-TACE (58 cases)	χ^2 value	*P* value
AST changes before and after surgery (U/L)	44.1 (10.4, 153.0)	102.7 (52.4, 254.8)	-2.086	0.05
ALT changes before and after surgery (U/L)	133.1 (31.6, 181.8)	110.3 (46.5, 309.7)	-1.382	0.176
TBil changes before and after surgery (μmol/L)	7.9 (5.4, 14.9)	11.6 (5.8, 21.6)	-1.842	0.081
ALB changes before and after surgery (g/L)	4.9 (3.2, 5.4)	2.6 (0.3, 5.3)	1.992	0.055
WBC changes before and after surgery ($\times 10^9$/L)	2.0 (0.9, 3.9)	2.1 (1.0, 4.4)	-0.214	0.832
RBC changes before and after surgery ($\times 10^{12}$/L)	0.3 (0.1, 0.5)	0.0 (-0.2, 0.3)	1.995	0.058
PLT changes before and after surgery ($\times 10^9$/L)	30.0 (9.0, 43.5)	36.0 (16.5, 59.2)	-1.616	0.120
AFP changes 1 mo before and after surgery (ng/mL)	0.8 (-0.3, 31.9)	19.0 (0.0, 554.6)	-1.219	0.228

D-TACE: Drug-loaded microspheres transcatheter arterial chemoembolization; C-TACE: Traditional/conventional transcatheter arterial chemoembolization; AST: Aspartate aminotransferase; ALT: Alanine transaminase; TBil: Total bilirubin; ALB: Albumin; WBC: White blood cell; RBC: Red blood cell; PLT: Platelet; AFP: Alpha fetoprotein.

Table 3 Postoperative response of patients, *n* (%)

Postoperative response	D-TACE (15 cases)	C-TACE (58 cases)	t/χ^2 value	*P* value
Body temperature (℃)	38.0 ± 0.9	38.3 ± 0.7	-1.414[1]	0.162
24 h PONV score postoperative			14.33	0.014
1	6 (40.0)	3 (5.2)		
2	4 (26.7)	20 (34.5)		
3	3 (20.0)	20 (34.5)		
4	2 (13.3)	9 (15.5)		
5	0 (0.0)	4 (6.9)		
6	0 (0.0)	2 (3.4)		
Postoperative pain score			32.967	0.000
0	5 (33.3)	15 (25.9)		
2	7 (46.7)	0 (0.0)		
4	3 (20.0)	39 (67.2)		
6	0 (0.0)	4 (6.9)		

[1]Result of *t* test.

D-TACE: Drug-loaded microspheres transcatheter arterial chemoembolization; C-TACE: Traditional/conventional transcatheter arterial chemoembolization; PONV: Postoperative nausea and vomiting.

there was no statistical difference between the two groups. The number of interventions received during the follow-up period was 1 in the drug-laden microsphere group; There were 32 patients who received 1 treatment, 24 cases received 2 treatments, and 2 patients received 3 treatments in the conventional TACE group, with a mean of 1.48 treatments. And the number of interventions in the two groups was statistically different. We briefly described three typical cases diagnosed as primary liver cancer for references (Figure 1, Figure 2, and Figure 3).

Table 4 Follow-up status of patients 1 and 3 mo after operation, *n* (%)

Follow-up status	D-TACE (15 cases)	C-TACE (58 cases)	χ^2 value	*P* value
Efficacy evaluation one month postoperative			3.307	0.347
CR	2 (13.3)	20 (34.5)		
PR	8 (53.3)	21 (36.2)		
SD	3 (20.0)	7 (12.1)		
PD	2 (13.3)	10 (17.2)		
Evaluation of curative effect in 3 mo postoperative			4.091	0.252
CR	2 (13.3)	18 (31.0)		
PR	7 (46.7)	21 (36.2)		
SD	0 (0.0)	5 (8.6)		
PD	6 (40.0)	14 (24.1)		
Number of interventional treatments			10.444	0.005
1	15 (100.0)	32 (55.2)		
2	0 (0.0)	24 (41.4)		
3	0 (0.0)	2 (3.4)		

D-TACE: Drug-loaded microspheres transcatheter arterial chemoembolization; C-TACE: Traditional/conventional transcatheter arterial chemoembolization; CR: Complete response; PR: Partial response; SD: Stable disease; PD: Disease progression.

DISCUSSION

HCC is the most common type of liver cancer and a main cause of tumor-related mortality[22]. As a palliative local treatment for advanced liver cancer, TACE is widely used and is a standard treatment for advanced liver cancer because it is not limited to the location and size of the tumor[23]. However, based on the adverse effects of systemic chemotherapy, HCC may be a tumor relatively resistant to chemotherapy, so the additional role of chemotherapeutic drugs in the embolization process has been controversial[24]. Also, delays or failures in successful treatment can also be attributed to poor health literacy and insurance-specific barriers[25]. We know that TACE acts mainly through embolization of the blood supply artery to the HCC, resulting in tumor tissue ischemia, hypoxia necrosis, and ischemia. Hypoxia may induce angiogenesis, resulting in tumor recurrence and metastasis. Previous studies have confirmed a correlation between polymorphisms of the angiopoietin-2 gene and prognosis in patients after TACE[26]. There is another view that incomplete hypoxia or incomplete devascularization of tumors is a powerful stimulating factor for angiogenesis[27].

Due to the complexity of the tumor blood supply (including the blood supply of the lateral hepatic artery and potential portal vein)[28] and the hemodynamics, it is difficult to achieve complete ischemia and hypoxia-induced tumor cell death after liver cancer embolization, which is the main reason for its recurrence and metastasis after tumor treatment. The basic principle of adding chemotherapeutic drugs to hepatic artery embolization is based on the assumption that chemotherapeutic drugs can enhance the antitumor effect of embolization agents in ischemia and hypoxia and counteract the stimulation of angiogenesis caused by ischemia and hypoxia. Therefore, during treatment, chemotherapeutic drugs are injected into the blood supply artery to improve the antitumor efficacy, and the enhanced cytotoxicity may contribute to the control and reduced recurrence of tumors. However, this hypothesis has not been confirmed in some clinical studies[29,30] because in these reports, TACE combined with local chemotherapy did not show significant survival benefits compared with TAE embolization alone.

There are two main reasons for this result. First, since cTACE has not been standardized in the implementation process, there are certain differences in the use of embolic materials, the selection of chemotherapeutic drugs, the selection of patients and operation technology among different regions and teams, especially in the selection of embolic agents and operation technology. This has caused certain difficulties in the formulation of treatment standards and efficacy evaluation, resulting in differences between different research results.

Therefore, in this study, to avoid the impact of these technical reasons on the results, the authors referred to the treatment recommendations jointly formulated by experts in the global TACE treatment field in 2016[31]. In terms of the selection of chemotherapeutic drugs, adriamycin or platinum-based chemotherapeutic drugs were mainly used in both groups. For the choice of embolization particles, the

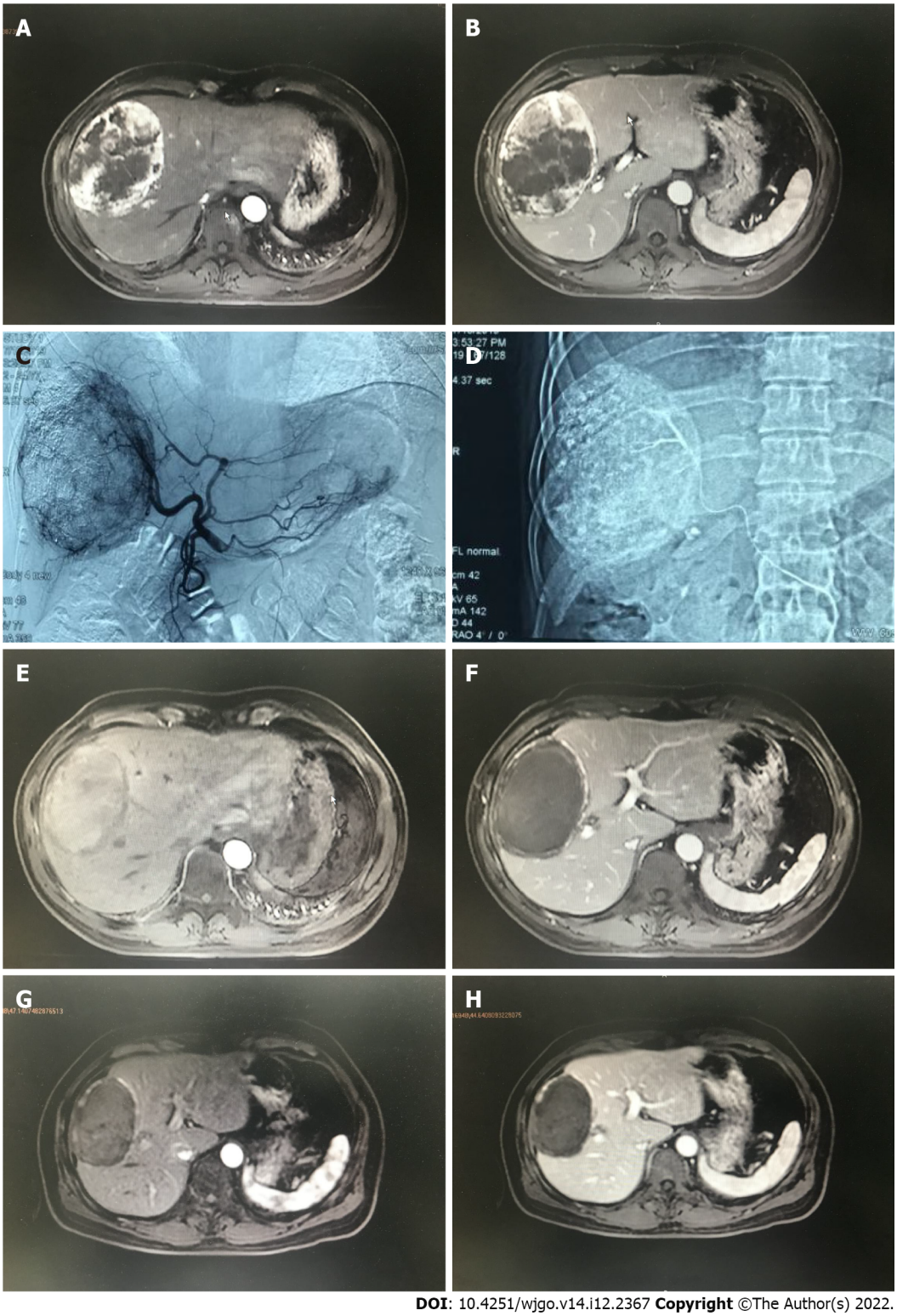

DOI: 10.4251/wjgo.v14.i12.2367

Figure 1 A 47 years old male diagnosed as primary liver cancer. Preoperative magnetic resonance imaging (MRI) T1WI enhanced axial position. A: In the arterial phase, there is a 105 mm × 85 mm × 119 mm uneven abnormal enhancement of the right lobe of the liver; B: The portal vein can be cleared. Transcatheter arterial chemoembolization treatment with drug-loaded microspheres was performed in July 2019; C: Digital subtracted angiography under common hepatic arteriography during interventional surgery shows tumors with rich blood supply in the right lobe of the liver; D: Microcatheter superselection of the right hepatic artery for chemoembolization; E: A 103 mm × 69 mm × 109 mm mass in the right lobe of the liver can be seen in the arterial phase and no obvious enhancement is seen; F: There is no enhancement in the mass in the portal vein; G: MRI T1WI enhancement axis is re-examined 3 mo after the operation. The mass in the right lobe of the liver in the arterial phase is compared to the previous significantly reduced (86 mm × 57 mm × 88 mm); H: There was no enhancement of the portal venous mass.

two groups both received 100-300 μm permanent embolization agents. To ensure the thoroughness of tumor blood supply artery embolization, a variety of imaging techniques (CT, MRI enhancement, CBCT) and digital subtracted angiography were used to identify the tumor blood supply arteries before

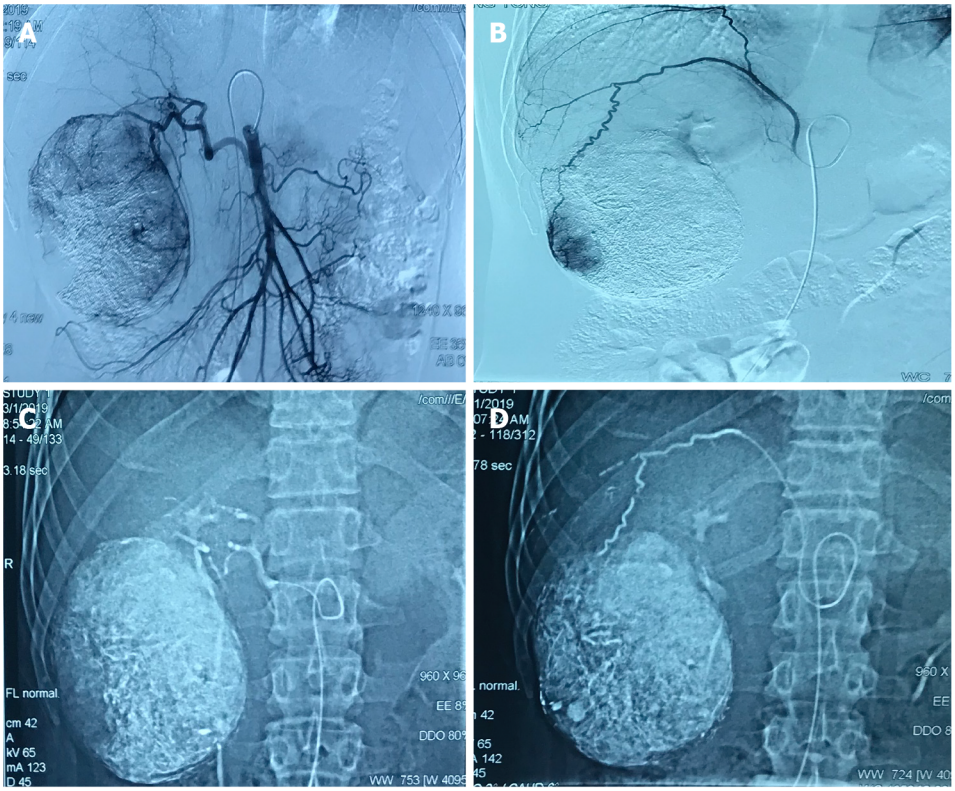

DOI: 10.4251/wjgo.v14.i12.2367 **Copyright** ©The Author(s) 2022.

Figure 2 A 38 years old male diagnosed as primary liver cancer. Traditional transcatheter arterial chemoembolization (TACE) treatment was performed in January 2019, and a follow-up examination was performed one month after the operation. Part of the lesion was alive. Later, the second traditional TACE treatment was performed in March 2019. A: Intraoperative digital subtracted angiography (DSA) angiography shows that the proper hepatic artery originates from the superior mesenteric artery, and the blood supply area of the right hepatic artery can be seen in the lesion; B: Intraoperative DSA angiography shows that the right inferior septal artery participates in the blood supply of the lesion; C: Intraoperative DSA Under the hepatic artery chemoembolization; D: Under DSA during the operation, the right inferior septal artery embolization was performed. Complete necrosis of the lesion was re-examined in January and March postoperative.

and after embolization. The microcatheter superselective technique was used during the embolization. Second, during the process of cTACE, chemotherapeutic drugs are often mixed with iodinated oil and injected after emulsification. Due to the unstable physical and chemical properties of this mixture, the chemotherapeutic drugs quickly separate from the oil phase into the water phase. It has been reported that this emulsifier is released completely into the circulation within 4 h after reaching the tumor[32]. Li *et al*[33] studied the response of HepG2 cells to epirubicin and other chemotherapeutic drugs under different hypoxia and low nutrition conditions *in vitro* and confirmed that the inhibition rate of HepG2 cells at 24 h was significantly higher than that at 2 h. Similar results published in 2019[34] also confirmed that the cytotoxicity of adriamycin in HepG2 and Huh7 cell models increased over time. Therefore, the chemotherapy effect of cTACE has been controversial for a long time, which may be related to its inability to remain near the tumor cells after application.

In recent years, DEB has been gradually used in TACE. After drug loading, the half-life of DEBs with diameters of 100–300 μm reached 150 h, and the half-life of DEBs with diameters of 700–900 μm reached 1730 h. This feature greatly improved the local action time and concentration of the chemotherapeutic drugs after TACE and reduced the systemic toxicity. The drug loading microsphere preparation process and drug loading concentration are standardized operations, so it is easier to control the differences between different teams. Therefore, in this study, PVA embolization particles with similar embolization effects were used as controls to evaluate the effect of chemotherapy drugs under the new DEB conditions.

HBV infection is usually considered to be an important factor leading to liver cancer and it affects the long-term prognosis of patients with liver cancer. This study enrolled patients with inactive HBV after treatment, so it was not a priority factor affecting the short-term efficacy after treatment. Tumor load is an important factor affecting the short-term efficacy after treatment. From Table 1, we can see that the tumor load of the drug-loaded microsphere group was larger, the average tumor size was 102.7 ± 44.4 mm, and the average tumor size of the traditional TACE group was 75.0 ± 34.1 mm. In the case of a large tumor load, the drug-loaded microsphere group achieved the same short-term effect as the traditional TACE group. To some extent, this suggests that chemotherapy drugs can play a role in TACE. Since the blood supply of large HCC is often complex and there are more or even some portal veins involved in the potential blood supply compared with small HCC, it is difficult to completely block the blood

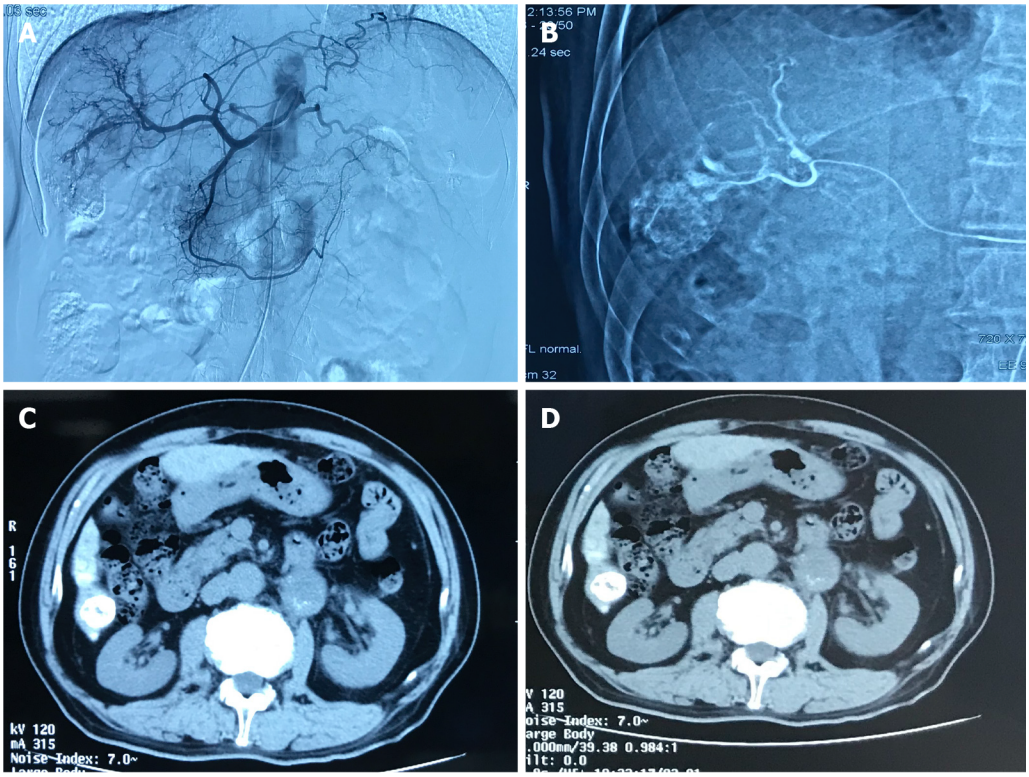

DOI: 10.4251/wjgo.v14.i12.2367 **Copyright** ©The Author(s) 2022.

Figure 3 A 70 years old male diagnosed as primary liver cancer. This patient underwent traditional transcatheter arterial chemoembolization treatment in May 2019. A: Intraoperative digital subtracted angiography (DSA) can be seen on angiography, and the blood supply area of the right hepatic artery can be seen in the lesion; B: Intraoperative DSA, superselective right hepatic artery branch chemoembolization; C: Abdominal computed tomography (CT) axial examination 1 mo after surgery, The lipiodol deposition in the lesion was good, and the lesion was completely necrotic; D: 3 mo after the operation, the abdominal CT axial examination was performed again, and the lipiodol deposition in the lesion was good, and no tumor recurrence was found.

supply by simple embolization. Drug-loaded microspheres can continuously release high-concentration chemotherapeutic drugs to the surrounding tumor for a long time and continue to kill tumor cells. Thus, it makes up for the deficiency of simple embolization treatment, improves the tumor control rate and reduces recurrence.

We also observed the safety of the two treatments. There was no significant difference in liver function biochemical or hematological indices between the two groups before and after the operation, suggesting that there was no significant difference in safety and toxicity between the two treatment methods. In terms of postoperative reactions, the traditional TACE group had more serious postoperative nausea, vomiting and pain symptoms. This is consistent with previous reports, indicating that drug-loaded microspheres can release chemotherapy drugs continuously and slowly, which can effectively reduce the incidence of systemic adverse drug reactions.

This study is a small sample retrospective study; inevitably, there is a certain bias. In addition, due to the many influencing factors on the long-term prognosis, its analysis was not performed. Therefore, the long-term prognosis of these two treatments for patients with advanced liver cancer needs to be further explored in large-sample randomized controlled trials.

CONCLUSION

In summary, the results of this study show that compared with traditional TACE, D-TACE may have more advantages in the short-term efficacy for treating large HCC in the middle and late stages, but the long-term clinical efficacy needs further follow-up studies. In terms of postoperative reactions, the patients in the drug-loaded microsphere group had less postoperative nausea, vomiting and pain and better subjective tolerance. In addition, the D-TACE can reduce the number of patients needing interventional treatment and improve their quality of life to a certain extent. Therefore, the D-TACE is worthy of clinical promotion.

ARTICLE HIGHLIGHTS

Research background

Liver cancer is a malignant tumor with high morbidity and mortality. One of the main reasons is that conventional Transcatheter arterial chemoembolization (TACE) is not a standardized procedure, and there are some differences in the use of embolization materials, selection of chemotherapeutic drugs, and operation techniques among different regions and teams.

Research motivation

This study compared the effect of using the same size of embolization particles and drug-eluting bead (DEB) during TACE. We investigated the effect and systemic response of chemotherapy drugs in TACE under the new local drug delivery mode.

Research objectives

This study aimed to explore the short-term efficacy of drug-loaded microspheres TACE (D-TACE) and traditional TACE in the treatment of advanced liver cancer.

Research methods

The clinical data of 73 patients with advanced liver cancer admitted to the First and Sixth Medical Centers of Chinese PLA General Hospital from January 2017 to October 2019 were retrospectively analyzed.

Research results

There were no statistical differences in the values of glutamic oxalyl transaminase, glutamic alanine transaminase, total bilirubin, serum albumin, leukocytes, red blood cells, and platelets before and after surgery in the drug-laden microsphere group and the conventional TACE group. In the postoperative 24 h postoperative nausea and vomiting score and postoperative pain score, the traditional TACE group was higher than the drug-loaded microsphere group, and the data of the two groups were statistically different.

Research conclusions

The authors found that compared with traditional TACE, D-TACE may have more advantages in the short-term efficacy for treating large hepatocellular carcinoma in the middle and late stages.

Research perspectives

D-TACE is worthy of clinical promotion. However, the long-term prognosis of D-TACE and traditional TACE for patients with advanced liver cancer needs to be further explored in large-sample randomized controlled trials.

FOOTNOTES

Author contributions: Ye T contributed to the research design and thesis writing; Shao SH collected and analyzed the data; Ji K contributed to the data collection; Yao SL overall supervise the study; and all authors proofed the revised manuscript.

Supported by National key research and development project of Ministry of Science and Technology, No. 2016YFC0103908.

Institutional review board statement: This study was approved by the First Medical Center, PLA General Hospital.

Informed consent statement: Patients were not required to give informed consent to the study because the analysis used anonymous clinical data that were obtained after each patient agreed to treatment by written consent.

Conflict-of-interest statement: No conflict of interest.

Data sharing statement: No additional data are available.

Country/Territory of origin: China

ORCID number: Ting Ye 0000-0002-0283-4565; Shi-Han Shao 0000-0002-3762-4031; Kan Ji 0000-0002-8369-0777; Shu-Lin Yao 0000-0003-4718-185X.

S-Editor: Wang JL
L-Editor: A
P-Editor: Wang JL

REFERENCES

1 **Yamashita T**, Kaneko S. [Liver Cancer]. *Rinsho Byori* 2016; **64**: 787-796 [PMID: 30695467]
2 **Chen W**, Zheng R, Baade PD, Zhang S, Zeng H, Bray F, Jemal A, Yu XQ, He J. Cancer statistics in China, 2015. *CA Cancer J Clin* 2016; **66**: 115-132 [PMID: 26808342 DOI: 10.3322/caac.21338]
3 **Heimbach JK**, Kulik LM, Finn RS, Sirlin CB, Abecassis MM, Roberts LR, Zhu AX, Murad MH, Marrero JA. AASLD guidelines for the treatment of hepatocellular carcinoma. *Hepatology* 2018; **67**: 358-380 [PMID: 28130846 DOI: 10.1002/hep.29086]
4 **European Association for the Study of the Liver**. EASL Clinical Practice Guidelines: Management of hepatocellular carcinoma. *J Hepatol* 2018; **69**: 182-236 [PMID: 29628281 DOI: 10.1016/j.jhep.2018.03.019]
5 **Forner A**, Reig M, Bruix J. Hepatocellular carcinoma. *Lancet* 2018; **391**: 1301-1314 [PMID: 29307467 DOI: 10.1016/S0140-6736(18)30010-2]
6 **Kudo M**, Han KH, Ye SL, Zhou J, Huang YH, Lin SM, Wang CK, Ikeda M, Chan SL, Choo SP, Miyayama S, Cheng AL. A Changing Paradigm for the Treatment of Intermediate-Stage Hepatocellular Carcinoma: Asia-Pacific Primary Liver Cancer Expert Consensus Statements. *Liver Cancer* 2020; **9**: 245-260 [PMID: 32647629 DOI: 10.1159/000507370]
7 **Tsochatzis EA**, Fatourou E, O'Beirne J, Meyer T, Burroughs AK. Transarterial chemoembolization and bland embolization for hepatocellular carcinoma. *World J Gastroenterol* 2014; **20**: 3069-3077 [PMID: 24695579 DOI: 10.3748/wjg.v20.i12.3069]
8 **Facciorusso A**. Drug-eluting beads transarterial chemoembolization for hepatocellular carcinoma: Current state of the art. *World J Gastroenterol* 2018; **24**: 161-169 [PMID: 29375202 DOI: 10.3748/wjg.v24.i2.161]
9 **Kim KW**, Van den Abbeele AD. Evolution of Transarterial Chemoembolization for the Treatment of Liver Cancer. *Radiology* 2019; **293**: 704-706 [PMID: 31617799 DOI: 10.1148/radiol.2019192090]
10 **Zhou GH**, Han J, Sun JH, Zhang YL, Zhou TY, Nie CH, Zhu TY, Chen SQ, Wang BQ, Yu ZN, Wang HL, Chen LM, Wang WL, Zheng SS. Efficacy and safety profile of drug-eluting beads transarterial chemoembolization by CalliSpheres® beads in Chinese hepatocellular carcinoma patients. *BMC Cancer* 2018; **18**: 644 [PMID: 29914435 DOI: 10.1186/s12885-018-4566-4]
11 **Yang B**, Liang J, Qu Z, Yang F, Liao Z, Gou H. Transarterial strategies for the treatment of unresectable hepatocellular carcinoma: A systematic review. *PLoS One* 2020; **15**: e0227475 [PMID: 32074102 DOI: 10.1371/journal.pone.0227475]
12 **Han T**, Yang X, Zhang Y, Li G, Liu L, Chen T, Zheng Z. The clinical safety and efficacy of conventional transcatheter arterial chemoembolization and drug-eluting beads-transcatheter arterial chemoembolization for unresectable hepatocellular carcinoma: A meta-analysis. *Biosci Trends* 2019; **13**: 374-381 [PMID: 31611486 DOI: 10.5582/bst.2019.01153]
13 **Liu YS**, Lin CY, Chuang MT, Tsai YS, Wang CK, Ou MC. Five-year outcome of conventional and drug-eluting transcatheter arterial chemoembolization in patients with hepatocellular carcinoma. *BMC Gastroenterol* 2018; **18**: 124 [PMID: 30075752 DOI: 10.1186/s12876-018-0848-1]
14 **Wu B**, Zhou J, Ling G, Zhu D, Long Q. CalliSpheres drug-eluting beads versus lipiodol transarterial chemoembolization in the treatment of hepatocellular carcinoma: a short-term efficacy and safety study. *World J Surg Oncol* 2018; **16**: 69 [PMID: 29587773 DOI: 10.1186/s12957-018-1368-8]
15 **Zhang ZS**, Li HZ, Ma C, Xiao YD. Conventional versus drug-eluting beads chemoembolization for infiltrative hepatocellular carcinoma: a comparison of efficacy and safety. *BMC Cancer* 2019; **19**: 1162 [PMID: 31783814 DOI: 10.1186/s12885-019-6386-6]
16 **Ma Y**, Zhao C, Zhao H, Li H, Chen C, Xiang H, Zheng C, Ma C, Luo C, Qiu H, Yao Y, Hu H, Xiong B, Zhou J, Zhu H, Long Q. Comparison of treatment efficacy and safety between drug-eluting bead transarterial chemoembolization with CalliSpheres® microspheres and conventional transarterial chemoembolization as first-line treatment in hepatocellular carcinoma patients. *Am J Transl Res* 2019; **11**: 7456-7470 [PMID: 31934293]
17 **Karalli A**, Teiler J, Haji M, Seth E, Brismar TB, Wahlin S, Axelsson R, Stål P. Comparison of lipiodol infusion and drug-eluting beads transarterial chemoembolization of hepatocellular carcinoma in a real-life setting. *Scand J Gastroenterol* 2019; **54**: 905-912 [PMID: 31287338 DOI: 10.1080/00365521.2019.1632925]
18 **Kang YJ**, Lee BC, Kim JK, Yim NY, Kim HO, Cho SB, Jeong YY. Conventional Versus Small Doxorubicin-eluting Bead Transcatheter Arterial Chemoembolization for Treating Barcelona Clinic Liver Cancer Stage 0/A Hepatocellular Carcinoma. *Cardiovasc Intervent Radiol* 2020; **43**: 55-64 [PMID: 31646378 DOI: 10.1007/s00270-019-02349-9]
19 **Melchiorre F**, Patella F, Pescatori L, Pesapane F, Fumarola E, Biondetti P, Brambillasca P, Monaco C, Ierardi AM, Franceschelli G, Carrafiello G. DEB-TACE: a standard review. *Future Oncol* 2018; **14**: 2969-2984 [PMID: 29987957 DOI: 10.2217/fon-2018-0136]
20 **Cerrito L**, Annicchiarico BE, Iezzi R, Gasbarrini A, Pompili M, Ponziani FR. Treatment of hepatocellular carcinoma in patients with portal vein tumor thrombosis: Beyond the known frontiers. *World J Gastroenterol* 2019; **25**: 4360-4382 [PMID: 31496618 DOI: 10.3748/wjg.v25.i31.4360]
21 **Lencioni R**. New data supporting modified RECIST (mRECIST) for Hepatocellular Carcinoma. *Clin Cancer Res* 2013; **19**:

1312-1314 [PMID: 23382112 DOI: 10.1158/1078-0432.CCR-12-3796]
22 **Mohamed AA**, Omar AAA, El-Awady RR, Hassan SMA, Eitah WMS, Ahmed R, Khater A, Tantawi OMS, Mohamed AA. MiR-155 and MiR-665 Role as Potential Non-invasive Biomarkers for Hepatocellular Carcinoma in Egyptian Patients with Chronic Hepatitis C Virus Infection. *J Transl Int Med* 2020; **8**: 32-40 [PMID: 32435610 DOI: 10.2478/jtim-2020-0006]
23 **Yang B**, Li CL, Guo WH, Qin TQ, Jiao H, Fei ZJ, Zhou X, Duan LJ, Liao ZY. Intra-arterial ethanol embolization augments response to TACE for treatment of HCC with portal venous tumor thrombus. *BMC Cancer* 2018; **18**: 101 [PMID: 29378532 DOI: 10.1186/s12885-018-3989-2]
24 **Lanza E**, Muglia R, Bolengo I, Poretti D, D'Antuono F, Ceriani R, Torzilli G, Pedicini V. Survival analysis of 230 patients with unresectable hepatocellular carcinoma treated with bland transarterial embolization. *PLoS One* 2020; **15**: e0227711 [PMID: 31935255 DOI: 10.1371/journal.pone.0227711]
25 **Gomes C**, Ginzberg D, Wong RJ. Delays and Gaps in Progressing Through the Hepatitis C Virus Cascade of Care: An Underserved Safety-net Hospital Experience. *J Transl Int Med* 2020; **8**: 261-267 [PMID: 33511053 DOI: 10.2478/jtim-2020-0039]
26 **Du Z**, Tang CH, Li LJ, Kang L, Zhao J, Jin L, Wang CQ, Su CM. Angiopoietin-2 gene polymorphisms are biomarkers for the development and progression of colorectal cancer in Han Chinese. *Int J Med Sci* 2020; **17**: 97-102 [PMID: 31929743 DOI: 10.7150/ijms.37675]
27 **Malagari K**, Pomoni M, Kelekis A, Pomoni A, Dourakis S, Spyridopoulos T, Moschouris H, Emmanouil E, Rizos S, Kelekis D. Prospective randomized comparison of chemoembolization with doxorubicin-eluting beads and bland embolization with BeadBlock for hepatocellular carcinoma. *Cardiovasc Intervent Radiol* 2010; **33**: 541-551 [PMID: 19937027 DOI: 10.1007/s00270-009-9750-0]
28 **Miyayama S**, Matsui O, Zen Y, Yamashiro M, Hattori Y, Orito N, Matsui K, Tsuji K, Yoshida M, Sudo Y. Portal blood supply to locally progressed hepatocellular carcinoma after transcatheter arterial chemoembolization: Observation on CT during arterial portography. *Hepatol Res* 2011; **41**: 853-866 [PMID: 21699636 DOI: 10.1111/j.1872-034X.2011.00836.x]
29 **Colombo GL**, Cammà C, Attili AF, Ganga R, Gaeta GB, Brancaccio G, Franzini JM, Volpe M, Turchetti G. Patterns of treatment and costs of intermediate and advanced hepatocellular carcinoma management in four Italian centers. *Ther Clin Risk Manag* 2015; **11**: 1603-1612 [PMID: 26527877 DOI: 10.2147/TCRM.S88208]
30 **Facciorusso A**, Bellanti F, Villani R, Salvatore V, Muscatiello N, Piscaglia F, Vendemiale G, Serviddio G. Transarterial chemoembolization *vs* bland embolization in hepatocellular carcinoma: A meta-analysis of randomized trials. *United European Gastroenterol J* 2017; **5**: 511-518 [PMID: 28588882 DOI: 10.1177/2050640616673516]
31 **de Baere T**, Arai Y, Lencioni R, Geschwind JF, Rilling W, Salem R, Matsui O, Soulen MC. Treatment of Liver Tumors with Lipiodol TACE: Technical Recommendations from Experts Opinion. *Cardiovasc Intervent Radiol* 2016; **39**: 334-343 [PMID: 26390875 DOI: 10.1007/s00270-015-1208-y]
32 **Lewis AL**, Gonzalez MV, Lloyd AW, Hall B, Tang Y, Willis SL, Leppard SW, Wolfenden LC, Palmer RR, Stratford PW. DC bead: *in vitro* characterization of a drug-delivery device for transarterial chemoembolization. *J Vasc Interv Radiol* 2006; **17**: 335-342 [PMID: 16517780 DOI: 10.1097/01.RVI.0000195323.46152.B3]
33 **Li Q**, Zhu LZ, Yang RJ, Zhu X. Cytotoxic activity of anticancer drugs on hepatocellular carcinoma cells in hypoxic-hyponutritional culture. *Int Surg* 2014; **99**: 745-752 [PMID: 25437582 DOI: 10.9738/INTSURG-D-14-00073.1]
34 **Dubbelboer IR**, Pavlovic N, Heindryckx F, Sjögren E, Lennernäs H. Liver Cancer Cell Lines Treated with Doxorubicin under Normoxia and Hypoxia: Cell Viability and Oncologic Protein Profile. *Cancers (Basel)* 2019; **11** [PMID: 31330834 DOI: 10.3390/cancers11071024]

World Journal of Gastrointestinal Oncology

Submit a Manuscript: https://www.f6publishing.com

World J Gastrointest Oncol 2022 December 15; 14(12): 2380-2392

DOI: 10.4251/wjgo.v14.i12.2380

ISSN 1948-5204 (online)

ORIGINAL ARTICLE

Observational Study

Deep learning-based radiomics based on contrast-enhanced ultrasound predicts early recurrence and survival outcome in hepatocellular carcinoma

Zhe Huang, Zhu Shu, Rong-Hua Zhu, Jun-Yi Xin, Ling-Ling Wu, Han-Zhang Wang, Jun Chen, Zhi-Wei Zhang, Hong-Chang Luo, Kai-Yan Li

Specialty type: Oncology

Provenance and peer review: Unsolicited article; Externally peer reviewed.

Peer-review model: Single blind

Peer-review report's scientific quality classification

Grade A (Excellent): 0
Grade B (Very good): B, B
Grade C (Good): C
Grade D (Fair): 0
Grade E (Poor): 0

P-Reviewer: Gupta T, India; Qazi Arisar FA, Pakistan; Tsoulfas G, Greece

Received: September 15, 2022
Peer-review started: September 15, 2022
First decision: October 19, 2022
Revised: October 21, 2022
Accepted: November 21, 2022
Article in press: November 21, 2022
Published online: December 15, 2022

Zhe Huang, Zhu Shu, Jun-Yi Xin, Ling-Ling Wu, Hong-Chang Luo, Kai-Yan Li, Department of Medical Ultrasound, Tongji Hospital, Tongji Medical College, Huazhong University of Science and Technology, Wuhan 430030, Hubei Province, China

Rong-Hua Zhu, Zhi-Wei Zhang, Institute of Hepato-pancreato-bililary Surgery, Tongji Hospital, Tongji Medical College, Huazhong University of Science and Technology, Wuhan 430030, Hubei Province, China

Han-Zhang Wang, Jun Chen, PDx Advanced Applications, GE Healthcare, Shanghai 200020, China

Corresponding author: Kai-Yan Li, MD, Director, Doctor, Department of Medical Ultrasound, Tongji Hospital, Tongji Medical College, Huazhong University of Science and Technology, No. 95 Jiefang Avenue, Qiaokou District, Wuhan 430030, Hubei Province, China.
liky20006@126.com

Abstract

BACKGROUND

Hepatocellular carcinoma (HCC) is the most common primary liver malignancy.

AIM

To predict early recurrence (ER) and overall survival (OS) in patients with HCC after radical resection using deep learning-based radiomics (DLR).

METHODS

A total of 414 consecutive patients with HCC who underwent surgical resection with available preoperative grayscale and contrast-enhanced ultrasound images were enrolled. The clinical, DLR, and clinical + DLR models were then designed to predict ER and OS.

RESULTS

The DLR model for predicting ER showed satisfactory clinical benefits [area under the curve (AUC)] = 0.819 and 0.568 in the training and testing cohorts, respectively), similar to the clinical model (AUC = 0.580 and 0.520 in the training and testing cohorts, respectively; $P > 0.05$). The C-index of the clinical + DLR

model in the prediction of OS in the training and testing cohorts was 0.800 and 0.759, respectively. The clinical + DLR model and the DLR model outperformed the clinical model in the training and testing cohorts (P < 0.001 for all). We divided patients into four categories by dichotomizing predicted ER and OS. For patients in class 1 (high ER rate and low risk of OS), retreatment (microwave ablation) after recurrence was associated with improved survival (hazard ratio = 7.895, P = 0.005).

CONCLUSION
Compared to the clinical model, the clinical + DLR model significantly improves the accuracy of predicting OS in HCC patients after radical resection.

Key Words: Hepatocellular carcinoma; Deep learning; Overall survival; Early recurrence; Contrast-enhanced ultrasound

Core Tip: Multivariate Cox regression analysis confirmed that age [hazard ratio (HR) = 1.01], carbohydrate antigen 19-9 (HR = 0.60), tumor size (HR = 1.11), echogenicity (HR = 0.82), and deep learning-based radiomics (DLR, HR = 4.33) were independent predictors of survival outcome (P < 0.05 for all). The concordance index of the clinical + DLR model in the training and testing cohorts was 0.800 and 0.759, respectively. We divided patients into four categories by dichotomizing predicted early recurrence and survival outcome. We found that for patients with class 1 (high early recurrence rate and low risk of survival outcome), retreatment after recurrence was associated with improved survival.

Citation: Huang Z, Shu Z, Zhu RH, Xin JY, Wu LL, Wang HZ, Chen J, Zhang ZW, Luo HC, Li KY. Deep learning-based radiomics based on contrast-enhanced ultrasound predicts early recurrence and survival outcome in hepatocellular carcinoma. *World J Gastrointest Oncol* 2022; 14(12): 2380-2392
URL: https://www.wjgnet.com/1948-5204/full/v14/i12/2380.htm
DOI: https://dx.doi.org/10.4251/wjgo.v14.i12.2380

INTRODUCTION

Hepatocellular carcinoma (HCC) is the most common primary liver malignancy[1]. Surgical resection is considered the mainstream intervention for early HCC treatment[2], and its therapeutic effect has gradually improved in recent years. However, the postoperative recurrence rate of HCC remains as high as 60% at the 5-year follow-up[3], and the 5-year average survival rate is less than 32%[4]. Previous studies have reported that the prognosis of patients with early recurrence (ER) of HCC (within 1 year) after surgical resection is poorer than that of patients with late recurrence (> 1 year)[5]. Therefore, to develop future treatment strategies, there is an urgent need to improve the identification of patients at high risk of recurrence and poor prognosis; this may help identify those who may benefit from adjuvant systemic therapy.

Clinical biomarkers, such as tumor burden, associated with postoperative recurrence and outcomes have been identified[6]. However, the model based on these clinical biomarkers could not provide sufficient predictive power, and quantifiable measures and radiological information were not included in the model, which could provide essential information. Therefore, new representations of biomarker technology must be urgently explored to predict postoperative recurrence and patient outcomes more accurately.

Medical imaging is a potential method for HCC diagnosis[7]. A previous study has developed a model that used clinical and contrast-enhanced computed tomography-based radiographic features to accurately predict the ER of HCC after surgical resection[8]. Ultrasonography is widely used in HCC examination as it is cost-effective, widely available, and time-saving and provides real-time results. More importantly, contrast-enhanced ultrasonography (CEUS) can visualize the microcirculatory perfusion of HCC in real-time[9]. The microbubble contrast agent can be safely used in patients with decreased renal function[10].

Accurate prediction of early HCC recurrence and patient outcome is required to make clinical decisions before surgical resection. Traditional imaging features are relatively poor indicators of tumor heterogeneity (*e.g.*, microvascular invasion and recurrence), are poor predictors of clinical outcomes [11], and are highly subjective, difficult to quantify, and challenging to apply further. Radiomics analysis transforms raw images into countable quantitative features and interprets tumor pathophysiology[12]. Neural network mining to link these features to biological and clinical endpoints can

help develop models to predict patient outcomes, thereby improving prediction-based cancer management[13]. Deep learning-based radiomics (DLR) has been applied to patients with HCC and has achieved promising results in predicting microvascular invasion and response to transarterial chemoembolization[14,15].

This study aimed to predict ER and overall survival (OS) in patients with HCC after radical resection by establishing a DLR model using ultrasonographic and CEUS images.

MATERIALS AND METHODS

Patients

The institutional review board of our institution approved this retrospective study and waived the requirement to obtain written informed consent of all participants.

We retrospectively screened 5466 patients with HCC meeting the Milan criteria who underwent curative resection for HCC at our institution between January 2008 and December 2018. HCC was diagnosed based on pathological findings[16]. The exclusion criteria were as follows: (1) CEUS not performed; (2) recurrent lesions or a history of radiofrequency ablation, microwave ablation, or transcatheter arterial chemoembolization before CEUS; and (3) incomplete follow-up. A total of 5052 patients were excluded, leaving 414 in the final analysis (Supplementary Figure 1). Clinical features, including basic patient information, biological test results, and treatment-related information, were obtained from patient records.

CEUS has the following clinical indications: Patients at risk for HCC in whom ultrasound screening is positive for liver nodules according to current clinical practice standards as well as the World Federation for Ultrasound in Medicine and Biology (WFUMB), European Federation of Societies for Ultrasound in Medicine and Biology (EFSUMB), and CEUS Liver Imaging Reporting and Data System guidelines; focal liver lesions observed on single-phase CT or unenhanced MRI performed for other clinical purposes; indeterminate focal liver lesions observed multiphase contrast-enhanced CT or MRI; and definite HCC on CT or MRI images in reparation for or during tissue sampling, surgical resection, or percutaneous ablation treatment.

Ultrasonographic examination

CEUS was performed using a GE Logiq 9 scanner (GE Healthcare, Wauwatosa, WI, United States) with a 25-MHz frequency range transducer and a 3-5 L probe. Contrast agent (2.4 mL, SonoVue, Bracco, Milan, Italy) was injected intravenously, followed by flushing with 10 mL of 0.9% saline. Continuous observation of three-stage contrast enhancement was performed, including the arterial phase (0-30 s), portal phase (31-120 s), and late phase (121-360 s). CEUS inspections were recorded as video clips for analysis. For the CEUS image used for research, a frame of image with peak contrast intensity of the lesion was selected, that is, the frame of image with the maximum intensity was selected by quantitatively analyzing the enhanced intensity of the lesion in 0-360 s.

Two sonographers (one with more than 8 years of experience in CEUS and the other with more than 5 years of experience) who were blinded to the pathology results evaluated each lesion. In the event of a difference of opinion between the two readers, the final decision was made by a third blinded sonographer (with more than 20 years of CEUS experience). Tumor size, number, and satellite nodules on CEUS were evaluated. Nodules close to the primary tumor (< 3 cm) were designated as satellite nodules. During the late phase, the presence of perfusion defects surrounding HCC lesions was evaluated. If a nodule exhibited hypoechogenicity compared with the surrounding enhanced liver parenchyma, it was defined as the "presence of a perfusion defect of satellite nodules." The degree of enhancement of each lesion was compared with that of the surrounding normal liver tissue and classified as hyper-enhanced, iso-enhanced, or hypo-enhanced.

Follow-up protocol

The patients were followed up at 1 mo, 3 mo, 6 mo, 9 mo, and 12 mo after operation, and every 3-6 mo after 12 mo. At each follow-up, serum alpha-fetoprotein levels were measured and imaging (contrast-enhanced computed tomography, CEUS, or contrast-enhanced MRI) was performed. ER was defined as intrahepatic and/or extrahepatic recurrence of HCC within 1 year after resection. Given that an increasing serum alpha-fetoprotein level alone does not necessarily mean recurrence, recurrence was confirmed by radiological evidence of a new tumor. All patients were followed up until death, ER, or for at least 1 year after curative resection. OS was calculated as the time interval between the date of surgery and the date of death or last follow-up.

Model construction and validation

Image quantification (radiomics feature extraction and DLR feature extraction of grayscale image and CEUS image, which was a frame of image with peak contrast intensity of the lesion (Supplementary Figure 2), OS prognostic model construction and validation (including the development of

DLR score and OS prognostic model using clinical variables and DLR score, and validation of the prognostic models), and construction and validation of the model for ER prediction are shown in the Supplementary material. We also assessed the ability of the DLR model to improve the ability of three clinicians (with 11, 5, and 2 years of experience, respectively) to predict ER, with or without the assistance of the DLR model. To demonstrate the impact of the DLR model on clinician-individualized assessment performance, three clinicians independently reassessed each patient's ER status on the same day after accounting for the DLR model predictions.

Statistical analysis

Differences in the distribution of clinical variables of the training and testing cohorts were assessed by Fisher's exact test or the chi-square test for categorical data and the nonparametric Mann-Whitney test for continuous data. To evaluate the predictive performance of different models, we plotted the receiver operating characteristic (ROC) curve and calculated the area under the ROC curve (AUC). Accuracy, sensitivity, and specificity were calculated from the confusion matrix to quantitatively evaluate the predictive models. For prognostic models predicting ER, we used Kaplan-Meier analysis and the log-rank test to assess survival differences in prognostic clinical variables and radiological characteristics between the training and test sets. Interclass correlation coefficients (ICCs) were calculated for inter-observer and intra-observer agreement. A two-tailed *P*-value less than 0.05 was considered statistically significant. All statistical analyses and graphic production were completed with Python (version 3.8) and R (version 3.6.1).

RESULTS

Demographic characteristics

A total of 414 patients were included in this study, of which 289 and 125 were assigned to the training and testing cohorts, respectively. Mean age of the 414 patients was 53 (45-60) years, and 375 (90.6) were male. The demographic characteristics of patients in the training and testing cohorts were comparable (Table 1; $P > 0.05$). During a median follow-up period of 68 mo (range, 1-137 mo), 217 (52.4%) patients developed recurrence after curative surgical resection.

Prediction models for ER

We considered 414 grayscale ultrasonographic images and 414 peak contrast intensities of CEUS images. A total of 11270 radiological features were extracted from 414 patients. After univariate logistic regression selection, 898 features were retained. After the selection of the maximum relevance minimum redundancy, 8 features were selected as candidate features, and a preoperative ER prediction model was designed using L1-regularized logistic regression machine learning. Inter-observer ICC for measuring DLR features ranged from 0.633 to 0.989. Intra-observer ICC for measuring DLR features ranged from 0.689 to 0.927. The DLR model had an AUC of 0.819 in the training cohort with a 74% accuracy and an AUC of 0.568 in the test cohort with a 58% accuracy.

In this study, the presence of satellites was selected to construct a clinical model based on the constants and satellites (Table 2). The clinical model had an AUC of 0.58 in the training cohort with a 56% accuracy and an AUC of 0.52 in the test cohort with a 56% accuracy.

We constructed a clinical + DLR model, including the presence of satellites and radiomics/DL features. The AUC, accuracy, sensitivity, and specificity of the clinical + DLR model were 0.83, 73%, 71%, and 76%, respectively; the corresponding values in the testing cohort were 0.57, 59%, 62%, and 56%. The DLR model exhibited good classification performance based on ROC curves (Figure 1) and satisfactory clinical benefit (Figure 1), similar to those of the satellite lesion-based clinical model ($P > 0.05$). Prediction accuracy did not improve when clinical variables were combined with the DLR model (AUC: 0.830 for the clinical + DLR model *vs* 0.819 for the DLR model in the training cohort; AUC: 0.572 for the clinical + DLR model *vs* 0.568 for the DLR model in the testing cohort).

In univariate Fine-Gray regression analysis, satellite nodules, DLR model, and multiple lesions were significantly associated with ER. Using these variables, we performed a multivariate Fine-Gray competitive risk regression analysis. This analysis showed that the DLR model remained a strong independent predictor of ER after adjusting for clinical variables [odds ratio (OR) = 132.847, $P < 0.001$].

We found that human performance in predicting ER was significantly enhanced after integrating the DLR model. For clinician 1, the sensitivity increased significantly from 0.250 to 0.856 in the training cohort and from 0.230 to 0.812 in the testing cohort. Likewise, for clinicians 2 and 3, the sensitivity of both testing cohorts increased significantly (0.248 to 0.855 and 0.268 to 0.818 in the training cohort; 0.289 to 0.784 and 0.307 to 0.823 in the testing cohort). Scores were consistent across clinicians with a κ value of 0.76-0.89 and were significantly improved by the integrated DLR model, with a κ value of 0.93-0.97.

Prognostic model for OS

We obtained 11270 radiomics/DL features from patient images and selected them through univariate

Table 1 Patient characteristics

	Study population (*n* = 414)	Training cohort (*n* = 289)	Testing cohort (*n* = 125)	*P* value
Age, yr	53.00 (45.00- 60.00)	52.059 ± 12.190	53.216 ± 11.380	0.1988
Gender, *n* (%)				
Male	375 (90.6)	262 (90.7)	113 (90.4)	0.9196
BMI, kg/m^2	24.50 ± 4.20	24.10 ± 3.20	24.70 ± 3.40	0.1889
HBsAg-positive, *n* (%)	375 (90.6)	264 (91.3)	111 (88.8)	0.5274
AFP > 7 ng/mL, *n* (%)	292 (70.5)	205 (70.9)	87 (69.6)	0.8761
CEA > 5 ng/ml, *n* (%)	31 (7.5)	24 (8.3)	7 (5.6)	0.4494
CA125 > 40 ng/mL, *n* (%)	15 (3.6)	8 (2.8)	7 (5.6)	0.2588
CA199 > 34 ng/mL, *n* (%)	46 (11.1)	295 (10.0)	17 (13.6)	0.3738
WBC count, /μL	6262 ± 1985	6232 ± 1756	6354 ± 2125	0.5668
ALT, U/L	49 ± 36	48 ± 39	51 ± 41	0.1654
AST, U/L	51 ± 35	49 ± 36	53 ± 42	0.2358
Liver cirrhosis, *n* (%)	345 (83.3)	244 (84.4)	101 (80.8)	0.3630
Microvascular invasion, *n* (%)	312 (75.4)	211 (73.0)	101 (80.8)	0.0910
Tumor size, cm				
x	2.40 [1.70-3.68]	2.957 ± 1.850	3.120 ± 2.050	0.3689
y	2.00 [1.42-3.10]	2.480 ± 1.490	2.670 ± 1.960	0.4820
Gray-scale echogenicity				0.5954
Hyperechoic	46 (11.1)	35 (12.1)	11 (8.8)	
Medium	4 (1.0)	3 (1.0)	1 (0.8)	
Hypoechoic	364 (87.9)	251 (86.9)	113 (90.4)	
Arterial phase				0.4639
Hyperenhancement	403 (97.3)	283 (97.9)	120 (96.0)	
Isoenhancement	8 (1.9)	4 (1.4)	4 (3.2)	
Hypoenhancement	3 (0.7)	2 (0.7)	1 (0.8)	
Portal phase				0.6669
Hyperenhancement	15 (3.5)	12 (4.2)	3 (2.4)	
Isoenhancement	232 (56.0)	162 (56.1)	70 (56.0)	
Hypoenhancement	167 (40.3)	115 (39.8)	52 (41.6)	
Late phase				0.1300
Hyperenhancement	2 (0.5)	1 (0.3)	1 (0.8)	
Isoenhancement	79 (19.1)	46 (15.9)	33 (90.4)	
Hypoenhancement	333 (80.4)	232 (80.3)	101 (80.8)	
Enhancing capsules	45 (10.9)	36 (12.5)	9 (7.2)	0.1598
Unsmooth margins	97 (23.4)	64 (22.19)	33 (26.4)	0.4168
Retreatment after recurrence	168 (40.3)	118 (40.5)	50 (40.0)	0.9270

BMI: Body mass index; AFP: Alpha-fetoprotein; CEA: Carcinoembryonic antigen; CA125: Carbohydrate antigen 125; CA19-9: Carbohydrate antigen 19-9; BCLC: Barcelona-clinic liver cancer; WBC: White blood cell; HBsAg: Hepatitis B surface antigen; ALT: Alanine aminotransferase; AST: Aspartate aminotransferase.

Table 2 Univariate and multivariable analyses of early recurrence of hepatocellular carcinoma patients

	Univariate cox regression				Multivariate logistic regression			
	HR	[0.025	0.975]	*P*	HR	[0.025	0.975]	*P*
Age, yr	0.991	0.971	1.011	0.383				
Gender	1.005	0.463	2.181	0.990				
HBsAg-positive	1.138	0.472	2.740	0.773				
AFP	0.622	0.361	1.071	0.087	0.709	0.406	1.239	0.227
CEA	0.944	0.352	2.535	0.910				
CA125	1.811	0.424	7.752	0.423				
CA19-9	1.636	0.727	3.684	0.234				
ALT, U/L	1.248	0.697	2.321	0.267				
AST, U/L	1.566	0.397	2.108	0.675				
FIB-4 score	1.212	0.431	1.986	0.742				
Liver cirrhosis	1.142	0.506	2.121	0.657				
Tumor size x	1.000	0.882	1.143	0.951				
Tumor size y	0.988	0.856	1.142	0.873				
Gray-scale echogenicity	0.731	0.493	1.087	0.121				
Arterial phase enhancement	0.924	0.351	2.438	0.874				
Portal phase enhancement	1.321	0.832	2.100	0.238				
Portal phase enhancement	0.982	0.512	1.885	0.957				
Enhancing capsules	0.930	0.413	2.096	0.862				
Satellite nodules	4.843	1.917	12.244	0.001	4.194	1.368	12.871	0.012
Unsmooth margins	0.839	0.462	1.522	0.563				
Constant					0.990	0.707	1.387	0.953

Fibrosis-4 score: Age (years) × aspartate aminotransferase (U/L) / [platelet count (10^9/L) × alanine aminotransferase (U/L)]$^{1/2}$.
HR: Hazard ratio; AFP: Alpha-fetoprotein; CEA: Carcinoembryonic antigen; CA125: Carbohydrate antigen 125; CA19-9: Carbohydrate antigen 19-9; ALT: Alanine aminotransferase; AST: Aspartate aminotransferase; FIB-4 score: Fibrosis-4 score; HBsAg: Hepatitis B surface antigen.

Cox proportional hazards regression, with 50 features with a Harrell's concordance index (C-index) > 0.58. Multivariate Cox regression with L1 penalization calculates survival hazard values and builds high-risk and low-risk groups based on hazard values. The optimal stratification threshold for X-tile generation was 0.52. Kaplan-Meier curves showed significant differences between the low- and high-risk subgroups in the training and testing cohorts (Figure 2). Inter-observer ICC for measuring DLR features ranged from 0.611 to 0.976. Intra-observer ICC for measuring DLR features ranged from 0.699 to 0.912. The C-indices in the training and testing cohorts were 0.792 and 0.741, respectively. Calibration curves at 1, 3, and 5 years showed good agreement between DLR model estimates and actual observations in the training and testing cohorts.

In univariate analysis, nine significant factors, including five clinical variables (age, sex, carcinoembryonic antigen, carbohydrate antigen 125, and carbohydrate antigen 19-9), three semantic imaging features (tumor size x, tumor size y, and unsmooth margins), and DLR, were significantly associated with OS ($P < 0.05$) (Supplementary Table 1). Multivariate Cox regression analysis confirmed that age [hazard ratio (HR) = 1.01, 95% confidence interval (CI): 1.00-1.03, $P = 0.02$], carbohydrate antigen 19-9 (HR = 0.6, 95%CI: 0.04-1.03, $P = 0.007$), tumor size y (HR = 1.11, 95%CI: 1.03-1.19, $P = 0.001$), and DLR (HR = 4.33, 95%CI: 3.45-5.45, $P < 0.005$) were independent predictors of OS (Table 3). Based on the multivariate Cox regression analysis of assigned coefficients, these independent predictor variables were linearly combined to build a clinical and clinical + DLR model. Kaplan-Meier curves showed significant differences between the low- and high-risk subgroups in the training and testing cohorts (Figure 2). The C-indices of the clinical model in the training and testing cohorts were 0.566 and 0.565, respectively. The C-indices of the clinical + DLR model in the training and testing cohorts were 0.800 and 0.759, respectively. The clinical + DLR model and DLR model outperformed the clinical model in the training cohort ($P < 0.001$ and $P < 0.001$, respectively). Similar results were observed in the testing

Table 3 Univariate and multivariable analyses of overall survival of hepatocellular carcinoma patients

	Univariate cox regression				Multivariate logistic regression			
	HR	[0.025	0.975]	*P*	HR	[0.025	0.975]	*P*
Age, yr	1.020	1.000	1.030	0.010	1.02	1.00	1.03	0.01
Gender	1.570	1.030	2.390	0.030	1.42	0.89	2.26	0.14
HBsAg-positive	1.600	1.030	2.490	0.040	1.32	0.82	2.12	0.25
AFP	1.100	0.830	1.460	0.500				
CEA	0.760	0.460	1.270	0.300				
CA125	0.580	0.280	1.220	0.150				
CA19-9	0.630	0.420	0.950	0.030	0.65	0.41	1.03	0.07
ALT, U/L	1.121	0.453	1.976	0.430				
AST, U/L	1.342	0.876	2.014	0.540				
FIB-4 score	1.012	0.547	1.743	0.720				
Liver cirrhosis	1.112	0.563	1.956	0.550				
Tumor size x	1.080	1.010	1.160	0.040	0.96	0.85	1.09	0.56
Tumor size y	1.090	1.020	1.170	0.010	1.17	1.02	1.33	0.02
Gray-scale echogenicity	0.830	0.670	1.020	0.080	0.77	0.60	0.99	0.04
Arterial phase enhancement	0.680	0.420	1.110	0.130				
Portal phase enhancement	1.270	0.990	1.620	0.060	1.25	0.95	1.63	0.11
Portal phase Enhancement	1.130	0.810	1.580	0.460				
Enhancing capsules	1.110	0.720	1.710	0.630				
Satellite nodules	1.190	0.780	1.830	0.420				
Unsmooth margins	0.720	0.520	0.990	0.040	0.79	0.56	1.13	0.19
Early reoccurrence	1.290	0.990	1.680	0.060	1.25	0.93	1.67	0.14
Retreatment after recurrence	0.710	0.540	1.160	0.300				
DLR	3.240	2.670	3.930	< 0.005				

HR: Hazard ratio; AFP: Alpha-fetoprotein; CEA: Carcinoembryonic antigen; CA125: Carbohydrate antigen 125; CA19-9: Carbohydrate antigen 19-9; ALT: Alanine aminotransferase; AST: Aspartate aminotransferase; FIB-4 score: Fibrosis-4 score; DLR: Deep learning-based radiomics.

cohort ($P < 0.001$ and $P < 0.001$, respectively). The corresponding prediction error curves show that the prediction error of the clinical + DLR model was consistently lower than that of the clinical model. Similar results were obtained for the combined Brier scores in the training and testing cohorts. Finally, we further quantified the improvement in survival prediction accuracy between the clinical + DLR model and the clinical model. This resulted in a net reclassification improvement in survival of 0.234 (0.009 to 0.312; $P < 0.001$) and an OS net reclassification improvement of 0.176 (0.076 to 0.293; $P < 0.001$) in the testing cohort.

Histological features [degree of differentiation (HR = 1.76, 95%CI: 0.56-3.01, $P = 0.012$) and microvascular infiltration (HR = 2.25, 95%CI: 0.75-5.12, $P = 0.023$)] were independent predictors of OS (Supplementary Table 2). The clinical + DL and DLR models had the same performance with the histological features in the training cohort ($P = 0.157$ and $P = 0.566$, respectively). Similar results were observed in the testing cohort ($P = 0.225$ and $P = 0.648$, respectively).

Evaluation of the model for predicting OS and benefit of retreatment after recurrence

In addition to evaluating the accuracy of the model in predicting ER and OS, we further evaluated the correlation between retreatment (microwave ablation) after recurrence and OS in patients. We divided patients into four categories by dichotomizing predicted ER and OS. We found that for patients in class 1 (high ER rate and low risk of OS), retreatment after recurrence was associated with improved survival (HR = 7.895, $P = 0.005$). In contrast, for patients in class 2 (high ER rate and high risk of OS) (HR = 1.542, $P = 0.214$), class 3 (low ER rate and low risk of OS) (HR = 0.357, $P = 0.500$), and class 4 (low ER rate and

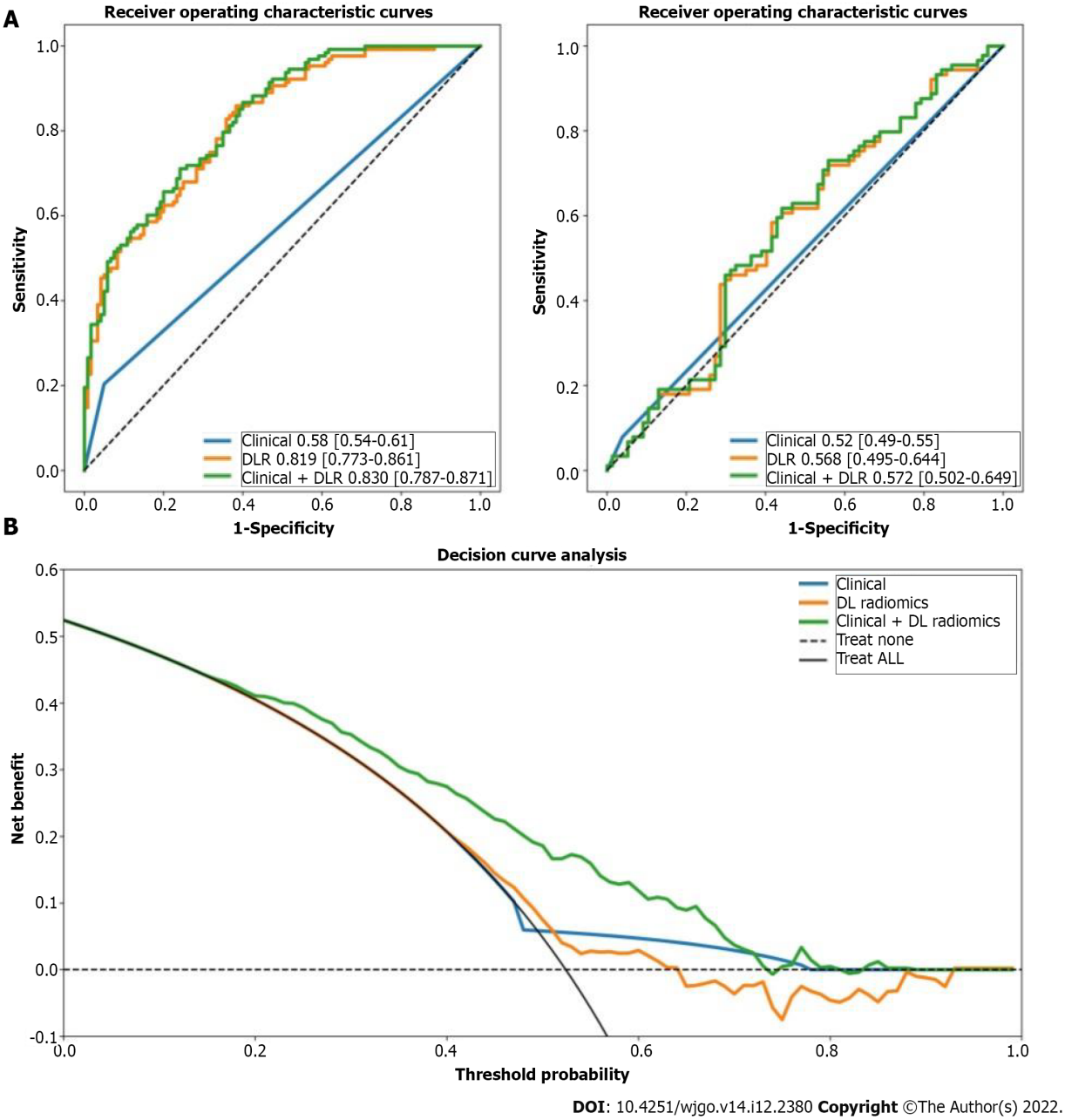

DOI: 10.4251/wjgo.v14.i12.2380

Figure 1 Receiver operating characteristic curves and decision curve analysis. A: Receiver operating characteristic curves of clinical, deep learning-based radiomics (DLR), and clinical + DLR models for predicting early recurrence in the training and testing cohorts; B: Decision curve analysis (DCA) of each model in predicting early recurrence. The vertical axis measures standardized net benefit. The horizontal axis shows the corresponding risk threshold. The DCA showed that if the threshold probability is between 0 and 1, using the DLR model derived in the present study to predict ER provided the same benefit as clinical model. ROC: Receiver operating characteristic; DCA: Decision curve analysis; DL: Deep learning; DLR: Deep learning-based radiomics.

high risk of OS) (HR = 1.416, P = 0.234), retreatment after recurrence did not affect survival (Figure 3).

DISCUSSION

This study aimed to develop and validate a predictive model for ER and OS in patients with early-stage HCC undergoing surgical resection. This model allows for better preoperative/pretreatment decision-making as to the best possible treatment options and timing. We transformed radiomics/DL signatures into quantitative radiomics/DL signatures and constructed a DLR model with a better ability to predict patient OS preoperatively than clinical models alone. This model may guide individualized treatment and survival monitoring.

Early-stage HCC still has a high recurrence rate after radical surgery. In our study, 52.4% of postoperative patients developed ER. Early HCC has high heterogeneity and different prognoses, which

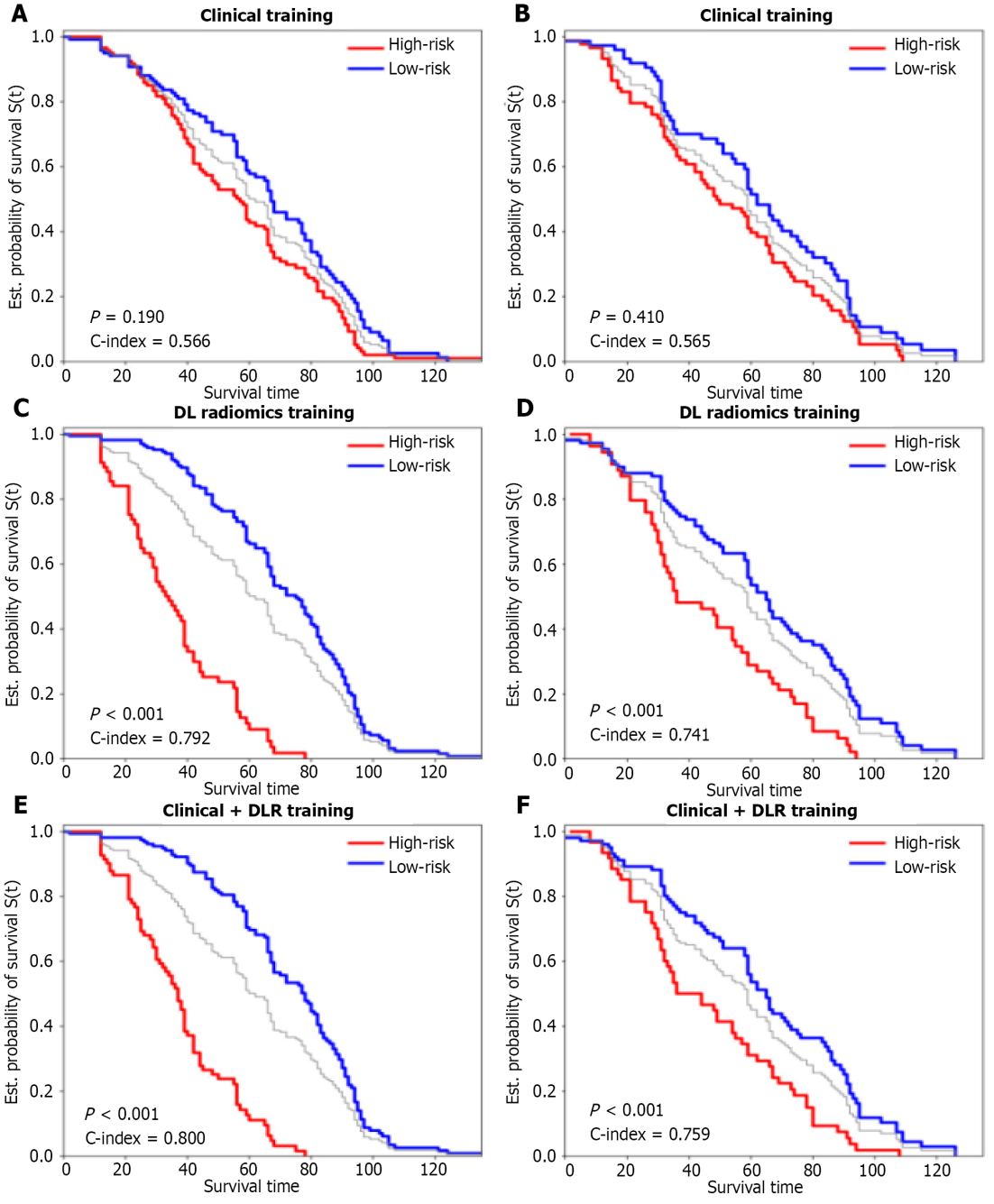

DOI: 10.4251/wjgo.v14.i12.2380

Figure 2 Kaplan-Meier curves of overall survival stratified by high and low risk for clinical, deep learning-based radiomics, and clinical + deep learning-based radiomics models. A and B: Clinical training; C and D: Deep learning-based radiomics testing; E and F: Clinical + DLR. DLR: Deep learning-based radiomics.

should be determined early and accurately. Gene signatures have been widely used in tumor identification but are rarely used in clinical applications because of their high cost and time consumption. Considering the high recurrence rate of HCC after radical resection, including disseminated or recurrent disease, early prediction of ER is critical for improving individualized treatment. As a routine examination, ultrasonography has a high potential for further investigation of ER-predictive radiological features. With the development of machine learning technology, a large amount of quantitative radiological data has been used to construct more predictive models than those developed by semantic radiological features. Our study found that the DLR score has the same or a higher ability to predict ER than satellite nodules. The DLR score can predict the patient's ER before surgery, helping guide treatment choices.

In this study, we developed an ER-related DLR model and evaluated its role in predicting OS. Furthermore, we combined clinical and DLR features to predict OS. In the multivariate analysis, we found that age was a significant risk factor for OS in patients with HCC, consistent with the results of

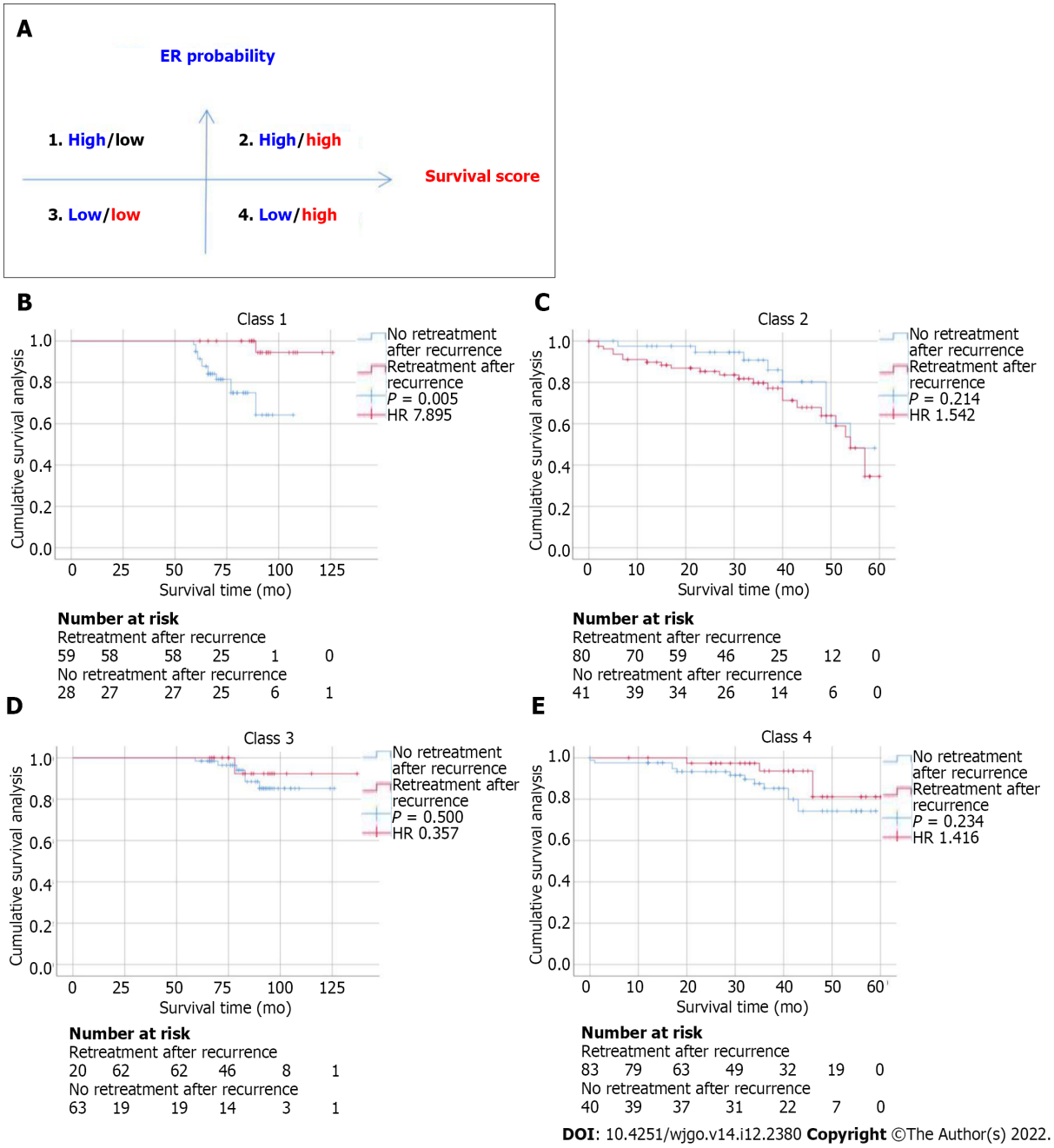

DOI: 10.4251/wjgo.v14.i12.2380

Figure 3 Relationship between the deep learning-based radiomics model and benefit from retreatment after recurrence in matched patients. A: Four different risk classes were defined by early recurrence and overall survival predicted by the deep learning-based radiomics model; B-E: Kaplan-Meier curves of disease-free survival for patients who were stratified according to receipt of retreatment after recurrence. HR: Hazard ratio.

other studies[8]. In addition, we found carbohydrate antigen 19-9, tumor size, and echogenicity were important risk factors for OS. However, the clinical + DLR and DLR models made a more dominant contribution in predicting OS than these clinical variables.

Re-surgical resection is considered a treatment for HCC recurrence. A key treatment issue is how to identify patients who may benefit from retreatment for HCC recurrence. However, given the costs associated with treatment, surgical trauma, and modest survival benefits, the optimal criteria for selecting candidates for retreatment for HCC recurrence remain unclear. The model developed in this study can help identify such patients. By combining information on ER risk and survival, our model can identify patients in class 1 who are more likely to benefit from re-surgical resection treatment.

HCC is a tumor with rich blood supply in which tortuous and dilated new vessels are continuously generated. In our study, the frame with the highest peak intensity in the arterial phase of CEUS was used, reflecting the density of neovascularization in the tumor. Studies have shown that the peak intensity in the recurrence group is lower than that in the non-recurrence group and that peak intensity is a risk factor for HCC recurrence[17].

Liu *et al*[18] analyzes CEUS images based on DLR to predict progression-free survival after radiofrequency ablation and surgical resection and optimize radiofrequency ablation and surgical resection treatment options for patients with HCC. Our study was also based on DLR analysis of CEUS images; the difference is that our study aimed to predict the ER and OS of patients with HCC after surgical resection and provide guidance for retreatment after recurrence.

Our study has two significant limitations. First, this is a single-center study, and a multicenter prospective study with a larger patient population is needed to further validate the performance of our model. Second, regions of interest were segmented manually and have not been fully automated. Finally, washout is also an important aspect of the assessment of HCC, and other images of CEUS need to be fully studied in the future.

CONCLUSION

The DLR model has the same satisfactory clinical benefit for predicting ER as the clinical model. Compared with the clinical model, the clinical + DLR model and the DLR model significantly improve the accuracy of predicting OS in HCC patients after radical resection.

ARTICLE HIGHLIGHTS

Research background

Hepatocellular carcinoma (HCC) is the most common primary liver malignancy.

Research motivation

To develop future treatment strategies, there is an urgent need to improve the identification of patients at high risk of recurrence and poor prognosis; this may help identify those who may benefit from adjuvant systemic therapy.

Research objectives

To predict early recurrence (ER) and overall survival (OS) in patients with HCC after radical resection using deep learning (DL)-based radiomics.

Research methods

A total of 414 consecutive patients with HCC who underwent surgical resection with available preoperative grayscale and contrast-enhanced ultrasound images were enrolled. The clinical, DLR, and clinical + DLR model were then designed to predict ER and OS.

Research results

The DLR model for predicting ER showed satisfactory clinical benefits [area under the curve (AUC)] = 0.819 and 0.568 in the training and testing cohorts, respectively), similar to the clinical model (AUC 0.580 and 0.520 in the training and testing cohorts, respectively; $P > 0.05$). The C-indices of the clinical + DLR model in prediction of OS in the training and testing cohorts were 0.800 and 0.759, respectively. The clinical + DLR model and the DLR model outperformed the clinical model in the training and testing cohorts ($P < 0.001$ for all). We divided patients into four categories by dichotomizing predicted ER and OS. For patients in class 1 (high ER rate and low risk of OS), retreatment (microwave ablation) after recurrence was associated with improved survival (hazard ratio = 7.895, $P = 0.005$).

Research conclusions

As compared to the clinical model, the clinical + DLR model significantly improves the accuracy of predicting OS in patients with HCC after radical resection.

Research perspectives

As compared to the clinical model, the clinical + DLR model significantly improves the accuracy of predicting OS in patients with HCC after radical resection.

FOOTNOTES

Author contributions: Huang Z contributed to study concept and design, data acquisition, analysis, and interpretation, and manuscript drafting; Wang HZ and Chen J contributed to the implementation and analysis of all machine learning methods; Huang Z, Zhu S, Wu XB, and Zhu RH contributed to image interpretation and segmentation; Zhu S, Wu XB, Zhang ZW, and Li KY contributed to data acquisition; Huang Z, Li KY, Wang HZ, and

Zhu RH contributed to study concept and design, critical revision of the manuscript for important intellectual content, and study supervision.

Institutional review board statement: The study was reviewed and approved by the Ethics Committee of Tongji Hospital, Tongji Medical College, Huazhong University of Science and Technology (Approval No. TJ-IRB20190401).

Informed consent statement: The Ethics Committee of Tongji Hospital waived the requirement to obtain written informed consent of all participants.

Conflict-of-interest statement: There are no conflicts of interest to report.

Data sharing statement: All data generated or analyzed during this study are included in this article and/or its supplementary material files. Further inquiries can be directed to the corresponding author.

STROBE statement: The authors have read the STROBE Statement—checklist of items, and the manuscript was prepared and revised according to the STROBE Statement—checklist of items.

Country/Territory of origin: China

ORCID number: Rong-Hua Zhu 0000-0002-8588-7493; Kai-Yan Li 0000-0003-3332-6325.

S-Editor: Chen YL
L-Editor: Wang TQ
P-Editor: Chen YL

REFERENCES

1 **Omata M**, Cheng AL, Kokudo N, Kudo M, Lee JM, Jia J, Tateishi R, Han KH, Chawla YK, Shiina S, Jafri W, Payawal DA, Ohki T, Ogasawara S, Chen PJ, Lesmana CRA, Lesmana LA, Gani RA, Obi S, Dokmeci AK, Sarin SK. Asia-Pacific clinical practice guidelines on the management of hepatocellular carcinoma: a 2017 update. *Hepatol Int* 2017; **11**: 317-370 [PMID: 28620797 DOI: 10.1007/s12072-017-9799-9]

2 **Hobeika C**, Nault JC, Barbier L, Schwarz L, Lim C, Laurent A, Gay S, Salamé E, Scatton O, Soubrane O, Cauchy F. Influence of surgical approach and quality of resection on the probability of cure for early-stage HCC occurring in cirrhosis. *JHEP Rep* 2020; **2**: 100153 [PMID: 32995713 DOI: 10.1016/j.jhepr.2020.100153]

3 **Lim KC**, Chow PK, Allen JC, Siddiqui FJ, Chan ES, Tan SB. Systematic review of outcomes of liver resection for early hepatocellular carcinoma within the Milan criteria. *Br J Surg* 2012; **99**: 1622-1629 [PMID: 23023956 DOI: 10.1002/bjs.8915]

4 **El-Serag HB**. Hepatocellular carcinoma. *N Engl J Med* 2011; **365**: 1118-1127 [PMID: 21992124 DOI: 10.1056/NEJMra1001683]

5 **Poon RT**, Fan ST, Ng IO, Lo CM, Liu CL, Wong J. Different risk factors and prognosis for early and late intrahepatic recurrence after resection of hepatocellular carcinoma. *Cancer* 2000; **89**: 500-507 [PMID: 10931448]

6 **Villanueva A**. Hepatocellular Carcinoma. *N Engl J Med* 2019; **380**: 1450-1462 [PMID: 30970190 DOI: 10.1056/NEJMra1713263]

7 **Llovet JM**, Brú C, Bruix J. Prognosis of hepatocellular carcinoma: the BCLC staging classification. *Semin Liver Dis* 1999; **19**: 329-338 [PMID: 10518312 DOI: 10.1055/s-2007-1007122]

8 **Lee IC**, Huang JY, Chen TC, Yen CH, Chiu NC, Hwang HE, Huang JG, Liu CA, Chau GY, Lee RC, Hung YP, Chao Y, Ho SY, Huang YH. Evolutionary Learning-Derived Clinical-Radiomic Models for Predicting Early Recurrence of Hepatocellular Carcinoma after Resection. *Liver Cancer* 2021; **10**: 572-582 [PMID: 34950180 DOI: 10.1159/000518728]

9 **Alzaraa A**, Gravante G, Chung WY, Al-Leswas D, Morgan B, Dennison A, Lloyd D. Contrast-enhanced ultrasound in the preoperative, intraoperative and postoperative assessment of liver lesions. *Hepatol Res* 2013; **43**: 809-819 [PMID: 23745715 DOI: 10.1111/hepr.12044]

10 **Wilson SR**, Feinstein SB. Introduction: 4th Guidelines and Good Clinical Practice Recommendations for Contrast Enhanced Ultrasound (CEUS) in the Liver-Update 2020 WFUMB in Cooperation with EFSUMB, AFSUMB, AIUM and FLAUS. *Ultrasound Med Biol* 2020; **46**: 3483-3484 [PMID: 32888748 DOI: 10.1016/j.ultrasmedbio.2020.08.015]

11 **Renzulli M**, Brocchi S, Cucchetti A, Mazzotti F, Mosconi C, Sportoletti C, Brandi G, Pinna AD, Golfieri R. Can Current Preoperative Imaging Be Used to Detect Microvascular Invasion of Hepatocellular Carcinoma? *Radiology* 2016; **279**: 432-442 [PMID: 26653683 DOI: 10.1148/radiol.2015150998]

12 **Bi WL**, Hosny A, Schabath MB, Giger ML, Birkbak NJ, Mehrtash A, Allison T, Arnaout O, Abbosh C, Dunn IF, Mak RH, Tamimi RM, Tempany CM, Swanton C, Hoffmann U, Schwartz LH, Gillies RJ, Huang RY, Aerts HJWL. Artificial intelligence in cancer imaging: Clinical challenges and applications. *CA Cancer J Clin* 2019; **69**: 127-157 [PMID:

30720861 DOI: 10.3322/caac.21552]
13 **Avanzo M**, Wei L, Stancanello J, Vallières M, Rao A, Morin O, Mattonen SA, El Naqa I. Machine and deep learning methods for radiomics. *Med Phys* 2020; **47**: e185-e202 [PMID: 32418336 DOI: 10.1002/mp.13678]
14 **Xu X**, Zhang HL, Liu QP, Sun SW, Zhang J, Zhu FP, Yang G, Yan X, Zhang YD, Liu XS. Radiomic analysis of contrast-enhanced CT predicts microvascular invasion and outcome in hepatocellular carcinoma. *J Hepatol* 2019; **70**: 1133-1144 [PMID: 30876945 DOI: 10.1016/j.jhep.2019.02.023]
15 **Chen M**, Cao J, Hu J, Topatana W, Li S, Juengpanich S, Lin J, Tong C, Shen J, Zhang B, Wu J, Pocha C, Kudo M, Amedei A, Trevisani F, Sung PS, Zaydfudim VM, Kanda T, Cai X. Clinical-Radiomic Analysis for Pretreatment Prediction of Objective Response to First Transarterial Chemoembolization in Hepatocellular Carcinoma. *Liver Cancer* 2021; **10**: 38-51 [PMID: 33708638 DOI: 10.1159/000512028]
16 **European Association for the Study of the Liver**. EASL Clinical Practice Guidelines: Management of hepatocellular carcinoma. *J Hepatol* 2018; **69**: 182-236 [PMID: 29628281 DOI: 10.1016/j.jhep.2018.03.019]
17 **Xuan Z**, Wu N, Li C, Liu Y. Application of contrast-enhanced ultrasound in the pathological grading and prognosis prediction of hepatocellular carcinoma. *Transl Cancer Res* 2021; **10**: 4106-4115 [PMID: 35116708 DOI: 10.21037/tcr-21-1264]
18 **Liu F**, Liu D, Wang K, Xie X, Su L, Kuang M, Huang G, Peng B, Wang Y, Lin M, Tian J. Deep Learning Radiomics Based on Contrast-Enhanced Ultrasound Might Optimize Curative Treatments for Very-Early or Early-Stage Hepatocellular Carcinoma Patients. *Liver Cancer* 2020; **9**: 397-413 [PMID: 32999867 DOI: 10.1159/000505694]

World Journal of Gastrointestinal Oncology

Submit a Manuscript: https://www.f6publishing.com

World J Gastrointest Oncol 2022 December 15; 14(12): 2393-2403

DOI: 10.4251/wjgo.v14.i12.2393

ISSN 1948-5204 (online)

ORIGINAL ARTICLE

Observational Study

Clinical value of regional lymph node sorting in gastric cancer

Chuan Li, Xiao-Jie Tian, Geng-Tao Qu, Yu-Xin Teng, Zhu-Feng Li, Xin-Yang Nie, Dong-Jie Liu, Tong Liu, Wei-Dong Li

Specialty type: Oncology

Provenance and peer review: Unsolicited article; Externally peer reviewed

Peer-review model: Single blind

Peer-review report's scientific quality classification

Grade A (Excellent): 0
Grade B (Very good): B
Grade C (Good): C
Grade D (Fair): 0
Grade E (Poor): 0

P-Reviewer: Huang HL, Japan; Wu C, China

Received: October 3, 2022
Peer-review started: October 3, 2022
First decision: October 21, 2022
Revised: October 26, 2022
Accepted: November 30, 2022
Article in press: November 30, 2022
Published online: December 15, 2022

Chuan Li, Xiao-Jie Tian, Geng-Tao Qu, Yu-Xin Teng, Zhu-Feng Li, Xin-Yang Nie, Dong-Jie Liu, Tong Liu, Wei-Dong Li, Department of General Surgery, Tianjin General Surgery Institute, Tianjin Medical University General Hospital, Tianjin 300000, China

Corresponding author: Wei-Dong Li, Doctor, MD, PhD, Surgical Oncologist, Department of General Surgery, Tianjin General Surgery Institute, Tianjin Medical University General Hospital, No. 154 Anshan Road, Heping District, Tianjin 300000, China.
tjmughgs_lwd@163.com

Abstract

BACKGROUND

Increasing evidence have shown that regional lymph node metastasis is a critical prognostic factor in gastric cancer (GC). In addition, lymph node dissection is a key factor in determining the appropriate treatment for GC. However, the association between the number of positive lymph nodes and area of lymph node metastasis in GC remains unclear.

AIM

To investigate the clinical value of regional lymph node sorting after radical gastrectomy for GC.

METHODS

This study included 661 patients with GC who underwent radical gastrectomy at Tianjin Medical University General Hospital between January 2012 and June 2020. The patients were divided into regional sorting and non-sorting groups. Clinicopathological data were collected and retrospectively reviewed to determine the differences in the total number of lymph nodes and number of positive lymph nodes between the groups. Independent sample *t*-tests were used for intergroup comparisons. Continuous variables that did not conform to a normal distribution were expressed as median (interquartile range), and the Mann-Whitney *U* test was used for inter-group comparisons.

RESULTS

There were no significant differences between the groups in terms of the surgical method, tumor site, immersion depth, and degree of differentiation. The total number of lymph nodes was significantly higher in the regional sorting group (n = 324) than in the non-sorting group (n = 337) (32.5 *vs* 21.2, $P < 0.001$). There was no significant difference in the number of positive lymph nodes between the two groups. A total of 212 patients with GC had lymph node metastasis in the lymph

node regional sorting group, including 89 (41.98%) cases in the first dissection station and 123 (58.02 %) cases in the second dissection station. Binary and multivariate logistic regression results showed that the number of positive lymph nodes ($P < 0.001$) was an independent risk factor for lymph node metastases at the second dissection station.

CONCLUSION

Regional sorting of lymph nodes after radical gastrectomy may increase the number of detected lymph nodes, thereby improving the reliability and accuracy of lymph node staging in clinical practice.

Key Words: Radical gastrectomy; Regional lymph node sorting; Lymph node dissection; Lymph node staging; Metastasis; Gastric cancer

Core Tip: The lymph node metastasis rates of different groups of gastric cancer (GC) lymph nodes in different parts of GC differ. Understanding the mechanisms of lymph node metastasis to guide lymph node dissection during surgery is of great significance. Regional sorting of lymph nodes after radical gastrectomy for GC may increase the number of detected lymph nodes, thereby allowing a more accurate and reliable lymph node staging, which is helpful in clinical practice.

Citation: Li C, Tian XJ, Qu GT, Teng YX, Li ZF, Nie XY, Liu DJ, Liu T, Li WD. Clinical value of regional lymph node sorting in gastric cancer. *World J Gastrointest Oncol* 2022; 14(12): 2393-2403
URL: https://www.wjgnet.com/1948-5204/full/v14/i12/2393.htm
DOI: https://dx.doi.org/10.4251/wjgo.v14.i12.2393

INTRODUCTION

There has been a decline in the incidence and mortality rates of gastric cancer (GC) over the past five decades globally; however, GC remains the third leading cause of cancer-related deaths[1]. Studies have reported that 3%-20% of patients with early-stage GC have lymph node metastasis[2,3]. Therefore, lymph node dissection is a key factor in selecting an appropriate treatment for GC. Clarifying lymph node staging is also a critical evaluation in the planning of GC treatment.

Accurate lymph node staging can be used to evaluate the effectiveness of surgery and provide a reliable basis for the choice of follow-up treatment. To obtain a sufficient number of lymph nodes and accurately classify lymph node staging, Japanese scholars began to involve surgeons in the study of lymph node detection as early as 1996[4]. In China, Cao *et al*[5] studied patients with GC who underwent D2 lymph node dissection and found that the number of detected lymph nodes increased significantly in patients who had been regionally sorted, indicating that regional sorting improved the accuracy and reliability of lymph node staging in GC. However, it remains unclear whether regional lymph node sorting increases the number of positive lymph nodes.

Using the number of lymph nodes with metastasis alone, the current classification criteria are not sufficient for clinical and surgical guidance[6]. Therefore, it is essential to study the regions of lymph node metastasis. By knowing the metastasis rates of lymph nodes at various tumor sites preoperatively, surgeons can remove all possible positive lymph nodes, enabling a 'root-and-branch' effect of the operation, thus improving patient outcomes.

Lymph node staging and lymph node metastasis regions are important considerations in the diagnosis and treatment of GC. Researchers have compared the current lymph node staging system with the lymph node metastasis region system used in Japan and found that these two systems have the same advantages in determining prognosis. The authors, therefore, concluded that the lymph node metastasis system should be incorporated into the current lymph node staging system[7]. However, few studies have focused on the relationship between the current lymph node staging system and regions of lymph node metastasis. Therefore, the aim of this study was to investigate the clinical value of regional lymph node sorting after radical gastrectomy in patients with GC.

MATERIALS AND METHODS

We evaluated the role of regional lymph node sorting in clinical settings by comparing the number of

lymph nodes detected between regional sorting and non-sorting groups. For patients in the lymph node regional sorting group, the lymph node metastatic rate was summarized for different tumor regions, providing an analytical basis for surgical dissection of the lymph nodes. The relationship between the number of positive lymph nodes and location of lymph node metastasis was analyzed to evaluate the current lymph node staging system and provide a theoretical basis for further treatment of patients in the lymph node regional sorting group with lymph node metastasis.

Study population

Based on the inclusion and exclusion criteria, 661 patients with gastric tumors were admitted to the Department of Gastrointestinal Surgery at Tianjin Medical University General Hospital from January 2012 to June 2020. Patients were divided into two groups according to the examination method: The regional sorting group and non-sorting group. The inclusion criteria were: (1) Diagnosis of GC by imaging and pathology; (2) No history of malignant tumors; and (3) Standard radical gastrectomy for GC. The exclusion criteria were: (1) New auxiliary chemotherapy; and (2) A history of gastric resection. The study complied with the Declaration of Helsinki and was approved by the ethics committee of Tianjin Medical University General Hospital (approval number: IRB2022-WZ-167). The need for informed consent was waived by the ethics committee.

General baseline information

General information collected in this study included sex, age, surgical method (near-end gastrectomy, far-end gastrectomy, and total gastrectomy), tumor sites [primary lesions in the upper third of the stomach (U), primary lesions in the middle third of the stomach (M), primary lesions in the lower third of the stomach (L) (the main tumor body was considered if the tumor invaded into two regions)], immersion depth, differentiation degree [differentiated carcinoma (DCA) (highly DCA, mediated carcinoma, papilloma cancer), undifferentiated carcinoma (UCA) (low differentiation carcinoma, mucus carcinoma, anti-cell carcinoma, undifferentiated cancer)], total number of lymph nodes, number of positive lymph nodes, metastatic lymph node ratio (MLNR): The ratio of the number of positive lymph nodes to the number of lymph nodes detected, and lymph node metastatic regions (first dissection station: Group Nos. 1-7; second dissection station: group Nos. 8a-12a). The order of lymph node metastasis may vary depending on the location of the primary tumor. Additionally, if the primary tumor is more infiltrated or poorly differentiated, lymph nodes may be more prone to metastases. Gong *et al*[8] have indicated that the prognosis of patients with N2 stage GC is similar to that of GC patients with regional lymph node metastasis who only underwent first-stage dissection. Therefore, 6 positive lymph nodes can be used as a boundary for the analysis of the relationship between lymph node metastasis areas and current lymph node staging. Moreover, these data are intuitive and easy to analyze clinically. Therefore, tumor sites, immersion depth, differentiation degree, and number of positive lymph nodes were included as variables in our multivariate logistic regression analysis.

Lymph node regional sorting method

Specimens collected from gastrectomy were flushed to remove the blood and afterward dried using sterile towels. According to the original anatomical position in the body, the specimens were flattened, expanded, measured, and recorded. Lymph nodes were further sorted using the following procedure: The tissue was sequentially cut according to the dissected lymph nodes, and the staging, location, and definition of the peritoneal lymph nodes (lymph nodes on the small curved side and their surrounding soft tissues, lymph nodes on the peritoneal stem and its branch root, and lymph nodes on the large curved side and the surrounding soft tissue) were recorded and placed in the corresponding specimen bags. Afterward, the gastric wall along the opposite side (large or small curved side) was dissected, the tissue of the gastric mucosa was fully exposed, and indistinguishable tumor sites were marked with silk threads to enable the pathologist to locate the lesion. Next, the gastric tissue was unfolded, measured, and photographed. Finally, the excised stomach, peritoneal fat blood vessels, lymphoid tissue, and large omentum were fixed with 10% formaldehyde solution and sent to the Department of Pathology for further examination (Figure 1).

Statistical analysis

Statistical analysis was performed using the IBM SPSS statistical software (Version 26.0; IBM Corp., New York, United States). Categorical variables are expressed as frequencies and percentages. The chi-square test was used for intergroup comparisons ($n < 40$ cases with Fisher's exact probability method). The continuous variables that conformed to the normal distribution measured in this study were expressed as mean ± SD. Independent sample *t*-tests were used for intergroup comparisons. Continuous variables that did not conform to a normal distribution were expressed as median (interquartile range), and the Mann-Whitney *U* test was used for inter-group comparisons. The MLNR in each group were expressed as percentages. Risk factors for lymph node metastasis in the second dissection station were identified using binary and multivariate logistic regression analyses. Statistical significance was set at $P < 0.05$. Statistical review of the study was performed by a biomedical statistician from Tianjin Medical University.

Table 1 Baseline data of gastric cancer cases in the regional sorting group and non-sorting group

	Regional sorting group (*n* = 324)	Non-sorting group (*n* = 337)	χ^2	*P* value
Surgery			1.727	0.422
Proximal gastrectomy	19	27		
Distal gastrectomy	177	189		
Total gastrectomy	128	121		
Tumor location			2.744	0.254
U	46	38		
M	92	85		
L	186	214		
Immersion depth			2.071	0.558
T1	69	60		
T2	42	38		
T3	19	21		
T4	194	218		
Differentiation degree			2.891	0.089
DCA	181	166		
UCA	143	171		

U: Upper third; M: Middle third; L: Lower third; DCA: Differentiated carcinoma; UCA: Undifferentiated carcinoma.

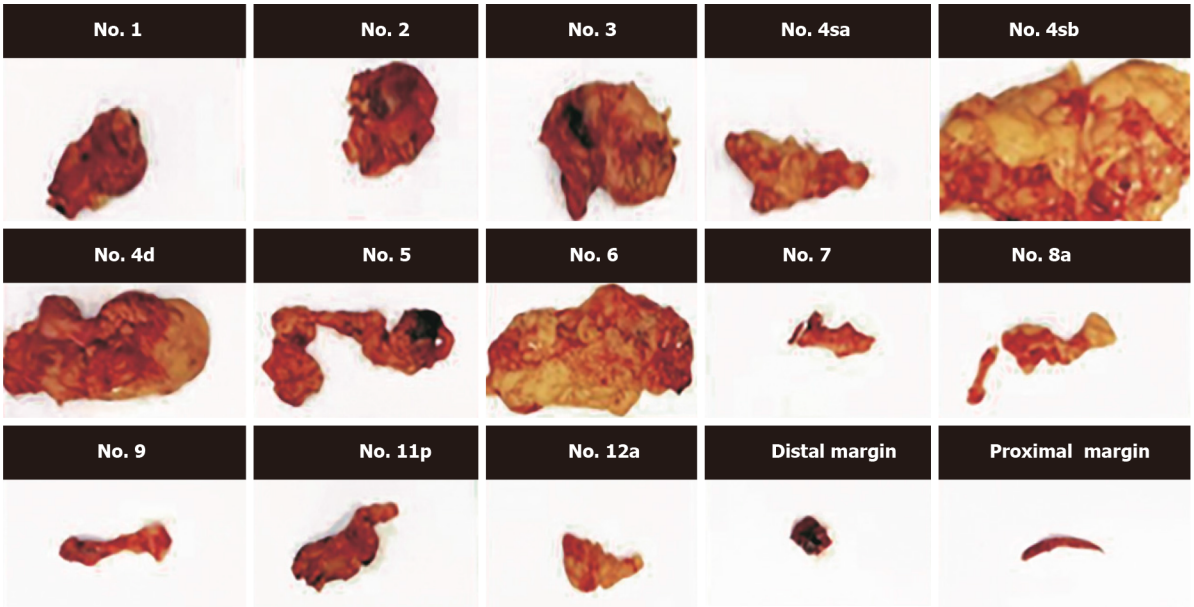

DOI: 10.4251/wjgo.v14.i12.2393

Figure 1 Regional sorted lymph nodes of gastric cancer.

RESULTS

Baseline characteristics of patients with GC

The mean patient age was 63.3 ± 10.2 (31-92), of which 457 (69.14%) were male and 204 (30.86%) were female. Three hundred and twenty-four patients (49.02%) were included in the regional sorting group and 337 (50.98%) were included in the non-sorting group. The surgical method (P = 0.422), tumor site (P = 0.254), immersion depth (P = 0.558), and degree of differentiation (P = 0.089) were not significantly different between the regional sorting and non-sorting groups (Table 1).

Comparison of the number of retrieved lymph nodes and lymph node metastasis ratios between the regional sorting and non-sorting groups

A total of 18977 lymph nodes were detected in all patients, of which 11111 (58.55%) were detected in the regional sorting group and 7866 (41.45%) in the non-sorting group. A total of 4399 positive lymph nodes were identified, of which 2264 (51.47%) were in the regional sorting group and 2135 (48.53%) in the non-sorting group. The number of detected lymph nodes in the two groups was significantly different ($P < 0.001$); however, there were no significant differences in the number of detected positive lymph nodes between the groups ($P = 0.863$) (Table 2).

Analysis of the lymph node metastasis ratios

Among the 324 patients in the regional sorting group, the highest lymph node metastasis ratio was found in group 3 (34.45%), followed by group 6 (22.46%). The lowest ratio was found in group 11p (13.81%) (Figure 2). Among the 46 patients with GC, region U showed the highest lymph node metastasis ratio in group 3 (31.48%). The ratios were low in groups 4 (7.56%), 5 (8.89%), and 6 (7.14%) (Figure 3A). Among the 92 patients with GC, region M had the highest lymph node metastasis in group 3 (41.44%) and the lowest ratio in group 11p (15.56%) (Figure 3B). Among the 186 patients, the highest lymph node metastasis ratio in region L was 30.50% in group 3, followed by 25.36% in group 6 and 9.68% in group 2 (Figure 3C).

Logistic regression of the lymph node metastasis

A total of 212 patients with GC in the lymph node regional sorting group had lymph node metastasis, including 89 cases (41.98%) at the first dissection station and 123 cases (58.02%) at the second dissection station. Binary and multivariate logistic regression results showed that the number of positive lymph nodes ($P < 0.001$) was an independent risk factor for lymph node metastases at the second dissection station (Tables 3 and 4).

DISCUSSION

Anatomy-based GC lymph node staging cannot ensure objectivity in clinical practice[8]. Therefore, the tumor-node-metastasis staging detailed in the 5th edition published by the Union for International Cancer Control (UICC)/American Joint Committee on Cancer is no longer based on anatomy, but on the number of metastatic lymph nodes[9]. Although the methods for lymph node staging were adjusted through multiple versions of the UICC publication, the standard method based on the number of metastatic lymph nodes did not change. Furthermore, the 14th edition, published by the Japanese Gastric Cancer Association abandoned the method of determining lymph node stages based on the location of the primary lesions and lymphatic metastasis[10]. Thus, the number of lymph nodes, one of the key factors in lymph node staging, has become the focus of current research.

A previous study showed that the number of lymph nodes detected is closely related to the pathological staging and prognosis of GC[11]. Currently, it is believed that the number of lymph nodes should be > 16. With improvements in lymph node detection methods and technology, the total number of lymph nodes detected is gradually increasing. Therefore, 16 lymph nodes are now considered the minimum requirement for staging and prognosis, and their use alone cannot guarantee an accurate prognosis of patients with GC[12,13]. One study revealed that the greater the number of lymph nodes detected, the greater the credibility of lymph node staging, which in turn leads to an accurate assessment of patient prognosis and the development of appropriate follow-up treatments[14]. In the current study, more than 16 lymph nodes (median, 32.5) were detected in the regional sorting group. Therefore, we considered that the number of lymph nodes obtained from the lymph node region was sufficient for lymph node staging.

The number of detected lymph nodes can be affected by many factors, such as surgery[15,16], lymph node sorting, and detection techniques[17]. Among these, postoperative lymph node sorting methods have not been fully studied. Presently, scholars generally believe that regional lymph node sorting after surgery can increase the number of lymph nodes detected[5,18]; however, the effect of regional sorting on the detection of positive lymph nodes remains debatable. Jiang *et al*[19] showed that lymph node sorting can increase the number of positive lymph nodes detected after surgery in patients with GC. However, in a prospective study, Wang *et al*[20] proved that regional lymph node sorting did not increase the number of positive lymph nodes. In our study, significantly more lymph nodes were detected in the regional sorting group than in the non-sorting group ($P < 0.001$). The increased number of detected lymph nodes was due to regional sorting; a pathologist who may not be familiar with gastric circumferential anatomy can easily identify the lymph nodes, rather than striving to identify "at least 16" lymph nodes[10]. The regional sorting method used in our study largely reduced the number of undetected lymph nodes. Similar to the findings of other studies, the number of positive lymph nodes in our study did not increase with the number of lymph nodes detected in the regional sorting group. This may be due to the fact that the diameter of positive lymph nodes is usually larger than that of negative

Table 2 Comparison of the number of lymph nodes and the number of positive lymph nodes between the regional sorting group and non-sorting group

	Pieces, median (interquartile range)		Z	*P* value
	Regional sorting group	Non-sorting group		
The number of lymph nodes detected	32.5 (24.0, 42.0)	21.0 (17.0, 28.0)	-10.775	< 0.001
Number of positive lymph nodes	2.0 (0.0, 9.0)	3.0 (0.0, 9.0)	-0.172	0.863

Table 3 Binary logistic regression analysis of risk factors of lymph node metastasis in the second dissection station (*n* = 123)

	B	SE	Wald	df	*P* value	OR	95%CI	
							Upper	Lower
Tumor location								
U			1.067	2	0.587			
M	-0.087	0.460	0.036	1	0.850	0.917	0.372	2.258
L	-0.346	0.421	0.675	1	0.411	0.708	0.310	1.615
Immersion depth								
T1			5.468	3	0.141			
T2	1.872	0.829	5.092	1	0.024	6.500	1.279	33.034
T3	1.504	0.850	3.132	1	0.077	4.500	0.851	23.801
T4	1.464	0.865	4.567	1	0.033	4.324	1.129	16.557
Differentiation degree								
DCA/UCA	0.415	0.282	2.201	1	0.138	1.515	0.875	2.621
The number of positive lymph nodes (pieces)								
≤ 6/> 6	1.707	0.305	31.284	1	< 0.001	5.514	3.031	10.029

OR: Odds ratio; CI: Confidence interval; U: Upper third; M: Middle third; L: Lower third; DCA: Differentiated carcinoma; UCA: Undifferentiated carcinoma; df: Degree of freedom.

lymph nodes. Noda *et al*[21] showed that positive lymph nodes have an average diameter of approximately 7.80 mm, whereas negative lymph nodes have an average diameter of only 5.30 mm; therefore, positive lymph nodes are more likely to be detected by pathologists. It is reasonable to assume that, due to the smaller diameter, some negative lymph nodes may not have been detected in the past, but this did not affect lymph node staging. Regional sorting of lymph nodes increases the number of detected lymph nodes and the credibility of lymph node staging; therefore, it has important clinical benefits.

Clarifying the role of lymph node metastasis in GC can provide basic guidance for the surgical dissection of lymph nodes. In this study, we found that the most likely regions of lymph node metastases were near the lesser curvature in group 3 and near the gastric sinus in group 6, which may indicate that these sites are potential locations for GC progression. Furthermore, in studying the lymph node metastasis patterns of gastric tumors located at different sites, we found that the most easily metastasized region was group 3, regardless of the primary lesion site (U, M, and L stomach), which is consistent with the location near the lesser curvature and with the main direction of lymphatic reflux in the stomach. In region U, lymph node metastasis was mainly located in groups 1-3 and 7-12a, whereas in groups 4-6, significantly fewer positive lymph nodes were observed. In region M, the lymph nodes in groups 1-12a were susceptible to aggression. In region L, lymph node metastasis was mainly located in groups 3-6, whereas groups 2 and 12a had less aggressive metastases than those in the other groups. The results suggest that although the direction of lymphatic drainage of stomach cancer varies in different regions, lymph nodes that are closer to the tumor's primary lesions or in the main direction of lymphatic reflux are more likely to metastasize. Therefore, for gastric tumors located at different sites, lymph nodes detected throughout the stomach can be used as a guide for further treatment.

The current lymph node staging system is based on the number of positive lymph nodes and cannot provide additional information for surgical guidance. Therefore, the standard lymph node metastasis location system for GC as a lymph node staging method has been studied and improved[22]. Duchon *et*

Table 4 Multivariable logistic regression analysis of risk factors of lymph node metastasis in the second dissection station (*n* = 123)

	B	SE	Wald	df	*P* value	OR	95%CI	
							Upper	Lower
Tumor location								
U			0.601	2	0.741			
M	-0.299	0.511	0.344	1	0.558	0.741	0.273	2.017
L	-0.358	0.463	0.599	1	0.439	0.699	0.282	1.732
Immersion depth								
T1			4.710	3	0.194			
T2	1.817	0.875	4.316	1	0.038	6.153	1.108	34.160
T3	0.956	0.922	1.075		0.300	2.601	0.427	15.852
T4	0.884	0.735	1.445	1	0.229	2.420	0.573	10.223
Differentiation degree								
DCA/UCA	0.124	0.323	0.147	1	0.701	1.132	0.601	2.130
The number of positive lymph nodes (pieces)								
≤ 6/> 6	1.718	0.322	28.541	1	< 0.001	5.576	2.968	10.473
Constant	-1197	0.829	2086	1	0.149	0.302		

The Hosmer-Lemshaw test results showed good fit for the multifactorial logistic regression (P = 0.611).
OR: Odds ratio; CI: Confidence interval; U: Upper third; M: Middle third; L: Lower third; DCA: Differentiated carcinoma; UCA: Undifferentiated carcinoma; df: Degree of freedom.

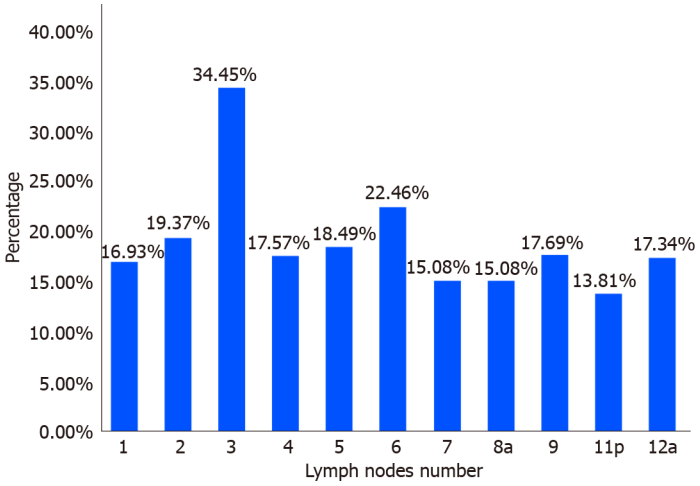

DOI: 10.4251/wjgo.v14.i12.2393 **Copyright** ©The Author(s) 2022.

Figure 2 The lymph node metastasis ratios of lymph nodes of patients with gastric cancer.

al[23] showed that lymph node staging based on lymph node metastasis location is correlated with patient prognosis and that there is no difference between these two lymph node staging methods in evaluating patient prognosis. Son *et al*[7] studied 4043 patients with GC and found that when No. 2-7 and No. 14 lymph node metastasis occurred in patients with GC, their prognosis was worse than that of patients with only No. 1-6 lymph node metastasis. The authors suggested that inclusion of the examination of lymph node metastasis in the current lymph node staging system could more accurately predict patient prognosis. Other researchers believe that lymph node metastasis is an independent survival predictor and that lymph node metastasis sites should be considered in future staging systems [24]. However, these studies did not analyze the relationship between the location of lymph node metastasis and current lymph node staging.

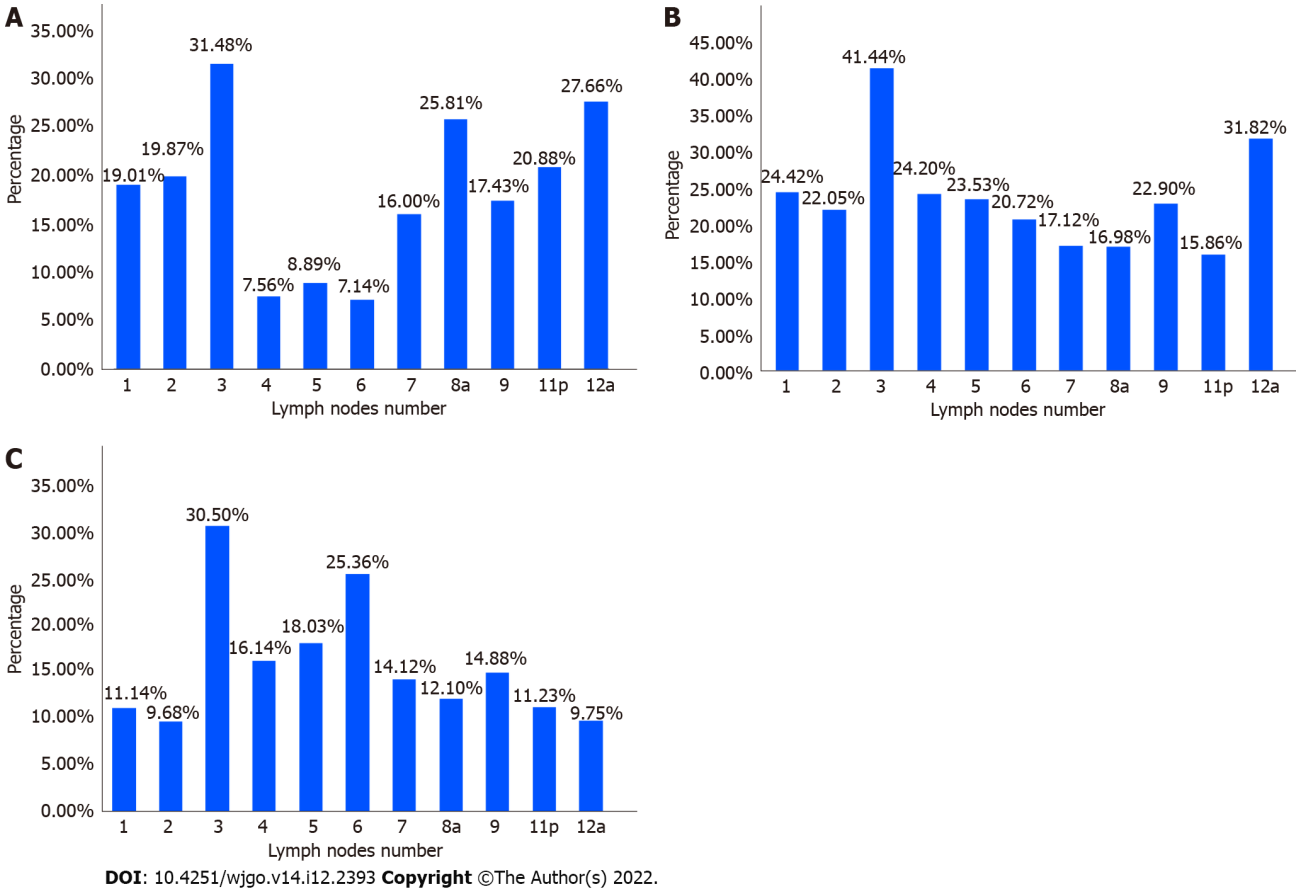

DOI: 10.4251/wjgo.v14.i12.2393

Figure 3 The lymph node metastasis ratios in region of patients with gastric cancer. A: Upper third of stomach; B: Middle third of stomach; C: Lower third of stomach.

Some studies have shown that the prognosis of patients with 2 stage GC in the current lymph node staging system is similar to that of patients with GC who were in the first dissection station of lymph node metastasis[8]. Therefore, we analyzed the relationship between the lymph node metastasis region system and the current lymph node staging system using a cutoff of six positive lymph nodes (Tables 3 and 4). Binary and multivariable logistic regression results showed that the number of positive lymph nodes was an independent risk factor for lymph node metastasis in the second dissection station, indicating that lymph node metastases in the second dissection station increased with the progression of lymph node staging. Inevitably, some limitations were present in our study. Firstly, the data collection in this study originated from a single surgical center over 8 years, so data bias was inevitable. In addition, the sorting of lymph nodes in surgical specimens of GC was completed by multiple people, and therefore measurement deviations were inevitable. Secondly, the Lauren classification was not included in the pathology report of Tianjin Medical University general hospital, which may have affected the richness of the analysis of this study.

CONCLUSION

Overall, with an increase in lymph node metastasis, lymph node metastasis occurred from the first to the second dissection station. Therefore, identifying the region of lymph node metastasis may increase the accuracy of lymph node staging. The inclusion of regional lymph node sorting into a lymph node staging system should be further studied in future research.

ARTICLE HIGHLIGHTS

Research background

In recent years, the morbidity and mortality of gastric cancer (GC) remain high worldwide. Its incidence ranks fifth among malignant tumors, and its mortality ranks fourth. The progression of GC involves direct tumor invasion, lymph node metastasis, and organ and peritoneal metastasis. Lymph node

metastasis is one of the main ways of GC metastasis. Even in patients with early GC, 3% to 20% of patients with early GC can develop lymph node metastasis. Therefore, surgical dissection of lymph nodes is the key to the treatment of GC, and obtaining accurate lymph node staging is also a non-negligible part of the treatment of GC.

Research motivation

Accurate lymph node staging can evaluate the therapeutic effect of surgery, and can also provide a reliable basis for patients to choose subsequent treatment options. Since the current lymph node staging takes the number of metastatic lymph nodes as the staging standard, the number of detected lymph nodes in postoperative specimens of GC is particularly important.

Research objectives

To explore the clinical application value of lymph node region sorting after radical gastrectomy for GC, summarize the rules of lymph node metastasis in different parts of GC around the stomach, and further explore the relationship between the number of positive lymph nodes and the lymph node metastasis area.

Research methods

The clinicopathological data of patients who underwent radical gastrectomy for GC in the Gastrointestinal and Anorectal Surgery Department of Tianjin Medical University General Hospital from January 2012 to June 2020 were collected, and the number of lymph nodes, positive lymph nodes in the lymph node regional sorting group and the unsorted group were analyzed. Differences in the number of lymph nodes; GC patients who had undergone regional sorting were grouped according to tumor sites, and the lymph node metastasis rates in each group were statistically analyzed, and the relationship between the number of positive lymph nodes and the lymph node metastasis area was analyzed by logistic regression.

Research results

The number of lymph nodes sent for examination in the regional sorting group was more than that in the unsorted group ($P < 0.001$); there was no significant difference in the number of positive lymph nodes between the two groups ($P = 0.863$). The lymph nodes with higher metastasis rate in upper cancer were No. 3 group (31.48%), while No. 4 group (7.56%), No. 5 group (8.89%), and No. 6 group (7.14%). The lymph node metastasis rate is low; in the middle cancer, the lymph node metastasis rate is higher in each group; in the lower cancer, the lymph nodes with higher metastasis rate are No. 3 group (30.50%), No. 2 group (9.68%), No. 12a (9.75%) had low lymph node metastasis rate. The multivariate logistic regression results showed that the number of positive lymph nodes was positively correlated with the risk of lymph node metastasis in the second station dissection area.

Research conclusions

Regional lymph node sorting after radical gastrectomy for GC can increase the number of detected lymph nodes and make lymph node staging more accurate and credible, which is worthy of clinical implementation. The lymph node metastasis rates of different groups of GC lymph nodes in different parts of GC are different. It is of great significance to understand the rules of lymph node metastasis to guide the lymph node dissection during operation. With the increase of the number of positive lymph nodes, the site of lymph node metastasis spreads from the first-stage dissection area to the second-stage dissection area. Identifying the location of lymph node metastasis can make lymph node staging more accurate.

Research perspectives

The current lymph node staging has a certain degree of consistency with the location of lymph node metastasis. With the increase in the number of lymph node metastases, the location of lymph node metastasis spreads from the first-stage dissection area to the second-stage dissection area. Identifying the lymph node metastasis location can make lymph node staging more accurate. Optimization of lymph node staging by including lymph node metastases requires further study.

FOOTNOTES

Author contributions: Li C and Tian XJ was the guarantor and designed the study; Qu GT, Teng YX, Li ZF, Nie XY and Liu DJ participated in the acquisition, analysis, and interpretation of the data, and drafted the initial manuscript; Li WD and Liu T revised the article critically for important intellectual content.

Supported by the Fundamental Scientific Research Project of Tianjin Universities of China, No. 2017KJ191.

Institutional review board statement: The study complied with the Declaration of Helsinki and was approved by the

ethics committee of Tianjin Medical University General Hospital (Ethics approval number: IRB2022-WZ-167).

Informed consent statement: The need for informed consent was waived by the ethical committee of Tianjin Medical University General Hospital.

Conflict-of-interest statement: All the authors report no relevant conflicts of interest for this article.

Data sharing statement: The data from this study are available from the corresponding author upon reasonable request.

STROBE statement: The authors have read the STROBE statement-checklist of items, and the manuscript was prepared and revised according to the STROBE statement-checklist of items.

Country/Territory of origin: China

ORCID number: Chuan Li 0000-0002-9535-9563; Yu-Xin Teng 0000-0002-9610-4423; Zhu-Feng Li 0000-0002-7070-907X; Tong Liu 0000-0002-9039-2364; Wei-Dong Li 0000-0003-0411-5924.

S-Editor: Wang JJ
L-Editor: A
P-Editor: Wang JJ

REFERENCES

1 **Thrift AP**, El-Serag HB. Burden of Gastric Cancer. *Clin Gastroenterol Hepatol* 2020; **18**: 534-542 [PMID: 31362118 DOI: 10.1016/j.cgh.2019.07.045]
2 **Lee JH**, Choi IJ, Han HS, Kim YW, Ryu KW, Yoon HM, Eom BW, Kim CG, Lee JY, Cho SJ, Kim YI, Nam BH, Kook MC. Risk of lymph node metastasis in differentiated type mucosal early gastric cancer mixed with minor undifferentiated type histology. *Ann Surg Oncol* 2015; **22**: 1813-1819 [PMID: 25344305 DOI: 10.1245/s10434-014-4167-7]
3 **Ren G**, Cai R, Zhang WJ, Ou JM, Jin YN, Li WH. Prediction of risk factors for lymph node metastasis in early gastric cancer. *World J Gastroenterol* 2013; **19**: 3096-3107 [PMID: 23716990 DOI: 10.3748/wjg.v19.i20.3096]
4 **Bunt AM**, Hermans J, van de Velde CJ, Sasako M, Hoefsloot FA, Fleuren G, Bruijn JA. Lymph node retrieval in a randomized trial on western-type versus Japanese-type surgery in gastric cancer. *J Clin Oncol* 1996; **14**: 2289-2294 [PMID: 8708719 DOI: 10.1200/jco.1996.14.8.2289]
5 **Cao Y**, Xiong L, Deng S, Shen L, Li J, Wu K, Wang J, Tao K, Wang G, Cai K. The effect of perigastric lipolymphatic tissue grouping by surgeon on the number of pathologic sampled lymph nodes after radical gastrectomy. *Medicine (Baltimore)* 2018; **97**: e11411 [PMID: 29979440 DOI: 10.1097/MD.0000000000011411]
6 **Lu J**, Zheng ZF, Xie JW, Wang JB, Lin JX, Chen QY, Cao LL, Lin M, Tu RH, Huang CM, Zheng CH, Li P. Is the 8th Edition of the AJCC TNM Staging System Sufficiently Reasonable for All Patients with Noncardia Gastric Cancer? *Ann Surg Oncol* 2018; **25**: 2002-2011 [PMID: 29725896 DOI: 10.1245/s10434-018-6447-0]
7 **Son T**, Hyung WJ, Kim JW, Kim HI, An JY, Cheong JH, Choi SH, Noh SH. Anatomic extent of metastatic lymph nodes: still important for gastric cancer prognosis. *Ann Surg Oncol* 2014; **21**: 899-907 [PMID: 24276641 DOI: 10.1245/s10434-013-3403-x]
8 **Gong Y**, Pan S, Wang X, Zhu G, Xu H, Zhu Z. A novel lymph node staging system for gastric cancer including modified Union for cancer Control/American Joint Committee on cancer and Japanese Gastric Cancer Association criteria. *Eur J Surg Oncol* 2020; **46**: e27-e32 [PMID: 32631708 DOI: 10.1016/j.ejso.2020.06.005]
9 **Sobin LH**, Fleming ID. TNM Classification of Malignant Tumors, fifth edition (1997). Union Internationale Contre le Cancer and the American Joint Committee on Cancer. *Cancer* 1997; **80**: 1803-1804 [PMID: 9351551 DOI: 10.1002/(sici)1097-0142(19971101)80:9<1803::aid-cncr16>3.0.co;2-9]
10 **Japanese Gastric Cancer Association**. Japanese classification of gastric carcinoma: 3rd English edition. *Gastric Cancer* 2011; **14**: 101-112 [PMID: 21573743 DOI: 10.1007/s10120-011-0041-5]
11 **Chen HN**, Chen XZ, Zhang WH, Chen XL, Yang K, Liu JP, Zhang B, Chen ZX, Chen JP, Zhou ZG, Hu JK. Necessity of harvesting at least 25 lymph nodes in patients with stage N2-N3 resectable gastric cancer: a 10-year, single-institution cohort study. *Medicine (Baltimore)* 2015; **94**: e620 [PMID: 25761190 DOI: 10.1097/MD.0000000000000620]
12 **Bouvier AM**, Haas O, Piard F, Roignot P, Bonithon-Kopp C, Faivre J. How many nodes must be examined to accurately stage gastric carcinomas? *Cancer* 2002; **94**: 2862-2866 [PMID: 12115373 DOI: 10.1002/cncr.10550]
13 **Kim YI**. Does the retrieval of at least 15 lymph nodes confer an improved survival in patients with advanced gastric cancer? *J Gastric Cancer* 2014; **14**: 111-116 [PMID: 25061538 DOI: 10.5230/jgc.2014.14.2.111]
14 **Deng J**, Zhang R, Pan Y, Wang B, Wu L, Jiao X, Bao T, Hao X, Liang H. Comparison of the staging of regional lymph

nodes using the sixth and seventh editions of the tumor-node-metastasis (TNM) classification system for the evaluation of overall survival in gastric cancer patients: findings of a case-control analysis involving a single institution in China. *Surgery* 2014; **156**: 64-74 [PMID: 24929759 DOI: 10.1016/j.surg.2014.03.020]

15 **Ichikura T**, Ogawa T, Chochi K, Kawabata T, Sugasawa H, Mochizuki H. Minimum number of lymph nodes that should be examined for the International Union Against Cancer/American Joint Committee on Cancer TNM classification of gastric carcinoma. *World J Surg* 2003; **27**: 330-333 [PMID: 12607061 DOI: 10.1007/s00268-002-6730-9]

16 **Lee WJ**, Hong RL, Lai IR, Chen CN, Lee PH, Chung KC. Reappraisal of the new UICC staging system for gastric cancer: problem in lymph node stage. *Hepatogastroenterology* 2002; **49**: 860-864 [PMID: 12064008]

17 **Cai YQ**, Liang YX, Yu SY, Tu RS. [Clinical value of carbon nanoparticles tracer in gastric cancer surgery to increase the number of lymph nodes retrieval]. *Zhonghua Wei Chang Wai Ke Za Zhi* 2020; **23**: 984-989 [PMID: 33053994 DOI: 10.3760/cma.j.cn.441530-20191031-00469]

18 **Afaneh C**, Levy A, Selby L, Ku G, Tang L, Yoon SS, Coit D, Strong VE. Ex Vivo Lymphadenectomy During Gastrectomy for Adenocarcinoma Optimizes Lymph Node Yield. *J Gastrointest Surg* 2016; **20**: 165-71; discussion 171 [PMID: 26403717 DOI: 10.1007/s11605-015-2948-3]

19 **Jiang L**, Yao Z, Zhang Y, Hu J, Zhao D, Zhai H, Wang X, Zhang Z, Wang D. Comparison of lymph node number and prognosis in gastric cancer patients with perigastric lymph nodes retrieved by surgeons and pathologists. *Chin J Cancer Res* 2016; **28**: 511-518 [PMID: 27877010 DOI: 10.21147/j.issn.1000-9604.2016.05.06]

20 **Wang P**, Zhang K, Xi H, Liang W, Xie T, Gao Y, Wei B, Chen L. Lymph Node Yield Following Packet Submission After Isolation By Surgeon During Gastrectomy. *Cancer Manag Res* 2019; **11**: 9871-9881 [PMID: 31819624 DOI: 10.2147/CMAR.S211218]

21 **Noda N**, Sasako M, Yamaguchi N, Nakanishi Y. Ignoring small lymph nodes can be a major cause of staging error in gastric cancer. *Br J Surg* 1998; **85**: 831-834 [PMID: 9667718 DOI: 10.1046/j.1365-2168.1998.00691.x]

22 **Japanese Gastric Cancer Association**. Japanese gastric cancer treatment guidelines 2018 (5th edition). *Gastric Cancer* 2021; **24**: 1-21 [PMID: 32060757 DOI: 10.1007/s10120-020-01042-y]

23 **Duchon R**, Bernadic M Jr, Pindak D. Impact of the anatomical location and the number of metastatic lymph nodes on gastric cancer patient´s survival. *Bratisl Lek Listy* 2020; **121**: 253-258 [PMID: 32356438 DOI: 10.4149/BLL_2020_038]

24 **Anderegg MC**, Lagarde SM, Jagadesham VP, Gisbertz SS, Immanuel A, Meijer SL, Hulshof MC, Bergman JJ, van Laarhoven HW, Griffin SM, van Berge Henegouwen MI. Prognostic Significance of the Location of Lymph Node Metastases in Patients With Adenocarcinoma of the Distal Esophagus or Gastroesophageal Junction. *Ann Surg* 2016; **264**: 847-853 [PMID: 27429034 DOI: 10.1097/SLA.0000000000001767]

World Journal of Gastrointestinal Oncology

Submit a Manuscript: https://www.f6publishing.com

World J Gastrointest Oncol 2022 December 15; 14(12): 2404-2414

DOI: 10.4251/wjgo.v14.i12.2404

ISSN 1948-5204 (online)

CASE REPORT

Edema of limbs as the primary symptom of gastric signet-ring cell carcinoma: A case report and literature review

Bei Wang, Jing Chen, Ying Wang, Ling-Li Dong, Gui-Fen Shen

Specialty type: Oncology

Provenance and peer review: Unsolicited article; Externally peer reviewed.

Peer-review model: Single blind

Peer-review report's scientific quality classification

Grade A (Excellent): 0
Grade B (Very good): 0
Grade C (Good): C, C, C
Grade D (Fair): 0
Grade E (Poor): 0

P-Reviewer: Brigode WM, United States; Chang A, Thailand

Received: August 26, 2022
Peer-review started: August 26, 2022
First decision: September 8, 2022
Revised: September 17, 2022
Accepted: November 28, 2022
Article in press: November 28, 2022
Published online: December 15, 2022

Bei Wang, Ling-Li Dong, Gui-Fen Shen, Department of Rheumatology and Immunology, Tongji Hospital, Tongji Medical College, Huazhong University of Science and Technology, Wuhan 430030, Hubei Province, China

Jing Chen, Division of Cardiology, Department of Internal Medicine and Gene Therapy Center, Tongji Hospital, Tongji Medical College, Huazhong University of Science and Technology, Wuhan 430030, Hubei Province, China

Ying Wang, Department of Pathology, Tongji Hospital, Tongji Medical College, Huazhong University of Science and Technology, Wuhan 430030, Hubei Province, China

Corresponding author: Gui-Fen Shen, MD, PhD, Doctor, Department of Rheumatology and Immunology, Tongji Hospital, Tongji Medical College, Huazhong University of Science and Technology, Jiefang Avenue 1095, Wuhan 430030, Hubei Province, China.
guifenshen@126.com

Abstract

BACKGROUND

Metastatic skin cancers are relatively rare dermatological malignancies. They usually present as nodules, erythematous lesions, scar-like lesions or other lesion types. Signet-ring cell carcinoma (SRCC) is an uncommon histological type of gastric cancer that usually behaves aggressively and has a poor prognosis. Skin metastasis may be the first sign of clinically silent visceral cancer or recurrence of an internal malignancy.

CASE SUMMARY

Herein we report on the case of a 55-year-old man with edema of a lower extremity as the primary symptom which progressed from local to generalized pitting edema in the year following skin involvement. Pathological evidence from gastroscopic specimens and subcutaneous tissue biopsy showed typical signet-ring cells and gland-like structures. Consistently, immunohistochemical analysis revealed positive pan-cytokeratin expression in tumor cells. A diagnosis of gastric SRCC with skin metastasis was established. Moreover, lymphoscintigraphy showed an obvious accumulation of radiotracer on the anterior and posterior sides of the right leg which indicated lymphedema. We reviewed the relevant literature on subcutaneous metastases of gastric SRCC.

CONCLUSION

This rare case emphasizes the importance of physical examination as it may help

elucidate the etiology of edema.

Key Words: Gastric cancer; Signet-ring cell carcinoma; Skin metastasis; Lymphedema; Prognosis; Case report

Core Tip: Metastatic skin cancers are relatively rare dermatological malignancies. They usually present as nodules, erythematous lesions, scar-like lesions or other lesion types. We report on a case of skin metastases from gastric signet-ring cell carcinoma in which lymphedema of the limbs presented as an initial symptom. This rare case emphasizes the importance of physical examination as it may help elucidate the etiology of edema.

Citation: Wang B, Chen J, Wang Y, Dong LL, Shen GF. Edema of limbs as the primary symptom of gastric signet-ring cell carcinoma: A case report and literature review. *World J Gastrointest Oncol* 2022; 14(12): 2404-2414
URL: https://www.wjgnet.com/1948-5204/full/v14/i12/2404.htm
DOI: https://dx.doi.org/10.4251/wjgo.v14.i12.2404

INTRODUCTION

Metastatic skin cancers (MSCs) are relatively rare dermatological malignancies. They constitute 2% of all skin tumors and the reported incidence rates range from 0.7% to 9.0%[1]. MSCs originate most commonly from breast, lung and gastrointestinal tissues and are recognized as having a poor prognosis [1,2]. Furthermore, cutaneous metastases from gastric signet-ring cell carcinoma (SRCC) are uncommon [3]. The clinical presentation of cutaneous metastases from gastric adenocarcinoma is usually single or multiple nodules or erythematous lesions; only 6.4 % to 7.8 % of these cutaneous metastases are the first clinical manifestation[4,5]. Moreover, to the best of our knowledge, there is no report describing edema of the limbs as the primary symptom of MSCs originating from signet-ring cell gastric carcinoma.

The causes of edema vary. Most causes of edema are due to increased capillary filtration overwhelming the normal lymphatic system[6]. Under some conditions, lymphedema occurs when lymph transport capacity is impaired. Lymphedema can be classified into primary and secondary categories[7]. Both primary and secondary forms of lymphedema are often chronic and insidious in nature. Infections such as lymphatic filariasis are a frequent cause of secondary lymphedema in developing countries, whereas in developed countries, a common cause of secondary lymphedema is cancer treatment. Of note, the metastasis or, rarely, direct invasion of active tumor into the lymphatic network can also produce a severe form of lymphedema[8].

In this study, we present a case of atypical gastric adenocarcinoma with signet-ring cell morphology which presented with cutaneous lymphedema as the primary symptom.

CASE PRESENTATION

Chief complaints

A 55-year-old Chinese male first presented with cutaneous edema of the right lower limb, which developed as systemic edema of all limbs over the course of a year (Figure 1).

History of present illness

In April 2019, the patient developed edema of the right lower limb with an unknown cause. The edema began to spread from the end of the lower extremity to the groin and trunk area. At a local hospital, he was diagnosed with slight renal insufficiency (estimated glomerular filtration rate: 59 mL/min/1.73 m^2). Additionally, cardiac insufficiency and hepatic insufficiency was excluded and the patient underwent magnetic resonance imaging of the lower extremity. The results showed obvious swelling of subcutaneous soft tissue in the right thigh, slight edema in the subcutaneous soft tissue of the left thigh and edema of the long and short head of the biceps femoris. One year after skin involvement, the patient presented with newly diagnosed poly-serous effusions (thoracic cavity, abdominal cavity and pericardium).

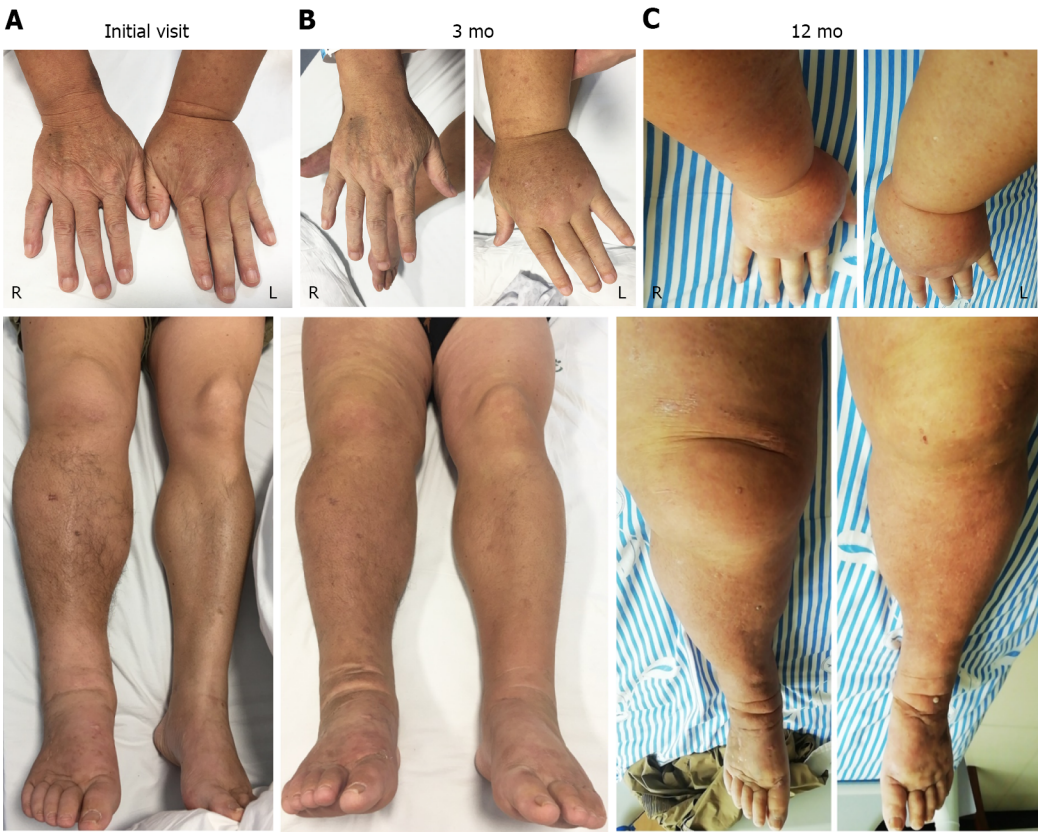

DOI: 10.4251/wjgo.v14.i12.2404 **Copyright** ©The Author(s) 2022.

Figure 1 The 55-year-old male patient with systemic edema. A: The images of fingers and legs of this patient at the initial visit; B: The images of fingers and legs of this patient at 3-mo visit; C: The images of fingers and legs of this patient at 12-mo visit.

Personal and family history

The patient had no significant personal history and denied any health issues or genetic problems in his family. There was no obvious weight loss or significant family history.

Physical examination

On admission, the patient's temperature was 36.0 ℃, heart rate was 91 beats/min, respiratory rate was 20 breaths/min and blood pressure was 143/92 mmHg. No abnormality was found in the heart and the lungs were clear to bilateral auscultation without any wheezes, rales or rhonchi. Furthermore, there was no tenderness or rebound pain in the abdomen. Additionally, there is no sign of associated gastrointestinal symptoms such as nausea, vomiting, hematemesis or any change in bowel habits. However, he had obvious pitting edema in the right lower limb but not in the left limb. When pressure was applied to the right lower limb, an indentation remained in the soft tissue after the pressure was removed.

Laboratory examinations

The main characteristics of laboratory examinations during the initial 3-mo and 12-mo visits are listed in Table 1. Specifically, the results showed that the patient's carbohydrate antigen 724 Levels were slightly elevated during the initial (16.41 U/mL, reference value range < 6.9 U/mL), 3-mo (15.51 U/mL) and 12-mo (15.67 U/mL) visit, while serum carcinoembryonic antigen (CEA) and carbohydrate antigen 19-9 Levels were within the normal range. The levels of urea nitrogen (8.97 mmol/L, 12.54 mmol/L, and 12.83 mmol/L for the initial, 3-mo and 12-mo visits, respectively) were slightly elevated. Similarly, creatinine levels (126 μmol/L, 130 μmol/L, and 152 μmol/L for the initial, 3-mo and 12-mo visits, respectively) were also slightly elevated. Kidney function was evaluated as chronic kidney disease (CKD) G3a by calculating the estimated glomerular filtration rate[9]. However, the results were normal for the patient's kidney, ureter, and bladder on color Doppler ultrasound. Routine urine tests indicated no proteinuria or hematuria. Thyroid function test results were normal.

Imaging examinations

No obvious abnormality was found on computed χ-ray tomography of the chest and abdomen. The 18F-fluorodeoxyglucose (FDG) positron emission tomography was performed. No pathological FDG uptake was detected in the liver, spleen, kidneys, gastrointestinal system, or in either the abdominal or pelvic

Table 1 Characteristics of laboratory examinations

Parameter	Initial visit	3 mo	12 mo	Reference value range
Full blood count				
White cell count as × 10^9/L	6.4	7.55	3.58	(3.5-9.5)
Neutrophils as × 10^9/L	4.51	5.56	2.25	(1.8-6.3)
Lymphocytes as × 10^9/L	1.3	1.32	0.68	(1.1-3.2)
Monocytes as × 10^9/L	0.36	0.5	0.23	(0.1-0.6)
Platelets as × 10^9/L	218	223	208	(125-350)
Hemoglobin in g/L	144	136	157	(130-175)
Tumor markers				
Carbohydrate antigen 724 in U/mL	16.41	15.51	15.67	(< 6.9)
Carbohydrate antigen 199 in U/mL	15.88	16.84	4.43	(≤ 34)
Carcinoembryonic antigen in ng/mL)	2.81	2.86	0.78	(≤ 5)
Blood biochemical indicators				
Alanine aminotransferase in U/L	16	11	14	(≤ 41)
Aspartate aminotransferase in U/L	13	13	15	(≤ 41)
Globulin in g/L	28.9	25.5	19	(64-83)
Albumin in g/L	38.2	32.2	25	(35-52)
Creatine kinase in U/L	93	56	24	(≤ 190)
Lactic dehydrogenase in U/L	163	156	202	(135-225)
Urea nitrogen in mmol/L	8.97	12.54	12.83	(3.1-8.0)
Creatinine in μmol/L	126	130	152	(59-104)
Estimated glomerular filtration rate in mL/min/1.73 m^2	55	52.9	49.5	(> 90)
Random blood glucose in mmol/L	6.22	5.39	6.12	(< 11.1)
Serum potassium in mmol/L	4.2	3.88	3.89	(3.5-5.1)
Serum sodium in mmol/L	141.5	141	142	(136-145)
Cardiac troponin T in pg/mL	2.2	2.5	2.7	(≤ 34.2)
N terminal pro B type natriuretic peptide in pg/mL	53	45	59	(< 161)
Fibrinogen in g/L	4.31	5.03	5.88	(2-4)
D-Dimer in μg/mL FEU	1.36	1.05	7.19	(< 0.5)
Other indicators				
Antinuclear antibodies	1:100	1:100	Not available	(negative)
Immunoglobulin IgG in g/L	9.31	8.57	9.27	(7-16)
Complement C3 in g/L	1.46	1.32	1.39	(0.8-1.8)
Complement C4 in g/L	0.67	0.39	0.51	(0.1-0.4)
Erythrocyte sedimentation rate in mm/h	20	21	25	(0-15)
High sensitivity C-reactive protein in mg/L	5.52	6.43	6.83	(0-5)
Interleukin 6 in pg/mL	2.72	3.56	2.98	(0.1-2.9)
Tumor necrosis factor α in pg/mL	2.07	2.97	3.12	(0.1-23)
T lymphocyte (CD3 + CD19 -) as /μL	830	977	780	(955-2860)
B lymphocyte (CD3 + CD19 -), as /μL	62	84	52	(90-560)
Proteinuria	negative	negative	negative	(negative)
Antineutrophil cytoplasmic antibody	negative	negative	negative	(negative)

Procalcitonin	< 0.05	< 0.05	< 0.05	(< 0.05)

lymph node groups. Moreover, lymphoscintigraphy labeled with ^{99m}Tc-DX showed an obvious accumulation of radiotracer in the right leg on both the anterior and posterior sides after 3 and 6 h diffusion (Figure 2), indicating lymph angiodysplasia and lymphedema. Color Doppler ultrasound of the heart and blood vessels of both lower limbs showed no abnormality.

Pathological and gastrointestinal endoscopic examination

First, the biopsy of the skin on the lower limb revealed infiltration of the suspicious cells with a signet-ring appearance cells and gland-like structures (Figure 3A-C). Biopsy specimens of the lesions showed reactive epithelial changes [pan-cytokeratin (panCK) positive) (Figure 3C). Because the gastrointestinal tract is the most common source of SRCC, a gastrointestinal endoscopic examination (Figure 3D and E) was subsequently performed. The results showed multiple gastric ulcers without solid neoplasm (Figure 3D and E). However, biopsies of both the body and antrum gastric mucosa showed infiltrating signet ring cell type adenocarcinoma (Figure 3F and G), which were very strongly panCK positive (Figure 3H and I) and CEA positive. Additionally, histopathology showed a less differentiated signet cell ring carcinoma with approximately 20% ki-67 positivity. Taken together, gastrointestinal metastasis was confirmed as the source of the signet-ring cells in skin biopsies. Thus, a diagnosis of metastatic SRCC, most likely from the stomach, was made.

FINAL DIAGNOSIS

Gastric SRCC with skin metastases.

TREATMENT

Surgical intervention is not possible for advanced or metastatic gastric cancer. First-line systemic therapy regimens with 2 cytotoxic drugs are preferred for these patients[10]. The preferred regimens for first-line systemic therapy includes fluoropyrimidine (fluorouracil or capecitabine) combined with either oxaliplatin or cisplatin (category 2B)[10]. Given the renal insufficiency in this patient, oxaliplatin or cisplatin was not suitable[11]. Thus, from August 21 to September 2, 2019, the patient received a combination of chemotherapy with tegafur (a prodrug of 5-fluorouracil, 60 mg/PO/bid), and paclitaxel (second-line systemic therapy; 100 mg/iv/QW). Over the next 5 mo, he received another five cycles of chemotherapy.

OUTCOME AND FOLLOW-UP

At the 3-mo visit, his limb edema had worsened. By the 12-mo visit, edema had spread from the lower limbs to the entire body (Figure 1), and the patient presented with newly diagnosed polyserous effusions (thoracic cavity, abdominal cavity and pericardium). After 6 mo of treatment, the patient declined further chemotherapy and received palliative diuretic therapy.

DISCUSSION

This report describes a rare case in which cutaneous metastasis led to the detection of gastric SRCC. Additionally, this gastric SRCC primarily presented as lymphedema of the limbs after the subcutaneous metastases. The typical sites for metastasis of gastric cancer are the liver, peritoneal cavity and regional lymph nodes[12]. The incidence rate of cutaneous metastasis from gastric SRCC is less than 2%; however, when present, the median survival time is 6.5 mo. Common cutaneous manifestations of gastric SRCC include single or multiple red, violet or hyperpigmented asymptomatic nodules, or more rarely, as cellulitis-like or erysipelas-like erythematous plaques[12]. However, our report presents a case of a patient with gastric SRCC who developed carcinomatous lymphangitis, which is very rare in clinical practice.

Skin metastases from internal tumors are uncommon in clinical practice. In women, the most common origin of skin metastases is adenocarcinoma of the breast, whereas squamous cell carcinoma of the lung is the most common in men. Skin metastases in patients with gastric SRCC are extremely rare. The largest series of patients with skin metastases came from a study by Lookingbill *et al*[3] with a total of 4020 patients. Current information about skin metastases from cancer of the stomach comes from the

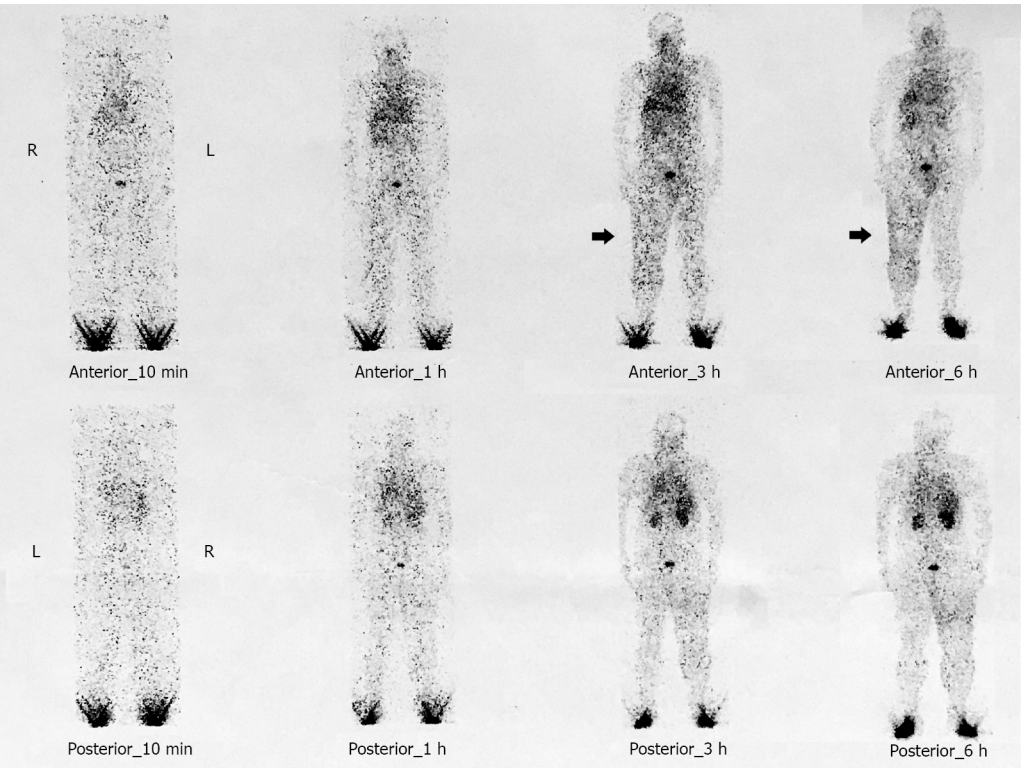

DOI: 10.4251/wjgo.v14.i12.2404

Figure 2 99mTc-DX lymphoscintigraphy. Images were recorded 10 min, 1h, 3h, and 6h after infusion with the 99mTc-DX indicators at both feet. Lymphoscintigraphy showed an obvious accumulation of the radiotracer both the anterior and posterior sides of the right leg.

publication of small series or case reports. The first thorough review of a cutaneous metastases from gastric cancer was performed in 2014 by Cesaretti *et al*[13] and included 72 reported patients with cutaneous lesions at various locations on the body surface. However, to the best of our knowledge, skin metastases from gastric SRCC as the first manifestation have not yet been reviewed.

An electronic literature search was conducted using Medline (PubMed) and Google Scholar databases in August 2022 with the terms "gastric SRCC and cutaneous metastases". The data of publication ranged from 1989 to 2022. There were a total of 30 studies, of which 5 lacked main information; thus, we present a review of 25 studies on cutaneous metastases from gastric signet-ring cell adenocarcinoma (Table 2). The 25 studies included 17 male and 8 female patients with an average age of approximately 58.0-years-old. Although reliable allocation of a skin metastasis to the original tumor is not possible, some preferential associations are obvious. Previous data showed that gastrointestinal and colorectal tumors mainly develop distant skin metastases in the abdomen[14]. In our review, the locations of skin metastases from gastric signet-ring cell adenocarcinoma included the abdomen (10/26, 40.0%), face (7/25, 28.0%), head (5/25, 20.0%), neck (6/25, 24.0%), back (8/25, 32.0%), chest (3/25, 12.0%), armpits (1/25, 4.0%), groin (2/25, 8.0%), arms (3/25, 12.0%) and limbs (3/25, 12.0%). Only one patient presented with initial symptoms and without any local or general clinical symptoms[15]. In all cases, only seven patients presented with weight loss and gastrointestinal symptoms (such as vomiting, loss of appetite, dyspepsia or abdominal pain)[16,17] as the first manifestation. For the cutaneous manifestations, seven patients presented with skin lesions[18-20] (scar-like or other types of lesions), nine patients with nodules[21] and five with erythema. Ours is a rare case, not only due to dramatic skin metastasis as the first presenting sign but also because the patient presented with obvious edema of the lower limbs. In addition, the prognosis of skin metastases from gastric signet cell carcinoma is poor. In all 25 cases reviewed, only 4 patients survived. Most patients died a few weeks (mean 6.1 wk) later after skin involvement[16]. Currently, the patient in our case is alive, but also has advanced symptoms (systemic edema in all limbs) (Figure 1).

In the review by Cesaretti *et al*[13] in 2014, 80% of the patients received a management approach ranging from local excision to chemotherapy or chemoradiation therapy to treat their cutaneous metastases. In our review, 16 patients were treated with chemotherapy (11/16), chemoradiation therapy (1/16), surgery (3/16), or radiotherapy (1/16). Chemotherapy is the first choice for the treatment of advanced gastric signet-ring cell adenocarcinoma. In particular, chemotherapy regimens 5-fu/fa/oxaliplatin (5-fluorouracil, folinic acid, and oxaliplatin) and S-1 (tegafur plus cisplatin) were preferred in our review of cutaneous metastases after gastric signet-ring cell adenocarcinoma.

Table 2 Gastric signet ring cell adenocarcinoma

Patients	Sex/age	Sites of skin involvement	Initial present symptoms	Stage	Follow-up	Management	Ref.
1	Male/67	Nodular lesions on his eyelid, cheeks, scalp, and back	Weight loss of 8 kg within 1 mo	Not available	DOD 3 mo after skin	XELOX chemotherapy (oxaliplatin and capecitabine)	[23]
2	Male/69	On forehead, back, neck, and arms	Dysphagia from eating and multiple cutaneous nodules	Not available	DOD 1 mo after skin	Surgery	[24]
3	Female/53	On abdomen and thighs	Livedo reticularis	Not available	DOD 7 mo after skin	Chemoradiation	[25]
4	Female/72	Skin infiltration in the lower limbs, abdomen, and root of the upper limbs	Lymphangitis	Stage IIIa	DOD 5 mo after skin	Adjuvant chemotherapy with capecitabine + oxaliplatin	[26]
5	Female/75	On the abdomen	Indurated scarlike lesions on the epigastric area	Stage IIIa (T4aN1M0)	DOD 3 mo after skin	Chemotherapy (5-fluorouracil, infusional folinic acid, and oxaliplatin)	[27]
6	Female/57	On the abdomen	With growing lesions on skin	Stage IIIa (T3N2M0)	Not available	Adjuvant chemotherapy [infusional folinic acid + 5-fluorouracil] and radiotherapy, a second round of chemotherapy	[20]
7	Female/45	On head and the back	The cutaneous metastases disappeared		Survival	Chemotherapy with S-1 (Tegafur) plus cisplatin	[28]
8	Male/52	Armpits, axillae, groin, and neck folds	Progressive dermal, mucosal, and perianal lesions, weight loss	T3N2M1	Not available	N/A	[18]
9	Male/21	Cutaneous nodule on his chest	Cutaneous nodule	Stage IV	Survival	Chemotherapy with oxaliplatin (day 1) and S-1	[29]
10	Male/85	A lesion of the right occipital scalp	Abdominal pain, malaise	T4N1M0	DOD 5 mo after skin	Not available	[30]
11	Male/35	Cutaneous nodules on the upper chest, abdomen and left scapular region	Without any local or general clinical symptoms	Not available	Not available	Not available	[15]
12	Male/76	Skin ulcer on right hypochondrium	Hematemesis, weight loss and loss of appetite	T4N2M0	DOD 1 mo after skin	Chemotherapy with irinotecan and oxaliplatin	[16]
13	Female/50	Large erythematous plaque on the left side of the neck; and an erythematous lesion in the perineal region	Bowel habit and weight loss	Not available	DOD 0.5 mo after skin	Not available	[31]
14	Male/59	Painless nodule of the left flank	Painless nodule of the left flank	Not available	DOD 0.5 mo after skin	Metastatic infiltration of a 32-yr-old surgical scar	[32]
15	Male/50	The umbilical area	With a single asymptomatic skin lesion	Not available	Not available	Not available	[19]
16	Male/69	Asymptomatic indurated scar-like lesion	Asymptomatic indurated scar-like lesion	Stage IV	DOD 10 mo after skin	Chemotherapy with cisplatin, Taxotere, and xeloda	[33]
17	Female/71	Limited cyan erythema on the right side of the middle and lower abdomen	Abdominal skin	Not available	DOD 12 mo after skin	Chemotherapy (unknown medication)	[34]
18	Male/48	Bracelet bracelet ("tripe palm"); and hyperkeratosis of fingers	Skin edema with pigmentation	Not available	DOD 36 mo after skin	Chemotherapy with cisplatin, 5-fluorouracil and folic acid	[35]
19	Male/44	Multiple cutaneous eruptions on face and neck	Vomiting and weight loss	Not available	N/A	Not available	[17]
20	Male/51	Abdominal and back	Without any symptom	Not available	DOD 2 mo after skin	Surgery	[36]
21	Male/67	Diffuse erythematous and warm induration over his right cheek	Dyspepsia	Stage IV	DOD 0.75 mo after	Radiotherapy	[37]

		and neck			skin		
22	Male/55	Lower part of face and neck	With multiple itchy nodules	Not available	DOD 7~8 mo after skin	Not available	[21]
23	Female/58	Right inguinal erythema with itching	With chylothorax	Not available	DOD 4 mo after skin	Not available	[38]
24	Male/44	On the face, trunk, and upper extremities	Multiple cutaneous nodules	Stage IV	Survival	Chemotherapy with an oxaliplatin-based regimen and denosumab	[39]
25	Male/68	Right chin region and on the left forehead	Erythematous skin lesion, nodular skin lesion	T4N0M0	Not available	Surgical treatment	[40]

DOD: Dead of disease; N/A: Not applicable.

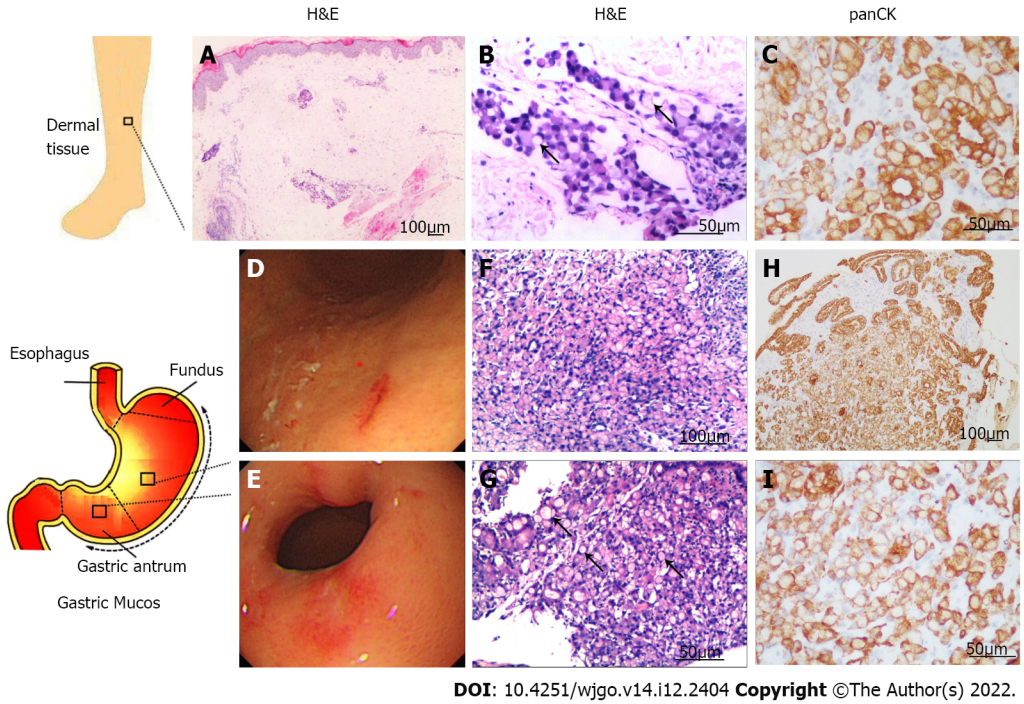

DOI: 10.4251/wjgo.v14.i12.2404 **Copyright** ©The Author(s) 2022.

Figure 3 The immunohistochemistry and gastric endoscopy. A: H&E histological samples of the skin tissue on the right lower limb, 10 ×; B: H&E histological samples of the skin tissue on the right lower limb, 20 ×; C: Histological samples of the skin tissue on the right lower limb stained for panCK, 20 ×; D: Images of gastric endoscopy: Gastric body; E: Images of gastric endoscopy: Gastric antrum; F: H&E histological samples of the mucosa in gastric body, 10 ×; G: Gastric antrum, 20 ×; H: Histological samples of the mucosa in gastric body stained for panCK, 20 ×; I: Gastric antrum, 20 ×. Note the abundant signet-ring cells (black arrows) (B) and (G). H&E: Hematoxylin and eosin; panCK: Pan-cytokeratin.

Because carcinomas generally spread preferentially *via* the lymphatic route and gastrointestinal tumors are known to spread to lymph nodes or lymph-vessels, in this case, it is hypothesized that an aggressive clone of signet cell gastric carcinoma metastasized to the lymph-vessels and then, by making a blockage of lymph-vessels, appeared in the dermis of the skin as an apparently primary skin edema or lymphedema. Lymphedema is a clinical condition characterized by an increased volume of subcutaneous soft tissues due to impairment of the lymphatic system. Lower limb edema is a very common symptom; the most common underlying mechanisms include venous and lymphatic disease, volume overload, increased capillary permeability and decreased oncotic pressure. The most commonly associated diseases are deep vein thrombosis and chronic venous insufficiency, heart failure, hepatic or renal failure hypoproteinemia, idiopathic cyclic edema and drug-induced edema. Lymphedema induced by gastric SRCC is rare and has not been previously reported.

Additionally, the patient's kidney function was evaluated as CKD G3a by calculating the estimated glomerular filtration rate. Renal dysfunction is classified into nonuremic and uremic stages. Patients with non-uremic renal failure (NURF) are defined as having impaired renal function, but are dependent on their own kidneys. The reason is currently unknown. Recently, owing to the increase in the aged population and the incidence of diabetes mellitus, the number of patients with gastric cancer associated

with NURF have been increasing[22]. Whether gastric cancer itself or other factors led to the NURF in this patient remains unclear.

CONCLUSION

We report on a case of skin metastases from gastric SRCC in which lymphedema of the limbs presented as an initial symptom. This case emphasizes the importance of excluding malignancy from the differential diagnosis of edema. Thus, a careful clinical physical examination must be performed on patients with edema to ensure that no information is missing and to obtain further clinical data which could pave the way for further studies.

FOOTNOTES

Author contributions: Wang B wrote the manuscript; Chen J and Wang Y diagnosed and treated the patient; Dong LL collected associated references; Shen GF commented on the manuscript and all authors discussed the results, read and approved the manuscript.

Supported by The National Nature Science Foundation of China, No. 81900363.

Informed consent statement: Informed written consent was obtained from the patient for the publication of this report and any accompanying images.

Conflict-of-interest statement: All the authors report no relevant conflicts of interest for this article.

CARE Checklist (2016) statement: The authors have read the CARE Checklist (2016), and the manuscript was prepared and revised according to the CARE Checklist (2016).

Country/Territory of origin: China

ORCID number: Gui-Fen Shen 0000-0002-3040-4482.

S-Editor: Liu XF
L-Editor: Filipodia
P-Editor: Liu XF

REFERENCES

1 **Wong CY**, Helm MA, Helm TN, Zeitouni N. Patterns of skin metastases: A review of 25 years' experience at a single cancer center. *Int J Dermatol* 2014; **53**: 56-60 [PMID: 23432658 DOI: 10.1111/j.1365-4632.2012.05635.x]
2 **Disibio G**, French SW. Metastatic patterns of cancers: results from a large autopsy study. *Arch Pathol Lab Med* 2008; **132**: 931-939 [PMID: 18517275 DOI: 10.5858/2008-132-931-MPOCRF]
3 **Lookingbill DP**, Spangler N, Helm KF. Cutaneous metastases in patients with metastatic carcinoma: A retrospective study of 4020 patients. *J Am Acad Dermatol* 1993; **29**: 228-236 [PMID: 8335743 DOI: 10.1016/0190-9622(93)70173-q]
4 **Nashan D**, Müller ML, Braun-Falco M, Reichenberger S, Szeimies RM, Bruckner-Tuderman L. Cutaneous metastases of visceral tumours: A review. *J Cancer Res Clin Oncol* 2009; **135**: 1-14 [PMID: 18560891 DOI: 10.1007/s00432-008-0432-0]
5 **Saeed S**, Keehn CA, Morgan MB. Cutaneous metastasis: A clinical, pathological, and immunohistochemical appraisal. *J Cutan Pathol* 2004; **31**: 419-430 [PMID: 15186430 DOI: 10.1111/j.0303-6987.2004.00207.x]
6 **Mortimer PS**. Managing lymphoedema. *Clin Exp Dermatol* 1995; **20**: 98-106 [PMID: 8565266 DOI: 10.1111/j.1365-2230.1995.tb02665.x]
7 **Szuba A**, Rockson SG. Lymphedema: Classification, diagnosis and therapy. *Vasc Med* 1998; **3**: 145-156 [PMID: 9796078 DOI: 10.1177/1358836X9800300209]
8 **Rockson SG**, Keeley V, Kilbreath S, Szuba A, Towers A. Cancer-associated secondary lymphoedema. *Nat Rev Dis Primers* 2019; **5**: 22 [PMID: 30923312 DOI: 10.1038/s41572-019-0072-5]
9 **Levin A**, Stevens PE. Summary of KDIGO 2012 CKD Guideline: Behind the scenes, need for guidance, and a framework for moving forward. *Kidney Int* 2014; **85**: 49-61 [PMID: 24284513 DOI: 10.1038/ki.2013.444]
10 **Ajani JA**, D'Amico TA, Bentrem DJ, Chao J, Corvera C, Das P, Denlinger CS, Enzinger PC, Fanta P, Farjah F, Gerdes H,

Gibson M, Glasgow RE, Hayman JA, Hochwald S, Hofstetter WL, Ilson DH, Jaroszewski D, Johung KL, Keswani RN, Kleinberg LR, Leong S, Ly QP, Matkowskyj KA, McNamara M, Mulcahy MF, Paluri RK, Park H, Perry KA, Pimiento J, Poultsides GA, Roses R, Strong VE, Wiesner G, Willett CG, Wright CD, McMillian NR, Pluchino LA. Esophageal and Esophagogastric Junction Cancers, Version 2.2019, NCCN Clinical Practice Guidelines in Oncology. *J Natl Compr Canc Netw* 2019; **17**: 855-883 [PMID: 31319389 DOI: 10.6004/jnccn.2019.0033]

11 **Taguchi T**, Nazneen A, Abid MR, Razzaque MS. Cisplatin-associated nephrotoxicity and pathological events. *Contrib Nephrol* 2005; **148**: 107-121 [PMID: 15912030 DOI: 10.1159/000086055]

12 **Liu F**, Yan WL, Liu H, Zhang M, Sang H. Cutaneous metastases from gastric adenocarcinoma 15 years after curative gastrectomy. *An Bras Dermatol* 2015; **90**: 46-50 [PMID: 26312672 DOI: 10.1590/abd1806-4841.20153829]

13 **Cesaretti M**, Malerba M, Basso V, Boccardo C, Santoni R, D'Alessandro G, Weiss A, Campisi C, De Cian F. Cutaneous metastasis from primary gastric cancer: A case report and review of the literature. *Cutis* 2014; **93**: E9-E13 [PMID: 24818191]

14 **Rendi MH**, Dhar AD. Cutaneous metastasis of rectal adenocarcinoma. *Dermatol Nurs* 2003; **15**: 131-132 [PMID: 12751347]

15 **Fekete GL**, Cotoi OS, Fekete JE. Multiple nodular cutaneous metastases as the first clinical sign of signet ring cell gastric carcinoma: Case report. *Acta Dermatovenerol Croat* 2012; **20**: 34-37 [PMID: 22507473]

16 **Karayiannakis AJ**, Bolanaki H, Tsalikidis C, Simopoulos C. Cutaneous metastasis at a surgical drain site after gastric cancer resection. *Case Rep Oncol* 2010; **3**: 495-497 [PMID: 21611104 DOI: 10.1159/000323559]

17 **Acikalin MF**, Vardareli E, Tel N, Saricam T, Urer S. Erysipelas-like cutaneous metastasis from gastric signet ring cell carcinoma. *J Eur Acad Dermatol Venereol* 2005; **19**: 642-643 [PMID: 16164730 DOI: 10.1111/j.1468-3083.2005.01214.x]

18 **Schulmann K**, Strate K, Pox CP, Wieland U, Kreuter A. Paraneoplastic acanthosis nigricans with cutaneous and mucosal papillomatosis preceding recurrence of a gastric adenocarcinoma. *J Clin Oncol* 2012; **30**: e325-e326 [PMID: 23008315 DOI: 10.1200/JCO.2012.42.5454.]

19 **Zadeh VB**, Kadyan R, Al-Abdulrazzaq A, Al-Otaibi S, Sarhan A, Najem N. Sister Mary Joseph's nodule: A case of umbilical cutaneous metastasis with signet ring cell histology. *Indian J Dermatol Venereol Leprol* 2009; **75**: 503-505 [PMID: 19736432 DOI: 10.4103/0378-6323.55396]

20 **Gündüz Ö**, Emeksiz MC, Atasoy P, Kidir M, Yalçin S, Demirkan S. Signet-ring Cells in the Skin: A Case of Late-onset Cutaneous Metastasis of Gastric Carcinoma and a Brief Review of Histological Approach. *Dermatol Reports* 2016; **8**: 6819 [PMID: 28326183 DOI: 10.4081/dr.2016.6819]

21 **Essa K**, Pervez S, Shah LM, Soomro IN. Signet cell gastric carcinoma presenting as multiple large skin nodules. *Australas J Dermatol* 2001; **42**: 219-220 [PMID: 11510466 DOI: 10.1046/j.1440-0960.2001.00522.x]

22 **Mori S**, Sawada T, Hamada K, Kita J, Shimoda M, Tagaya N, Kubota K. Gastrectomy for patients with gastric cancer and non-uremic renal failure. *World J Gastroenterol* 2007; **13**: 4589-4592 [PMID: 17729411 DOI: 10.3748/wjg.v13.i34.4589]

23 **Bulut E**, Taştekin E, Topuz C, Öztürk S, Gökyer A. Exceptional Variant with Distant Cutaneous Metastasis as the First Clinical Sign in Gastric Signet-Ring Carcinoma. *J Gastrointest Cancer* 2021 [PMID: 34786642 DOI: 10.1007/s12029-021-00747-2]

24 **Chen JW**, Zheng LZ, Xu DH, Lin W. Extensive cutaneous metastasis of recurrent gastric cancer: A case report. *World J Clin Cases* 2021; **9**: 6575-6581 [PMID: 34435028 DOI: 10.12998/wjcc.v9.i22.6575]

25 **Demircioğlu D**, Öztürk Durmaz E, Demirkesen C, Şahin S. Livedoid cutaneous metastasis of signet-ring cell gastric carcinoma. *J Cutan Pathol* 2021; **48**: 785-788 [PMID: 33476049 DOI: 10.1111/cup.13969]

26 **Souza BDS**, Bonamigo RR, Viapiana GL, Cartell A. Signet ring cells in carcinomatous lymphangitis due to gastric adenocarcinoma. *An Bras Dermatol* 2020; **95**: 490-492 [PMID: 32487420 DOI: 10.1016/j.abd.2019.12.004]

27 **Cokgezer S**, Samanci NS, Bektas M, Kepil N, Demirelli FH. Cutaneous Metastasis of Signet Cell Gastric Carcinoma. *Indian J Dermatol* 2020; **65**: 148-150 [PMID: 32180605 DOI: 10.4103/ijd.IJD_263_18]

28 **Matsuoka T**, Hosaka S, Inada K, Kawamoto S. [A case of delayed subcutaneous metastases of gastric carcinoma effectively treated with S-1 plus cisplatin chemotherapy]. *Gan To Kagaku Ryoho* 2013; **40**: 2262-2264 [PMID: 24394079]

29 **Qiao J**, Fang H. Cutaneous nodule in a young man. *JAMA* 2012; **308**: 812-813 [PMID: 22910759 DOI: 10.1001/jama.2012.9637]

30 **Alcaraz I**, Santonja C, Kutzner H, Requena L. Signet-ring cell gastric adenocarcinoma metastasizing into a primary cutaneous squamous cell carcinoma of the scalp. *J Cutan Pathol* 2012; **39**: 568-569, 570 [PMID: 22616597 DOI: 10.1111/j.1600-0560.2012.01928_1.x]

31 **Ismaili Z**, Dekhay S, Moussaoui A, Jahid A. Primary gastric, duodenal, and rectal signet ring cell carcinoma revealed by cutaneous metastasis. *Endoscopy* 2011; **43** Suppl 2: E209-E210 [PMID: 21590608 DOI: 10.1055/s-0030-1256399]

32 **Kerkeni N**, Fazaa B, Ezzine N, Zeglaoui F, Kamoun MR, Jaada N, Khedher MA, Zermani R. Cutaneous metastasis in an old surgical scar revealing gastric linitis. *Int J Dermatol* 2011; **50**: 629-632 [PMID: 21506987 DOI: 10.1111/j.1365-4632.2009.04425.x]

33 **Xavier MH**, Vergueiro Tde R, Vilar EG, Pinto JM, Issa MC, Pereira GB, Carocha AP. Cutaneous metastasis of gastric adenocarcinoma: An exuberant and unusual clinical presentation. *Dermatol Online J* 2008; **14**: 8 [PMID: 19094846]

34 **Müller CS**, Pföhler C, Reichrath J, Tilgen W. [Gastric signet ring cell carcinoma presenting. An erysipelas-like cutaneous metastasis of the abdominal skin]. *Hautarzt* 2008; **59**: 992-994 [PMID: 18712325 DOI: 10.1007/s00105-008-1541-z]

35 **Kleikamp S**, Böhm M, Frosch P, Brinkmeier T. [Acanthosis nigricans, papillomatosis mucosae and "tripe palms" in a patient with metastasized gastric carcinoma]. *Dtsch Med Wochenschr* 2006; **131**: 1209-1213 [PMID: 16721709 DOI: 10.1055/s-2006-941753]

36 **Sánchez-Muñoz A**, Gravalos Castro C, Colomer Bosch R, García Velasco A, García JP, Cortés-Funes H. [Generalized cutaneous-nodal metastatic spread as initial manifestation of the recurrence of a gastric adenocarcinoma]. *Rev Clin Esp* 2003; **203**: 597-598 [PMID: 14622511 DOI: 10.1157/13053731]

37 **Foo KF**, Tao M, Tan EH. Gastric carcinoma presenting with cellulitis-like cutaneous metastasis. *Singapore Med J* 2002; **43**: 37-38 [PMID: 12008775]

38 **Shibata K**, Kitagawa S, Fujimura M, Matsuda T. Chylothorax associated with inflammatory carcinoma. *Intern Med* 1998;

37: 538-541 [PMID: 9678689 DOI: 10.2169/internalmedicine.37.538]

39 **Bajoghli AA**, Piselli A, Kemprecos H, Khosravi H, Cardis MA, Noel MS. Gastric carcinoma's primary presentation as multiple cutaneous nodules throughout the body. *Cancer Treat Res Commun* 2022; **31**: 100532 [PMID: 35217487 DOI: 10.1016/j.ctarc.2022.100532]

40 **Eckardt AM**, Back W. Facial Cutaneous Metastases of Gastric Signet-ring Cell Carcinoma: Resection and Reconstruction as a Palliative Surgical Treatment Option. *In Vivo* 2022; **36**: 1508-1512 [PMID: 35478122 DOI: 10.21873/invivo.12859]

World Journal of Gastrointestinal Oncology

Submit a Manuscript: https://www.f6publishing.com

World J Gastrointest Oncol 2022 December 15; 14(12): 2415-2421

DOI: 10.4251/wjgo.v14.i12.2415

ISSN 1948-5204 (online)

CASE REPORT

Rare massive hepatic hemangioblastoma: A case report

De-Fu Li, Xue-Jun Guo, Shi-Peng Song, Hong-Bing Li

Specialty type: Oncology

Provenance and peer review: Unsolicited article; Externally peer reviewed.

Peer-review model: Single blind

Peer-review report's scientific quality classification

Grade A (Excellent): 0
Grade B (Very good): B
Grade C (Good): C, C
Grade D (Fair): 0
Grade E (Poor): 0

P-Reviewer: Mahmoud MZ, Saudi Arabia; Reis F, Brazil

Received: August 30, 2022
Peer-review started: August 30, 2022
First decision: September 23, 2022
Revised: October 2, 2022
Accepted: November 6, 2022
Article in press: November 6, 2022
Published online: December 15, 2022

De-Fu Li, Hong-Bing Li, Department of Radiology, Fuyong People's Hospital of Shenzhen Baoan, Shenzhen 518103, Guangdong Province, China

Xue-Jun Guo, Department of Radiology, Peking University Shenzhen Hospital, Shenzhen 518036, Guangdong Province, China

Shi-Peng Song, Department of Hepatobiliary Surgery, Fuyong People's Hospital of Shenzhen Baoan, Shenzhen 518103, Guangdong Province, China

Corresponding author: Hong-Bing Li, MD, MMed, Associate Chief Physician, Department of Radiology, Fuyong People's Hospital of Shenzhen Baoan, No. 81 Defeng Road, Fuyong Street, Baoan District, Shenzhen 518103, Guangdong Province, China. lihongbing.2@163.com

Abstract

BACKGROUND

Hepatic hemangioblastoma is an extremely rare disease; only three cases have been reported in the literature, and its magnetic resonance imaging (MRI) findings are unreported.

CASE SUMMARY

We report a case of incidental hepatic hemangioblastoma. The patient had no history of von Hippel-Lindau disease or associated clinical signs. Computed tomography and MRI showed a large tumor occupying almost half of the right side of the liver with expansive growth, well-defined borders, heterogeneous mildly progressive enhancement, and visibly enlarged blood supply vessels. Flow voids were observed on T2-weighted imaging. Both diffusion-weighted imaging (DWI) and apparent diffusion coefficient (ADC) map findings of the mass were predominantly inhomogeneous. Postoperative pathology indicated a diagnosis of hemangioblastoma.

CONCLUSION

Enlarged peripheral blood-supplying vessels and progressive enhancement seem to be typical imaging features of hepatic hemangioblastoma. However, a solid significantly enhanced mass with a low signal on DWI and a high signal on ADC may also be helpful for the diagnosis of hepatic hemangioblastoma.

Key Words: Computed tomography; Hemangioblastoma; Magnetic resonance imaging; Liver; von Hippel Lindau disease; Case report

Core Tip: Hepatic hemangioblastoma is mostly huge in size, and images of flow void vessels within the tumor can be seen on T2-weighted imaging, and enlarged peripheral blood-supplying vessels and progressive enhancement seem to be typical imaging features of hepatic hemangioblastoma. However, a solid significantly enhanced mass with a low signal on diffusion-weighted imaging and a high signal on apparent diffusion coefficient may also be helpful for the diagnosis of hepatic hemangioblastoma.

Citation: Li DF, Guo XJ, Song SP, Li HB. Rare massive hepatic hemangioblastoma: A case report. *World J Gastrointest Oncol* 2022; 14(12): 2415-2421
URL: https://www.wjgnet.com/1948-5204/full/v14/i12/2415.htm
DOI: https://dx.doi.org/10.4251/wjgo.v14.i12.2415

INTRODUCTION

Hemangioblastomas are rare benign tumors, accounting for 1%-2% of all central nervous system tumors [1,2]. The cerebellum is the most common location, followed by the spinal cord and brainstem[3]; however, hemangioblastomas can also occur in the peripheral nervous system, adrenal gland, and liver [4]. Hemangioblastomas are present in 25%-30% of patients with von Hippel-Lindau disease (VHLD), and in these cases, retinal hemangioblastomas and endolymphatic sac tumors may also be detected[5].

Only three cases of VHLD with hepatic hemangioblastoma have been reported in the literature. Here, we report a case of hepatic hemangioblastoma that was not clearly related to VHLD, and we combined computed tomography (CT) and magnetic resonance imaging (MRI) findings with postoperative pathology findings and reports in the literature to further elucidate the imaging findings of hepatic hemangioblastoma.

CASE PRESENTATION

Chief complaints

A 42-year-old Chinese man complained of left lumbar abdominal pain for 3 d and decreased vision in his right eye for 3 mo.

History of present illness

Three days earlier, there was no obvious cause of the left-sided lumbar abdominal pain and discomfort with persistent distension, which radiated to the left lower abdomen and was accompanied by urine frequency, urgency, and dysuria. Ultrasonography performed at the local community health center showed a calculus in the distal portion of the left ureter with mild dilated effusion in the ureter and kidney.

History of past illness

The patient had a history of hyperlipidemia for 3 years and denied any history of infectious diseases, such as "hepatitis or tuberculosis".

Personal and family history

The patient's family members were fit and healthy with no genetic diseases or history of hepatitis B.

Physical examination

On physical examination, the abdomen was flat, and a hard mass was palpable under the hepatic rib cage. No enlargement was palpable under the splenic rib cage. There was no percussion pain in the liver or left kidney areas.

Laboratory examinations

The laboratory examinations were as follows: Aspartate aminotransferase 86 U/L, alanine aminotransferase 95 U/L, total bilirubin 25.2 μmol/L, direct bilirubin 11.6 μmol/L, hepatitis B virus surface antibody (luminescence method) 106.90 mIU/mL, hepatitis B virus core antibody (luminescence method) 3.90 cut off index, erythrocyte count 4.07 × 10^{12}/L, and hemoglobin concentration 114 g/L.

Imaging examinations

Ultrasonography revealed a left distal ureteral calculus with dilatation. A mixed-density mass (approximately 160 mm × 184 mm × 122 mm in size) in the right lobe of the liver was accidentally found on a

plain CT scan of the urinary system after admission. Subsequently, CT and MRI images of the liver revealed an oval-shaped mass with heterogeneous density and signal (Figures 1 and 2), which resembled different types of meteorites in different series images. A multidisciplinary team consultation, considering hepatic mesenchymal tumors, concluded that atypical hemangioma or solitary fibrous tumor was likely.

FINAL DIAGNOSIS

Hepatic hemangioblastoma.

TREATMENT

After all examinations and a full assessment were made, the intrahepatic mass was surgically resected with the patient's signed consent. Intraoperatively, the total volume of the liver was significantly enlarged, and there was a huge mass (200 mm in diameter) in the right lobe of the liver, occupying half of the right liver, with the left lower margin closing to the left edge of the gallbladder bed and the upper margin closing to the right edge of the inferior vena cava. The right liver was partially lifted out of the abdominal cavity. The right hemihepatic mass was completely resected. The mass had an intact envelope during the resection. The surgical procedure was uneventful, with satisfactory intraoperative anesthesia, no adverse effects, stable vital signs, and bleeding of about 400 mL. Postoperative radiotherapy and chemotherapy were not performed. The patient was advised to undergo genetic examination for VHLD, but the patient refused.

OUTCOME AND FOLLOW-UP

The patient recovered well without complications after 8 mo of follow-up.

DISCUSSION

The current patient had no clinical features related to VHLD. MRI did not reveal hemangioblastoma in the cerebellum, the red blood cell count was normal, and the hemoglobin concentration was close to normal, indicating a sporadic hemangioblastoma. However, three previous reports indicated that hepatic hemangioblastoma can be related to VHLD[6-8]. The three previous cases were also found to have hemangioblastoma in the cerebellum, spinal cord, retina, lung, or mesentery, with a history of surgery for cerebellar and spinal cord hemangioblastoma. The features of the three cases of hepatic hemangioblastoma are shown in Table 1.

The imaging features of the lesion in this case are as follows: The tumor was massive, with expansive growth and well-defined boundaries, the real capsule was not observed on pathology, and there was no invasion of adjacent hepatic vessels or breakthrough of the hepatic capsule. There were no emboli in the portal vein or enlarged lymph nodes in the hepatic portal or retroperitoneum. Contrast-enhanced scans showed heterogeneous mild progressive enhancement. There was no definitive liquefaction or necrosis in the tumor, which may be because the tumor itself was composed of many capillary components and numerous vacuolar stromal cells, and it had a low tumor proliferation index and low oxygen demand. The density or signal of the tumor parenchyma was heterogeneous, with low density on unenhanced CT and obvious high signal on T2-weighted imaging (T2WI) (Figures 1 and 2). There was no enhancement in those areas of the lesion on the enhanced scan, and it is considered that the cytoplasm of tumor cells contained more liquid components and some lipid-like bubbles. Patchy areas with high diffusion-weighted imaging (DWI) and low apparent diffusion coefficient (ADC) signals appeared in some parts of the lesion, and the CT findings were relatively high-density (rectangular areas in Figures 2D-G), which may be related to two aspects. First, intratumoral hemorrhage was confirmed by pathology. The incidence of hemorrhage in hemangioblastomas is low[9]. The intratumoral hemorrhage occurred possibly because the tumor contained more immature thin-walled vessels and the tumor volume was large. Second, the tumor-feeding artery originated from the blood vessels below the tumor and the blood supply in the lower part of the tumor was relatively abundant; as such, there were many closely arranged spindle stromal cells. A vascular flow void signal can be seen on the T2WI sequence (black arrow in Figure 2B), which may indicate a hemangioblastoma. In other tumors, a vascular flow void signal occurs only when the blood supply is very abundant[1]. The lower part of the tumor and the scattered areas showed a slightly high signal on T2WI and a slightly low signal on T1WI, and the low signal on DWI and high signal on ADC were mildly enhanced (triangles in Figures 2D, 2E and 2G).

Table 1 Characteristics of hepatic hemangioblastoma reported in three papers

Case	Sex	Age (yr)	Location	Size (cm^2)	US	CT	DSA	VHLD	First or preoperative diagnosis	Other parts
1	Female	42	Left and right liver	1.5 × 1.5 (largest)	A central hypoechoic solid mass	Enlarged liver with multiple nodules, some of which have necrosis or bleeding within them	No abnormalities in the kidneys and other abdominal organs	Yes	/	Cerebellum, cervical spine
2	Female	39	The right lobe of the liver	9 × 11	Solid hyperechoic mass with a hypoechoic central portion	Hypodense lesion, significant peripheral enhancement, and incomplete filling inward after enhancement	Early stage with obvious vascularization and extensive tumor redness involving almost the whole liver	Yes	A giant cavernous hemangioma	Cerebellum, cervical medulla, lung
3	Male	30	The right lobe of the liver	/	Two hypoechoic solid masses with simple cysts in the kidneys and pancreas	Progressively enhanced liver and mesenteric mass with collateral veins, and pancreatic cysts	Richly vascularized and supplied by the right hepatic and right renal perineural arteries and collateral veins	Yes	Metastases from hepatic and mesenteric hemangioblastoma or renal cell carcinoma	Mesentery, retina, cerebellum, and spinal cord

US: Ultrasound; CT: Computed tomography; DSA: Digital subtraction angiography; VHLD: von Hippel-Lindau disease.

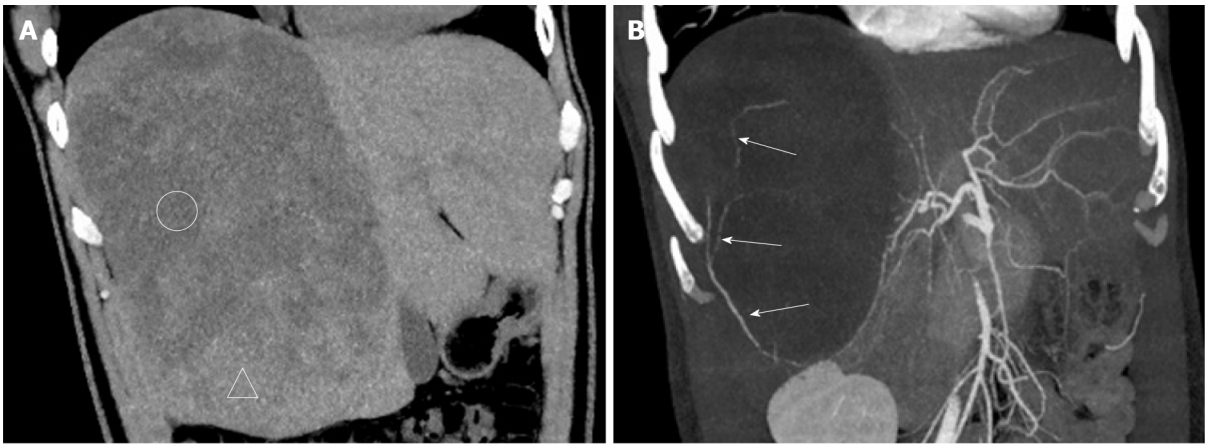

DOI: 10.4251/wjgo.v14.i12.2415 **Copyright** ©The Author(s) 2022.

Figure 1 Computed tomography images. A: Plain computed tomography (CT) coronary reconstruction image; B: CT-enhanced arterial phase maximum intensity projection (MIP) reconstruction image. Compared with the liver parenchyma, many areas of the lesions appear as low density (circled areas) on CT. The mass resembles a meteorite. The MIP image shows that the tumor-feeding artery originates from the right posterior hepatic artery, from bottom to top, with multiple branches (white long arrows in Figure 1B).

These findings are suggestive of hemangioblastoma. The solid area of cerebellar hemangioblastoma often exhibits a low signal on DWI with ADC corresponding to a high signal, which is significantly enhanced, and it may be related to the tumor having abundant vascular interstitial spaces[10]. The signal in the other areas on DWI and ADC was equally highly inhomogeneous (Figures 2D and 2E), and this may be related to the tumor cell composition, arrangement, and vascular network structure. The lesions had heterogeneous and progressive enhancement (Figures 1 and 2), but the degree of enhancement was significantly lower than reported previously[7,8]. After reviewing the pathology (Figure 3), we speculated that this was due to the following reasons: (1) There were many interstitial cells with vacuolar structures in the tumor; (2) Although there were many capillaries in the tumor, most were immature vessels lacking a normal vascular structure (a large amount of blood remained in the capillaries, resulting in increased vascular resistance, which made it difficult for contrast agents to penetrate the tumor parenchyma); and (3) The tumor was too large and the feeding arteries were relatively small, resulting in insufficient blood supply. Multiple irregular strip-like obvious enhancement foci with irregular shape and course were seen in the mass after contrast enhancement and are

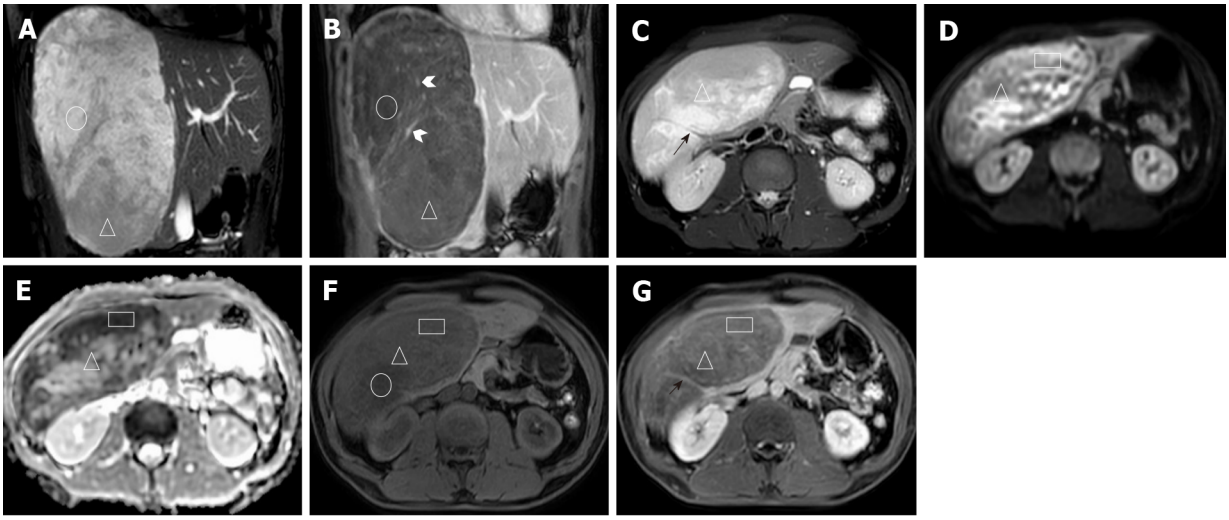

DOI: 10.4251/wjgo.v14.i12.2415 **Copyright** ©The Author(s) 2022.

Figure 2 Magnetic resonance imaging images. A: Coronal balanced fast field echo (B-FFE) image; B: Coronal T1-weighted image (T1WI) after 150-s gadolinium enhancement; C: Axial image, including T2-weighted imaging (T2WI); D: Diffusion-weighted imaging (DWI); E: Apparent diffusion coefficient (ADC); F: T1WI; G: After 7-min gadolinium enhancement, the lesions showed a high signal on B-FFE, a low signal on T1WI, and no definitive enhancement (circled areas). In the lesions, a strip-shaped flow void vascular signal (black short arrow in Figure 2C) can be seen on T2WI. Multiple irregular strip-like obvious enhancement foci with irregular shapes are shown (white arrowhead in Figure 2B). Some areas of high signal on DWI and low signal on ADC and B-FFE (triangular areas) showing progressive and heterogeneous enhancement with gadolinium contrast enhancement. The mass resembled different meteorites in the various sequences.

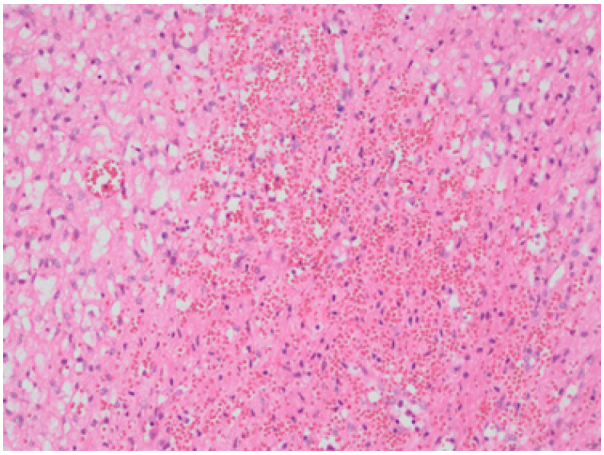

DOI: 10.4251/wjgo.v14.i12.2415 **Copyright** ©The Author(s) 2022.

Figure 3 Pathology map (200 ×, hematoxylin-eosin staining). The tumor was mainly composed of capillaries and eosinophilic, vacuole-containing stromal cells. The cell morphology was mild, the nuclei were small and uniform, and division was rare. The blood vessels were full of blood, with some blood spilling out from the blood vessels.

related to different types of arteries and veins observed pathologically (white swallowtail shaped arrow in Figure 2B). Nodular enhancement foci were observed in the tumor, suggesting that the contrast agent leaked from relatively immature blood vessels to form blood sinuses.

We carefully compared the features of this case with those of the lesions of the previous three cases and found some similar features. The patients were aged 30-45 years when the lesion was found, the tumors were large, all were predominantly solid with heterogeneous density and were mostly found in the right lobe of the liver, with obvious blood supply vessels visible on either angiography or MRI, and all were progressively enhanced. However, clinical symptoms were variable and most could have been related to VHLD. MRI or CT can replace angiography for detecting vascular supply, thus reducing unnecessary invasive examinations.

The present report has some limitations. The first limitation is the lack of pathological sections consistent with CT or MRI, thereby preventing the appropriate analysis of the imaging features corresponding to the pathology. Further, our report only included a single case, which was too few to allow a summary of lesion characteristics.

The main advantage of CT and MRI is the ability to optimally demonstrate the internal composition of the tumor, blood supply, and relationship with surrounding structures, which provide the necessary basis for surgical planning. Because of the abundance of capillaries in hemangioblastoma related to the increased expression of vascular endothelial growth factor, this tumor demonstrates elevated relative cerebral blood volume seen in perfusion sequences. Thus, DWI imaging combined with perfusion cerebral blood volume can provide more diagnostic information[11].

CONCLUSION

Because of the rarity of hepatic hemangioblastoma, the understanding of its imaging features is in the preliminary stages. The patient had no clinical features of VHLD, indicating a sporadic hemangioblastoma. Enlarged peripheral supplying arteries and progressive enhancement may be typical imaging features of hepatic hemangioblastoma. Low signal on DWI and high signal on ADC with significant enhancement may be indicative of a diagnosis of hepatic hemangioblastoma.

ACKNOWLEDGEMENTS

The authors thank Dr. Wang Rui-An (Department of Pathology, Shenzhen Hospital, Southern Medical University, Guangdong Province, China) for providing pathological pictures, consultation, and annotations.

FOOTNOTES

Author contributions: Li DF contributed to the methodology and original draft writing; Guo XJ and Song SP were involved in the data curation and editing the manuscript; Li DF and Li HB contributed to the formal analysis; Guo XJ and Li HB participated in the manuscript writing and review.

Informed consent statement: The local institutional review board of Fuyong People's Hospital of Shenzhen Baoan approved the study and waived the need for written informed consent due to the study's retrospective design.

Conflict-of-interest statement: All the authors report no relevant conflicts of interest for this article.

CARE Checklist (2016) statement: The authors have read the CARE Checklist (2016), and the manuscript was prepared and revised according to the CARE Checklist (2016).

Country/Territory of origin: China

ORCID number: De-Fu Li 0000-0001-7486-3739; Xue-Jun Guo 0000-0003-4769-7426; Hong-Bing Li 0000-0002-4686-4168.

S-Editor: Wang JJ
L-Editor: Wang TQ
P-Editor: Wang JJ

REFERENCES

1 **Duan M**, Yang L, Kang J, Wang R, You H, Feng M. Neuroimaging Features of Optic Nerve Hemangioblastoma Identified by Conventional and Advanced Magnetic Resonance Techniques: A Case Report and Literature Review. *Front Oncol* 2021; **11**: 763696 [PMID: 34868983 DOI: 10.3389/fonc.2021.763696]
2 **Kano H**, Shuto T, Iwai Y, Sheehan J, Yamamoto M, McBride HL, Sato M, Serizawa T, Yomo S, Moriki A, Kohda Y, Young B, Suzuki S, Kenai H, Duma C, Kikuchi Y, Mathieu D, Akabane A, Nagano O, Kondziolka D, Lunsford LD. Stereotactic radiosurgery for intracranial hemangioblastomas: a retrospective international outcome study. *J Neurosurg* 2015; **122**: 1469-1478 [PMID: 25816088 DOI: 10.3171/2014.10.JNS131602]
3 **Hussein MR**. Central nervous system capillary haemangioblastoma: the pathologist's viewpoint. *Int J Exp Pathol* 2007; **88**: 311-324 [PMID: 17877533 DOI: 10.1111/j.1365-2613.2007.00535.x]

4 **Bisceglia M**, Muscarella LA, Galliani CA, Zidar N, Ben-Dor D, Pasquinelli G, la Torre A, Sparaneo A, Fanburg-Smith JC, Lamovec J, Michal M, Bacchi CE. Extraneuraxial Hemangioblastoma: Clinicopathologic Features and Review of the Literature. *Adv Anat Pathol* 2018; **25**: 197-215 [PMID: 29189208 DOI: 10.1097/PAP.0000000000000176]

5 **Mourão JLV**, Borella LFM, Duarte JÁ, Dalaqua M, Fernandes DA, Reis F. Imaging manifestations of von Hippel-Lindau disease: an illustrated guide focusing on the central nervous system. *Radiol Bras* 2022; **55**: 188-192 [PMID: 35795602 DOI: 10.1590/0100-3984.2021.0080-en]

6 **Rojiani AM**, Owen DA, Berry K, Woodhurst B, Anderson FH, Scudamore CH, Erb S. Hepatic hemangioblastoma. An unusual presentation in a patient with von Hippel-Lindau disease. *Am J Surg Pathol* 1991; **15**: 81-86 [PMID: 1898683]

7 **McGrath FP**, Gibney RG, Morris DC, Owen DA, Erb SR. Case report: multiple hepatic and pulmonary haemangioblastomas--a new manifestation of von Hippel-Lindau disease. *Clin Radiol* 1992; **45**: 37-39 [PMID: 1740034 DOI: 10.1016/s0009-9260(05)81467-9]

8 **Hayasaka K**, Tanaka Y, Satoh T, Mutoh H. Hepatic hemangioblastoma: an unusual presentation of von Hippel-Lindau disease. *J Comput Assist Tomogr* 1999; **23**: 565-566 [PMID: 10433288 DOI: 10.1097/00004728-199907000-00016]

9 **Ene CI**, Morton RP, Ferreira M Jr, Sekhar LN, Kim LJ. Spontaneous Hemorrhage from Central Nervous System Hemangioblastomas. *World Neurosurg* 2015; **83**: 1180.e13-1180.e17 [PMID: 25727302 DOI: 10.1016/j.wneu.2015.02.009]

10 **She D**, Yang X, Xing Z, Cao D. Differentiating Hemangioblastomas from Brain Metastases Using Diffusion-Weighted Imaging and Dynamic Susceptibility Contrast-Enhanced Perfusion-Weighted MR Imaging. *AJNR Am J Neuroradiol* 2016; **37**: 1844-1850 [PMID: 27173365 DOI: 10.3174/ajnr.A4809]

11 **Neska-Matuszewska M**, Zimny A, Bladowska J, Czarnecka A, Sąsiadek M. The role of diffusion and perfusion magnetic resonance imaging in differentiation of haemangioblastomas and pilocytic astrocytomas. *Pol J Radiol* 2018; **83**: e197-e203 [PMID: 30627235 DOI: 10.5114/pjr.2018.75870]

Published by **Baishideng Publishing Group Inc**
7041 Koll Center Parkway, Suite 160, Pleasanton, CA 94566, USA
Telephone: +1-925-3991568
E-mail: bpgoffice@wjgnet.com
Help Desk: https://www.f6publishing.com/helpdesk
https://www.wjgnet.com